Investigating the neuromechanical control of healthy gait modulation and pathological gaits observed in cerebral palsy using neuromuscular simulations

Andrea DI RUSSO

Acknowledgements

In these few pages, it is difficult to express my gratitude for all the people who took part in my life in this academic adventure. I cannot help to thank first Prof. Auke Ijspeert for giving me the opportunity to work on this exciting project, always finding the perfect balance between providing guidance and independence, and for keeping on making the Biorobotics Laboratory not only a stimulating academic environment but also a fun place full of social activities that made this PhD experience very special for me. I would like to thank the funding agency of the SimGait project, the Swiss National Science Foundation, together with my scientific collaborators Prof. Stephane Armand, head of the Kinesiology Lab at the University Hospital of Geneva, Prof. Alexandros Kalousis, head of the Data Mining and Machine Learning team at University of Applied Sciences Western Switzerland, and Dr. Olivier Michel, CEO of Cyberbotics. I thank my jury members Prof. Silvestro Micera, Prof. Friedl De Groote, Prof. Hartmut Geyer, and Prof. Gregoire Courtine for their time and valuable insights that greatly improve the final quality of my research work. A special thank goes to my scientific collaborators outside the SimGait project, Prof. Simon Danner, Prof. Jessica Ausborn, Prof. James Finley, and Dr. Mohamed Bouri, and to all the students who chose to conduct their semester, bachelor, and master projects under my supervision without whom a great part of my scientific work would not have been possible.

Through my experience at BIOROB before and during my PhD, I had the luck of working with many scientific mentors who guided me toward what I am today. A great thanks to Prof. Amy Wu, Dr. Florin Dzeladini, Prof. Anne Koelewijn, and especially Dr. Dimitar Stanev who has been supportive in providing research guidance and suggestions even after leaving the Biorobotics Lab. A very special thank goes to all other BIOROB members who made these four and half years full of laughs and fun. From the first period, thanks to Tomislav, Peter, Salman, Hamed, Behzad, and especially Simon and Mehemet for the many magic raclette nights and boardgames crepe mornings! A warm thanks to the friends that mostly shared this PhD adventure with me. Thanks to Shravan, Jon, Laura and Kamilo for the uncountable funny moments and trips we did together. Many thanks to Luca, Iselin, Matt, Xiangxiao, and Mohsen for many great moments as well. Big thanks to new generations of BIOROB members Alice, Gizem, Ozge, Astha, Alessandro (Alex), Alexandros, Andrea, Milad, Guillaume, Anastasia,

Abstract

Locomotion is based on a sophisticated interaction among the environment, the musculoskeletal system, the spinal cord, and the brain locomotor areas. Quality of life is strongly related to the proper capability of this movement. However, many pathologies, like cerebral palsy (CP), lead to motor impairments that limit locomotor capabilities. The proper treatment choice depends on the relationship between biomechanical or neural impairments and the observed gait deviations. Predictive neuromuscular simulations can be powerful tools for testing how specific impairments influence gait deviations and the roles of different neural structures in controlling locomotion. This thesis has two main objectives to pursue using neuromuscular simulations: (1) investigating the roles of spinal reflexes and central pattern generator (CPG) circuits in the control and modulation of healthy human locomotion, (2) investigating the gait deviations associated with biomechanical and neural impairments commonly observed in CP patients and evaluating the effects of muscle-tendon surgeries. First, we perform these investigations using purely reflex-based controllers guided by finite state-machines adapted from previous studies. Our results suggest that reflex gains and thresholds of hip muscles and ankle plantarflexors can be modulated by the descending mechanisms to achieve different gait behaviors in healthy human locomotion. Furthermore, pathological behaviors like heel and toe walking can be related to both biomechanical and neural impairments. More specifically, contracture or hyperreflexia applied to plantarfleor can reproduce toe walking, whereas partial heel walking was achieved through plantarflexor biomechanical or neural weaknesses. Then, we developed a new neuromuscular controller composed of a CPG network with five locomotor synergies and a more sophisticated reflex network built using leaky integrator neurons without relying on a finite state-machine. This controller is used to explore the two investigation objectives of this thesis. A vast range of walking speeds can be reproduced with this model, and results suggested that CPGs could be an important component in generating rhythmic locomotion by preventing or enabling reflexes to affect gait in specific gait cycle phases. Furthermore, CPG's frequency seems to be crucial in modulating step duration. Concerning gait pathologies, we use the newly developed controller to investigate the effect of biomechanical contractures and neural spasticity affecting the hamstring muscle in generating crouch gait behaviors. Results suggest that crouch gait could be generated with moderate or severe levels of contracture and spasticity or a combination of these. Then, we simulate the benefit of different levels of hamstring lengthening surgery

for several combinations of biomechanical and neural impairments. Results suggest that a moderate level of surgery could improve gait deviations related to muscle contractures by decreasing the amount of passive force generated. The surgery appears much less effective when the gait deviation is primarily due to neural spasticity. Furthermore, severe surgeries may result in problems in generating meaningful tension in the hamstring muscle-tendon unit. Our work shows the great potentialities of predictive neuromuscular simulations in investigating open questions in motor control, the emergence of pathological behaviors, and the possible effects of clinical treatments.

Résumé

La locomotion est basée sur des interactions sophistiquées entre l'environnement, le système musculo-squelettique, la moelle épinière et les zones locomotrices du cerveau. La qualité de vie est étroitement liée à la capacité de ce mouvement. Cependant, de nombreuses pathologies, telle que la paralysie cérébrale (PC), entraînent des altérations biomécaniques et neurologiques qui limitent les capacités locomotrices. Le bon choix de traitement dépend du rapport entre toute altération biomécanique ou neurologique et les déviations observées lors de la marche du patient. Les simulations neuromusculaires prédictives peuvent être de puissants outils pour tester comment les altérations spécifiques affectent les déviations de la marche et les rôles des différentes structures neurales dans le contrôle de la locomotion. Cette thèse a deux objectifs principaux à poursuivre en utilisant des simulations neuromusculaires : (1) étudier les rôles des réflexes spinaux et des circuits du réseau locomoteur spinal (CPG) dans le contrôle et la modulation de la locomotion humaine saine, (2) étudier les déviations de la marche associées à des altérations biomécaniques et neurologiques communément observées chez les patients PC et évaluer les effets des interventions chirurgicales orthopédiques. Tout d'abord, nous effectuons ces études en utilisant des contrôleurs basés exclusivement sur le mécanisme de réflexes spinaux ajustés en fonction des états précis de la marche et basés sur des contrôleurs provenant d'études antérieures. Nos résultats suggèrent que les gains et les seuils d'activation des réflexes des muscles de la hanche et du mollet pourraient être modulés par les mécanismes descendants pour obtenir différents types de marche dans la locomotion humaine saine. En outre, des comportements pathologiques tels que la marche sur la pointe des pieds ou sur le talon peuvent être liés à des troubles biomécaniques et neurologiques. Plus précisément, la contracture ou l'hyperréflexie appliquée aux muscles du mollet peut reproduire la marche sur la pointe des pieds, tandis que la marche sur le talon peut être reproduite avec une faiblesse biomécanique ou neurologique aux muscles du mollet. Plus tard, nous avons développé un nouveau contrôleur neuromusculaire composé de CPG avec cinq synergies locomotrices et un réseau de réflexes plus sophistiqué construit à l'aide de modèles de neurones indépendants des phases de marche. Ce contrôleur est utilisé pour explorer les deux objectifs de cette thèse. Un large éventail de vitesses de marche peut être reproduit avec ce modèle, et les résultats ont suggéré que les CPG pourraient être un composant important en créant la locomotion rythmique en empêchant ou en permettant à des réflexes d'influencer la marche dans étapes de la marche. De plus, la fréquence des CPG semble être cruciale dans la

modulation de la durée du pas. En ce qui concerne la marche pathologique, nous avons utilisé le contrôleur nouvellement conçu pour étudier l'effet des contractures biomécaniques et de la spasticité nerveuse qui affectent le biceps fémoral dans la génération de la marche à genoux fléchie. Les résultats suggèrent qu'une telle démarche pourrait être générée avec des niveaux modérés ou graves de contracture et de spasticité ou une combinaison de ceux-ci. Ainsi, nous avons simulé l'avantage de différents niveaux de chirurgie d'étirement du biceps fémoral pour différentes combinaisons d'altérations biomécaniques et neurologiques. Les résultats suggèrent qu'un niveau modéré de chirurgie pourrait améliorer les déviations de marche liées aux contractures musculaires en diminuant la quantité de force passive générée. L'intervention apparaît beaucoup moins efficace lorsque la déviation de la marche est principalement due à la spasticité. En outre, les interventions chirurgicales extrêmes peuvent causer des problèmes pour générer une tension importante dans le biceps fémoral. Notre travail montre le grand potentiel des simulations prédictives neuromusculaires dans l'étude des questions en suspens sur le contrôle moteur, l'émergence de comportements pathologiques et les effets possibles des traitements cliniques.

Mots clefs : locomotion humaine, paralysie cérébrale, modulation, spasticité, contracture musculaire, faiblesse musculaire, interventions chirurgicales musculaires, simulations, modélisation

Sommario

La locomozione si basa su sofisticate interazioni tra l'ambiente, il sistema muscolo-scheletrico, il midollo spinale e le aree locomotrici del cervello. La qualità della vita è strettamente legata alla capacità di questo movimento. Tuttavia, molte patologie, come la paralisi cerebrale (PC), portano ad alterazioni biomeccaniche e neurologiche che limitano le capacità locomotorie. La scelta corretta del trattamento dipende dal rapporto tra ogni alterazione biomeccanica o neurologica e le deviazioni osservate nella camminata del paziente. Le simulazioni neuromuscolari predittive possono essere potenti strumenti per testare come le specifiche alteraioni influenzino le deviazioni della camminata e i ruoli delle diverse strutture neurali nel controllo della locomozione. Questa tesi ha due obiettivi principali da perseguire utilizzando simulazioni neuromuscolari: (1) studiare i ruoli dei riflessi spinali e dei circuiti dei generatori centrali di schema (CPG) nel controllo e nella modulazione della locomozione umana sana, (2) studiare le deviazioni della camminata associate ad alterazioni biomeccaniche e neurologiche comunemente osservati nei pazienti con PC e valutare gli effetti di interventi chirurgici ortopedici. In primo luogo, eseguiamo queste indagini usando controllori basati esclusivamente sul meccanismo di riflessi spinali regolati in base alle precise fasi della camminata e basati su controllori proposti da studi precedenti. I nostri risultati suggeriscono che i guadagni e le soglie di attivazione dei riflessi dei muscoli dell'anca e del polpaccio potrebbero essere modulati dai meccanismi discendenti per ottenere diversi tipi di camminata nella locomozione umana sana. Inoltre, comportamenti patologici come la deambulazione in punta di piedi o su tallone potrebbero essere correlati a disturbi biomeccanici e neurologici. Più specificamente, la contrattura o l'iperriflessia applicata ai muscoli del polpaccio possono riprodurre la camminata in punta di piedi, mentre la camminata su tallone può essere riprodotta con debolezza biomeccanica o neurologica ai muscoli del polpaccio. Successivamente, abbiamo sviluppato un nuovo controllore neuromuscolare composto da CPG con cinque sinergie locomotrici e una rete di riflessi più sofisticata costruita utilizzando modelli di neuroni senza fare affidamento sugli stati della camminata. Questo controllore viene utilizzato per esplorare i due obiettivi di questa tesi. Una vasta gamma di velocità di deambulazione può essere riprodotta con questo modello ed i risultati hanno suggerito che i CPG potrebbero essere una componente importante nella generazione della locomozione ritmica impedendo o permettendo che i riflessi influenzino la camminata nelle fasi della deambulazione. Inoltre, la frequenza dei CPG sembra essere cruciale nella modulazione della durata del passo. Per quanto riguarda la

camminata patologica, abbiamo utilizzato il controllore di nuova concezione per indagare l'effetto delle contratture biomeccaniche e della spasticità neurale che influenzano il bicipite femorale nel generare la deambulazione a ginocchio flesso. I risultati suggeriscono che tale andatura potrebbe essere generata con livelli moderati o gravi di contrattura e spasticità o una combinazione di queste. Quindi, abbiamo simulato il beneficio di diversi livelli di chirurgia di allungamento del bicipite femorale per diverse combinazioni di disturbi biomeccanici e neurologici. I risultati suggeriscono che un livello moderato di chirurgia potrebbe migliorare le deviazioni di camminata relative alle contratture muscolari diminuendo la quantità di forza passiva generata. L'intervento appare molto meno efficace quando la deviazione della camminata è dovuta principalmente alla spasticità. Inoltre, interventi chirurgici estremi possono causare problemi nel generare una tensione significativa nel bicipite femorale. Il nostro lavoro mostra le grandi potenzialità delle simulazioni predittive neuromuscolari nell'indagare le questioni aperte sul controllo motorio, l'emergere di comportamenti patologici e i possibili effetti dei trattamenti clinici.

Parole chiave: locomozione umana, paralisi cerebrale, modulazione, spasticità, contrattura muscolare, debolezza muscolare, interventi chirurgici muscolari, simulazioni, modellazione

Contents

List of Figures

List of Tables

1 Introduction

Locomotion is defined as the ability to move from one place to another and relies on a sophisticated interaction among high brain centers, spinal circuits, body biomechanics, and the external environment. This movement has always been a key feature in the evolution of mammals and lower vertebrates, and also in humans, walking is often considered the most important activity in daily living (Chiou and Burnett, 1985). The ability to move without pain, fatigue, or gait deviations is closely related to the quality of life (Cuomo et al., 2007; van Schie, 2008). However, many pathologies lead to abnormal conditions that limit locomotor capabilities, consistently influencing the life quality of people affected by these pathologies. Therefore, preserving or restoring a normal walking behavior with the minimum amount of deviations is the main objective of clinical treatments. The optimal choice of these treatments relies on the understanding of gait deviation mechanisms and the effect that each impairment has on walking behavior.

Among the many pathologies causing gait deviations, cerebral palsy (CP) is the most frequent cause of motor impairments in children in Europe, with a prevalence of 1.77 cases for 1000 births (Sellier et al., 2016). Brain injury happening during early development affects the maturation of both the neural and musculoskeletal systems abnormally (Cappellini et al., 2020; Graham and Selber, 2003). Therefore, the understanding of gait deviations in CP patients presents numerous challenges, given the high complexity of the human neuro-musculoskeletal system and the dynamic nature of walking. In order to optimize treatment strategies, it is necessary to establish the relationship between each biomechanical and neural impairment and the emerging gait deviations. However, this relationship is rarely elucidated (Boudarham et al., 2014). Currently, instrumented gait analysis is generally the most used tool affecting clinical decision-making (Armand et al., 2016; Davids et al., 2003; Gough and Shortland, 2008; States et al., 2021; Wren et al., 2011). Yet, the measurement of joint kinematics, kinetics, and muscular electrical activity may provide an objective record that quantifies the magnitude of deviations between pathological and normal gait(Baker, 2006), but it is difficult to derivate the effect of each impairment. In addition to instrumented gait analysis, complex locomotor characteristics of patients with gait deviations are assessed through clinical testing.

This testing is composed of assessments that evaluate the functionality of neuromuscular and musculoskeletal structures. These assessments permit the identification and characterization of the impairments. However, their reliability is limited, and it is difficult to define the different impairments quantitatively (Biering-Sørensen et al., 2006).

Although not yet widely used in clinics, computer simulations able to perform "what-if" scenarios and estimate the contribution of each control component by evaluating different models and parameters could be a resourceful tool both to investigate the neuromechanical control principles of healthy locomotion and to isolate the effect of each impairment in simulations. Over the years, the BioRobotics laboratory has been investigating aquatic, quadruped, and human locomotion, both using mathematical models and robotic platforms. This thesis aims at using computer simulations to have possible insights about the spinal components controlling the modulation of healthy human locomotion and for the investigation of motor impairments observed in CP and their effects on gait deviations.

Before we move to the specific studies, let me first briefly introduce the main motor impairments in CP and the state of the arts in computational models for human locomotion.

1.1   Motor impairments in CP

Cerebral palsy is a broad term that defines the clinical conditions linked to a brain lesion that happened during early development (Sankar and Mundkur, 2005). The motor disorders associated with this pathology depend on the brain areas affected by the lesion. Figure 1.1 shows the motor impairments emerging from different brain injuries commonly observed in CP. Spasticity, generally defined as a form of hypertonia due to hyperexcitable tonic stretch reflexes (Sheean, 2002), is linked to injuries to the motor cortex. Damages involving one side of the motor cortex (left or right) will generate motor impairments to the controlateral bodyside leading to hemiplegic conditions, whereas damages involving both sides of the motor cortex lead to diplegic (all the lower part of the body is affected) or quadriplegic conditions (lower and upper body are affected) depending on the extension of the region involved (Azar et al., 2020). This thesis mainly targets spastic diplegic gaits with symmetric behaviors in gait deviations.

Concerning motor cortex lesions, the primary impairments are paresis, soft tissue contractures, and spasticity (Gracies, 2005a, 2005b).

- Paresis is the direct consequence of a central nervous system lesion (Gracies, 2005a, 2005b), leading to muscular activation failure and muscle weakness.

- Spasticity is defined as a muscle overactivity due to a velocity-dependent increase in the tonic stretch reflexes with exaggerated tendon jerks resulting from hyperexcitability to the stretch reflex because of lack of inhibitory inputs from pre-synaptic and reciprocal inhibition (Gracies, 2005b; Lance, 1980a).

- Soft tissue contractures are defined as the inability of a joint to move through its full
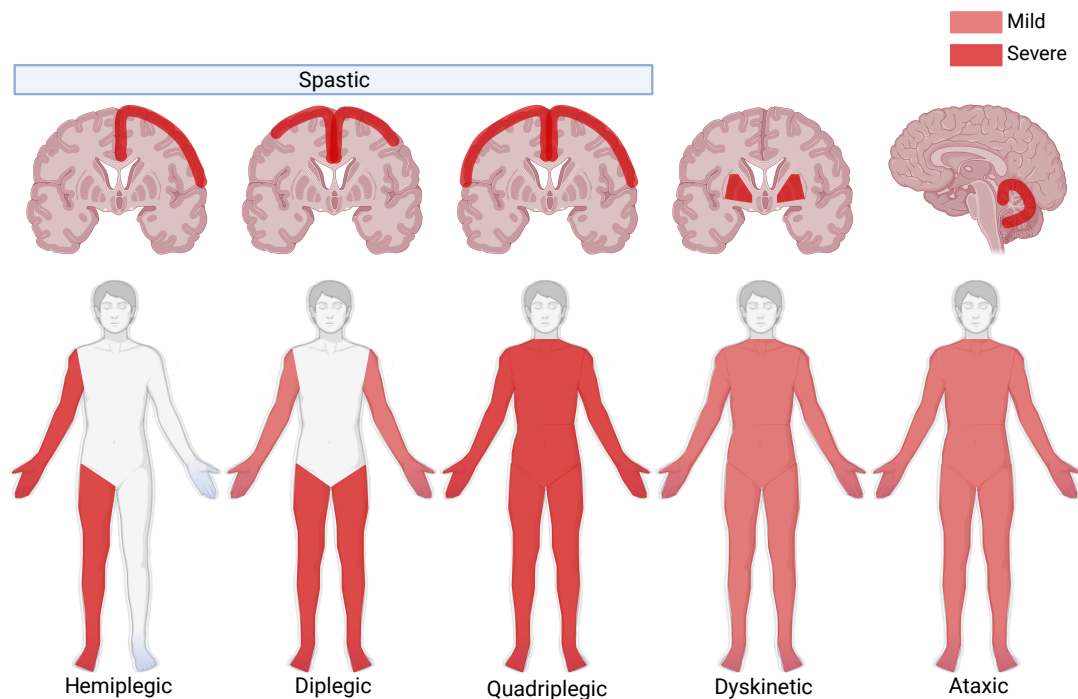
Figure 1.1: Brain injuries in cerebral palsy - adapted from Azar et al. (2020) (Created with BioRender.com)
Spastic conditions result from damage to the motor cortex. Depending on the portion of the motor cortex involved, patients may present hemiplegic, diplegic, or quadriplegic behavior. Damages to the basal ganglia or cerebellum result in dyskinetic and ataxic movements, respectively. Dyskinesia is a movement disorder in which involuntary sustained or intermittent muscle contractions cause twisting and repetitive movements, whereas ataxia is characterized by an impairment of the coordination of goal-directed movements, resulting in gait and trunk disturbances (Eggink et al., 2017). The red color highlights the brain areas affected and the corresponding effects on body parts.

range of motion and an excessive resistance during passive mobilization of this joint (Gaudreault et al., 2009). Over time, spasticity causes a relative shortening of the musculotendinous unit because the skeleton grows at a faster pace than the musculotendinous unit can lengthen, leading to abnormal joint motion (Azar et al., 2020). Therefore, soft tissue contractures are characterized by a decreased number of sarcomeres in series in the muscle fiber and increased stiffness due to increased collagen in the extracellular matrix (Dayanidhi and Lieber, 2018; L. R. Smith et al., 2011).

Because of the difficulty in characterizing and assessing precisely the mechanism of spasticity, there was a lack of consensus around its definition (Malhotra et al., 2009). A European consensus proposed to use the term hyper-resistance to describe the phenomenon of impaired neuromuscular response during passive stretch instead of spasticity or hypertonia (van den Noort et al., 2017). They conclude that it is essential for therapeutic strategies to distinguish the non-neural component (soft tissue contractures) from the neural component (involuntary activation of muscles) of the hyper-resistance. For simplicity, this document uses the term

"spasticity" for the neural component that comes from muscle overactivity due to exaggerated proprioceptive feedback from the spindles.

In addition to these three motor impairments, reduced selective motor control is considered an important impairment in CP, and it is defined as the inability to isolate the activation of muscles in a selected pattern in response to demands of a voluntary movement or posture (Sanger et al., 2006). This thesis studies mainly the modeling of weakness, soft tissue contractures, and spasticity.

1.2 Common treatments for CP patients

The treatments to improve the pathological conditions of CP patients differ among nonoperative treatments, orthopedic surgeries, and neuro-surgeries (Azar et al., 2020).

1.2.1 Nonoperative treatments

Nonoperative modalities, such as medication, splinting and bracing, and physical therapy, are commonly used as primary treatment to treat neural spasticity or in conjunction with surgeries (Azar et al., 2020). Some medication agents like diazepam and baclofen act centrally, increasing inhibitory neurotransmitter activity (Azar et al., 2020). Others, like dantrolene, act at the level of skeletal muscle, decreasing muscle calcium ion release and abnormal muscle stretch reflexes and tone. Alternative drug delivery systems are intrathecal baclofen, and intramuscular botulinum toxin (a potent neurotoxin used to weaken muscles) injections, decreasing the dose required to affect spasticity and some of the side effects like sedation (Azar et al., 2020). Physical therapy is an essential component in treating CP patients and is used as a primary treatment modality and in conjunction with other modalities, such as casting, bracing, BTX-A, and surgery (Azar et al., 2020). Bracing in patients with cerebral palsy is most commonly used to prevent or slow the deformity's progression. The most commonly used braces are ankle-foot orthoses, hip abduction braces, and spinal braces or jackets (Azar et al., 2020).

1.2.2 Operative treatments

Operative treatments can be divided into neuro and orthopedic surgeries.

Neurosurgeries

The most common neurosurgery performed in CP patients is selective dorsal root rhizotomy, a technique to reduce spasticity and balance muscle tone. This treatment is performed by identifying the rootlets from the muscle spindle carrying excessive stimulatory information and sectioning them to reduce the stimulatory input from the dorsal sensory fibers. This

procedure requires extensive physical therapy postoperatively since patients have a significant weakness in the early postoperative period (Azar et al., 2020).

Orthopedic surgeries

Operative treatment is typically indicated when contractures or deformities decrease function, cause pain, or interfere with activities of daily living (Azar et al., 2020). These treatments include procedures to correct static or dynamic deformity, balance muscle power across a joint, reduce spasticity, and stabilize uncontrollable joints. Often, procedures can be combined (Azar et al., 2020). Severe or rigid deformities usually require osteotomies or capsulotomies, whereas flexible static and dynamic deformities are typically corrected with a muscle-tendon lengthening procedure using a recession or release of the muscular aponeurosis at the musculotendinous junction, or a complete tenotomy depending on the circumstances. Operative lengthening of the musculotendinous unit causes a weakening of the muscle with the restoration of more normal forces and motion across the joint (Azar et al., 2020).

In this thesis, we will model the effect of muscle-tendon lengthening in alleviating the gait deviations observed in CP patients.

1.3   Computer simulations

Several frameworks have been promoted in the literature to simulate human gait. The most common frameworks are inverse dynamics-based optimization and predictive forward dynamics-based optimization. The first one aims to compute joint torques from joint kinematics and ground reaction forces and moments and then solve the muscle redundancy problem by minimizing an objective function. The second one aims to compute joint kinematics and ground reaction forces and moments based on an initial muscular state. These controllers can either send pre-defined commands to muscles (open-loop) or have the muscle commands modulated by the muscles themselves (closed-loop) (Mansouri and Reinbolt, 2012). Both forward and inverse approaches rely on a model representing the biomechanics of the human musculoskeletal system (Delp et al., 1990). This model is generally actuated by Hill-type muscles composed of an active contractile element representing the muscle fibers, a passive element in parallel with the contractile element representing the connective tissue in the muscle matrix, and a passive element in series representing the tendon (Zajac, 1989). The passive or active force generated by these elements depends on the muscle activation, length, velocity, and strain (De Groote et al., 2016; Millard et al., 2013; Thelen, 2003). Inverse dynamics-based optimization is highly dependent on the experimental data quality used to input into the model (Riemer and Hsiao-Wecksler, 2008). Several other frameworks have been proposed to overcome this limitation, like optimal inverse dynamics (Farahani et al., 2011; Fluit et al., 2014; Rasmussen et al., 2000).

This thesis explores the capabilities of predictive forward dynamics-based optimization first

to investigate the control of healthy gait modulation in human walking and then to predict gait deviations in CP.

Over the past 20 years, the studies on simulations of human gaits have focused their investigation on the role of feedforward and feedback circuits in human locomotion (Gerasimenko et al., 2017). The role of feedforward spinal circuits generating rhythmic commands and called central pattern generators (CPGs) in controlling locomotion has been observed in mammals and lower vertebrates (Akay, 2020; Brown, 1911; Grillner, 1975; Kiehn, 2006; Whelan, 2010). However, there is only indirect evidence of these circuits in humans (Minassian et al., 2017). Several studies investigated the potential role of these circuits with computational models being able to reproduce human movements and flexibly modulate gait speed (Aoi et al., 2010; Dzeladini et al., 2014; Haghpanah et al., 2017; Matsuoka, 1985; Taga, 1995). On the other hand, sensory feedback also plays a significant role in controlling human locomotion (Edwards and Prilutsky, 2017; Sinkjær et al., 2000). To highlight this aspect, influential models based on feedback loops representing spinal reflexes could reproduce detailed aspects of human kinematics, dynamics, ground reaction forces, and muscle activation without relying on feedforward commands (Geyer and Herr, 2010; Ogihara and Yamazaki, 2001; Ong et al., 2019; Song and Geyer, 2013).

The aforementioned studies demonstrated that both feedback and feedforward controllers could reproduce human walking behaviors highlighting the complexity of the neuromusculoskeletal systems as highly redundant mechanisms (Allen and Ting, 2016; Stanev and Moustakas, 2019).

1.4 SimGait project

The studies reported in this thesis are part of the SimGait Sinergia project funded by the Swiss National Science Foundation (http://p3.snf.ch/project-177179). The main objective of this project is to combine different expertises to record and model gait deviations in CP patients. In particular, the Biorobotics laboratory collaborated with the Kinesiology laboratory at the University Hospital of Geneva, which performs instrumented gait analysis on patients with spastic cerebral palsy. The team comprises experts in clinical gait analysis and biomechanics and a clinician specialist in neuro-orthopedic pathologies in the pediatric population. The Kinesiology team continuously interacted with the Biorotics team providing instructions on key features of the cerebral palsy population and the characteristics of orthopedic interventions.

1.5 Thesis organization and main contributions

This thesis reports the contribution of the Biorobotics Laboratory to the SimGait project. The reported studies use the simulation framework SCONE (Geijtenbeek, 2019) to generate gait simulations. With these experiments, we aim to address the following research questions:

- RQ1: How can the modulation of spinal cord circuits like reflexes and CPGs produce different target behaviors in healthy human locomotion?

- RQ2: Can we identify the effects of specific biomechanical and neural impairments inducing pathological gait deviations and predict the effects of orthopedic treatments using neuromuscular models?

We start studying the capabilities of existing neuromuscular controllers relying on sensory-feedback commands governed by state-machine mechanisms to control healthy gait modulation and reproduce pathological gaits. For this purpose, we consider the models proposed by Geyer and Herr (2010) and Ong et al. (2019). Then, we propose a novel neuromuscular controller modeling spinal circuits more suitable to model spastic pathological behavior. We first explore the performances of this novel controller in modeling healthy human locomotion, and then we use this controller to reproduce spasticity in a generic musculoskeletal model. The thesis is organized into the following chapters:

- Chapter 1: The introduction chapter introduced the reader to the main motor impairments in CP and the current tools used in simulations of human locomotion.

- Chapter 2: The first study investigates the modulation of sensory reflexes in controlling gait speed, step length, and step duration using the neuromuscular controller proposed by Ong et al. (2019).

- Chapter 3: We started investigating the effects of neural and biomechanical impairments producing heel and toe walking in a generic musculoskeletal model extending the neuromuscular controller proposed by Geyer and Herr (2010).

- Chapter 4: We propose a novel neuromuscular controller composed of CPGs synergies generators and spinal reflexes implemented as neural networks rather than finite state-machines. We evaluate the controller's performances in speed modulation and investigate the role of CPGs and reflexes in generating different human gait behaviors.

- Chapter 5: We use the neuromuscular controller presented in the previous chapter to propose a novel model of spastic behavior and generate different levels of spasticity and contractures to the hamstring muscle to reproduce crouch and jump gaits commonly observed in CP. In addition, we model and evaluate the effects of hamstring lengthening in treating the impairments investigated.

- Chapter 6: The concluding chapter summarizes the main findings reporting the insights that the proposed study suggested as possible answers to the two main research questions previously described. Finally, the chapter concludes with the future directions that could be developed starting from this work.

Table 1.1 provides a schematic organization of the thesis chapters.

> **Main contributions:**
> - We identified the reflex gain parameters that could be modulated by the central nervous system to achieve different target behaviors in speed, step length, and step duration.
>
> - We modeled the effects of hyperreflexia, contractures, and neural and biomechanical weaknesses in plantarflexor muscles generating heel and toe walking behaviors.
>
> - We developed a novel neuromuscular controller composed of CPGs generating locomotor primitives and a detailed representation of spinal reflexes modeling afferents activities and reciprocal inhibition mechanism between agonists and antagonists muscles.
>
> - We explored the role of CPGs and spinal reflex circuits in controlling locomotor speed.
>
> - We proposed a model of spasticity using the developed neuromuscular controller.
>
> - We reproduced crouch and jump gait behaviors commonly observed in CP by applying the spastic model and a modelization of soft tissue contracture to the hamstring muscle.
>
> - We modeled the effect of tendon lengthening surgery and evaluated the reduced gait deviations in crouch and jump gaits.

	State-machine controllers	Spinal neuromuscular controller
Healthy gait modulation (RQ1)	Chapter 2	Chapter 4
Pathological gaits (RQ2)	Chapter 3	Chapter 5

Table 1.1: Chapters organizations.

Chapters 2 and 3 use already established neuromuscular controllers to investigate healthy gait modulation and pathological gaits, respectively, whereas chapters 4 and 5 investigate the same research questions with a newly developed neuromuscular controller.

2 Sensory modulation of gait characteristics in human locomotion: a neuromusculoskeletal modeling study

Overview

In this first study, we start investigating the capabilities of traditional state-machine controllers based on sensory feedback in reproducing gait modulation in human locomotion. It is well known that sensory feedback gains are modulated in a phase and task-dependent manner during locomotion. However, it is not yet well understood which gains the central nervous system modulates in order to achieve different gait behaviors. Here, we use neuromuscular models to investigate this aspect of human locomotor control.

My contributions:

- I conceptualized and conducted the study and the experiments to perform.

- I analyzed the data obtained from optimizations and interpreted the results.

- I wrote the original draft of the manuscript and updated it according to co-authors and reviewers' comments.

2.1 Abstract

The central nervous system of humans and other animals modulates spinal cord activity to achieve several locomotion behaviors. Previous neuromechanical models investigated the modulation of human gait, changing selected parameters belonging to CPGs (Central Pattern Generators) feedforward oscillatory structures or to feedback reflex circuits. CPG-based models could replicate slow and fast walking by changing only the oscillation's properties. On the other hand, reflex-based models could achieve different behaviors through optimizations of large dimensional parameter spaces. However, previous studies seldom tried to identify individual key reflex parameters responsible for gait characteristics' modulation. This study investigates which reflex parameters modulate gait characteristics through neuromechanical simulations. A recently developed reflex-based model is used to perform optimizations with different target behaviors on speed, step length, and step duration to analyze the correlation between reflex parameters and their influence on these gait characteristics. We identified nine key parameters that may affect the target speed ranging from slow to fast walking (0.48 and 1.71 m/s) as well as a large range of step lengths (0.43 and 0.88 m) and step duration (0.51, 0.98 s). The findings show that specific reflexes during stance significantly affect step length regulation, mainly given by positive force feedback of the ankle plantarflexors' group. On the other hand, stretch reflexes active during swing of iliopsoas and gluteus maximus regulate all the gait characteristics under analysis. Additionally, the results show that the hamstrings' group's stretch reflex during the landing phase is responsible for modulating the step length and step duration. Additional validation studies in simulations demonstrated that the modulation of identified reflexes is sufficient to regulate the investigated gait characteristics. Thus, this study provides an overview of possible reflexes involved in modulating speed, step length, and step duration of human gaits.

2.2 Introduction

The interactions between the nervous system and the musculoskeletal system allow humans and other animals to move and interact in their environment, choosing among different motor patterns through a complex and redundant interaction of neural circuits. However, the strategies used to control the different gait patterns have not been elucidated yet. It is well-known that the central nervous system controls locomotion in a hierarchical and distributed way by modulating the activity of its control subsystems such as spinal reflexes and central pattern generators (CPGs) (Kiehn, 2006, 2016). These networks are modulated by descending cortical and brainstem pathways and sensory feedback to regulate the motor outputs for the required motion (Bouvier et al., 2015; Büschges, 2017; Garcia-Rill and Skinner, 1987; Hägglund et al., 2010; Matsuyama et al., 2004). It is also well-established that the modulation of sensory feedback relies on the control of reflex responses through reciprocal and presynaptic inhibition (Mutha, 2017; Prochazka, 1989, 2010). In mammals and lower vertebrates, stereotyped movements are executed with low sensorimotor gains, whereas locomotion relies on higher feedback gains during demanding tasks or unfamiliar conditions (Prochazka, 2010).

These observations led to the conclusion that the central nervous system modulates sensory transmission by adjusting reflex gains to develop adaptive responses to the environment. In addition to gains, specific reflexes such as the stretch response can also be modulated through changes in their activation threshold (Mutha, 2017). These reflex features are cyclically regulated in stereotyped rhythmic activities like locomotion (Prochazka, 1989) and are subject to task-dependent modulation (Mutha, 2017). Furthermore, feedback pathways might be more important than central circuits in controlling human biped locomotion. In fact, experiments on subjects with lost limb proprioception demonstrated that the amount of motor control delegated to sensory feedback is more prominent in humans compared to other mammals, and lower vertebrates (Giuliani and Smith, 1987; Goldberger, 1977; Grillner, 1975; Guertin, 2009; Lajoie et al., 1996). However, it is not yet fully understood which of the mentioned reflex's features are tuned nor at what time during the gait cycle in order to modulate human locomotion.

Neuromusculoskeletal simulations are powerful tools to test hypotheses in neuroscience. In particular, past studies used these tools to investigate the interaction between biomechanical properties, sensory inputs, and spinal circuits (Falisse et al., 2019; Ijspeert, 2008; Prochazka et al., 2017). Several proposed models aimed to reproduce the healthy behavior of human locomotion and its modulation. Many studies explored the modulation of feedforward CPGs circuits able to generate changes in gait speed (Aoi et al., 2010; Aoi et al., 2019; Dzeladini et al., 2014; Haghpanah et al., 2017; Matsuoka, 1985; Taga, 1995; Van der Noot et al., 2015; Van der Noot et al., 2018), demonstrating how the modulation of selected feedforward components in the spinal cord can reproduce a wide range of walking behaviors. However, these models do not consider the potential effect of reflex circuits' modulation in changing gait characteristics.

On the other hand, other studies highlighted the contribution of sensory feedback to motor control. Ogihara and Yamazaki (2001) gave one of the first contributions in this direction with a neural controller composed of motoneurons receiving inputs from a common CPG and reflexes from stretch and force receptors. Additionally, in that model, the spindle reflexes included inhibitory inputs to antagonist muscles, and the parameters were optimized using genetic algorithm optimization. Subsequently, Geyer and Herr (2010) developed a purely reflex-based neuromechanical model reproducing kinematics, dynamics, and muscle activation of human walking behavior without the contribution of any CPG circuit. The modulation of speed for this model was explored by Song and Geyer (2012). Performing different optimizations for six different speeds ranging from 0.8 to 1.8 m/s, they identified nine key reflex control parameters that show a significant trend and increase speed. Three key parameters were related to trunk balance, three to stance behavior, and three to swing generation. The model could generate speed transitions from slow to fast speed, optimizing the identified parameters. However, these key parameters did not include only reflex mechanisms but also balance and prevention of overextension parameters that were simplified in a way that could hardly be related to specific physiological proprioceptive information. Subsequently, the same authors added supraspinal layers on top of a generalized reflex model in the three-dimensional space (Song and Geyer, 2013) able to reproduce walking and running behaviors (Song and

Geyer, 2015). These behaviors were achieved by optimizing stance reflex parameters and the modulation of two supraspinal parameters: desired foot placements and the desired minimum swing leg length. Therefore, gait modulation relied on integrating these descending pathways without identifying and selecting the feedback circuits contributing to this modulation.

More recently, Ong et al. (2019) developed a detailed reflex-based controller modeling each control component based on the physiology of proprioception, with mechanisms for trunk balance and gait phase switching being the only non-physiological components. The model is designed to walk in sagittal plane, and it is optimized for different target speeds between 0.50 m/s and 2.00 m/s, reproducing kinematic, kinetic, and metabolic trends observed in human walking experiments (Schwartz et al., 2008). This present study will use the model proposed by Ong et al. in order to identify the reflexes taking part in the modulation of speed, step length, and step duration.

The aforementioned studies demonstrated that both feedback and feedforward controllers could faithfully reproduce various walking behaviors highlighting the complexity of the neural and musculoskeletal systems as highly redundant mechanisms (Allen and Ting, 2016; Stanev and Moustakas, 2019). CPG-based models partially uncovered the contribution of spinal feedforward oscillatory mechanisms generating diverse walking behaviors with CPGs parameters' modulation. However, previous reflex-based models could not identify physiologically relevant reflex parameters responsible for gait modulation. Furthermore, previous studies in neuromechanical simulations focused mainly on achieving different target speeds rather than separating the components controlling step length and step duration. Lim et al. (2017) investigated the relations between these gait characteristics in an experimental study where subjects walked with combinations of small, nominal, and large step lengths (i.e., 0.584, 0.730, and 0.876 m) and short, nominal, and long step durations (i.e., 0.43, 0.52, and 0.65 s). The resulting range of speeds was between 0.89 and 2.04 m/s. The study showed that the activity of gluteus maximus, gluteus medius, vastus, gastrocnemius, and soleus are dedicated to vertical support and forward progression independent of changes made to either step length or step duration. In addition, increased step length results majorly from the larger contribution of hip and knee extensors. This study aims to understand the potential mechanisms of task-dependent reflex modulation behind various behaviors of human locomotion. In particular, we aim to answer the following questions:

1. To what extent can the modulation of reflexes modify speed, step length, and step duration during walking?

2. Can these quantities be controlled independently?

3. Which specific reflexes should be modulated to adjust each quantity?

It is undoubtedly true that other mechanisms, such as modulation of CPGs, muscle synergies, vestibular, visual, and cerebellar circuits also play an essential role in modulating

locomotion. However, the present goal is to focus on the potential role of reflex modulation in gait adaptation and to analyze to what extent reflex modulations alone could explain the modulation of some gait characteristics. More specifically, we aim to understand the effect of the task-dependent modulation of the reflex circuits rather than the neural mechanism that performs this modulation since this would require the modeling of much more complex supraspinal neural networks. Therefore, in the implemented neuromechanical simulations, the spinal feedback mechanisms are isolated from human walking's other neural components. Other neural circuits essential for locomotion, such as the vestibular feedback and the cyclic activation of spinal reflexes, are simplified to engineered components like a state machine and proportional derivative controls. The primary focus of this study is dedicated to the modulation of speed together with the independent modulation of step length and step duration. Three different sets of optimizations having various target speeds, step lengths, and step durations are performed. The results suggest that the reflex-based model can generate different gait behaviors, including low and high speed, step length, and step duration. Furthermore, walking patterns ranging among small and large step lengths could be achieved by maintaining the step duration fixed and vice versa. Finally, all these behaviors can be controlled with the modulation of nine identified reflex parameters that showed the highest correlation with the changing of gait characteristics.

2.3   Materials and methods

The analysis performed in this study is conducted using the optimization and control framework SCONE (Geijtenbeek, 2019). The musculoskeletal model and the reflex controller are based on the ones used by Ong et al. (2019) and are described in more detail in the following sections. We present the musculoskeletal model, the reflex controller, the optimization protocol, the description of the dataset analysis, and the validation steps.

2.3.1   Musculoskeletal model

The musculoskeletal model (Figure 2.1) is based on the one developed by Delp et al. (1990), which is composed of a skeleton of height = 1.8 m and weight = 75.16 kg. The model movement is constrained in the sagittal plane and has nine DoFs in total: a 3-DoFs planar joint between the pelvis and the ground and other 3 for each leg, one at the hip, one at the knee, and one at the ankle. Three spheres are also included as contact model to estimate the ground reaction forces when they touch the ground. The contact model is taken from Sherman and Delp (2011) and is composed of one bigger sphere of radius equal to 5 cm at the anatomical reference of calcaneus and two smaller of radius 2.5 cm at the anatomical reference of toes. The model is also composed of nine Hill-type muscle-tendon units (Millard et al., 2013) per leg: gluteus maximus (GMAX), biarticular hamstrings (HAMS), iliopsoas (ILPSO), rectus femoris (RF), vasti (VAS), biceps femoris short head (BFSH), gastrocnemius (GAS), soleus (SOL), and tibialis anterior (TA).
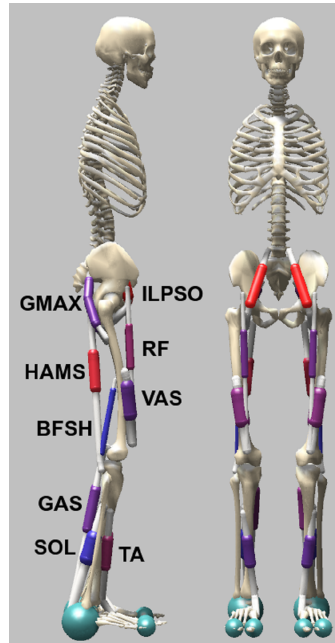
Figure 2.1: Musculoskeletal model used to study human locomotion.
The model is constrained in the sagittal plane and has 9 DoFs: hip and knee flexion/extension, ankle plantar/dorsal flexion for each leg, and a 3-DoFs planar joint between the pelvis and the ground. The movements are generated by the activation of 9 muscles per leg: gluteus maximus (GMAX), biarticular hamstrings (HAMS), iliopsoas (ILPSO), rectus femoris (RF), vasti (VAS), biceps femoris short head (BFSH), gastrocnemius medialis (GAS), soleus (SOL), and tibialis anterior (TA).

2.3.2 Reflex controller

In the reflex controller proposed by Ong et al. (2019) that we reused in the present study, the type of stimulation provided to each muscle depends on the phases of the gait cycle. The gait cycle is divided into five different gait subphases, three for the stance phase and two for the swing: early stance (ES), mid-stance (MS), pre-swing (PS), swing (S), and landing preparation (LP). Taking as reference the division of the gait cycle defined in clinical gait analysis (Baker and Hart, 2013), it is possible to classify the division in subphases proposed by Ong et al. (2019) as follows:

- early stance (ES): first double support and early stance in single support

- mid-stance (MS): mid and late stance in single support

- pre-swing (PS): second double support

- swing (S): early and middle swing

- landing preparation (LP): late swing

The controller is based on three different kinds of feedback: positive force feedback from the Golgi tendon organs, length and velocity feedback based on the muscle spindles' stretch reflex.

Furthermore, Proportional Derivative (PD) controllers regulating the trunk's forward-lean angle are integrated in the hip muscles' stimulation to help maintain balance. A constant feedforward stimulation only dependent on the state of the gait cycle is also integrated. The types of stimulation provided to muscles are mathematically described in the equations below:

Feedforward stimulation:

$$u_C = k_C \tag{2.1}$$

Length feedback:

$$u_L = k_L \cdot max(0, (\tilde{l}(t - t_D) - l_0)) \tag{2.2}$$

Velocity feedback:

$$u_V = k_V \cdot max(0, \tilde{v}(t - t_D)) \tag{2.3}$$

Force feedback:

$$u_f = k_f \cdot \tilde{f}(t - t_D) \tag{2.4}$$

PD balance controller:

$$u_{PD} = k_p(\theta(t - t_D) - \theta_0) + k_v\dot{\theta}(t - t_D) \tag{2.5}$$

where k_C is a constant, k_L, k_V and k_F are the gains of the reflex controller, l_0 is the length offset of the stretch response. This offset defines the threshold value of the muscle length, after which the length feedback stimulates the muscle itself. Concerning the stimulation given by the PD balance controller, k_p and k_v are the proportional and derivative controller's gains, and θ_0 is the desired forward lean angle regulating the proportional feedback of the actual forward lean angle θ. On the other hand, t_D represents the parameter for the time delay, and it depends on the muscle proximity to the vertebral column: $t_D = 5ms$ for the hip, $t_D = 10ms$ for the knee, and $t_D = 20ms$ for the ankle. The variables used in the controller (muscle length l, contraction velocity v, and force generated f) are taken normalized according to specific muscle parameters: optimal length (l_{opt}) and maximum isometric force (f_{max}).

$$\tilde{l} = \frac{l}{l_{opt}}, \quad \tilde{v} = \frac{v}{l_{opt}}, \quad \tilde{f} = \frac{f}{f_{max}} \tag{2.6}$$

Finally, a state controller regulating threshold parameters that define the switching between one sub-phase of gait and another is also integrated. In this context, muscle activation is linked to the stimulation given by the controller through first-order dynamics:

$$\frac{da}{dt} = \frac{u - a}{\tau} \tag{2.7}$$

where a represents the muscle activation, u the muscle stimulation, and τ the dynamic time constant equal to 0.01 s. Furthermore, from the equations above, the stimulation provided to the muscle depends on the model's state (muscle force, muscle length, or forward-leaning of the trunk) and independent parameters represented by the constant feedforward stimulation k_C, the reflex gains k_L, k_V and k_F, the length offset of the stretch reflex l_0 and the parameters of the PD controller k_p, k_v and θ_0. These parameters are the ones optimized to evaluate the ability of reflexes to modulate human gait. For this reason, the parameters under study are only the reflex gains, and offsets since the other feedback mechanisms, such as the PD balance controller, are necessary to stabilize the gait but do not rely on physiological evidence.

In the next sections of this study, the reflex parameters are indicated with the following notation:

$$KX^{subphases}_{muscle} \text{ for the reflex gains}$$
$$L0^{subphases}_{muscle} \text{ for the length offsets}$$

where X represents the type of feedback (either L (length), V (velocity) or F (force)) $subphases$ specify in which subphase of the gait cycle the reflex referred by the parameter is active (either ES, MS, PS, S, LP), and $muscle$ represents the specific muscle targeted by the reflex (either ILPSO, GMAX, RF, HAMS, VAS, BFSH, GAS, SOL or TA). The parameters presented in the Results section are also included in the list of abbreviations.

2.3.3 Optimization

The Covariance Matrix Adaptation Evolutionary Strategy (CMA-ES) method is used to optimize the parameters and obtain the different walking behaviors. The optimization parameters are the maximum number of generations equal to 1500, the samples per iteration $\lambda = 16$, and the step size $\sigma = 1$.

The cost function used is divided in seven different components:

- A penalty preventing the falling condition: the termination height parameter is used to detect if the model has fallen. This parameter is defined as the ratio between the center of mass (COM) height to the initial state. The simulation is terminated in advance when $\frac{COM\_height}{initial\_COM\_height} < th = 0.8$ (termination-height). The amount of this penalty is defined by equation 2.8.

$$p_{stability} = w_{stability} \cdot \left(\frac{time_{max} - time_{sim}}{time_{max}} \right) \tag{2.8}$$

  where $time_{max}$ represents the maximum simulation's duration set to 15 seconds, $time_{sim}$ is the time after which the simulation is terminated ($time_{max} = time_{sim}$ if the model does not fall), and $w_{stability}$ is the weight assigned.

- A penalty minimizing the difference between the target speed and the model's actual speed:

$$p_{speed} = w_{speed} \cdot |speed_{model} - speed_{target}| \qquad (2.9)$$

where $speed_{model}$ represents the actual average speed recorded in the simulation, $speed_{target}$ represents the desired speed to optimize, and w_{speed} the weight assigned.

- A penalty minimizing the difference between the target step length and the model's actual step length:

$$p_{sl} = w_{sl} \cdot |sl_{model} - sl_{target}| \qquad (2.10)$$

where sl_{model} is the average step length recorded in simulation, sl_{target} is the desired step length and w_{sl} is the assigned weight.

- A penalty minimizing the difference between the target step duration and the model's actual step duration:

$$p_{sd} = w_{sd} \cdot |sd_{model} - sd_{target}| \qquad (2.11)$$

where sd_{model} is the average step duration recorded in simulation, sd_{target} is the desired step duration, and w_{sd} is the assigned weight.

- A penalty minimizing the walking effort: the effort is computed taking the implementation of Umberger metabolic model (Umberger, 2010; Umberger et al., 2003) with updates from Uchida et al. (2016):

$$p_{effort} = w_{effort} \cdot effort \qquad (2.12)$$

Computing the total heat rate (tot_heat_rate), the mechanical work rate ($mech\_work\_rate$), and the mass for each muscle, the effort is obtained according to equation 2.13

$$effort = \frac{basal\_energy + \sum_{n=1}^{N_{muslces}} (tot\_heat\_rate_i + mech\_work\_rate_i) \cdot mass_i}{distance \cdot mass_{model}}$$

$$(2.13)$$

According to Uchida's model, the basal energy is computed as $1.2 \cdot mass_{model}$.

- A penalty minimizing the overcoming of joints' ranges: this penalty is linked to the distance between the actual joints' angle values and the desired joints' ranges. Desired joints ranges in degrees are defined as [-16.2, 42.0] for the hip (positive flexion), [-1.3, 68.2] for the knee (positive flexion), and [-27.7, 15.5] for the ankle (positive dorsiflexion) (Schwartz et al., 2008):

$$p_{joints} = w_{joints} \cdot |joints\_ranges_{model} - joints\_ranges_{target}| \qquad (2.14)$$

where $joints\_ranges_{model}$ represents the joints ranges recorded in simulation, $joint\_ranges_{target}$ represents the desired joints ranges, and w_{joints} is the assigned weight.

- A penalty minimizing the head's acceleration for head stability: the acceptable ranges in m/s^2 where no penalty is applied are [-4.9, 4.9] for the vertical direction and [-2.45, 2.45] for the forward direction.

$$p_{head} = w_{head} \cdot |head\_acc_{model} - head\_acc_{target}| \tag{2.15}$$

where $head\_acc_{model}$ represents the head acceleration recorded in simulation, $head\_acc_{target}$ represents the desired ranges for head acceleration, and w_{head} is the assigned weight.

The final value of the cost function is given by equation 2.16:

$$cost\_function = p_{stability} + p_{speed} + p_{sl} + p_{sd} + p_{effort} + p_{joints} + p_{head} \tag{2.16}$$

Three different sets of optimizations are performed with different targets implemented in the objective functions:

- Optimization set 1: different target speeds ranging from slow to fast gait

- Optimization set 2: different target step lengths ranging from small to large, maintaining a fixed value of step duration

- Optimization set 3: different target step duration ranging from small to large, maintaining a fixed value of step length

The first set of optimizations changes the target speed in every optimization covering a wide range, from the slowest to the fastest speed that the model's stability can handle. The following optimizations for step length and step duration are performed starting from the initial condition of the best solution found in the mid-range at 1.0 m/s of speed with a value of step length and step duration around 0.7 m and 0.7 s, respectively. The second set investigates the modulation of step length having this gait characteristic as target varying in the different optimizations and a fixed target step duration in the range of [0.68, 0.72] s. Similarly, for the third set, the step length is kept fixed to the defined range of [0.68, 0.72] m, and the step duration is the varying target. Different weights are assigned to each cost function's component depending on the optimization set. These weights are shown in Table 2.1.

Since forcing a fixed step length or step duration while varying the gait characteristics increases the task's effort, the weight for effort minimization is reduced from 1 to 0.1 for the last two sets of optimizations, not to penalize the task's achievement.

	set 1	set 2	set 3
$w_{stability}$	100	100	100
w_{speed}	100	100	100
w_{sl}	0	1	0
w_{sd}	0	0	1
w_{effort}	1	0.1	0.1
w_{joints}	0.1	0.1	0.1
w_{head}	0.25	0.25	0.25

Table 2.1: Assigned weight for each cost function component for the three optimization sets.

2.3.4 Solutions' selection

The three sets of optimizations obtained contain several solutions where the achieved values of speed, step length, and step duration are recorded together with the amount of effort and joint ranges. Among these solutions, the ones selected for the current study satisfy the following conditions:

- stability: from the solutions that reached the maximum simulation time without falling condition, the stable solutions are the ones that show a convergence toward a constant oscillation of joint angles.

- effort: the efficient solutions from the energy point of view are the ones with an effort value lower than 4 $J/(kg \cdot m)$ for speed between 0.8 and 1.3 m/s, and lower than 8 $J/(kg \cdot m)$ for slower and faster speeds since these types of gaits requires higher energy expenditure.

- joints limits: the solutions selected for the analysis are the ones that have a penalty lower than 0.5 for the knee and hip angles. In contrast, the ankle angle's penalty limit is set to 3 since the model tends to have high dorsiflexion.

Additionally, the second and third set of optimization also need to maintain the values of step duration and step length in the ranges reported previously. From the data obtained, it is possible to evaluate the three gait characteristics' ranges when the human model's movement is driven by reflexes allowing to answer the first research question.

2.3.5 Dataset analysis

For the identification of key parameters, the focus is purely on reflex circuits. Therefore, the parameters related to balance, feedforward stimulation, and thresholds are not analyzed. The identification of critical parameters for gait modulation is found by examining the correlation coefficient between the parameter and the variation of the gait characteristics analyzed. Therefore, a reflex parameter is considered a candidate key parameter for gait modulation if it

presents a correlation coefficient larger than 0.6 for at least one of the three gait characteristics' modulation. Then, each identified parameter is analyzed through three different regressions, one for the solutions obtained by each of the three optimization sets. The regression analysis is performed with a similar methodology as previously done by Van der Noot et al. (2018). However, we consider all the good solutions extracted instead of their average. Then, data are regressed, finding the lowest order polynomial function that can model the distribution with a coefficient of determination (R^2) larger than 0.7, which is commonly considered a value above which it is possible to define a strong correlation (Akoglu, 2018). If the solutions extracted are widely spread, the maximum polynomial order allowed is set to three.

2.3.6 Validation of gait behaviors

The previous stage allowed us to identify the parameters that mostly correlate with gait modulation. However, in the case of stretch reflexes, the same stimulation level can be achieved by modulating the gain (k_L) or the length offset (l_0). Therefore, when one of these stretch parameters is identified as a key parameter, the other belonging to the same reflex is also considered a key modulator for the validation study. Once the key reflexes are identified, we demonstrate that the variation of these is sufficient to achieve the same ranges of gait variability achieved in the previous experiments. This process is done by performing new optimizations exploring the gait characteristics' boundaries (minimum and maximum speed, step length, and step duration). During these optimizations, reflexes that were not identified as relevant are not allowed to change, and their value is kept constant. On the other hand, the key reflexes are optimized together with the parameters regulating balance, feedforward stimulation, and states. Further validation is done by optimizing only the non-relevant reflexes for the gait modulation and keeping the key parameters to a constant value with the target objective of obtaining the same boundaries of the gait characteristics obtained previously. This process is done to demonstrate the model's reduced ability to modulate the gait without the possibility of changing the key reflex parameters. The other parameters not belonging to the reflex controller are also optimized in this case. Other experiments explored the capability of key parameters to modulate the gait characteristics without the contribution of PD balance controller and states' threshold since also these non-physiological parameters may contribute to gait modulation.

The identification of key reflexes and the validation process permit us to answer the last two research questions allowing us to define which reflex controls which gait characteristics and if these characteristics can be controlled independently. The study then presents the gait analysis of joint kinematics, ground reaction forces, and muscular activity, considering minimum, intermediate, and maximum values of the obtained speed, step length, and step duration.

2.4 Results

This section presents first the gait limits that the model can reach in terms of speed, step length, and step duration, then the identified key parameters. These parameters are divided depending on whether they control step length, step duration, or both. The identification of the key parameters is made by analyzing the linear correlation for the three gait characteristics and the tendency of the data distribution shown together with the regression model.

Three different sets of optimizations were performed. Specifically, set 1 contains 147 solutions extracted from 12 optimizations, whereas set 2 and set 3 respectively include 134 and 75 solutions, both extracted from 9 optimizations from each set. The multiple solutions extracted from a single optimization represent simulations with a low effort level with different values of the spatiotemporal gait characteristics. This allowed obtaining several gait characteristics values minimizing the number of optimizations. Furthermore, we verified that a specific target behavior could be reached through optimizations starting from different initial conditions. Table 2.2 shows the minimum and maximum boundaries reached during the optimization processes. From the first one investigating the speed modulation, the solutions were extracted within the speed range from 0.45 to 1.71 m/s, step length from 0.45 and 0.87 m, and step duration from 0.51 to 1.04 s. The solutions in the second set of optimizations achieved a minimum step length of 0.45 and a maximum of 0.88 m, covering the same range already obtained in the first set with an increasing target speed. The step duration was maintained constant at 0.69 s, and this condition was satisfied for all the solutions selected with a tolerance of 0.01 s. Consequently, the range of speed obtained in this second set is reduced compared to the first one because of the imposed fixed step duration, which is included between 0.69 and 1.48 m/s. Finally, the third set presents solutions with values of step duration ranging from 0.51 to 0.91 s. The target step length is maintained fixed to 0.72 m, and the solutions extracted from optimizations satisfied this condition with a tolerance of 0.02 m. The range of speed obtained out of this optimization set is included between 0.78 and 1.46 m/s.

Optimization set [min, max]	Speed [m/s]	Step length [m]	Step duration [s]
Set 1	[0.45, 1.71]	[0.45, 0.87]	[0.51, 1.04]
Set 2	[0.69, 1.48]	[0.45, 0.88]	[0.68, 0.70]
Set 3	[0.78, 1.46]	[0.70, 0.74]	[0.51, 0.91]

Table 2.2: Boundaries of the three gait characteristics targeted during the three optimization sets.
The first set shows the optimizations' results where the gait target to reach is the desired speed that varied from the lower to the upper boundary. The second set shows the optimizations' results with a fixed step duration and a varying target step length. Finally, the third set shows the optimizations' results with a fixed value of step length, changing the target step duration.

Changing parameters' values with gait characteristics' modulation permits identifying the

reflexes controlling speed, step length, and step duration. Table 2.3 presents the correlation coefficients of the nine key parameters identified. Among these, some reflexes are linked with specific gait characteristics. Specifically:

- three key reflexes for the modulation of speed by modulating only the step length.

- four key reflexes for the modulation of speed by modulating both step length and step duration.

- Two additional reflexes modulating both step length and step duration, such that together this results in keeping speed more or less constant.

- no reflex parameter has been found to modulate step duration independently from step length.

	Speed	Step length	Step duration
Step length modulators			
$L0_{HAMS}^{ES-MS}$	0.4892	0.7827	0.1312
KF_{SOL}^{MS-PS}	0.9082	0.8156	0.3632
KF_{GAS}^{MS-PS}	0.8978	0.7074	0.1348
Step length and step duration modulators with effects on speed			
KL_{ILPSO}^{PS}	0.6931	0.8029	0.6363
$L0_{ILPSO}^{S}$	0.4689	0.2328	0.7409
KL_{GMAX}^{LP}	0.7285	0.4041	0.6454
$L0_{TA}^{LP}$	0.8121	0.5978	0.3431
Step length and step duration modulators without effects on speed			
KL_{HAMS}^{LP}	0.1452	0.4781	0.6072
$L0_{HAMS}^{LP}$	0.3382	0.8707	0.7602

Table 2.3: Correlation coefficients of identified key reflex parameters.
Three reflexes were found to have a significant effect on speed through the modulation of step length, four to have an impact on all three gait characteristics, and two able to modulate step length and step duration accordingly with small effects on speed.

Since we did not find parameters that could modulate step duration without significantly affecting step length, step duration is mainly modulated by reflexes that interact with step length's regulation as well. Therefore, the solutions presented where step duration modulation

is achieved while maintaining the step length fixed could be obtained only with other reflex circuits' compensation mechanisms.

2.4.1 Step length modulators

In total, three parameters have been selected for step length modulation, namely $L0_{HAMS}^{ES-MS}$: (length offset of hamstrings' stretch reflex during early and mid-stance), KF_{GAS}^{MS-PS} (positive force feedback's gain of gastrocnemius muscle during mid-stance and pre-swing), and KF_{SOL}^{MS-PS} (positive force feedback's gain of soleus muscle during mid-stance and pre-swing). These are the ones that showed a high correlation coefficient with speed and step length and a low correlation coefficient with step duration, indicating a minor effect on this latter gait characteristic. All these parameters regulate the stimulation given by reflexes activated during the stance phase. The length offset of the hamstrings' stretch reflex in the first two sub-phases of stance shows a high correlation coefficient with the modulation of step length ($c = 0.7827$) and a lower correlation with the modulation of speed ($c = 0.4892$) and with a significant low correlation with the modulation of step duration ($c = 0.1312$). The graphs in the first row in Figure 2.2 show the linear relationship with the step length modulation ($R^2 = 0.7827$). However, parameter variation also affects the step duration, as shown by the quadratic regression ($R^2 = 0.78198$). Therefore, the same parameter value can generate two different gaits patterns with different step durations depending on the other reflex parameters' compensatory mechanisms. This nonlinear effect on the step duration results in a less clear dependency between the hamstrings stretch offset and the increase in speed. In fact, the values of this parameter are very spread around the linear regression for the speed modulation. However, the global increasing tendency seems to follow the one found for step length modulation.

On the other hand, the propulsive muscles seem to have a key role in modulating step length. Indeed, both gastrocnemius and soleus' positive force feedback has a high linear correlation with step length modulation with $R^2 = 0.81562$ for soleus and $R^2 = 0.70738$ for gastrocnemius. This linear dependency is also present in the speed's modulation that can be modeled as a linear regression with $R^2 = 0.90818$ for soleus and $R^2 = 0.89783$ for gastrocnemius. The changing of these two parameters shows minor effects on the modulation of step duration with low correlation coefficients. Indeed, the parameters' values were maintained roughly constant for longer step durations than 0.6 s. Nevertheless, shorter durations more proper of high speeds may affect the parameters' values. Indeed, the positive force feedback gain of soleus increases when step duration goes below 0.6 s while gastrocnemius' one decreases. It is also possible to notice that the value that the parameters can reach is limited if constraints to the gait characteristics are applied. This is especially true for the gastrocnemius's positive force feedback gain that cannot reach values larger than 1.1 if a fixed step length or step duration is imposed.
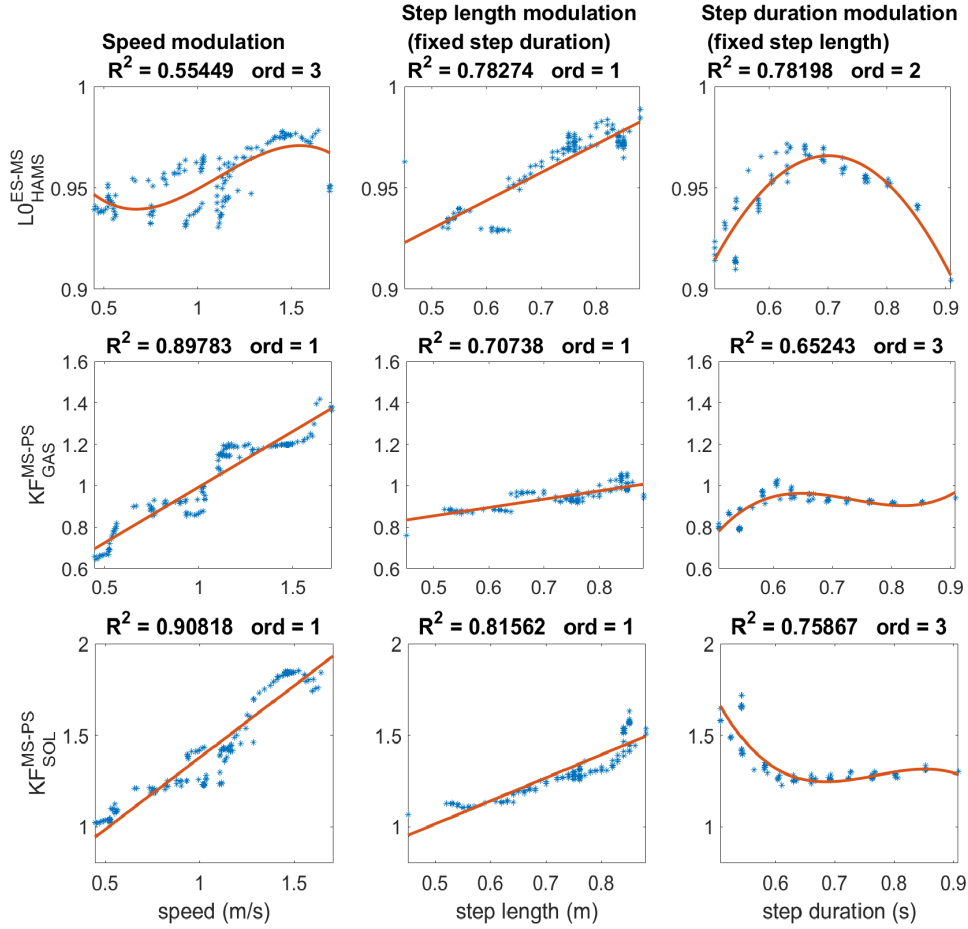
Figure 2.2: Regression analysis of step length modulators.
The solutions obtained by the three sets of optimizations are represented by the blue dots, whereas the red curve represents the regression. The plot on the left shows the data distribution and regression for the speed modulation, while the plots on the center and the right show the step length and step duration modulation, respectively. The reflexes presented facilitate speed and step length increase with minimal effect on the step period. The offset length of the hamstrings' stretch reflex presents an influence on step duration modulation, but the global increasing tendency of speed reflects the behavior found in the modulation of step length.

2.4.2 Step length and step duration modulators

The following results present the key parameters affecting both step length and step duration significantly. These parameters are separated into two groups: those that affect speed modulation and those that do not affect speed. This diversification is made because possible parameters that influence step length and duration coherently maintain the ratio between these two gait characteristics roughly constant, minimizing the effect on speed modulation.

With effects on speed

KL_{ILPSO}^{PS} (stretch reflex's gain of iliopsoas muscle during pre-swing), $L0_{ILPSO}^{S}$ (length offset of iliopsoas' stretch reflex during swing), KL_{GMAX}^{LP} (stretch reflex's gain of gluteus maximus muscle during the landing phase) and $L0_{TA}^{LP}$ (length offset of tibialis anterior's stretch reflex during the landing phase) are the key reflex parameters that influence both step length and step duration, significantly affecting speed. The graphs at the top of Figure 2.3 described the behavior of the stretch reflex gain of the iliopsoas during pre-swing. This parameter decreases linearly with the increasing step length and increases with the rising step duration, resulting in a global decrease in speed.

In the following phase of the gait cycle, we can observe a decreasing length offset of iliopsoas' stretch reflex during swing with the increase of speed. However, the parameter's values start to decrease only after 1 m/s while it remains roughly constant for slower gaits, as described in the plots presented in the second row of Figure 2.3. The decrease with increasing speed is coherent with the step duration observed tendency that increases linearly with the increase of length offset value. The step length modulation shows that the parameter maintains values close to 0.8 except for small step lengths below 0.6 m, where the parameter slightly increases from 0.7 to 0.8. This dependency found for small step length contrasts with the step duration's increasing behavior, possibly explaining the low effect of this parameter for slow speed modulation.

The length feedback gain of the gluteus maximus during landing linearly influences speed modulation. However, this linearity is not found in the modulation of step length and step duration as observed in the third row of Figure 2.3. The critical contribution to the modulation of step length is given mainly at values larger than 0.7 m showing a drastic decreasing behavior of the parameter. It is also possible to observe that the reflex gain increases from a value of 0.1 to 0.2 for small step lengths. This increasing behavior is probably the main contributor to the growing speed modulation behavior for slow speed. However, the parameter values keep increasing for the fastest speed, although they decrease for large step lengths. Therefore, at the fastest speeds, the modulation is given by the effect on the step duration that decreases rapidly when the reflex gain increases.

The last parameter for speed modulation is represented by the length offset of the tibialis anterior's stretch reflex. Concerning speed modulation, despite the data being regressed efficiently with a linear function, the parameter values were kept at around 0.75 for slow speeds until reaching 1 m/s. After this speed value, the length offset constantly decreases and maintains a decreasing behavior for the fastest gaits. Coherent decreasing of the parameter's value can also be found for large step lengths and short step durations typical of fast speeds. On the other hand, the parameter remains roughly constant for small step lengths and long step durations typical of slow speeds.
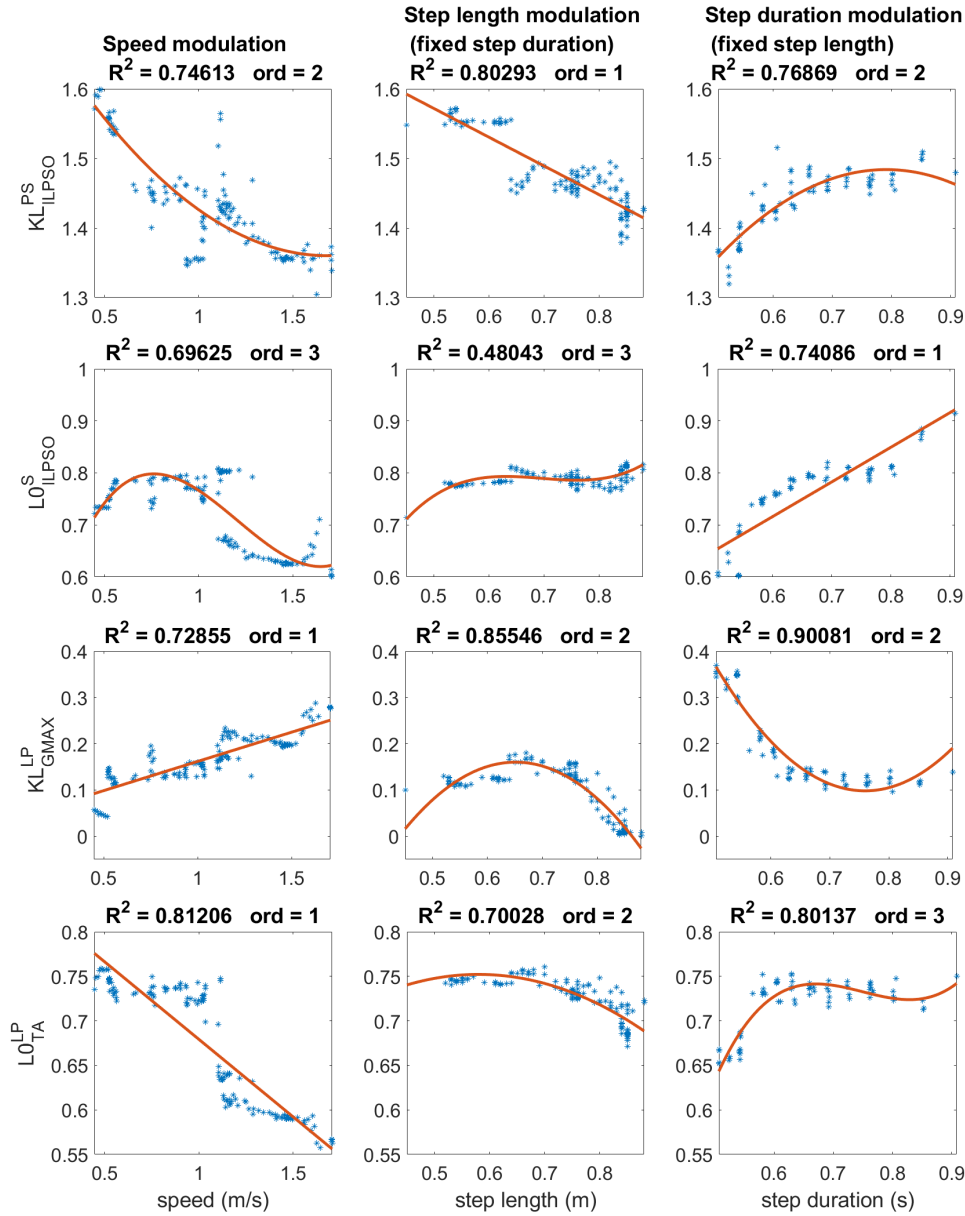
Figure 2.3: Regression analysis of step length and step duration modulators with effects on speed

The stretch reflex gain of iliopsoas during pre-swing and the length offset during swing have a decreasing impact on speed due to decreasing step length and increasing step duration for the former and primarily for step duration increasing for the latter. On the other hand, the stretch reflex gain of gluteus maximus in landing preparation has an increasing linear effect on the speed with nonlinear effects on step length and step duration. The length offset of tibialis anterior's stretch reflex can modulate fast speed with large step lengths and short step durations but has less effect in the modulation of slow gaits.

Without effects on speed

KL_{HAMS}^{LP} (stretch reflex's gain of hamstrings muscle during the landing phase) and $L0_{HAMS}^{LP}$ (length offset of hamstrings' stretch reflex during the landing phase) control the modulation

on both step length and step duration, maintaining their relation roughly constant with a minimal effect on speed. Both these parameters are related to the hamstring's stretch reflex activity during landing preparation and are represented by the gain and the length offset. From the graphs at the top of Figure 2.4, the gain decreases accordingly with both step length and step duration resulting in a null effect on the speed modulation as shown by the spread distribution of data and from the low coefficient of determination of the third-order polynomial ($R^2 = 0.19406$). The increasing length offset values with the increasing step length and step duration also contribute to the stretch response's reduced activity when the two gait characteristics increase, as shown in the bottom graphs in Figure 2.4. Also in this case, the global effect is less efficient in the modulation of gait velocity.
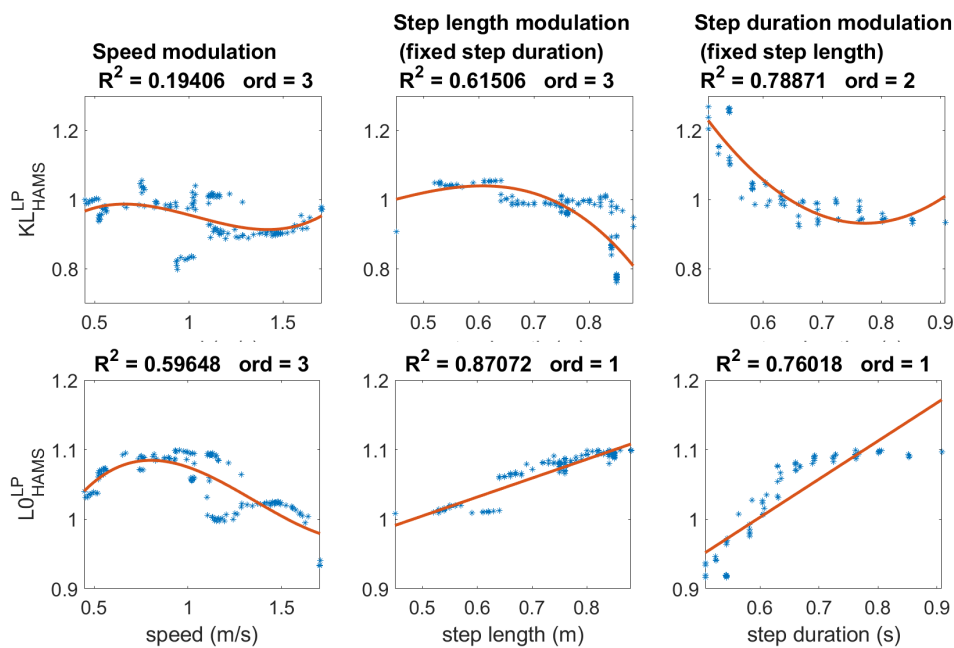
Figure 2.4: Regression analysis of step length and step duration modulators with effects on speed.
Increasing the stretch reflex gain of hamstrings during landing preparation leads to a decrease in step length and step duration resulting in a low influence in speed modulation. Similarly, the increasing length offset of hamstrings' stretch reflex during landing preparation results in an increased step length and step duration with a small effect on speed modulation.

2.4.3 Modulation of key parameters

From the previous section, we could identify the reflexes that may affect gait modulation. These key reflexes are highlighted in the control diagram of Figure 2.5. Step length modulators are highlighted in yellow, whereas step length and step duration modulators are highlighted in green and red depending on whether they have or do not affect speed, respectively.

This section presents the largest ranges reached for the modulation of the three gait charac-

Figure 2.5: Diagram of the reflex controller with key reflexes modulating gait highlighted
The reflexes that were found to modulate mainly step length are highlighted in yellow. In contrast, those modulating step length and step duration together are highlighted in green and red depending on whether they showed a significant effect on speed (green) or not (red).

teristics, optimizing only the key reflexes identified together with the feedforward, balance, and state controller parameters. These boundaries are compared with the ones obtained previously, optimizing all the parameters. Another comparison is made with the achieved boundaries resulting from optimizations of all non-relevant parameters (not selected as key parameters).

Table 2.4 presents the largest boundaries obtained by optimizing the key reflexes identified. Compared to Table 2.2, the modulation of key parameters could generate locomotion behaviors from slow to fast gaits with large and small step lengths and short and long step durations. The boundaries of the three gait characteristics cover the same ranges as those obtained with all reflex parameters' optimization. Similar results are obtained for the modulation of step length and step duration. Therefore, the key reflexes selected demonstrated to be able to modulate gait with the same performances of the modulation of all reflexes.

Optimization set [min, max]	Speed [m/s]	Step length [m]	Step duration [s]
Speed modulation	[0.48, 1.71]	[0.43, 0.88]	[0.51, 0.98]
Step length modulation	[0.77, 1.26]	[0.52, 0.87]	[0.69, 0.70]
Step duration modulation	[0.79, 1.30]	[0.70, 0.71]	[0.54, 0.91]

Table 2.4: Boundaries of the three gait measures reached with the optimization of key reflexes. The optimization of the key reflexes alone could obtain the same performances of the gaits obtained optimizing all the reflexes suggesting that the major role of modulation is delegated to the key reflexes.

However, some reflexes that were not considered key modulators could still significantly affect locomotion modulation since the neural system is highly redundant. The results from the optimizations of non-relevant reflexes targeting the same ranges achieved in the previous stages show that the model fails to achieve slow and fast speed targets when the key identified reflexes are kept constant and not included in the optimization. For step length modulation maintaining a fixed value of step duration, the model cannot reproduce stable locomotion with a small step length. However, large step gaits could be achieved with similar performances obtained previously without modulating the identified reflex modulators. On the other hand, the optimization could not reach long step durations maintaining an intermediate value of 0.67 s when trying to target high values. However, the optimization could converge to a behavior able to reproduce short durations comparable to those previously obtained.

These results suggest that there are parameters beyond the key reflexes identified to modulate large step length and short step duration. These parameters do not necessarily belong to the reflex controller but could be part of the feedforward, balance, or state controller. In order to verify this, we performed optimizations varying the key reflex parameters alone and other optimizations varying only the other reflexes maintaining constant in all cases feedforward, balance, and state controller parameters. We verified that the modulation of state threshold parameters alone could achieve large step lengths. By fixing these parameters, we could reach a step length value of 0.87 m with the optimization of key parameters. In contrast, the optimization of other reflexes could only reach a step length below 0.8 m. On the other hand, the modulation of short step duration could be achieved with PD balance parameters' contribution. Maintaining these parameters constant, a short step duration of 0.54 s could be achieved by optimizing the key reflex parameters. In comparison, the other reflexes could not converge to solutions with a step duration value lower than 0.62 s. Therefore, the key reflexes identified describe a large variance in the neural feedback mechanism's modulation, whereas the other reflexes do not seem to affect gait modulation significantly.

2.4.4   Gait analysis

This section presents the gait analysis of the different solutions obtained, considering low, intermediate, and high values of speed, step length, and step duration when modulating the key reflexes. Firstly, the joint angles are presented, followed by ground reaction forces and muscle activation. These results are also compared to findings reported in past experimental studies (Y. P. Ivanenko et al., 2006; Lim et al., 2017; Moissenet et al., 2019; Wu et al., 2019). It can be noted that the reflex controller could generate human-like locomotion behaviors as shown in Figure 2.6 for the specific solution from the first set of optimization at the intermediate speed of 1.2 m/s.
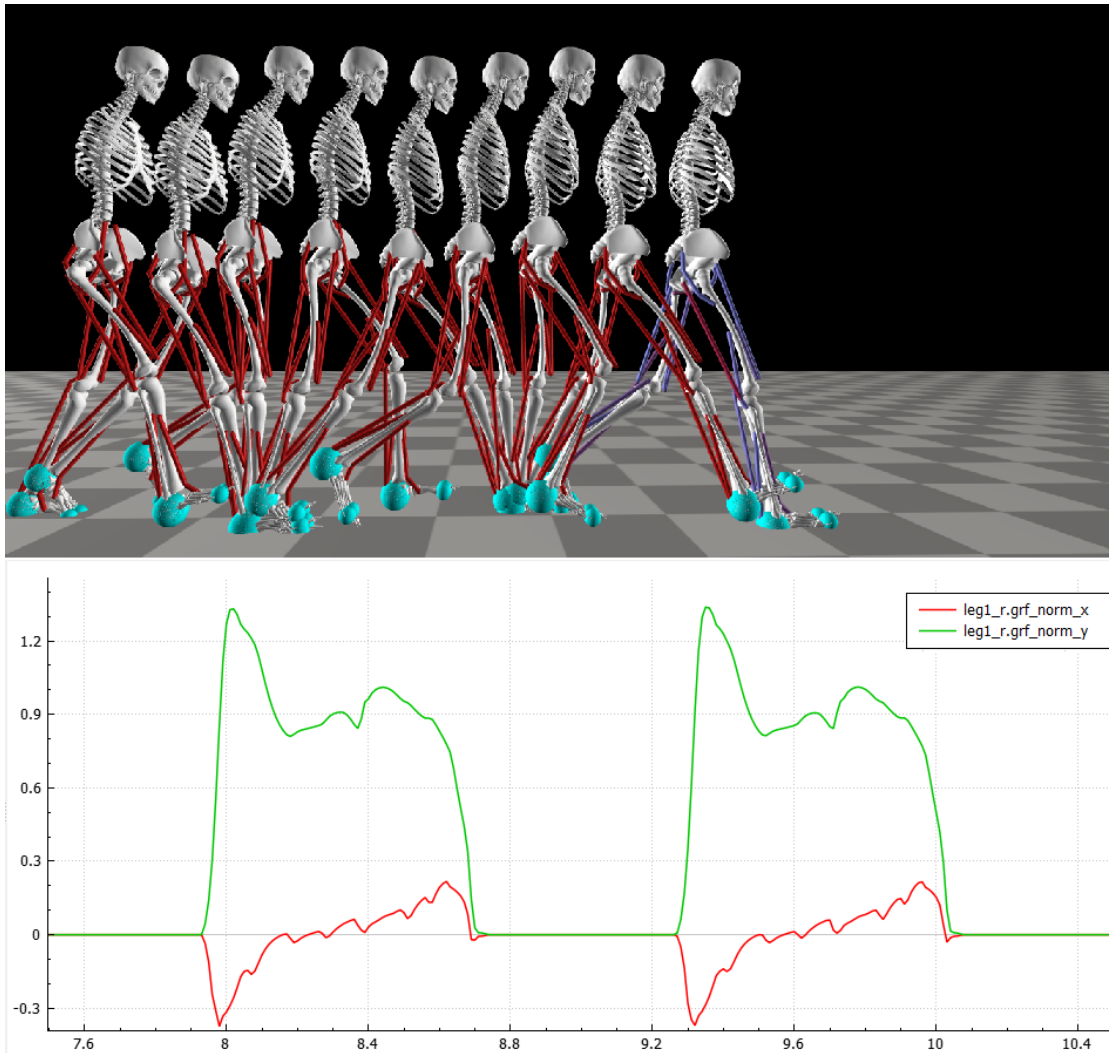
Figure 2.6: Representation of gait behavior with snapshots taken at different frames for the speed modulation solution with target speed equal to 1.2 m/s.
The instant taken is represented together with the behavior of vertical and horizontal ground reaction forces.

Kinematics and GRFs

Figure 2.7 describes the behavior of joint kinematics and ground reaction forces. The hip angle has larger oscillation amplitudes for fastest speeds and largest step lengths. Wu et al., Schwartz et al., and Moissenet et al. also observed the same behavior in their experimental results about speed modulation (Moissenet et al., 2019; Schwartz et al., 2008; Wu et al., 2019). Besides, Lim et al. observed that the hip flexion's peaks were increasing with the step length's increase, whereas no significant changes in step duration's modulation are observed (Lim et al., 2017). Indeed, our results show that, in these conditions, fast speed and large step lengths start from a flexion value around 40 degrees, decrease during stance to a maximum extension around -25 degrees and increase in swing to a maximum flexion value close to 50 degrees. By contrast, at slow speeds and small step lengths, the gait cycle starts with a hip flexion value of 20 degrees, decreases during stance to a minimum extension of -10 degrees, and increases during swing to a maximum extension value below 40 degrees. This behavior is not preserved in the modulation of step duration, where the hip flexion maintains roughly the same oscillation amplitudes with a tendency to maintain flexion for short step durations. Indeed, the hip flexion values vary from 30 to -20 degrees for long durations and from below 50 to -10 degrees for short durations. Therefore, the changing of speed shares more similarities with the changing of step length rather than step duration when considering hip flexion variation (Lim et al., 2017).

Then, for the knee flexion, we can observe that the modulation of speed step length, and step duration does not significantly affect the knee flexion observed during the swing phase. Indeed, we can only observe that this flexion is around 70 degrees for all the proposed values of speed and step length with a small decrease of maximum flexion to 60 degrees for long step durations. However, it is possible to notice that difference is more important for the smaller knee flexion observed at the beginning of the stance phase. In fact, the amplitude of this flexion is larger with the increase in speed and can be observed only for large step lengths. Furthermore, the flexion is delayed to 40% of the gait cycle for very slow speed gait simulations. Concerning the modulation of step duration with fixed step length, the knee angle remains fully extended during the stance phase and starts to flex only at the beginning of the swing phase with the large knee flexion. These results slightly differ from the observations provided by experimental studies. Indeed, Wu et al., Schwartz et al., and Moissenet et al. observed a decrease in the small peak's amplitude present in stance for slow speeds, as also observed in our experiments (Moissenet et al., 2019; Schwartz et al., 2008; Wu et al., 2019). However, a decrease in knee flexion in swing is reported for very slow speeds. In addition, Lim et al. noticed an increase in knee flexion for large step lengths and short step durations.

Concerning the ankle joint, compared to experimental results, there is excessive dorsiflexion between 10 and 20 degrees, and the plantarflexion is anticipated to 30% of the gait cycle instead of the 50%. The results show that the peak dorsiflexion in stance increases when speed rises. The same behavior can be observed for the peak plantarflexion in pre-swing. Furthermore, it is possible to notice a consistent delay of ankle dorsiflexion from 60 to 80% of
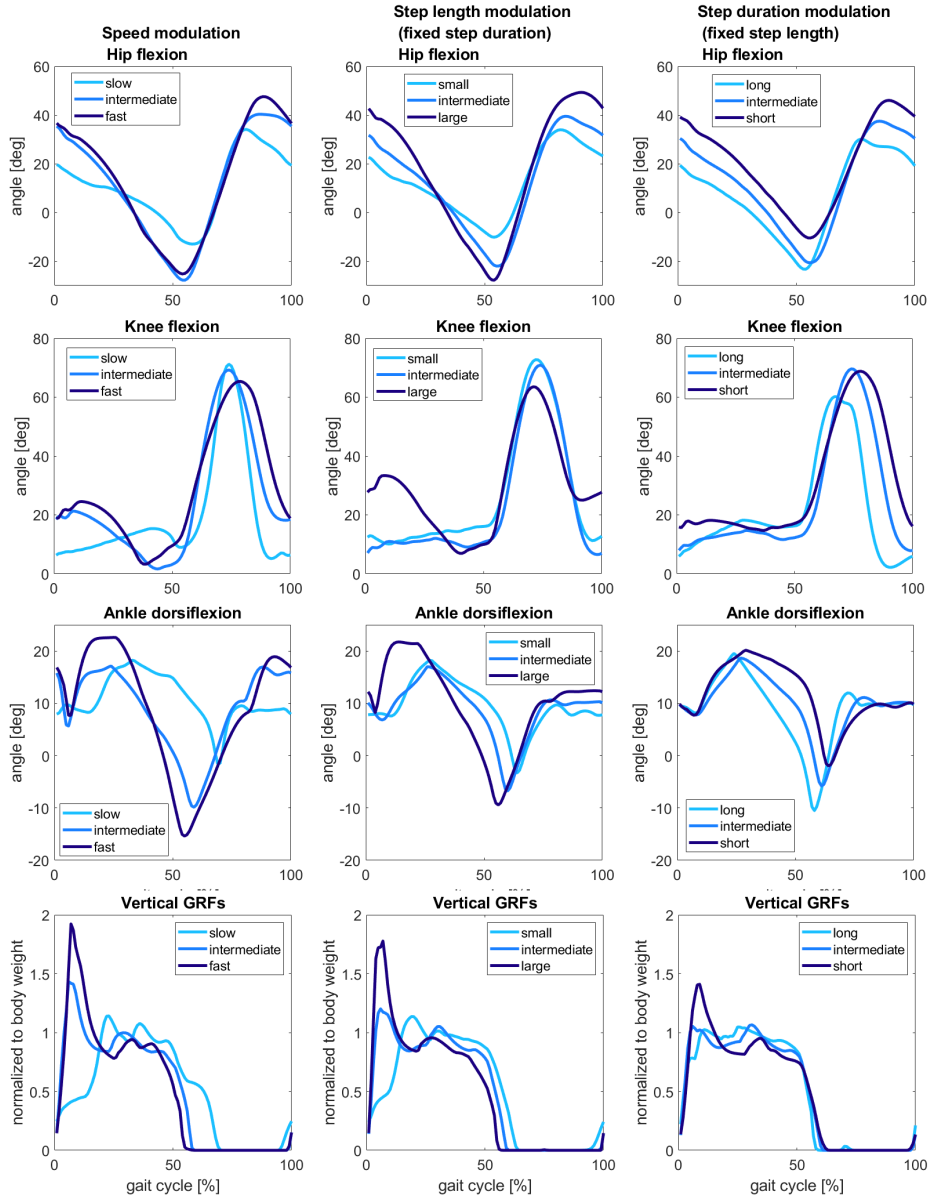
Figure 2.7: Joints angles and ground reaction forces for low, intermediate, and high values of the three gait characteristics.
The cyan curves describe the slow gaits with small step lengths and long step durations, whereas the dark blue curves describe the fast gaits with large step lengths and short step durations. The change observed in speed modulation is closer to the only step length modulation than the modulation of step duration.

the gait cycle for slow gait simulations. The curves' tendency appears similar for speed and step length modulation. Concerning the effects of modulation of step duration, higher values for plantarflexion are reached with long durations, and it keeps on decreasing with the step duration's decrease. The shown results seem to agree with the experiments performed by Wu et al. for the amplitudes of ankle dorsiflexion and plantarflexion (Wu et al., 2019). However, it

should be noted that Schwartz et al. and Moissenet et al. observed higher first dorsiflexion for very slow speeds compared to fast speeds (Moissenet et al., 2019; Schwartz et al., 2008). On the other hand, Lim's experiments partially confirm our results since he observed that ankle plantarflexion increases with rising speed (Lim et al., 2017). Nevertheless, he also observed that a decrease in step duration results in a slight increase in ankle plantarflexion, whereas in our results, this peak is kept small for short durations.

From the shapes of ground reaction forces, it is possible to observe a high peak at the beginning of the cycle for fast speeds, large step lengths, and short durations due to the fast collision with the ground. Furthermore, the second peak of the GRFs curve is anticipated compared to the ones usually found in experimental data. Moreover, the curve is flattened with small oscillations for slow speeds, small step lengths, and long step duration. These plots also provide information on the duration of the stance and swing phase in the gait cycle percentage. The stance phase ends around 60% of the gait cycle, except for slow gaits, where the stance phase is prolonged to 70%. These results resemble the observations found in experimental data from Wu et al. (2019) and Schwartz et al (2008).

Muscle activity

Figure 2.8, Figure 2.9, and Figure 2.10 show the muscle activity changes for the hip, knee, and ankle muscles, respectively. From the activation of the gluteus maximus, we noticed that the muscle is active mainly at the beginning and at the end of the gait cycle. It has a higher activity at fast speed during the stance phase despite the reflex gain and offset parameters have been maintained constant since it was not considered a key reflex for gait modulation. Higher activity at the beginning of the gait cycle is also observed at large step lengths and short step durations. Gluteus maximus activation reaches significant levels around 0.2 during the landing preparation due to the stretch reflex activity. This activation appears to be higher at fast speeds and short step durations but decreases significantly at large step lengths. Globally, the muscle never reaches a high activation through the gait cycle, as it is possible to see from the graphs where the activation is kept below 0.3. From the experimental studies performed by Ivanenko et al. and Lim et al., gluteus maximus' peak activation increases with increasing speed and step length and decreases with increasing step duration, as also observed in our results (Y. P. Ivanenko et al., 2006; Lim et al., 2017).

From the second row of Figure 2.8, the activation of hamstrings muscle through the gait cycle in early stance and mid stance and during landing increases significantly with the increase of speed and step length and decreasing of step duration. In fact, hamstrings activation passes from values around 0.3 for slow speeds, small steps, and long durations to values around 0.8 for large step lengths and short durations until reaching peak values close to saturation for fast speeds. The single peak obtained is not preserved for slow speeds and small step lengths where the activation curves show a double peak behavior. During landing, the muscle activation also shows higher activity with increasing speed and decreasing step duration, passing from values around 0 to 0.3. A slight activity increase is also observed for gait with

large step lengths with peak values below 0.2 and around 0.1 for small and intermediate step lengths. The experiments performed by Ivanenko et al. (2006), Schwartz et al. (2008), and Lim et al (2017) also observed an increased activity with speed and step length increase and step duration decreases.

The iliopsoas muscle is active during early stance, pre-swing, and swing phases with decreasing activity during landing. The muscle activity during stance driven by the proportional derivative controller increases slightly with speed from 0.2 to 0.6, but no significant changes are present for step length and step duration modulation, maintaining the peak activation values around 0.3. The activity of iliopsoas during pre-swing and swing phases is significantly high for fast speeds and short duration, reaching the maximum activation level during these phases. Significant changes of increasing activity are also present between slow and intermediate speeds, with peak activation values rising from 0.4 to 0.7. Nevertheless, there is no significant difference in amplitude between long and intermediate durations for the step duration's modulation where the peak activation values around 0.6. Still, the muscle activity decreasing during swing is anticipated for long durations. The increasing step length also increases muscle activation but less critically than the one observed for speed modulation. In contrast, the peak activity ranges between above 0.4 and below 0.8 for step length modulation. On the other hand, Ivanenko et al. (2006) recorded a low EMG signal from iliopsoas for every speed value investigated. However, Lim et al. (2017) found an increasing peak activity for large step lengths and short step durations, similarly to our results.

From the plots shown in the last row of Figure 2.8, the rectus femoris muscle is active only during pre-swing, and the activation does not change meaningfully for the different gait targets. The activation is kept low in all the conditions that do not overcome level 0.2 of activation. These results do not match what was observed in experiments from Ivanenko et al. (2006) and Schwartz et al. (2008), who recorded increasing activity with speed increase.

From Figure 2.9 showing the knee muscles activity, the vasti muscle group is active mainly during early stance, mid-stance, and landing. The increase in speed also increases muscle activation from 0.1 of slow speeds to 0.5 of fast speeds. Other increases in activity are present for large step lengths during stance and short duration gaits during landing, raising the muscle activity from 0.2 to 0.6 and from 0.2 to 0.4, respectively. Lim et al. (2017) and Ivanenko et al. (2006) also observed an increased peak activation of vasti muscles, increasing speed, step length, and decreasing step duration.

The activity of the biceps femoris short head is also higher with the increasing values of speed and step length. This increase is less consistent when passing from intermediate to fast speed than from slow to intermediate speed. Indeed, the peak activity increases from 0.4 for slow speeds and small step lengths to 0.7 for intermediate and fast speeds and intermediate and large step lengths. On the other hand, there is no consistent difference in muscle activity for the step period modulation that maintains the peak activity values at 0.6. No meaningful comparisons with experimental studies were possible since gait modulation experiments did
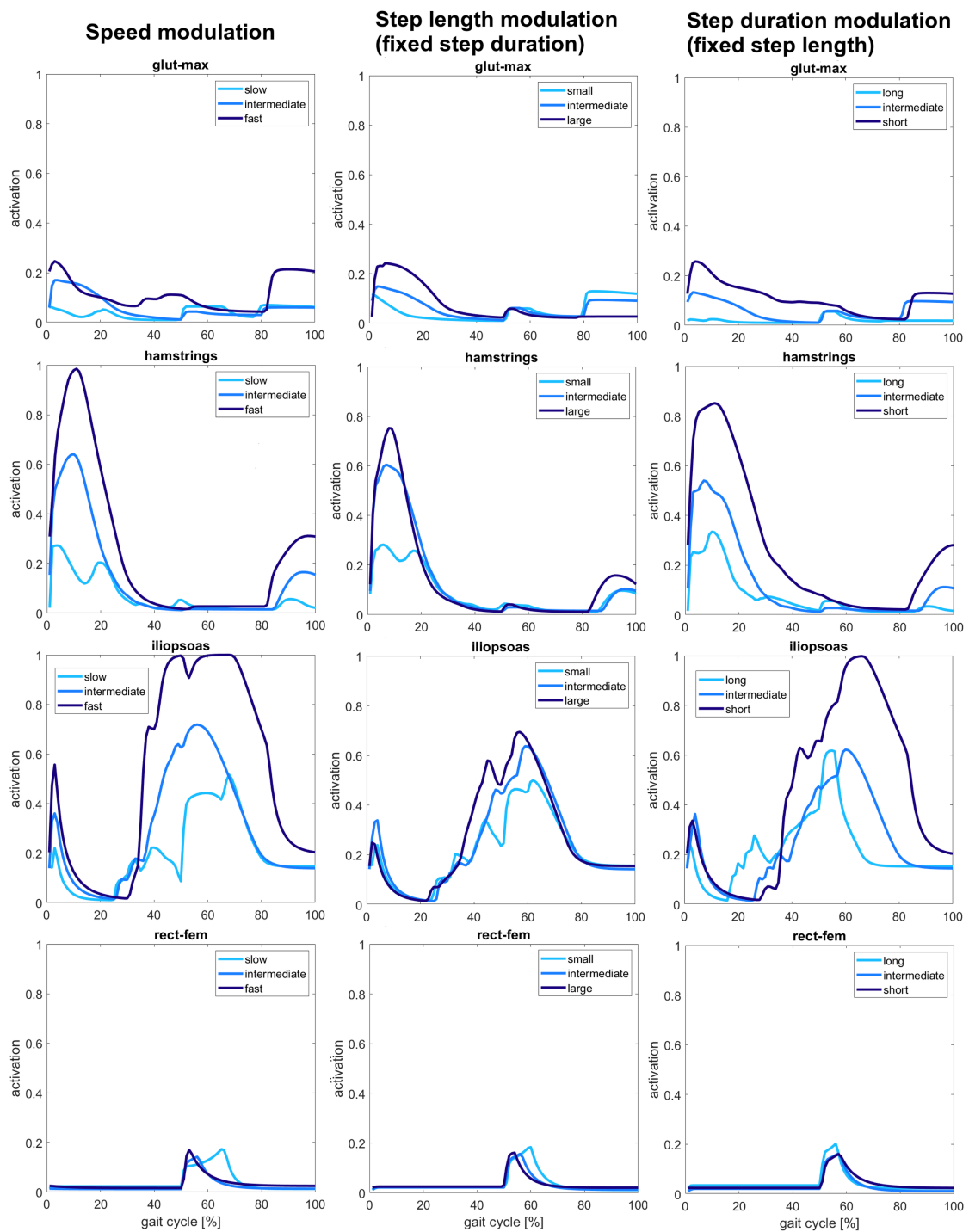
Figure 2.8: Hip muscles activity in gait modulation

Hamstrings and iliopsoas activity show a significant increase with increasing speed and step duration. Gluteus maximus activation is less evident, but it increases activation at the fastest speeds, whereas the rectus femoris does not show significant changes.
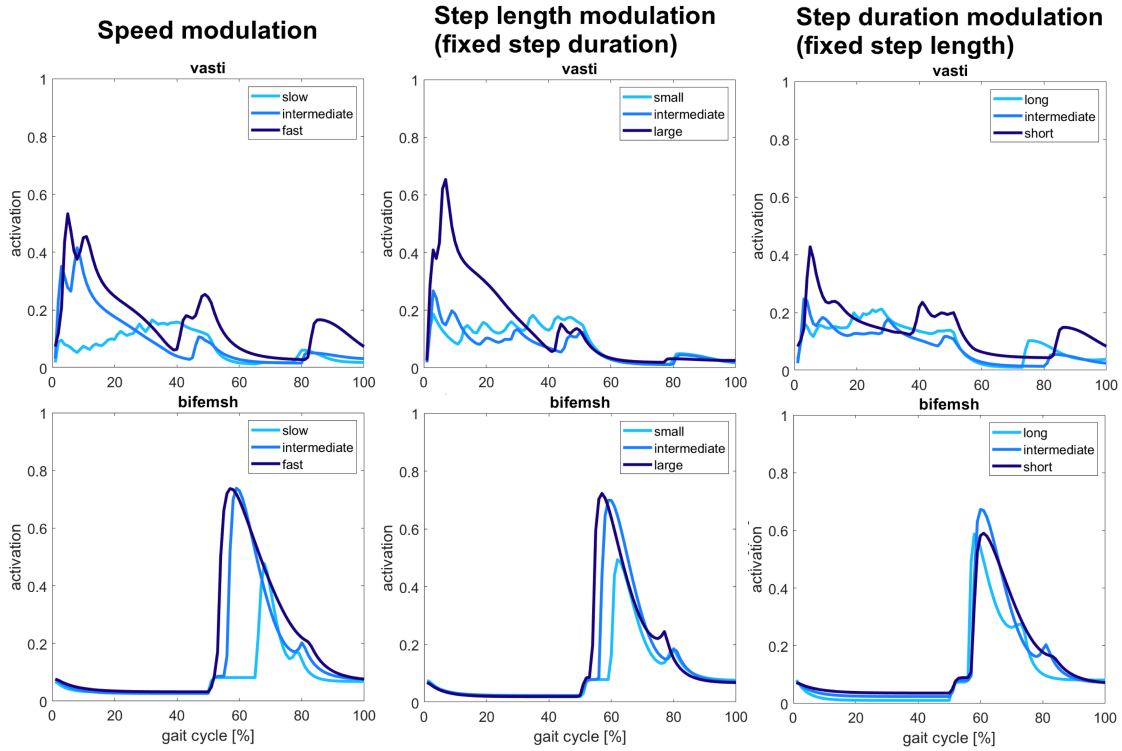
Figure 2.9: Knee muscles activity in gait modulation.
Higher activation is observed for both the vasti and biceps femoris short head muscles at fast speeds and large step lengths.

not record this muscle activity.

From Figure 2.10, it is possible to notice an increased activity for soleus and gastrocnemius muscle during mid-stance and pre-swing when speed increases with the peak activation value passing from 0.25 to 0.4. These results are validated from experiments by Lim et al. (2017) and Ivanenko et al. (2006). Furthermore, an activation delay is present for slow speeds. However, no other significant activity changes linked to the different gait targets are observed, with peak activation values kept to 0.3 for soleus and 0.5 for gastrocnemius. However, Lim et al. (2017) observed that both increasing step length and decreasing step duration resulted in increased soleus and gastrocnemius muscle activity.

Finally, the tibialis anterior is active at the beginning of stance phase and during swing. Also in this case, the activity is increasing with increasing speed with a delay observed for slow gaits. In particular, peak activation values pass from 0.3 for slow speeds to 0.5 for fast speeds. A smaller delay is also observed for smaller step lengths and shorter step durations without a large amplitude variation. The experimental results from Ivanenko et al. (2006) and Schwartz et al. (2008) found similar results of our simulations for speed modulation. However, Lim et al. (2017) did not perform recorded the tibialis anterior muscle, and no comparisons with experimental studies are possible for step length and step duration modulation.
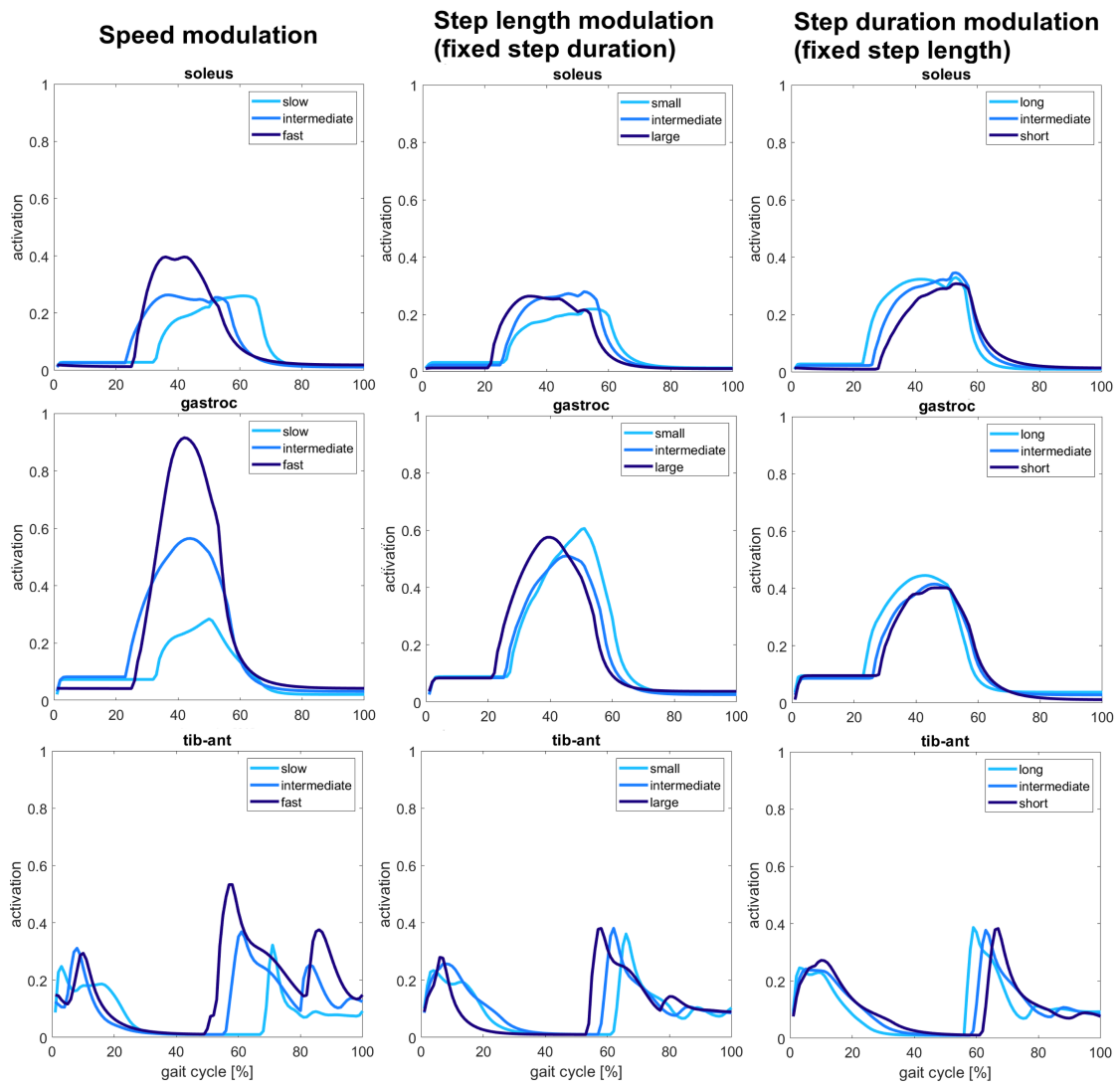
Figure 2.10: Ankle muscles activity in gait modulation.
Soleus and gastrocnemius activity increase with the increase of speed, but no significant changes are seen for the modulation of step length and step duration. Similarly, tibialis anterior activity increases with speed, whereas for step length and step duration modulation, it can be observed anticipation and delay of activation during the gait cycle for large step lengths and short durations, respectively.

2.5 Discussion

In this study, we aim first to understand how much a human model controlled by sensory-driven neural signals can replicate various gait behaviors at different speeds, step lengths, and step durations. Then, we aim to investigate whether these gait characteristics can be controlled independently, and finally to identify possible reflexes that the central nervous system can modulate in task-dependent locomotion. The results obtained from the optimizations show that the reflex controller could generate large ranges of these three gait characteristics. These results are coherent with the previous studies involving the application of sensory-driven

controllers (Geyer and Herr, 2010; Ong et al., 2019; Song and Geyer, 2015) that focused mainly on the single modulation of energy-efficient walking at different speeds. Our results demonstrated that sensory reflexes could modulate speed and energy-efficient gaits and control step length and step duration independently with less efficient gaits. These last generated behaviors can be performed by humans even though they are beyond their optimal energy efficiency. Furthermore, nine key reflex parameters are found to be good candidates to modulate human gait. Three of them modulate speed and step length, four modulate all three gait characteristics, and two modulate step length and step duration accordingly with small effects on speed. These results demonstrate that the modulation of these key reflexes is sufficient to generate various human locomotion behaviors, ranging from reduced to high values of speed, step length, and step duration similar to those obtained with the optimization of all the reflexes. Therefore, the modulation of a small subset of reflexes could, in principle, be involved in the strategies used by descending commands to change the gait behavior together with the already investigated modulation of feedforward circuits (Aoi et al., 2019; Dzeladini et al., 2014).

Some of the identified parameters, mainly active during stance, were found to influence speed and step length. Indeed, step length is affected by the level of propulsion that the stance leg muscles can give, pushing the body forward and lowering the center of mass. Coherently with experiments in human subjects (Francis et al., 2013), the soleus and gastrocnemius muscles give the main propulsion through their positive force feedback, as observed by the strong correlation that the two reflexes have with both speed and step length modulation. However, soleus and gastrocnemius muscle activation show a considerable change only with speed modulation. No significant variations are observed with the modulation of the step length. It should be observed that muscle activation does not depend solely on the values of reflex parameters. In fact, the stimulation given to the muscle depends on the reflex parameters and the muscle state. For this reason, the muscle activation that responds to stimulation as a first-order linear dynamics is also dependent on the state of the muscle itself. It has been verified that the positive force feedback gains of soleus and gastrocnemius change accordingly with the data distribution and regression laws described in the results section. Therefore, the unchanged activation level observed for the modulation of step length is due to an alteration of muscle states. An example can also be found in the activation of vasti which exhibits large variations depending on the target gait, although its reflexes are kept constant and are not modulated. This behavior is due to the state-dependent excitation provided to each muscle. Indeed, the muscle activation regulated by excitation may vary because of the different states that the muscle is having in different gait conditions (i.e., changing of the gait characteristics) even if the reflex parameters are kept constant. Therefore, the regulation that reflex parameters give to muscle excitation has the final effect of facilitating or preventing changes generated by the muscle state.

Another parameter affecting the step length is the length offset of the hamstrings' stretch reflex during the stance phase. More precisely, increasing the length offset of the hamstrings' stretch reflex results in a faster gait with larger steps. By contrast, decreasing this parameter results in

a slower gait with small steps. Indeed, the length offset defines the muscle fiber length level after which the stretch reflex is active. Therefore, a larger length offset allows the hamstrings to sustain a stretch level due to knee extension and hip flexion. This condition mainly happens in early stance at higher step lengths. Thus, an increased length offset prevents large stretch reflex responses that would produce an undesired knee flexion.

On the other hand, gait modulation with significant effects in all the gait characteristics relies largely on reflexes active during swing preparation or swing phases. The main stretch activity that plays a role in this modulation is the one governing iliopsoas' activity. In fact, the larger length offset of this muscle causes a slower response of the stretch activity resulting in a slower and lower leg lifting typical of gait with reduced speed. Moreover, the decreasing stretch activity of iliopsoas during the swing preparation allows a large hip extension necessary for larger steps when the step length increases.

Then, the fast execution of landing is guaranteed with the modulation of gluteus maximus and hamstring stretch reflexes. The activity of the gluteus maximus during the landing phase is crucial to determine the step period since its higher stretch response allows a faster landing of the foot, increasing the frequency of the gait. On the other hand, the stretch reflex of hamstrings during the landing phase regulates the coherent increase or decrease of step length and step period through the regulation of both reflex gain and offset. The increased activity of hamstrings helps a faster landing phase due to the hip, but it also prevents a full extension of the knee, slightly reducing the step length. Excessive knee flexion is prevented by regulating the length offset that tends to increase linearly with step length. Nevertheless, this regulation tends to slow down the reflex's stretch response less effectively in fast landing.

The modulation of reflex parameters described above involves the regulation of sensory-motor gains (k_F and k_L) and the threshold for the onset of the stretch response (l_0). Physiologically, the modulation of gains can be obtained with the involvement of presynaptic inhibition of afferent activity (Stein, 1991; Zehr and Stein, 1999). Besides, the regulation of descending modulation and γ-motoneurons is thought to contribute to the stretch reflex threshold's modulation (Matthews, 1959). The altered regulation of this reflex component also takes a role in generating motor impairments in gait pathology (Levin and Feldman, 1994).

For the comparison with experimental studies, we found a good match with kinematics and ground reaction forces, especially for hip angles showing higher flexion and extension peaks with increasing speed, step length. Concerning knee flexion, experiments observed lower peaks in knee flexion in swing for very slow gaits. However, we do not find this behavior in our simulations. Still, it should be pointed out that our sensory feedback controller is not able to replicate very slow walking that in experiments reach values of 0.1 m/s, whereas our model cannot walk at speeds below 0.4 m/s. The ankle angle is the one that shows the most important limitations in our simulations. In fact, the model tends to have excessive dorsiflexion in all the solutions found, and in some of them, it shows anticipation in the plantarflexion movement. This behavior is probably also causing anticipation in the second

peak of vertical GRFs. However, the ankle angle and GRFs' modulation resemble the behaviors observed in experiments with larger plantarflexions and higher peaks when speed increases.

Concerning muscle activation, the results are consistent with past experimental studies. The muscles that present the most relevant activity changes are the hamstrings, the iliopsoas, and the gastrocnemius. In simulations, the iliopsoas muscle is also active during the initial stance phase, whereas it is active only during pre-swing and swing in human experiments. This behavior is due to the PD controller stimulating iliopsoas muscle in early stance to maintain the model's balance. Furthermore, human experiments in speed modulation result in a low EMG signal for the iliopsoas muscle, while in our simulations, it appears to have high activity, especially for fast gaits. However, it should be noticed that experimental studies using surface EMGs are limited by muscle deepness. Indeed the iliopsoas is located deep in the trunk, and it is not easy to record its activity (Jiroumaru et al., 2014). Besides, Yokoyama et al. (2017) estimated the motoneurons' activity in the spinal cord and found that the activation ratio between lumbar and sacral segments increases with speed. Therefore, proximal muscles controlled by lumbar segments increase their activity more consistently than distal muscles controlled by sacral segments. We also observe this condition in our results. Indeed, there is a more significant increase in iliopsoas and hamstrings muscle activity than the increasing soleus and gastrocnemius activity when passing from slow to fast speeds.

Finally, the key reflexes' variation achieved the same gait behaviors obtained by optimizing all the controller parameters from the validation performed. Furthermore, not allowing the key parameters to change resulted in a severe limitation of gait modulation. Physiologically, the neural system may modulate additional feedback circuits for human locomotion than the one identified. Yet, the results suggest that the identified reflexes are sufficient to modulate the gait in the contest of purely sensory-driven mechanisms.

Other experimental studies tried to obtain information about the neural circuitries involved in locomotion through indirect measurements. Ivanenko et al. (2000) performed experiments applying vibration to hamstrings muscles. These local effects of vibration can be explained in the light of a lengthening illusion of the vibrated muscle in that phase of the gait cycle where the muscle is lengthened (Verschueren et al., 2002). The results showed that the perturbation to the hamstrings muscle evokes increments in walking speed. In our results, we similarly observed an influence of the hamstrings stretch reflex on walking speed in the first two subphases of stance. Nevertheless, Ivanenko et al. noticed that phasis stimulation was more effective in swing rather than in stance. On the other hand, Verschueren et al. applied tendon vibration separately to tibialis anterior and calf muscles (Verschueren et al., 2002). The results showed a decreased plantarflexion at toe-off when the perturbation was applied to tibialis anterior. In contrast, a decreased dorsiflexion was observed when the same perturbation was applied to the calf muscles. In the end, the authors suggest the involvement of Ia afferent input in the online control of joint rotations. Our study includes stretch Ia excitation for tibialis anterior, but not for calf muscles (soleus and gastrocnemius). However, a progressive decline in soleus H-reflex excitability has also been observed from standing to walking and from walking to

running due to an increased Ia presynaptic inhibition (Angulo-Kinzler et al., 1998; Brooke et al., 1997; Capaday and Stein, 1986; Crenna and Frigo, 1987; Koceja et al., 1995; Koceja et al., 1993; Mynark and Koceja, 1997; Stein and Capaday, 1988). Besides, increased stimulation of the tibialis anterior would probably result in excessive dorsiflexion weakening the plantarflexion in toe-off, as observed by Verschueren et al. (2002). Other studies investigated the effect of trans-spinal stimulation on short-latency tibialis anterior flexion reflex during walking (Zaaya et al., 2020). The reflex facilitation occurred at heel contact and then progressively from late stance reaching its peak at early and late swing phases. These results are coherent with our model's structure where the stretch reflex of the tibialis anterior is active in all the phases of the gait cycle, and it is strongly inhibited by the soleus muscle leading to a peak activity during the swing phase. However, it should be observed that experiments performed by increasing the afferent activity stretching the muscle or by electrical stimulation reveal the effect of the added afferent activity on top of the already ongoing natural baseline activity. Therefore, these experiments investigate primarily the impact of a sudden external perturbation rather than the contribution of afferent activity in locomotion (Nielsen and Sinkjaer, 2002).

A more reliable approach could be the removal of afferent feedback through the effect of sudden unloading. These kinds of experiments mainly investigate group Ib fibers' activity since these are more sensitive to load feedback than group Ia or II (Af Klint et al., 2010). Klint et al. (2008) used a robotic platform changing the surface's inclination to apply small dorsiflexion, and plantarflexion perturbations to the ankle joint in early stance. The results showed that in soleus and gastrocnemius muscles, the modulation of activity increased with inclines and decreased with declines suggesting these muscles to be modulated mainly through Ib fibers. This observation is coherent with the choice made in our controller to regulate plantarflexor activity with positive force feedback stimulation. In the context of task-dependent reflex modulation, significant studies were conducted applying acceleration and deceleration impulses delivered at the time of heel strike during treadmill walking Dietz et al., 1984. It has been observed that the gastrocnemius muscle was inhibited during deceleration and excited during acceleration linking polysynaptic spinal pathways activating gastrocnemius with the gait speed. This behavior is also observed in our analysis, where the positive force feedback gain of gastrocnemius muscle increases its amplitude according to the increasing walking speed.

Furthermore, Gerasimenko et al. (2017) gave a fascinating point of view in the context of sensory control in human locomotion. They proposed that conceptually all sensory information in real-time provided to the brain and spinal cord can be considered as a feedforward phenomenon. Indeed, the central nervous system processes sensory input in a feedforward manner to make fundamental decisions defining motor responses. Therefore, the sensory feedback system integrates into feedforward networks, and it is continuously regulated by them. In this context, the task and phase-dependent spinal reflexes' modulation explored in this study can be seen as part of these feedforward mechanisms in charge of regulating the gait characteristics.

Although this study's results largely reflect findings reported in past experimental studies, some limitations need to be highlighted. First, the lack of DoFs above the pelvis delegates the balance control to hip muscles that are generally not involved in trunk balance. Indeed, the PD controller efficiently stabilizes the gait. However, this mechanism is only a first approximation of the complex neural networks dedicated to regulating balance in human walking involving vestibular and cerebellar systems. The modeling of these networks is very challenging and would require a significant increase in the number o parameters. Nevertheless, the detailed representation of balance mechanisms is beyond the scope of this study. Furthermore, the controller investigated could not achieve extremely slow speeds below 0.4 m/s that we can observe in human experiments (Wu et al., 2019). This is probably because, at those speeds, there is a major involvement of descending control from brain areas (e.g. for balance control) that are not modeled in the reflex-based controller. Besides, the proposed controller relies on a state machine mechanism for the cyclic activation of reflexes, the control of which is most probably delegated to mutual inhibition of antagonist muscle or rhythmic circuits located in the spinal cord. Indeed, central pattern generators may play a crucial role in modulating locomotion through phasic feedforward signals and temporal activation of spinal circuits. In our study, we decided to focus on the modulation of sensory feedback mechanism alone since abstract models of central pattern generators basing their rhythmic patterns on sensory feedback and muscle synergies have already demonstrated to be able to modulate walking and running behaviors (Aoi et al., 2019; Dzeladini et al., 2014; Van der Noot et al., 2015).

The neuromotor control of gait modulation is a highly redundant problem. Multiple combinations could have similar effects since the model's simplification does not consider other circuits likely to influence gait modulation. Nevertheless, considering that direct experiments are challenging to perform on humans, this modeling approach could be informative and of significant value concerning the spinal sensory circuits that high-level centers may modulate to change gait characteristics. In this context, the modulation of key parameters investigated should be considered as one of the many possible strategies that the central nervous system may perform to modulate human gait. Future works should focus on the combined modulation of feedforward and feedback circuits with detailed models of the spinal cord, as already implemented for mouse models (Ausborn et al., 2019). Furthermore, other aspects of human walking modulation involving higher voluntary control should be investigated. More experiments could target the modeling of specific motor behaviors, such as high ground clearance, stair climbing, walking on slopes, and obstacle avoidance. Moreover, the investigation of bioinspired controllers by including neural feedback and feedforward mechanisms would permit to explore other neuromotor control theories in human locomotion, such as the proximal-distal gradient control observed in animal experiments (Daley et al., 2007).

2.6 Conclusion

In this work, we investigated the nature of sensory reflex modulation potentially behind the generation of different walking behaviors using neuromuscular simulation tools. We

focused on studying the modulation of speed, step length, and step duration, identifying the main reflexes that could be responsible for the modulation of the three gait characteristics. Hamstrings length stretch reflexes and plantarflexors positive force feedbacks during stance were found to have a primary effect on step length modulation. On the other hand, stretch reflexes of iliopsoas, hamstrings, gluteus maximus, and tibialis anterior active during pre-swing, swing, and landing were found to modulate both step length and step duration. These reflexes were found to be sufficient and necessary to modulate a wide range of the three gait characteristics under analysis. Furthermore, the solutions obtained showed similarities with previous experimental studies on gait modulation in terms of kinematics, ground reaction forces, and muscle activation (Y. Ivanenko et al., 2000; Lim et al., 2017; Schwartz et al., 2008; Wu et al., 2019; Yokoyama et al., 2017) and with experiments investigating the activation of sensory afferents in human walking (Dietz et al., 1984; Klint et al., 2008; Verschueren et al., 2002; Zaaya et al., 2020). This study provides a first contribution to the modulation of human locomotion in simulation environments based on physiologically relevant neural feedback circuits.

Future directions should focus on investigating the joint contribution of feedforward and feedback neural components in the modulation of human gait as well as the potential neural mechanisms behind the sensory feedback modulation. This investigation will be conducted in chapter 4 using a novel neuromuscular controller for human locomotion. Before presenting the new controller, we will first explore the capabilities of traditional sensory-based controllers to reproduce pathological gaits in the next chapter.

Supplementary Information

The data used, figures and videos can be found at the following link: https://doi.org/10.5281/zenodo.4719785.

3 Investigation of neural and biomechanical parameters leading to pathological toe and heel gaits through neuromusculoskeletal modeling

Overview

In the previous chapter, we investigated the capability of sensory-based controllers to reproduce different behaviors in healthy human locomotion. Here, we investigate the capability of the same kind of controllers to explain pathological behaviors commonly observed in CP patients, like toe and heel walking.

3.1 Abstract

This study investigates the pathological toe and heel gaits seen in human locomotion using neuromusculoskeletal modeling and simulation. In particular, it aims to investigate potential cause–effect relationships between biomechanical or neural impairments and pathological gaits. Toe and heel gaits are commonly present in spinal cord injury, stroke, and cerebral palsy. Toe walking is mainly attributed to spasticity and contracture at plantarflexor muscles, whereas heel walking can be attributed to muscle weakness of biomechanical or neural origin. To investigate the effect of these impairments on gait, this study focuses on the soleus and gastrocnemius muscles as they contribute to ankle plantarflexion. We built a reflex circuit model based on previous work by Geyer and Herr with additional pathways affecting the plantarflexor muscles. The SCONE software, which provides optimization tools for 2D neuromechanical simulation of human locomotion, is used to optimize the corresponding reflex parameters and simulate healthy gait. We then modeled various bilateral plantarflexor biomechanical and neural impairments and individually introduced them in the healthy model. We characterized the resulting simulated gaits as pathological or not by comparing ankle kinematics with the healthy optimized gait based on metrics used in clinical studies. Our simulations suggest that toe walking can be generated by hyperreflexia, whereas muscle and neural weaknesses partially induce heel gait. Thus, this 'what if' approach is deemed of great interest as it allows investigation of the effect of various impairments on gait and suggests an important contribution of active reflex mechanisms to pathological toe gait.

3.2 Introduction

Human locomotion relies on complex interactions between the musculoskeletal system, spinal circuits, sensory reflex pathways, descending pathways, and the environment (Rossignol et al., 2006). Neuromusculoskeletal modeling is a powerful tool to study these complex interactions and the contribution of each of these motor control components, as it allows for the systematic evaluation of different models and parameters. Neuromusculoskeletal modeling has thus been used to study and understand human locomotion. Nevertheless, abnormal gaits resulting from illness or injury are less often modeled. Indeed, pathological gaits can have several causes ranging from biomechanical to neural impairments. Neuromusculoskeletal modeling can help target and understand impaired mechanisms leading to pathological gaits by evaluating a model with altered parameters (Ong et al., 2019).

This study aims to investigate the effect of both biomechanical and neural impairments on gait using neuromusculoskeletal simulation. Two pathological gaits common in several conditions, such as spinal cord injury (SCI), stroke, and cerebral palsy (CP) are studied, namely toe and heel gaits. Toe walking, also called equinus gait, is a gait in which there is continuous ankle plantarflexion throughout the stance phase (Nieuwenhuys et al., 2016). This gait deviation is mainly attributed to spasticity and contracture at plantarflexor muscles that are present in SCI, stroke, and CP conditions (Armand et al., 2016; Attias et al., 2017; Crenna, 1998; Lamontagne

et al., 2002; Matjačić et al., 2006; Van Der Salm et al., 2005). The most common definition of spasticity is from Lancel et al. (1980b), stating that spasticity is a motor disorder, characterized by a velocity-dependent increase in tonic stretch reflexes, resulting from hyperexcitability of the stretch reflex. Spastic hyperreflexia is mainly due to increased alpha motor neuron excitability (Leech et al., 2018; Marque et al., 2001), reduction of presynaptic inhibition (Calancie et al., 1993; Faist et al., 1994), and reduction of reciprocal inhibition (Knikou and Mummidisetty, 2011) to reciprocal facilitation (Crone et al., 2003; Xia and Rymer, 2005). Biomechanical changes within both muscle–tendon unit cells and extracellular matrix collagen fibers can also contribute to spastic conditions by inducing a stiffer muscle–tendon unit (Diong et al., 2012; Lieber et al., 2004). In the long term, spasticity can also lead to the shortening of the muscle–tendon complex resulting in muscle contracture (Gracies, 2005b). For its part, heel walking, also called calcaneus gait, is a gait in which there is an excessive ankle dorsiflexion during the stance phase (Nieuwenhuys et al., 2016). This gait deviation is mainly attributed to muscle weakness that is also present in SCI, stroke, and CP conditions (Armand et al., 2016; Bohannon, 2007; Elder et al., 2003; Thomas et al., 1997). Muscle weakness is a lack of muscle strength that can be induced by muscle diseases, but also by deficits in the neural drive leading to muscle atrophy (Thomas et al., 1997). Thus, both toe and heel gaits present impaired mechanisms that can have neural or biomechanical origins.

Several neuromechanical models of human locomotion have been developed over the years. The existence and contribution of central pattern generators (CPGs) producing rhythmic patterns in spinal circuits appear to be fundamental for lower vertebrate locomotion (Kiehn, 2016). However, they are still discussed for human locomotion that would rely on more important sensory reflex pathways and descending pathways (Minassian et al., 2017; Sinkjær et al., 2000). Several neuromechanical models include both CPGs and sensory feedbacks to simulate human locomotion (Aoi et al., 2019; Ryu and Kuo, 2021; Taga, 1995. On another note, Geyer and Herr (2010) developed a purely reflex-based model encoding the principles of legged mechanics and reproducing human walking kinematics, dynamics, and muscle activation. Song and Geyer (2015) extended this model with additional muscle velocity feedback and generated various behaviors of human locomotion, from walking on a slope to running. Ong et al. (2019) also simulated human walking through a model based on muscle length, velocity, and force reflexes. The modulation of walking speed, step length, and step duration by these reflexes was further studied by Di Russo et al. (2021). These models, including more reflex pathways, are more in line with physiological mechanisms. The present study similarly builds on Geyer and Herr's model by introducing additional reflex pathways affecting the soleus (SOL) and gastrocnemius (GAS), and their antagonist muscle tibialis anterior (TA) to more closely reproduce physiological mechanisms and simulate impairments. This study focuses particularly on the SOL and GAS muscles as they contribute to ankle plantarflexion, and are thus usually involved in both toe and heel gaits.

Previous studies also modeled spasticity or muscle weakness through neural or biomechanical impairments. Van der Krogt et al. (2016) modeled spasticity in CP children with the velocity-dependent stretch reflex. That model replicated hamstrings (HAMS) EMG global shape during

passive stretching but did not reproduce EMG fast variations. Falisse et al. (2018) also studied spasticity in CP children and compared three models based on velocity, acceleration, and force feedback. The force-related model predicted HAMS and GAS activity that better correlated with measured activity during gait compared with the two other models. Jansen et al. (2014) simulated increased length and velocity feedbacks and altered reflex modulation patterns of lower limb muscles. They reproduced hemiparetic gait deviations, but they could not distinguish the contributions of the two pathways. Song and Geyer (2018) simulated the major contribution of loss of muscle strength and contraction speed in walking speed and efficiency decline with aging based on Song and Geyer (2015). Waterval et al. (2021) also reproduced most gait changes due to bilateral plantarflexor weakness based on Geyer and Herr's model. Similarly, Ong et al. (2019) modeled SOL and GAS weakness and contracture with respectively reduced maximal isometric force and reduced muscle fiber optimal length. Severe plantarflexor weakness resulted in heel walking, whereas severe contracture resulted in toe walking simulation.

By investigating the effect of both biomechanical and neural impairments on gait, the present study addresses the following question: can we identify specific biomechanical and neural causes inducing the pathological toe and heel gaits?

To answer this, we developed a reflex circuit model by extending Geyer and Herr's reflex circuits with additional pathways affecting the SOL and GAS muscles, and their antagonist muscle TA. The model introduces additional force, spindle, and length direct pathways for these three muscles and reciprocal spindle pathways between plantarflexors and TA. Since the objective of this study is to reproduce toe and heel walking, we focus our attention mainly on the ankle angle. The SCONE software (Geijtenbeek, 2019), which provides optimization tools for 2D neuromechanical simulation of human locomotion based on Geyer and Herr's work, is used to optimize the parameters of this reflex circuit model and simulate a healthy gait. We then modeled various bilateral plantarflexor biomechanical and neural impairments through decreased or increased parameter values. Biomechanical parameters are altered to model muscle weakness and reduced muscle fiber length. Regarding reflex parameters, they are modified to model hyperreflexia, reduction of presynaptic inhibition, reduction of reciprocal inhibition, and neural weakness. We individually introduced each of these modeled impairments in the healthy model and simulated the gait resulting from new optimization. All these simulated gaits then need to be characterized as pathological or not. To do so, we compared the ankle kinematics of each impaired evaluation with the healthy optimization based on metrics used in clinical studies.

3.3 Methods

This section presents the methods, including the SCONE software simulation framework, the developed reflex circuit model, the modeled biomechanical and neural impairments, and the pathological gait characterization. All the necessary files to reproduce this study are provided
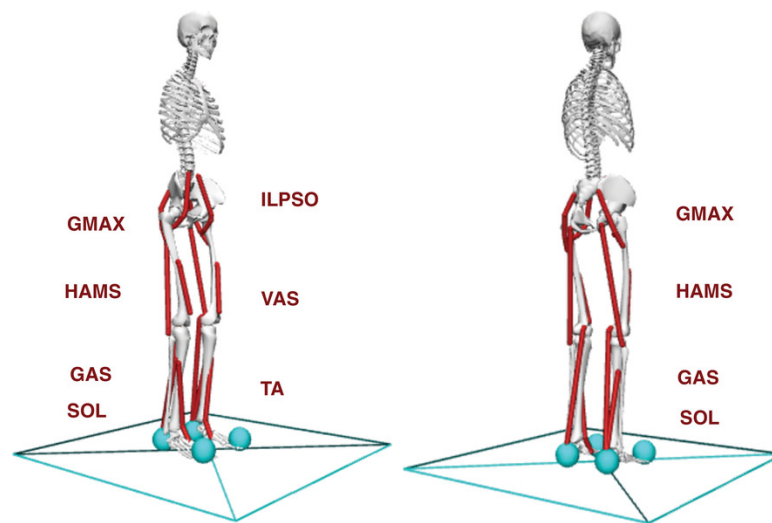
Figure 3.1: OpenSim musculoskeletal model.
Composed of three degrees of freedom per leg, at the hip, knee, and ankle joints, and seven Hill-based muscles per leg: iliopsoas (ILPSO), vasti (VAS) and tibialis anterior (TA), gluteus maximus (GMAX), hamstrings (HAMS), gastrocnemius (GAS), and soleus (SOL).

in a GitHub repository shared in https://github.com/AliceBrue/pathological_gait.git.

3.3.1 SCONE simulation

Gait simulations were performed with the SCONE software (Geijtenbeek, 2019). that is based on the following four blocks:

1. An OpenSim musculoskeletal model: here, we use a model based on Delp et al. (1990). This model represents an adult of about 1.8 m and 75 kg. It is constrained in the sagittal plane with three degrees of freedom (DOF) per leg, namely at the hip, knee, and ankle joints, and a 3 DOF planar joint between the pelvis and the ground. This model is composed of seven Hill-based muscles with tendon compliance (Millard et al., 2013) per leg shown in Figure 3.1: gluteus maximus (GMAX), HAMS, iliopsoas (ILSPO), vasti (VAS), gastrocnemius (GAS), soleus (SOL) and tibialis anterior (TA). Muscle–tendon parameters are taken from Delp et al. (1990), which is based on experimental data. To estimate the ground reaction forces, a compliant contact model is used with one viscoelastic Hunt–Crossley sphere representing the heel and another one representing the toes (Hunt and Crossley, 1975).

2. A controller: here, we use a reflex circuit controller adapted from Geyer and Herr's (2003) model. This controller is composed of several state-dependent control law primitives, including feedforward, muscle reflex and pelvis tilt proportional-derivative primitives. These different components are detailed below with the extended reflex circuit model

that is developed for this study.

3. Measures that are minimized through the optimization as components of the cost function: here, we considered the following human walking goals as measures:

- A gait measure penalizing falling and walking speed lower than a minimum speed: This gait measure takes values between 1, when the model falls at the first step, and 0, when the model does not fall, and the velocity condition is met. The model is considered to fall when the ratio between its center of mass height (h_{COM}) to the initial state ($h_{COM,i}$) is smaller than a termination height threshold set to 0.8 ($\frac{h_{COM}}{h_{COM,i}} < 0.8$). For each step ($s$), the step end time ($t_{s,end}$) and step speed ($v_s$) are then respectively compared to potential falling time (t_{fall}) and a minimum speed (v_{min}) set to 1.0 m/s. The resulting gait measure is:

$$J_{gt} = 1 - \frac{1}{N_{Steps}} \sum_{s \in Steps} p(t_{s,end}, v_s) \tag{3.1}$$

where:
$$\begin{aligned} p(t_{s,end}, v_s) &= 0 \quad \text{if} \quad t_{s,end} = t_{fall} \\ p(t_{s,end}, v_s) &= \frac{v_s}{v_{min}} \quad \text{if} \quad v_s < v_{min} \\ p(t_{s,end}, v_s) &= 1 \quad \text{if} \quad v_s \leq v_{min} \end{aligned}$$

- An effort measure from Wang et al. (2012) minimizing muscles metabolic energy:

$$J_{eff} = \frac{1}{m \cdot L} (\dot{B} + \sum_{m \in Muscles} \dot{E_m}) \tag{3.2}$$

where m is the body mass, L is the traveled distance, $\dot{B}$ is the basal metabolic energy rate set to 1.51 times the body mass, and $\dot{E_m}$ is the mean rate of metabolic energy expenditure for a given muscle throughout the simulation.

- A joint measure penalizing non-physiological movements by minimizing the knee limit force (F_{lim}) representing knee ligaments (Veerkamp et al., 2021). This measure also penalizes the overextension of the other joints (ankle, hip, pelvis) by penalizing the corresponding joint angles (α_{jt}) overcoming experimental ranges from Schwartz et al. (2008) ($[\alpha_{jt,min}, \alpha_{jt,max}]$). These experimental ranges are more precisely [0, 15] degrees for the pelvis retroversion–anteversion, [20, 40] degrees for the hip extension–flexion, and [30, 15] degrees for the plantarflexion–dorsiflexion. The resulting joint measure is:

$$J_{jt} = \int_0^{t_{end}} F_{lim}(t)dt + \sum_{jt \in Joints} \int_0^{t_{end}} max(\alpha_{jt}(t) - \alpha_{jt,max}, \alpha_{jt,min} - \alpha_{jt}(t), 0)dt \tag{3.3}$$

These measures finally result in the following cost of function with the same weights as Ong et al. (2019) who defined them to balance competing objectives:

$$J_{tot} = w_{gt} \cdot J_{gt} + w_{eff} \cdot J_{eff} + \sum_{jt \in Joints} w_{jt} \cdot J_{jt} \tag{3.4}$$

with $w_{gt} = 100$, $w_{eff} = 0.1$, and $w_{jt} = 1$

4. An optimizer that optimizes the initial conditions and controller parameters to minimize the previous measures: here the Covariance Matrix Adaptation Evolutionary Strategy (CMA-ES) from Igel et al. (2007) is applied to optimize about 100 parameters of the reflex circuit model. The population size of each generation (λ) is set to 40 and the initial step size (σ) is set to 5.

This optimization scheme is thus used to generate a healthy gait of 15 s. We stopped the optimization when a mean diminution of the cost function <5% was reached between successive optimization steps. About 5000 generations of CMA-ES were necessary to fulfill this condition. The corresponding simulated gait is stable and reproduces human walking kinematics and muscle activation as presented in more detail below. The generation of optimizations with modeling pathological impairments is described below.

3.3.2 Reflex circuit model

This subsection first presents the baseline reflex-based model developed by Geyer and Herr (2010). Our extension, which introduces additional pathways affecting the SOL and GAS muscles, and their antagonist muscle TA, is then presented.

Baseline reflex circuit model

The baseline reflex circuit model is taken from Geyer and Herr's work with a reflex-based controller composed of several state-dependent control law primitives, including feedforward, muscle reflex, and pelvis tilt proportional–derivative primitives as summarised in Figure 3.2. A feedforward component provides a feedforward constant excitation to each muscle actuator modeling supraspinal drive. A muscle reflex primitive accepts as input the sensed normalized fiber length (L) or force (F). A muscle reflex primitive based on X then provides the following muscle excitation:

$$u_X = KX \cdot [X(t - t_D) - X_0]_+ \tag{3.5}$$

where KX is the reflex gain, the sign of which is indicated by the sign of the reflex (X+) or (X-), t_D is the reflex delay, X_0 is the reflex offset and $[x]_+ = max(x, 0)$.

Geyer and Herr's reflex primitives are positive feedback laws onto the same muscle, except the negative force feedback law from the SOL to the TA and the length feedback law from the HAMS to the ILPSO. Reflex gains and offsets are optimized parameters, whereas reflex delays are fixed. Similarly, the pelvis tilt proportional derivative component provides such muscle excitation based on the pelvis angle and angular velocity for balance control. Muscle

	Stance			Swing	
	ES	MS	PS	S	LP
GMAX	PD+, C		C	F+	
HAMS	PD+, C			F+	
ILPSO	PD-, C		C	L+, L- (HAMS)	
VAS	C, F+				
SOL	F+				
GAS	F+				
TA	L+, F- (SOL)				

Figure 3.2: Reflex-based controller from Geyer and Herr (2010).
The controller is composed of feedforward (C), muscle reflexes, and pelvis tilt proportional-derivative (PD) primitives. The reflex primitives are based on normalized muscle length (L) or force (F). They are positive feedback laws onto the same muscle (L+, F+), except the negative force feedback law from the SOL to the TA ($F-_{(SOL)}$) and length feedback law from the HAMS to the ILPSO ($L-_{(HAMS)}$). All these components are state-dependent with 5 states: early stance (ES), mid stance (MS), pre-swing (PS), swing (S), and landing preparation (LP).

activation is then calculated from the sum of the muscle excitation using a first-order dynamic model, with activation and deactivation time constants of 10 and 40 ms, respectively.

Moreover, all these primitives are state-dependent on five states: early stance (ES), mid-stance (MS), and pre-swing (PS) for the stance phase, and swing (S) and landing preparation (LP) for the swing phase. This state dependency reproduces the phase-dependent modulation of neural pathways that occurs during gait. Neural feedbacks are indeed modulated between stance and swing phases due to presynaptic inhibition and other descending modulation mechanisms (Büschges and El Manira, 1998; Meunier and Pierrot-Deseilligny, 1998; Prochazka, 1989). Thresholds for the ground reaction force (GRF) on the ipsilateral foot and for the distance between the ipsilateral foot and pelvis are optimized to determine the transition between these states.

In order to better link Geyer and Herr's reflex rules to actual neural circuits and to facilitate the introduction of additional reflexes (see next section), we have mapped the rules to a neural circuit for SOL, GAS, and TA muscles in 3.3a. The Ib afferent disynaptic pathway from plantarflexor Golgi tendon organ (GTO) to alpha motor neuron provides the force feedback. The corresponding reflex is defined as positive and represented through an excitatory interneuron during the stance states to model Ib facilitation during late stance (Af Klint et al., 2010; Faist et al., 2006). Such a pathway providing feedback from a muscle to itself is referred to as a direct pathway. By opposition, a pathway that provides feedback from a muscle to its antagonist's muscle is a reciprocal pathway. TA is also included in this representation as it is coupled with

SOL by such an Ib reciprocal pathway. This force reflex from the SOL to the TA is defined as negative and represented through an inhibitory interneuron to model reciprocal inhibition. TA also receives positive length feedback from its muscle spindle through a II afferent disynaptic pathway. Regarding pathway delays, Ong et al. (2019) fix direct reflex delays to 20 ms (compared with 5 and 10 ms for hip and knee muscles, respectively). In contrast, Ong et al. fix the Ib reciprocal reflex from the SOL to the TA delay to 40 ms, since reciprocal reflexes involve longer pathways and are thus more delayed (Crone et al., 1987). Nevertheless, note that these delays are shorter than those recorded experimentally by an order of 50% (Frijns et al., 1997).

(a) Neural circuit from Geyer and Herr (2010).

(b) Neural circuit in our extended model.

(c) Reflex primitives from Geyer and Herr (2010).

(d) Reflex primitives in our extended model.
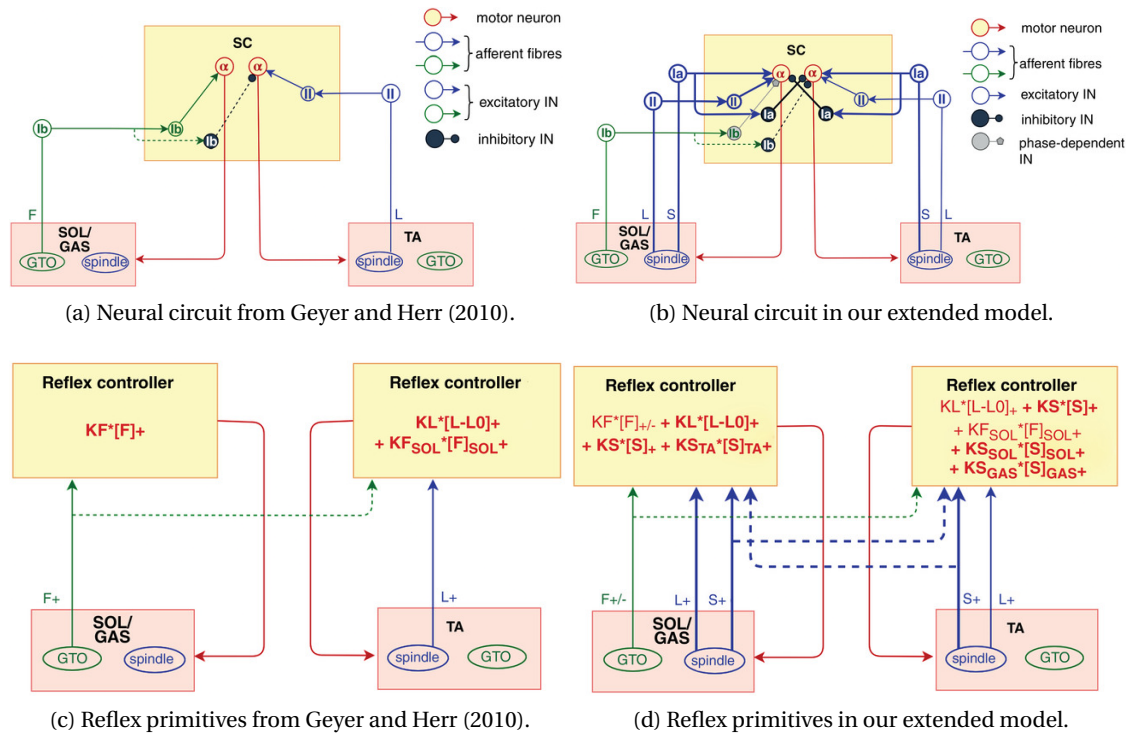
Figure 3.3: Representations of SOL, GAS, and TA reflex circuit model from Geyer and Herr (2010) and our extended model including additional direct and reciprocal pathways.
3.3a) neural circuit implementation of Geyer and Herr's reflex rules for SOL, GAS and TA muscles. The Ib disynaptic pathway from plantarflexor GTO to alpha motor neuron provides positive force (F) feedback, the Ib reciprocal pathway from SOL GTO to TA alpha motor neuron provides negative force feedback, and the II disynaptic pathway from TA spindle to plantarflexor alpha motor neuron provides positive length (L) feedback. 3.3b) neural circuit implementation of our extended model: the additional pathways are indicated in bold. The Ia monosynaptic pathway from muscle spindle to alpha motor neuron provides positive spindle (S) feedback reproducing the stretch reflex. The II disynaptic pathway from muscle spindle to alpha motor neuron provides positive length feedback. The Ia reciprocal pathway from muscle spindle to antagonist alpha motor neuron provides negative spindle feedback mimicking reciprocal inhibition. 3.3c) controller reflex primitives from Geyer and Herr (2010). 3.3d) controller reflex primitives corresponding to our extended model: SOL, GAS, and TA direct and reciprocal L and S reflexes are added to the previous primitives.

More complex reflex circuit model for SOL, GAS, and TA muscles

Based on the previous model, we developed a more complex reflex circuit model with additional SOL, GAS, and TA pathways. Spindle Ia and II afferent direct pathways are added to study three types of feedback, namely force, spindle, and length direct feedback. The Ia afferent pathway indeed provides major muscle velocity and length feedback and is involved in the common stretch reflex. As plantarflexors Ib and TA II direct pathways in Ong et al. (2019), we set the delay of these direct pathways to 20 ms. Moreover, reciprocal inhibition pathways between the antagonist's muscles are also present and important in physiological mechanisms. Indeed, if the antagonist's muscles contract simultaneously, they work against each other, leading to extra effort and potential muscle tear. Reciprocal inhibition pathways prevent such co-contraction and, in this way, participate in movement facilitation and muscle protection. Thus, to study these determinant pathways, we also introduced spindle Ia reciprocal reflexes between plantarflexors and TA in the model as represented in 3.3b and 3.3d. As SOL to TA Ib reciprocal pathway, these reciprocal reflexes are modeled with disynaptic pathways, and their delays are set to 40 ms. For the SOL to TA Ib reciprocal pathway, we modeled these reciprocal reflexes with disynaptic pathways and we set their delays to 40 ms. To summarise, the additional pathways introduced in this more complex model are tabulated in Figure 3.4 and are as follows:

- SOL, GAS, and TA Ia direct pathway: this pathway provides velocity and length feedback from the muscle spindle. The corresponding primitive in the SCONE controller is based on the spindle rate from Prochazka (1999)as a function of both muscle stretch velocity and length ($\alpha \cdot v^{0.6} + \beta \cdot l + \gamma$). It is modeled with a monosynaptic pathway and is defined as positive to reproduce the excitatory stretch reflex (Pierrot-Deseilligny and Burke, 2005). This reflex is mainly involved in plantarflexor activation during gait (Yang et al., 1991).

- SOL and GAS II direct pathway: this pathway provides length feedback from the muscle spindle. It is modeled with a disynaptic pathway and is defined as positive to mimic the disynaptic II excitation in line with the literature (Lundberg et al., 1987; Pierrot-Deseilligny and Burke, 2005);

- SOL and GAS Ib direct pathway during the swing: as described above, this pathway provides force feedback from the GTO. It is modeled with a disynaptic pathway in line with the literature (Pierrot-Deseilligny and Burke, 2005; Stephens and Yang, 1996). It is defined as positive during the stance states to reproduce the plantarflexor Ib facilitation that occurs during late stance (Af Klint et al., 2010; Faist et al., 2006). In contrast, it is defined as negative during the swing states to reproduce the common Golgi tendon reflex regulating muscle tension.

- Plantarflexor to TA Ia reciprocal pathway: this pathway provides negative spindle feedback from the plantarflexors to the TA. It is modeled with a disynaptic inhibitory pathway

and is defined as negative to mimic the common reciprocal inhibition between antagonist muscles (Pierrot-Deseilligny and Burke, 2005).

- TA to plantarflexor Ia reciprocal pathway: this pathway similarly provides negative spindle feedback from the TA to the plantarflexors through a disynaptic inhibitory pathway to mimic reciprocal inhibition.

	Stance			Swing	
	ES	MS	PS	S	LP
GMAX	PD+, C		C	F+	
HAMS	PD+, C			F+	
ILPSO	PD-, C		C	L+, L- (HAMS)	
VAS	C, F+				
SOL	F+, **L+, S+**			**F-, L+, S+**	
	S- (TA)			**S- (TA)**	
GAS	F+, **L+, S+**			**F-, L+, S+**	
	S- (TA)			**S- (TA)**	
TA	**L+, S+**			**L+, S+**	
	F- (SOL), S- (SOL), S- (GAS)			**F- (SOL), S- (SOL), S- (GAS)**	

Figure 3.4: Extended gait controller from Geyer and Herr (2010).
The additional SOL, GAS, and TA direct and reciprocal reflexes are indicated in blue. For instance, S_+ means a positive direct spindle reflex from the muscle to itself, whereas S_{-TA} means a negative reciprocal spindle reflex from the TA to the muscle.

As detailed above, we fixed the signs of the controller primitives (as opposed to being open for optimization) as there is experimental evidence of the excitatory or inhibitory nature of the corresponding pathways that we wanted to account for (Pierrot-Deseilligny and Burke, 2005).

3.3.3 Modeled impairments

The effect of biomechanical and neural impairments is investigated by individually modifying various bilateral plantarflexor biomechanical and reflex parameters. Biomechanical parameters are altered to reproduce plantarflexor weakness and reduced muscle fiber length. As

for reflex parameters, they are modified to mimic plantarflexor hyperreflexia, reduction of presynaptic and reciprocal inhibition, and neural weakness. This subsection presents these parameters of interest. For each of them, SOL and GAS values are altered simultaneously and by the same percentage of the corresponding healthy optimization values as these muscles are agonists and commonly impaired simultaneously (Armand et al., 2016; Neyroud et al., 2017; van der Krogt et al., 2010.

Biomechanical impairments

Muscle biomechanical properties are defined in the OpenSim musculoskeletal model through maximal isometric force, optimal muscle fiber length, tendon slack length, pennation angle parameters, and muscle fiber and tendon force–length and force–velocity curves. We investigate the following parameters:

- Plantarflexors maximal isometric force, F_{max}: this parameter is evaluated with decreased values to model muscle weakness;

- Plantarflexors optimal fiber length, $l_0{}^{fib}$: this parameter is evaluated with decreased values to reproduce muscle fiber shortening.

Neural impairments

Impairments of both direct and reciprocal pathways affecting the plantarflexors are modeled. As mentioned above, reflex feedbacks are modulated between gait phases. Thus, we investigate each of the following reflexes during the stance or swing states:

- Plantarflexor spindle reflex gains during the stance (ST) and swing (SW) phases, KS^{ST} and KS^{SW}: these parameters are evaluated with increased values to model spastic hyperreflexia and reduction of presynaptic inhibition. KS^{ST} is also evaluated with decreased values to model neural weakness. By contrast, KS^{SW} is not evaluated with decreased values as plantarflexor muscles are mainly activated during the stance phase.

- Plantarflexors length reflex gains during the stance and swing phases, KL^{ST} and KL^{SW}: these parameters are similarly evaluated with increased values to reproduce hyperreflexia and KL^{ST} is evaluated with reduced values to mimic neural weakness.

- Plantarflexors force reflex gain during the stance phase, KF^{ST}: this parameter is evaluated with both increased and decreased values to reproduce hyperreflexia and neural weakness, respectively.

- TA to plantarflexor spindle reflex gains during the stance and swing phases, KS_{TA}^{ST} and KS_{TA}^{SW}: as these reciprocal reflexes are negative, their gains are evaluated with decreased

absolute values corresponding to increased real values to reproduce a reduction of reciprocal inhibition. Further, positive gains mimic reciprocal facilitation that abnormally excites antagonist muscles after switching from reciprocal inhibition to facilitation.

3.3.4   Generation and automation of pathological gaits optimizations

Each parameter alteration of interest detailed above is individually induced in the model for a range of altered values, resulting in a gait without fall after optimization. To do so, we define a broad range of altered values as a percentage of the corresponding healthy optimization value. We set the altered values to both SOL and GAS of both legs for a biomechanical or reflex parameter. In this last case, the reflex parameter is fixed and will not be optimized. Meanwhile, the variation of the remaining reflex parameters is constrained. Some impairments occur gradually along with neural adaptations, such as in CP, whereas other impairments can be sudden, for instance, after stroke or SCI. Compensation through neural adaptations may also arise in these pathological conditions, especially after training (Knikou and Mummidisetty, 2011; A. C. Smith et al., 2015). Nevertheless, such adaptations are difficult to study through simulation as we do not know the cost function in pathological conditions. Indeed, in addition to effort minimization, pain avoidance, which is difficult to compute, might play an important role in defining the gait targets in pathological (Fish and Nielsen, 1993). The goal is here to systematically study the strict and short-term effect of various individual impairments on gait (and therefore to stay close to the healthy parameter values, except for the altered parameters). The remaining reflex parameters are thus set to the corresponding healthy optimization values with a limited variety of 5% allowed for the optimizer to act upon. Each parameter is drawn from a Gaussian distribution characterized by its mean and standard deviation (SD). Furthermore, each parameter is also upper and lower bounded to reject parameters outside a permissible range. Thus, to constrain a parameter from varying from the baseline, we set its upper and lower boundaries with a small SD from the healthy optimization results. For biomechanical parameter alterations, optimizations are run with all the reflex parameters set to their healthy optimization value with a limited variety of 5% (with smaller limited variations, optimizations could not reach gaits without falling for small alterations). We apply this strategy to limit potential compensation from other muscle reflexes while at the same time offering some flexibility that allows optimizations to reach gaits without falling.

We adapt the cost functions used for optimizing the healthy gait by considering a lower minimum speed set to 0.5 m/s and larger joint ranges for the joint measure. Each extremum is more precisely set to two times the previous extremum, leading to the following ranges: for the pelvis, hip, and ankle, respectively: [30, 15] degrees for the pelvis retroversion–anteversion, [40, 80] degrees for the hip extension–flexion and [60, 30] degrees for the plantarflexion–dorsiflexion. Each of these pathological gaits optimizations is then run over 500 iterations. Here we do not define any specific stopping condition, but we limit the number of iterations to reach a gait without immediate fall. If an optimization does not reach such a gait (i.e., if the simulation falls immediately without taking 12 steps), we do not consider the corresponding altered value.

The optimization method introduces randomness in the initial conditions and parameters so that the population of solutions tends to lead to similar conclusions. To further check the repeatability of our results, we ran several optimization trials with various initial conditions (IC) for some of the altered parameters. We consider the IC we use for the results presented above and modify each joint by +10 or 10°. We number these various IC from 1 to 6 with $IC1$ the IC used for the main results, $IC2$ the same IC with the right hip with +10 degrees, $IC3$ with the right knee with 10 degrees, $IC4$ with the right ankle with +10 degrees, $IC5$ with the left knee with 10 degrees and $IC6$ with the left ankle with +10 degrees. Then for each IC, we compute the mean absolute error between the mean ankle angle over the gait cycle and the mean ankle angle over the gait cycle of $IC1$ ($MAE_{IC1\alpha}$). Moreover, we compute the mean relative error between the optimized parameters and the optimized parameters of $IC1$ (MRE_{IC1p}). Thus, we can check if the various optimization trials result in similar results in terms of kinematics and parameter values.

Finally, we further this one-dimensional (1D) exploration with a two-dimensional (2D) exploration in which some reflex parameters are investigated together (see some examples below). We determine the pairs of parameters of interest later according to the results of the 1D exploration. optimizations are similarly run with the values of two parameters altered simultaneously, and limited variation is allowed on the remaining ones. The previous 1D exploration ranges define the 2D space of altered values.

3.3.5 Pathological gait characterizations

All these parameter alteration evaluations result in simulated gaits that need to be characterized as pathological or not. Toe walking is characterized by an excessive ankle plantarflexion throughout the stance phase, an absence of the first ankle rocker, and an early third ankle rocker (Alvarez et al., 2007). The first and third ankle rockers correspond to the ankle plantarflexion movements, respectively from heel-strike to flat foot on the ground at the beginning of the stance phase, and from heel-off to toe-off at the end of the stance phase (Brockett and Chapman, 2016). Severe toe gaits present all the previous deviations, whereas mild to moderate toe gaits do not necessarily present rocker deviations (Alvarez et al., 2007). Heel walking is characterized by an increased slope towards dorsiflexion or a dorsiflexion peak >20 degrees (Nieuwenhuys et al., 2016). Each simulated gait contains about 12 gait cycles that may present variability. To consider this variability while distinguishing initial transitions depending on initial conditions from steady-state behavior (the steady states can show variability), we compute each metric described below on each gait cycle except the first one and compute their mean and SD. Thus, we define the following metrics based on ankle kinematics to characterize simulated gaits.

Ankle kinematics comparison

For each investigated parameter, we plot the mean hip, knee, and ankle angles (ankle angle is noted α) over the gait cycles of each altered value. We extract and normalize each gait cycle to gait cycle percentage ([0, 100]). Then, we interpolate each gait cycle joint angle on the mean gait cycle and average the joint angles over the gait cycles. We similarly plot the mean joint angles of the healthy optimization (healthy ankle angle is noted α_h). Thus, we can compare the effect of the alterations on the ankle profile, particularly on the ankle rockers. The initiation time of the third ankle rocker is computed from the ankle velocity when it takes a null value. Based on Alvarez et al. (2007), we consider a simulated gait as toe gait if the third ankle rocker occurs before 30% of the gait cycle, compared to healthy gait presenting a third ankle rocker at the end of the stance phase (after 40% of the gait cycle). We name this criterium $C_{toe}1$.

For each simulation, we also compute the mean and the maximum ankle angle (α and α_{max}) during each MS and PS period that we hereafter name ST (ST = MS + PS):

$$\begin{cases} \bar{\alpha}^{ST} = \frac{1}{N_{ST}} \sum_{n \in ST} \alpha_n^{ST} \\ \\ \alpha_{max}^{ST} = max_{n \in ST}(\alpha_n^{ST}) \end{cases} \tag{3.6}$$

with N_{ST} the number of ST samples. The mean and SD of α^{ST} and α_{max}^{ST} over the gait cycles are finally computed. Based on Nieuwenhuys et al. (2016), we consider a simulated gait as heel walking if $\alpha_{max}^{ST} > 20 degrees$. We name this criterium $C_{heel}1$. The simulation's mean ankle angle estimates α^{ST} are first compared with reported ankle angles during pathological gaits. For instance, several studies analyzed the gait of CP children and provided experimental ankle angle measures, but with large intra- and inter-study variability as patients' conditions can be widely different (Granata et al., 2000; Kerkum et al., 2015; Papadonikolakis et al., 2003). We consider our healthy optimization as reference and the kinematics features based on the method used by Schwartz et al. (2008) to identify gait deviations. According to this identification system, plantarflexion (respectively dorsiflexion) is excessive during the stance phase if $\alpha^{ST} < \alpha_{ref}^{ST} - std(\alpha_{ref}^{ST})$ (respectively $\alpha^{ST} > \alpha_{ref}^{ST} - std(\alpha_{ref}^{ST})$) with α_{ref} a healthy reference. Based on the experimental healthy ankle angle with a mean SD of 3.5 degrees during the stance phase reported by Schwartz et al. (2008), we thus consider a simulated gait as toe or heel walking if $\Delta_h \alpha^{ST} = \alpha^{ST} - \alpha_h^{ST}$ is lower than 3.5 or larger than 3.5 degrees, respectively. We name these criteria C_{toe2} and C_{heel2}.

3.4 Results

This section first presents the healthy gait resulting from the optimization of our new reflex circuit model. We compare the simulation estimates of the pelvis tilt, hip, knee, and ankle angles, and ground reaction forces to healthy experimental data ranges. We also compare

muscle activations of the healthy optimization to experimental EMG timings. To further evaluate this healthy result, we analyze the optimized reflex gains with respect to pathway modulations during gait reported in the literature.

Simulations of altered biomechanical parameters are then outlined, followed by simulations of altered reflex parameters. All these results are tabulated, and those leading to pathological gaits are analyzed in more detail with the ankle kinematics. All the results are presented for the left leg (l).

3.4.1 Healthy optimization

The optimization of our new reflex circuit model (i.e. Geyer and Herr's model extended with additional reflexes) results in a healthy gait that can be visualized following the link provided in the Additional information section. Snapshots of the simulation are also presented in 3.5a. The resulting walking speed and step length are respectively 1.16 m/s and 0.8 m. The quality of this simulated gait is first evaluated through analysis of its joint angles, ground reaction forces, and muscle activation estimates. This gait analysis is presented in 3.5b. The simulation states of joint angles and ground reaction forces are plotted with healthy experimental data ranges reported by Schwartz et al. (2008). This gait analysis shows regular pelvis tilt, hip flexion, knee angles, and ground reaction forces. The ankle angle reproduces the experimental profile with a less pronounced plantarflexion at the push-off phase and slightly excessive dorsiflexion at the gait cycle transition. The third ankle rocker occurs well after 40% of the gait cycle, as reported in the literature (Alvarez et al., 2007). The knee flexion also shows excessive values at the beginning of the swing and stance phase, respectively. In comparison, Geyer and Herr's results show an ankle flexion profile that better reproduces experimental data, whereas Ong's results also show excessive dorsiflexion throughout the gait cycle. Geyer and Herr's results show better matching ankle kinematics, which may result from the fact that their model has fewer parameters than ours or Ong's. Parameter fine-tuning to minimize the cost function may then be easier.

Furthermore, similarly to Ong et al. (2019), Figure 3.6 compares the muscle activations of this healthy optimization to experimental EMG on–off timings reported by Perry and Burnfield (2010a). The timings of simulation states match the experimental ones correctly, except for ILPSO at the beginning of the stance phase and VAS at the end of the swing phase. Such muscle inactivity is also present in Geyer and Herr's, and Ong's results. This figure also shows a larger activation of GAS compared to SOL during the stance phase.

The optimized values of SOL, GAS, and TA reflex gains are also presented in Table 3.1. They highlight the following major modulations during gait that are in line with the literature:

- SOL spindle reflex gain is larger during the stance phase compared with the swing phase. This difference corresponds to the modulation of the stretch reflex that occurs between
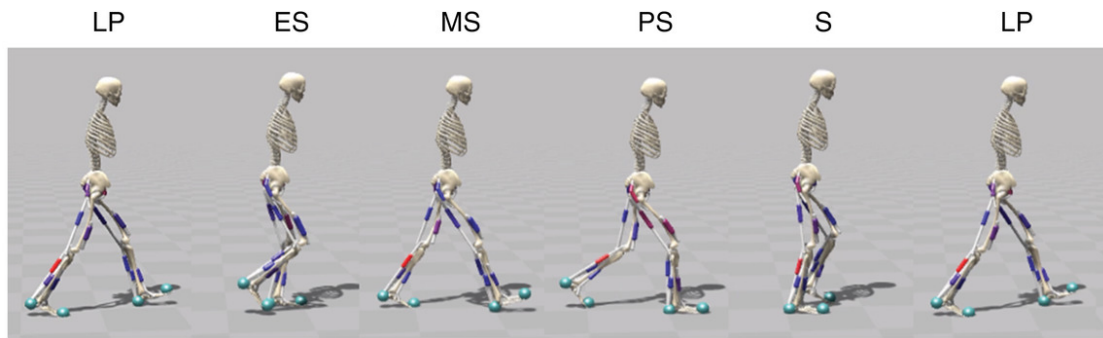
(a) Snapshots of the optimised healthy gait.
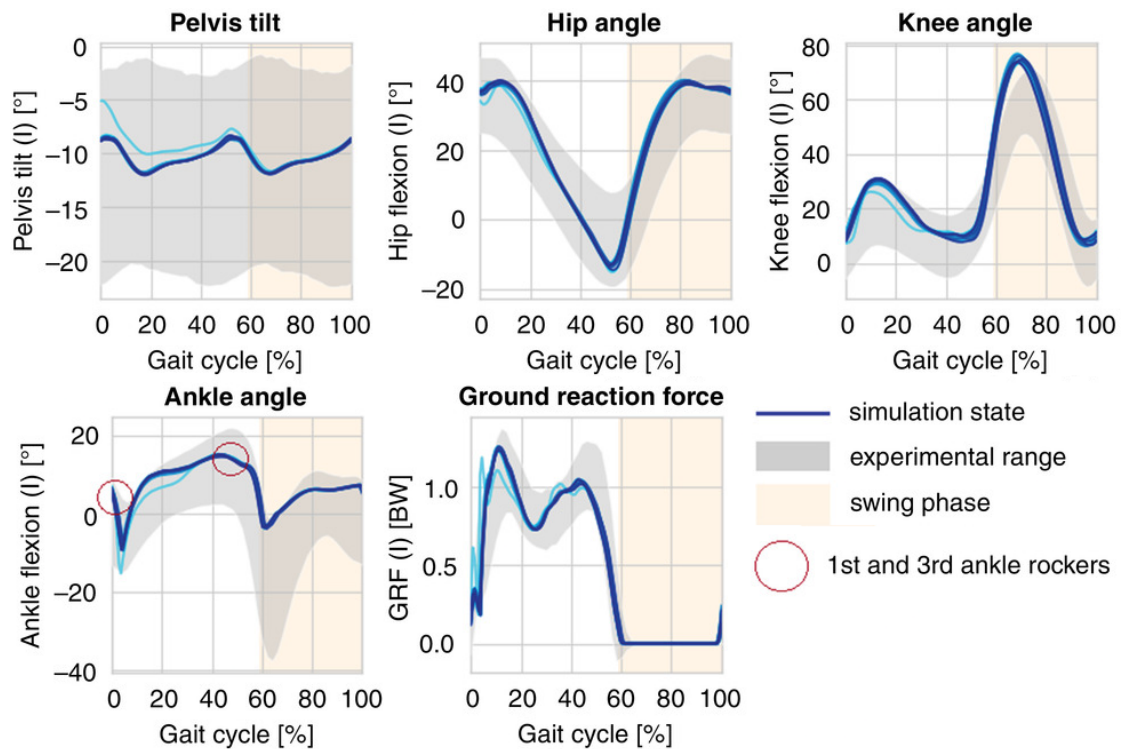
(b) Gait analysis of the optimised healthy gait.

Figure 3.5: Healthy reflex circuit model optimization.
3.5a) snapshots of the optimized healthy gait at the beginning of each controller state: LP, ES, MS, PS, S, and LP. 3.5b) gait analysis: simulation states of the pelvis tilt, hip, knee, and ankle angles, and ground reaction forces over the gait cycles are compared with healthy experimental data ranges reported by Schwartz et al. (2008) ($\mu \pm 2 \cdot std$) in grey. Curves from cyan to blue correspond to the 11 simulated gait cycles. The optimization result shows regular states. The ankle angle reproduces the experimental profile with a less pronounced plantarflexion at the push-off phase and slightly excessive dorsiflexion at the gait cycle transition. The first and third rockers are circled in red. The knee flexion also shows excessive values at the beginning of the swing and stance phases, respectively.

the stance and swing phases (Faist et al., 1996). The stretch reflex indeed participates in propulsion during the stance phase and stabilization during both stance and swing phases (Zehr and Stein, 1999). Regarding the GAS muscle, its spindle reflex gain is larger
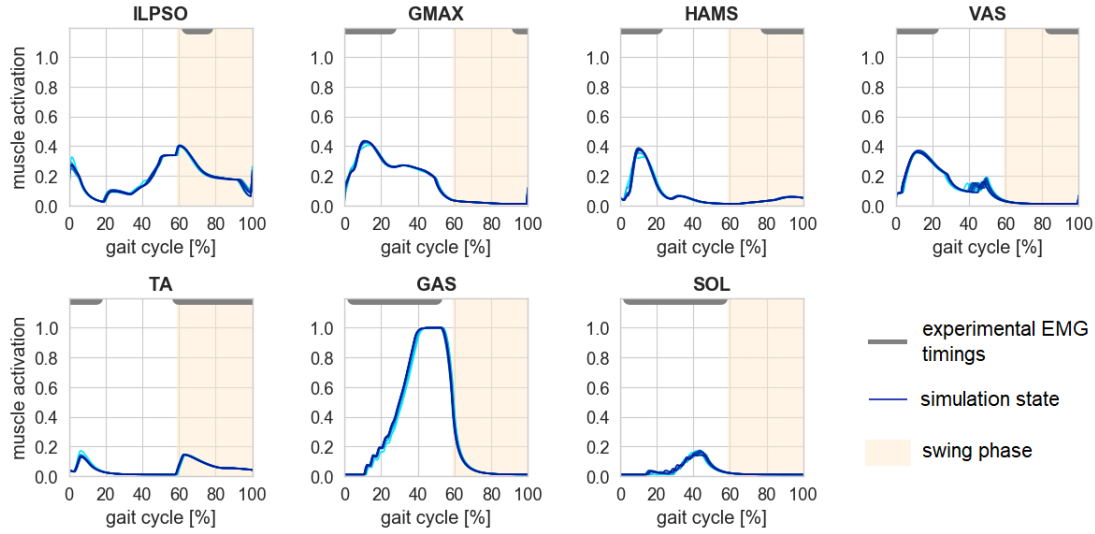
Figure 3.6: Muscle activations of the healthy optimization over the gait cycles.
The simulation states are compared to experimental EMG on–off timings in grey reported by Perry and Burnfield (2010a). Curves from cyan to blue correspond to the 11 simulated gait cycles. The timings of the simulation and experimental data match correctly, except for ILPSO at the beginning of the stance phase and VAS at the end of the swing phase.

| | Parameters | | | | | | | |
Phase	KS_{SOL}	KS_{GAS}	KL_{SOL}	KL_{GAS}	KF_{SOL}	KF_{GAS}	KS_{TA-SOL}	KS_{TA-GAS}
stance	0.16	0.17	4.0	0.08	0.23	1.4	-0.85	-0.34
swing	0.11	0.26	0.80	0.01	-0.91	-1.8	-3.3	-1.7

Table 3.1: Optimized values of SOL, GAS, and TA direct and reciprocal reflex gains during the stance and swing phases.

during the swing phase compared with the stance phase. As the GAS muscle is also involved in knee flexion (bi-articular muscle), it is reasonable that the modulation of its stretch reflex is different.

- TA to plantarflexor spindle reflex gains are smaller during the swing phase compared with the stance phase. As these reciprocal reflexes are negative, this difference corresponds to the reciprocal stretch inhibition between stance and swing phases. Thus, these reciprocal reflexes participate in the inactivation of the antagonist muscles in the appropriate phases of the gait cycle. Here, TA inhibits the plantarflexors during the swing phase to avoid plantarflexion (Petersen et al., 1999).

3.4.2 Pathological gaits optimizations

Biomechanical impairments

Figure 3.7 compares the simulated gait resulting from reduced plantarflexor F_{max} to 60%, mimicking muscle weakness with the healthy gait. The corresponding simulation can also be visualized following the link provided in the Additional information section. We can see that the altered condition induces a smaller step length, but no severe increase in dorsiflexion. The effect of reduced F_{max} on gait is further presented in Figure 3.8. The ankle kinematics comparison highlights large dorsiflexion and reduced plantarflexion during the late stance period compared with a healthy gait. The corresponding α_{max}^{ST} metric fulfil the criteria $C_{heel}1$ ($\alpha_{max}^{ST} > 20$ degrees), but the $\Delta_h \alpha^{ST}$ metric does not reach values characterizing heel gait (criterium $C_{heel}2$, $\Delta_h \alpha^{ST} > 3.5$ degrees).
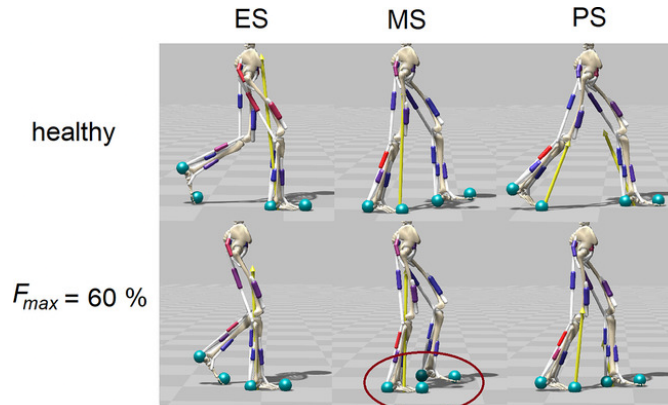
Figure 3.7: Comparison of the gait resulting from reduced plantarflexors F_{max} to 70% mimicking muscle weakness with the healthy gait.
Snapshots during ES, MS and PS phases. The yellow arrows represent ground reaction forces. There is a smaller step length in the altered condition compared to the healthy one, but no significantly larger dorsiflexion characterizing heel gait.

Table 3.2 summarises the two biomechanical parameter alterations investigated in this study. Reduced l_0^{fib} reproducing muscle shortening induces toe gait, whereas a reduction of F_{max} induces heel walking only partially.

Neural impairments

1D exploration

Figure 3.9 compares the simulated gait resulting from increased plantarflexor KS^{ST} to 400%, mimicking hyperreflexia with the healthy gait. We can observe that only the toes touch the ground during the MS phase in the altered condition as in typical toe gait. The effect of increased KS^{ST} on the ankle angle is further presented in Figure 3.9. The ankle kinematics
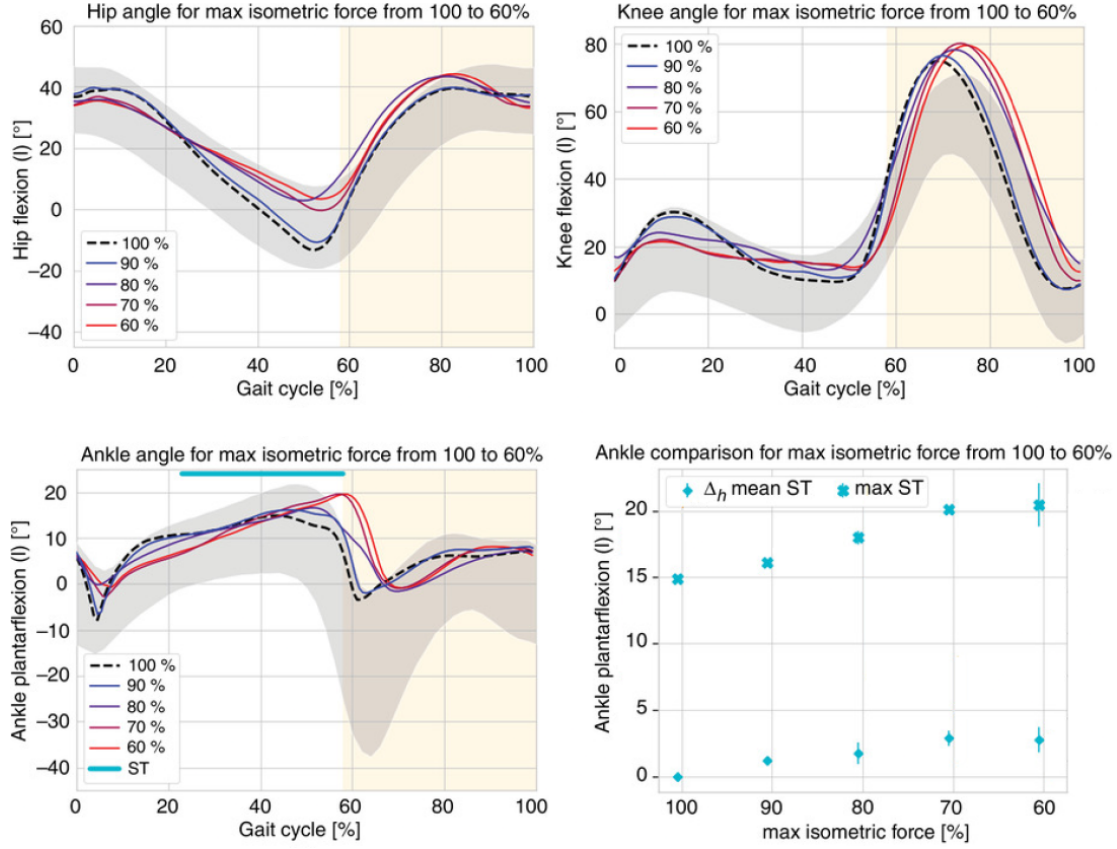
Figure 3.8: Effect of reduced plantarflexors maximal isometric force (F_{max}) mimicking muscle weakness on gait.
The grey area represents healthy experimental data ranges reported by Schwartz et al. (2008) ($\mu \pm 2 \cdot std$) and the light orange area indicates the healthy swing phase. For the ankle angle, alterations lead to large dorsiflexion during the late stance period. The ST period over which $\Delta_h \bar{\alpha}^{ST}$ and α_{max}^{ST} are computed as indicated by the cyan top line. The bottom right graph represents the corresponding $\Delta_h \bar{\alpha}^{ST}$ and α_{max}^{ST}.

comparison highlights early and large plantarflexion during the stance phase characterizing toe gait (3rd ankle rocker before 30% of the gait cycle and $\Delta_h \alpha^{ST} < 3.5 degrees$ corresponding to criteria $C_{toe}1$ and $C_{toe}2$). The knee kinematics comparison also reveals a larger knee flexion during the stance phase.

Table 3.3 summarises all the reflex parameter alterations investigated in this study. Increased plantarflexor F reflex gain mimicking hyperreflexia during the stance phase similarly induces toe gait. Increased KS_{TA}^{ST}, corresponding to decreased absolute values, reproduce a reduction of reciprocal inhibition and also lead to toe gait. The effects of increased KF^{ST} and KS_{TA}^{ST} on gait are similar to those of KS^{ST}.

By contrast, increased KL^{ST} and reflex gains during the swing phase do not induce toe gait. Early plantarflexion during the stance phase can still be observed for KL^{ST} increases, whereas increases in reflex gains during the swing phase do not have significant effects on the gait kinematics. Alterations of plantarflexor reflex parameters during the stance phase thus have

Parameters	Evaluated values as percentage of the healthy value	Toe gait range (the two toe gait criteria are fulfilled)	Partial heel gait range (some heel gait criteria are fulfilled, but not all)	Falling threshold
F_{max}	90,80...60%	$\emptyset$	$C_{heel}1$ but not $C_{heel}2$: [70, 60]%	50%
l_0^{fib}	95,90%	[85,90]%	$\emptyset$	85%

Table 3.2: Plantarflexor biomechanical parameter alterations and pathological gaits. This table outlines the evaluation of biomechanical parameters. For each, the evaluated values are provided as a percentage of the healthy value. The eventual range leading to toe gait and the eventual range leading to partial heel gait (some heel gait criteria are fulfilled, but not all) are also provided as a percentage of the healthy value. $\emptyset$ indicates that any parameter alteration leads to toe or heel gait before the falling threshold. The falling threshold corresponds to the parameter value at which the simulation falls immediately. If the simulation does not fall in the range of values of the parameter evaluation, the possible falling threshold beyond this range is indicated with the symbol > or <. Thus, reduced F_max mimicking muscle weakness induces partial heel gait, whereas reduced l_0^{fib} reproducing muscle contracture induces toe gait.
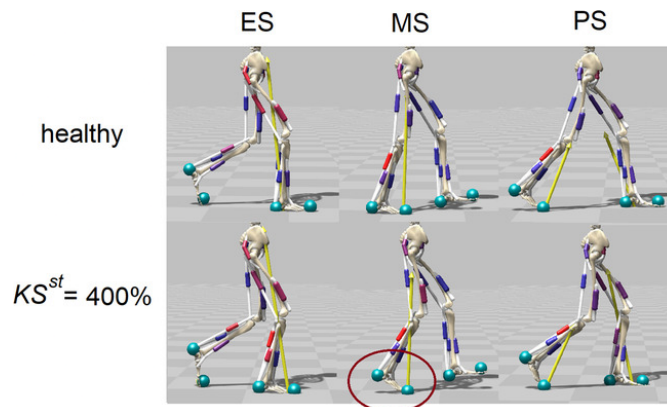
Figure 3.9: Comparison of the gait resulting from increased plantarflexor KS^{ST} to 400% mimicking hyperreflexia with the healthy gait.
Snapshots during ES, MS, and PS phases. The yellow arrows represent ground reaction forces. As in typical toe gait, only the toes touch the ground during the MS phase in the altered condition.

greater effects on gait compared to parameters during the swing phase.

Regarding decreased reflex gains reproducing neural weakness, they induce partial heel gait in a similar way to muscle weakness.

Finally, the qualitative effect of all evaluated biomechanical and reflex parameter alterations on gait is summarised in Figure 3.11.
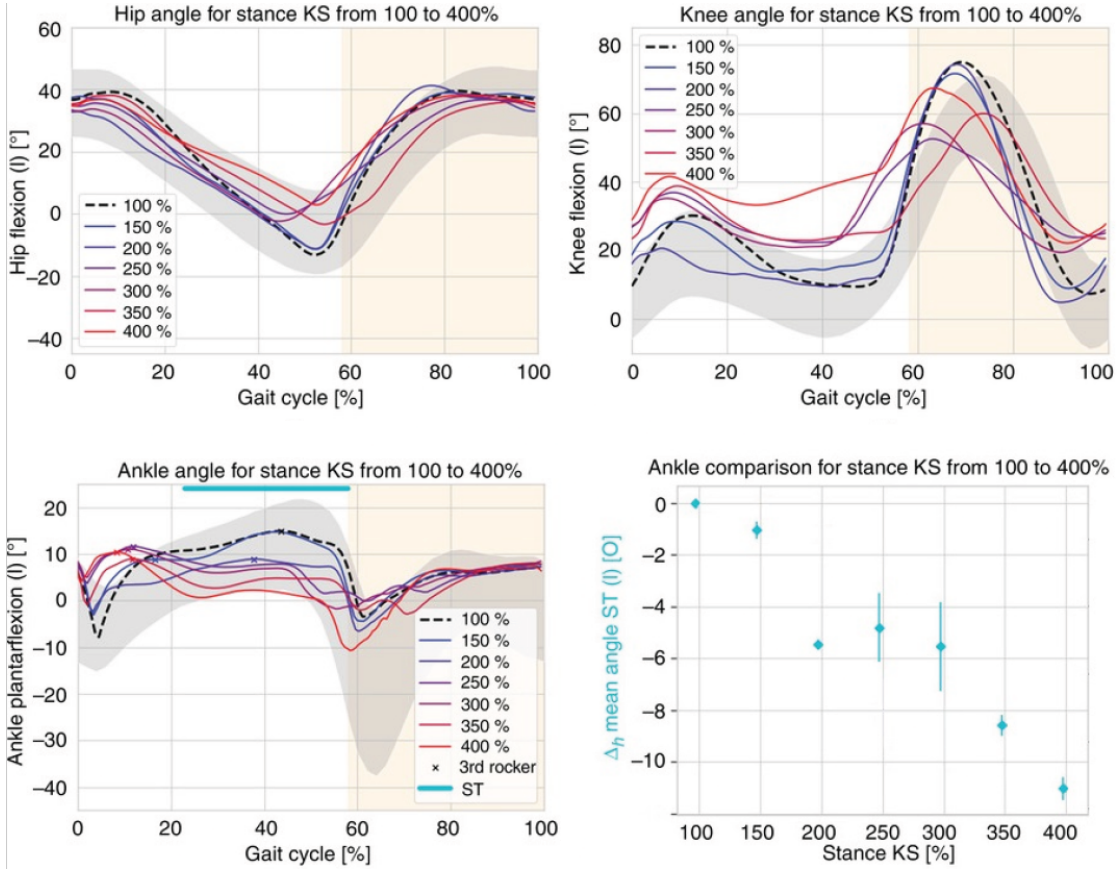
Figure 3.10: Effect of increased plantarflexor stance KS (KS_{ST}) from 100 to 400% mimicking hyperreflexia on gait.

The grey area represents healthy experimental data range reported by Schwartz et al. (2008) ($\mu \pm 2 \cdot std$) and the light orange area indicates the healthy swing phase. In the knee angle, alterations lead to larger knee flexion during the stance phase. For the ankle angle, alterations lead to early and large plantarflexion during the stance phase. The ST period over which $\Delta_h \bar{\alpha}^{ST}$ is indicated by the cyan top line. The bottom right graph represents the corresponding $\Delta_h \bar{\alpha}^{ST}$.

Repeatibility of results

Figure 3.12 presents the results of various optimization trials for the maximal isometric force altered to 70% and the stance spindle gain altered to 300% with various IC. These results show similar ankle kinematics and optimized parameter values for the various IC (small $MAE_{IC1\alpha}$ and MRE_{IC1p}) arguing for the repeatability of our results.

2D exploration

The previous 1D exploration is furthered by a 2D exploration of some pairs of reflex parameters of interest. As hyperreflexia usually occurs during both stance and swing phases, plantarflexor hyperreflexia is first modeled during both phases through KS and KL reflex gains. The investigation of neural weakness is similarly extended by reducing both KF and KL reflex gains during

Parameters	Evaluated values as percentage of the healthy value	Toe gait range (the two toe gait criteria are fulfilled)	Partial heel gait range (some heel gait criteria are fulfilled, but not all)	Falling threshold
KS^{ST}	150, 200...400%	[250, 400]%	$\emptyset$	450%
	95, 90...75%	$\emptyset$	[70, 75]%	70%
KS^{SW}	150, 200...450%	$\emptyset$	$\emptyset$	500%
KL^{ST}	150, 200...450%	$\emptyset$	$\emptyset$	500%
	90, 80...40%	$\emptyset$	$C_{heel}1$ but not $C_{heel}2$: 40%	30%
KL^{SW}	200, 300...700%	$\emptyset$	$\emptyset$	800%
KF^{ST}	200, 300...900%	[300, 900]%	$\emptyset$	>900%
	95, 90...80 %	$\emptyset$	$C_{heel}1$ but not $C_{heel}2$: 80%	75%
KS^{ST}_{TA}	90, 80...20%	[70, 20]%	$\emptyset$	10%
KS^{SW}_{TA}	90, 80...10%	$\emptyset$	$\emptyset$	0%

Table 3.3: Reflex parameter alterations and pathological gaits.
This table outlines the evaluation of parameters from the reflex circuit model with increased and decreased values. For each, the evaluated values are provided as a percentage of the healthy value. The eventual range leading to toe gait (the two toe gait criteria are fulfilled) and the eventual range leading to partial heel gait (some heel gait criteria are fulfilled, but not all) are also provided as a percentage of the healthy value. $\emptyset$ indicates that any parameter alteration leads to toe or heel gait before the falling threshold. The falling threshold corresponds to the parameter value at which the simulation falls immediately. If the simulation does not fall in the range of values of the parameter evaluation, the possible falling threshold beyond this range is indicated with the symbol > or <. Thus, increased F and S reflex gains mimicking hyperreflexia during the stance phase induce toe gait, whereas reduced reflex gains mimicking neural weakness do not induce heel gait.

the stance phase. The results of these 2D explorations are presented through color maps of the ankle kinematics metrics, $\Delta_h \alpha^{ST}$ and α^{ST}_{max}. Plantarflexor hyperreflexia thus leads to a more pronounced toe gait and neural weakness to a more pronounced heel gait.

Figure 3.13 shows smaller $\Delta_h \alpha^{ST}$ corresponding to more pronounced toe gaits induced by increased plantarflexor KS during both stance and swing phases compared to 1D exploration results. TA to plantarflexor KS and plantarflexor KL increases during the two phases also lead to more pronounced toe gait. These results also highlight further the main effect of increased reflex gains during the stance phase.

Figure 3.13 also shows larger α^{ST}_{max} and therefore more pronounced heel gaits induced by plantarflexor KF and KL reduction during the stance phase compared to 1D exploration results.

Figure 3.11: Qualitative effects of biomechanical and reflex parameters.
Increased and decreased values are represented by > and < symbols, respectively. As KS_{TA}^{ST} is negative, it is evaluated with decreased absolute values corresponding to increased real values to reproduce the reduction of reciprocal inhibition. Induced toe gait is highlighted in red, whereas induced large plantarflexion and dorsiflexion during the stance phase are shown in light red and light blue, respectively.

3.5   Discussion

This investigation of the effect of both biomechanical and neural impairments on gait is based on a reflex circuit model including plantarflexor force, spindle and length direct pathways, and additional reciprocal pathways with TA. We model pathways that were omitted by previous models to extend our investigation. optimization of this reflex circuit model results in a healthy gait model highlighting reported pathway modulations during gait. We then investigate the effect of plantarflexor SOL and GAS impairments from both biomechanical and neural origins. We explore the effect of each impairment while constraining the variation of the other parameters in order to study the strict and short-term effect on gait. On the one hand, toe gaits can be generated by increased spindle and force reflex gains modeling spastic hyperreflexia during the stance phase. These results reproduce both clinical observations (Armand et al., 2016; Chia et al., 2020) and previous simulations. In particular, they are comparable to Jansen et al.'s (Jansen et al., 2014) simulation that reproduces excessive plantarflexion with increased length and velocity feedback, and lack of suppression of the stretch reflex of plantarflexor muscles during the swing phase. Increased spindle reciprocal pathways from the TA to the plantarflexors reproducing reduction of reciprocal inhibition also lead to toe walking. These reflex increases modeling hyperreflexia coherently simulate toe gait. Moreover, these simulations of plantarflexor hyperreflexia reveal excessive knee flexion during the stance phase. This gait deviation corresponds to the pathological crouch gait that is also commonly present in CP and, in part, attributed to plantarflexor spasticity (Armand et al., 2016; Gage et al., 2009.

On the other hand, other impairments that were expected to generate pathological gaits only
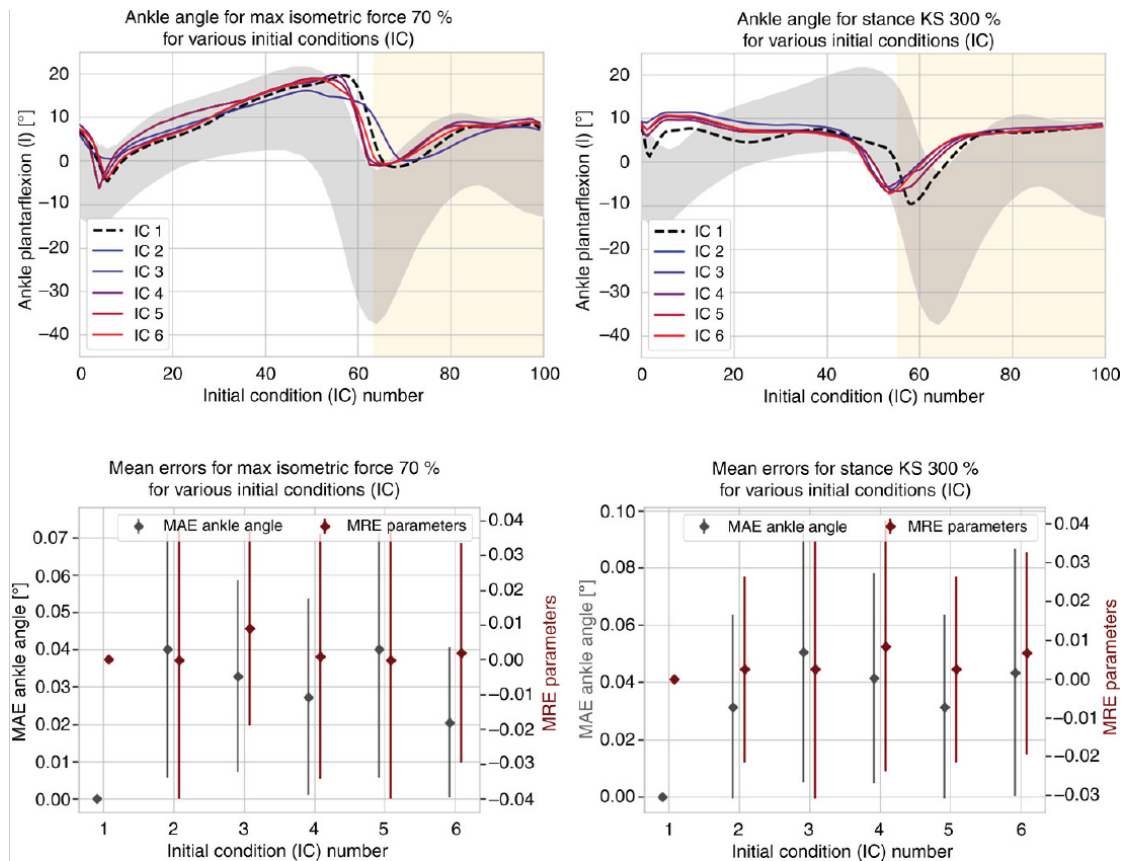
Figure 3.12: Results of optimizations for the maximal isometric force altered to 70% and the stance spindle gain altered to 300% with various IC.
On the left, various optimization trials for the maximal isometric force altered to 70% with various IC: small $MAE_{IC1\alpha}$ and MRE_{IC1p} indicate similar results. On the right, various optimization trials for the stance spindle gain altered to 300%: small $MAE_{IC1\alpha}$ and MRE_{IC1p} indicate similar results.

partially do so (some criteria are fulfilled, but not all). First, regarding biomechanical impairments, reduced maximal isometric force modeling muscle weakness induces partial heel gait. Reduced optimal fiber length still induces early ankle plantarflexion, whereas reduced maximal isometric force leads to large dorsiflexion, mainly during the late stance period corresponding to weak propulsion of the body. In comparison, Ong et al. (2019) simulate heel and toe walking by modeling SOL and GAS weakness and contracture, respectively. However, the corresponding optimized reflex parameters are not constrained to a small range around the healthy value as in the present study. Ong et al. (2019) also reproduce toe walking by modeling contracture to the SOL only. We considered alterations to the properties of both plantarflexors as they are agonist muscles and are commonly impaired simultaneously. Nevertheless, they do not have the exact same role (Attias et al., 2017; Lenhart et al., 2014; Matjačić et al., 2006) showed that SOL and GAS contractures do not have the same effects on gait kinematics. Perry and Burnfield (1992) also state that the main cause of heel gait is SOL weakness, whereas GAS weakness does not directly contribute to excessive ankle dorsiflexion. The present study
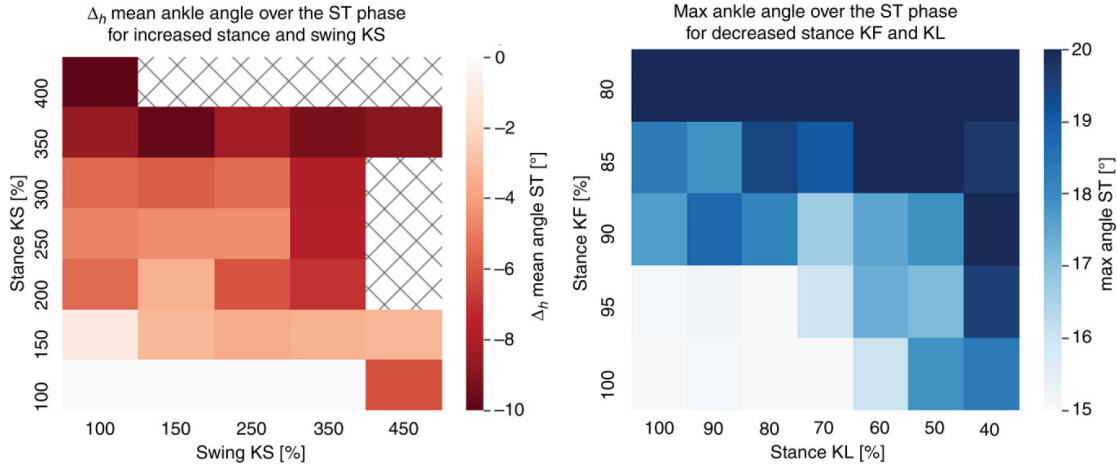
Figure 3.13: Effect of plantarflexors hyperreflexia and neural weakness on gait.
On the left, effect of increased plantarflexor KS during both stance and swing phases: smaller $\triangle_h \bar{\alpha}^{ST}$ corresponding to more pronounced toe gait are induced compared to 1D exploration results. The checked squares indicate simulations that fall immediately. On the right, effect of reduced plantarflexor KF and KS during the stance phase: larger α_{max}^{ST} corresponding to more pronounced heel gait are induced compared to 1D exploration results.

could thus be furthered by distinguishing the effect of SOL and GAS impairments on gait. On another note, plantarflexor weakness is also assumed to contribute to crouch gait (Steele et al., 2012). Nevertheless, similarly to Ong et al. (2019) and Waterval et al. (2021), our simulations of plantarflexor weakness do not induce such gait deviation, and thus do not support such a contribution of plantarflexor weakness in crouch gait.

Regarding neural impairment, increased reflex gains during the swing phase do not result in toe gait. Alterations of plantarflexor reflex parameters during the stance phase thus have more effect on gait than parameters during the swing phase. The plantarflexor muscles are indeed mainly activated during the stance phase to propel the body forward. However, decreased plantarflexor reflex gains during the stance phase mimicking neural weakness induce partial heel gait. Furthermore, investigation of both hyperreflexia and neural weakness through 2D exploration reproduces more pronounced toe and heel gaits.

The present investigation is limited by the fact that the model falls before reaching severe pathological gait. Nonetheless, the sensitivity and the effect of parameter alterations toward plantarflexion or dorsiflexion can be observed. These results are significant because the contributions of active reflex pathways and passive muscle properties in spastic stiffness can barely be distinguished in clinical examination (Lorentzen et al., 2010). Previous studies assumed that spastic stiffness is mainly caused by passive muscle properties (Dietz and Sinkjaer, 2007). However, the contribution of active reflex mechanisms is being progressively considered and reported as significant (Lorentzen et al., 2010; Mirbagheri et al., 2001). The present study suggests such an important contribution of active reflex mechanisms in pathological toe gait.

Nevertheless, the 'what if' approach applied in this study faces a major validation issue. On

the one hand, we modeled numerous pathways that intrinsically lead to redundancy. The solution space may then contain several local minima. Given an optimized healthy gait state, our model predicts that specific pathways can elicit a pathology but our results might not generalize. In a different condition (e.g., faster or slower gait), this might not be true. However, the problem is difficult to explore as there are infinite possible initial conditions and parameters. The optimization method still introduces randomness in the initial conditions and parameters (even for those constrained) so the population of solutions tends to lead to similar conclusions. To further argue for the repeatability of our results, we looked at suboptimal solutions and observed similar tendencies in both the gait kinematics and control parameter values. Furthermore, before impairing parameters, we had already formed hypotheses on the different cause–effect relationships, which were confirmed when we observed agreement between simulation and clinical studies.

On the other hand, parameters are modified individually to investigate their effect on gait, but SCI, stroke, or CP patients usually present many biomechanical and neural impairments together. Spasticity and muscle weakness can coexist in these conditions, leading to spastic paresis (Lamontagne et al., 2002). This study focuses on plantarflexors only, whereas these patients usually present multiple impaired muscles. Moreover, as mentioned previously, some impairments may be gradual, along with progressive compensation through neural adaptations. Such adaptations may also arise after sudden impairments, especially after training. This topic of long-term adaptation and compensation is of great interest, but the state-of-the-art in pathological modeling is not at the point to address such complex conditions, given that pathological gaits are normally more unstable than healthy ones. We plan to explore this topic in follow-up studies. Thus, validation of this study with clinical data is very challenging. This 'what if' approach is still deemed of great interest as one can postulate various hypotheses, then identify the conditions through simulation and finally design an experiment that can help test and validate the model.

Besides its validation issue, this study could be improved on several points. First, the optimization solution space could be further explored to look for other potential local minimums and reach a solution that better reproduces experimental observations. In particular, as outlined previously, knee angle and GAS activation present excessive values during the stance that could be refined. This exploration would require many optimizations that would take a long time to realize. More sophisticated balance controllers could also be included to allow simulations to reach more severe pathological gaits. We also considered similar cost functions for healthy and impaired models, whereas human walking goals may vary depending on individual conditions. minimization of effort might play a minor role compared to healthy conditions, whereas pain might play a more important role, for instance. Adapted measures for impaired optimization could thus also be considered to reach more severe pathological simulations. On another note, more reflex parameters could be evaluated. Indeed, reflex offsets were not investigated, whereas their contribution to impaired motor control has been highlighted in the literature (Levin and Feldman, 1994). Neither were reflex delays evaluated, whereas increased delays are reported in SCI conditions, for instance (Thomas et al., 2014). It

should also be noted that the reflex pathway delays used in this study based on Geyer and Herr (2010) and Ong et al. (2019) are shorter than those recorded experimentally by the order of 50%. Moreover, even with delays closer to physiological values, a reflex-based controller is still only a first approximation of all the underlying neural pathways. The introduction of neuron models for afferent fibers, interneurons, alpha motor neurons, and descending neurons would be a significant improvement to model in more detail descending pathways and presynaptic inhibition mechanisms, among others.

3.6   Conclusions

This study allows the targeting of various biomechanical and neural impairments leading to pathological gaits by simulating the effect of altered biomechanical and reflex parameters on gait. Our simulations suggest that toe walking can be generated by hyperreflexia, whereas muscle and neural weakness lead partially to heel gait. This 'what if' approach based on neuromusculoskeletal simulation is thus deemed of great interest and suggests an important contribution of both biomechanical contracture and active reflex mechanisms in pathological toe gait. Further modeling and simulation are essential to understand the cause–effect relationship between impaired mechanisms and pathological gaits in more detail. In this way, such neuromusculoskeletal simulation could help to target appropriate therapies. Furthermore, therapies such as drugs or epidural electrical stimulation themselves could be simulated to study their efficiency.

In this study, we had to extend the sensory controller for the ankle muscles to reproduce reciprocal inhibition mechanisms and properly model hypertonia. This modification required finding again a proper optimal solution for healthy gait in order to start from a reliable initial condition in the modeling of pathological gaits. However, if we aim at modeling other pathological gaits affecting different muscles, another extension of the original controller would be necessary with the consequent effort in finding the optimal healthy solution. This issue highlights the need for a new neuromuscular controller accounting for sensory inputs and reciprocal inhibition mechanisms in the spinal cord for all the modeled muscles. This kind of controller will be presented in the following chapter.

Supplementary Information

Videos of the healthy and pathological gait simulations can also be visualized in the following shared folder: https://drive.switch.ch/index.php/s/6uw4lbVapQc2Hrn.

4 Investigating the roles of reflexes and central pattern generators in the control and modulation of human locomotion using a physiologically plausible neuromechanical model

Overview

In the past chapter, we highlighted the limitations of sensory-based controllers to reproducing spastic hypertonia. In this chapter, we will present a new neuromuscular controller, including the main sensory reflexes and reciprocal inhibition between agonist and antagonist muscles. In Figure 3.3, we showed the neural representation of the reflex circuits and the corresponding modeling with reflex primitives. The new controller proposed will decrease the level of abstraction by modeling directly the neural representation of reflex circuits using leaky integrator neurons without relying on a finite state-machine. Furthermore, we included a model of CPG network on top of the reflex circuit. Before studying the capability of this controller to reproduce pathological gaits, we will first investigate how it can reproduce healthy human locomotion and gait modulation.

Abstract

Studying the neural components regulating movement in human locomotion is obstructed by the inability to perform invasive experimental recording. Neuromechanical simulations can provide insights by modeling the locomotor circuits. Past neuromechanical models proposed control of locomotion either driven by central pattern generators (CPGs) with simple sensory commands or by a purely reflex-based network regulated by state-machine mechanisms. However, the physiological interpretation of these state-machines remains unclear. Here, we present a physiologically plausible model to investigate spinal control and modulation of human locomotion. We propose a bio-inspired controller composed of two coupled central pattern generators (CPGs) that produce the rhythm and pattern and a reflex-based network simulating low-level reflex pathways and Renshaw cells. This reflex network is based on leaky-integration neurons, and the whole system does not rely on changing reflex gains according to the gait cycle state. The only component of the controller that maintains a state-machine mechanism is the balance controller of the trunk. The musculoskeletal model is composed of a skeletal structure and 9 muscles per leg generating movement in sagittal plane. After optimizing the open parameters, human locomotion replicating kinematics and muscle activation naturally emerged. Furthermore, when CPGs were not activated, no

stable and physiologically plausible gaits could be achieved through optimization, suggesting the necessity of this component to generate rhythmic behavior without a state machine mechanism regulating reflex activation. The controller could reproduce a wide range of speeds from 0.3 to 1.9 m/s. The results also showed that the net influence of feedback on motoneurons during perturbed locomotion is predominantly inhibitory and that the CPG network provides the timing of motoneurons' activation by exciting or inhibiting muscles in specific gait phases. The proposed bio-inspired controller could contribute to our understanding of locomotor circuits of the intact spinal cord and could be used to study neuromotor disorders.

4.1   Introduction

Limbs movements result from the complex interaction between brain centers, the spinal cord, and the musculoskeletal system (Rossignol et al., 2006). The spinal network is essential in the control, coordination, and modulation of locomotion (Kiehn, 2006). While there is direct evidence of a CPG in mammals and vertebrates (Akay, 2020; Kiehn, 2006), the lack of direct experimental access in humans means that there is only indirect evidence (Minassian et al., 2017). Furthermore, sensory feedback pathways may play a major role compared to other mammals, and lower vertebrates in humans (Goldberger, 1977; Grillner, 1975; Guertin, 2009; Lajoie et al., 1996). Different studies suggested that the muscle activity observed during human locomotion may be controlled by five locomotor primitives that could be generated by rhythmic neural circuits (Danner et al., 2015; Y. P. Ivanenko et al., 2004). Hypothesizing these questions about the roles of different spinal components in controlling locomotion is challenging since we possess only partial knowledge of the interaction between the different subsystems involved in this process. On top of that, limited experimental access complicates the observation of the sub-components functions leading to difficulties in model validation. Computer simulations are necessary and have been proven useful in the past by evaluating the contribution of each control component by evaluating different models, and parameters (Aoi et al., 2010; Di Russo et al., 2021; Dzeladini et al., 2014; Geyer and Herr, 2010; Ijspeert, 2008; Ong et al., 2019; Song and Geyer, 2015).

Various neuromechanical models have been proposed in the past to address these questions. In 1995, Taga (1995) proposed a musculoskeletal system controlled by a neural rhythm generator composed of 7 pairs of neural oscillators and simple sensory-motor signals. Successively, in 2001, Ogihara and Yamazaki (2001) developed a neural controller composed of motoneurons receiving inputs from a common CPG and reflexes from stretch and force receptors, where the spindle reflexes had inhibitory inputs to antagonist's muscles. In the context of locomotion controlled by CPG mechanisms, Aoi et al. (2010) constructed a CPG model based on a two-layered hierarchical network composed of a rhythm generator (RG) and a pattern formation (PF) layer. The RG model produced rhythmic information using phase oscillators and was regulated by phase resetting based on foot-contact gait events, whereas the PF model generated feedforward commands composed of five motor primitives based on the muscle synergies analysis performed by Ivanenko et al. (2004). On the other hand, Geyer and Herr

(2010) demonstrated that the kinematics and muscle activation observed in human locomotion could be reproduced without CPG commands by relying purely on sensory feedback activated at specific gait cycle phases. A similar controller with partial modifications has been then proposed by Ong et al. (2019). In these studies, the activation of sensory responses in the gait cycle is regulated by a state-machine mechanism, hinting at the need for a more sophisticated circuit that controls the underlying reflexes. Other studies have integrated CPG commands on top of these purely sensory-based controllers, showing the benefits of rhythmic circuits in gait modulation (Dzeladini et al., 2014; Van der Noot et al., 2015).

In this study, we propose a novel bio-inspired controller composed of a feedforward network inspired by Aoi et al. consisting of two CPGs that produce the locomotor rhythm and patterns and a new physiologically plausible implementation of spinal reflexes based on neurophysiological studies in locomotion (Windhorst, 1989; Zehr and Stein, 1999) without relying on any state machine mechanism. This network controls 9 muscle actuators generating torques in a previously assessed musculoskeletal model (Delp et al., 1990). The performance of this controller in replicating the behavior of human locomotion and its modulation are investigated and compared with previous experimental and neuromechanical studies. In addition, we investigate the performance of the sensory feedback controller alone to verify whether it is possible to generate human walking behavior with a purely reflex-based controller without relying on state machine mechanisms and to verify the benefit of CPG mechanisms. Finally, we examine the contribution given by pattern generation and reflex circuits to the motoneurons at slow, intermediate, and fast speeds performing a correlation analysis to identify possible parameters responsible for speed modulation. With these experiments, we aim to address the following questions:

1. What is the role of CPGs and reflex circuits in the generation of muscle activation in human locomotion?

2. Can low-level feedback circuits produce stable locomotion without a CPG or state-machine?"

3. Is the contribution of these two neural components changing with increasing of gait speed?

Our results show that the reflex rules implemented in previous models (Geyer and Herr, 2010; Ong et al., 2019) could be reproduced into less abstract models of neural circuits. The insights given by the proposed controller suggest that spinal reflexes alone could not reproduce rhythmic locomotion without a state machine mechanism regulating the activation of reflexes in specific phases of the gait cycle. CPG networks appear to play the role of state machines in previous models and to be necessary to promote muscle activation in specific gait cycle phases. In addition, the modulation of CPG frequency seems necessary to modulate step duration. The modulation of either reflexes, CPG network, or both could generate gaits in a wide speed range, highlighting the high level of versability of the neurospinal control of human locomotion.

4.2 Methods

This study used the SCONE software simulation framework (Geijtenbeek, 2019), which was extended to implement and optimize the new spinal model generating gait simulations of 10 s. The SCONE simulation comprises the following four blocks:

- An OpenSim musculoskeletal model.

- A controller.

- A cost function composed of several locomotion metrics

- An optimizer that optimizes the initial conditions and controller parameters to minimize the cost function.

4.2.1 Musculoskeletal model

The musculoskeletal model (Figure 4.1) has the skeletal structure presented by Delp et al. (1990) with a height of 1.8 m and weight of 75.16 kg. The model is constrained in the sagittal plane and has a total of nine degrees of freedom (DoFs): a 3-DoFs planar joint between the pelvis and the ground and 3 rotational DoFs per leg: hip flexion/extension, knee flexion/extension, and ankle dorsiflexion/plantarflexion. Three spheres per leg are used as contact models with the ground: one of radius 5 cm at the calcaneus and two of radius 2.5 cm at the toes. The musculoskeletal model is actuated by nine Hill-type muscle-tendon units per leg: gluteus maximus (GMAX), biarticular hamstrings (HAMS), biceps femoris short head (BFSH), rectus femoris (RF), iliopsoas (ILPSO), vasti muscle group (VAS), gastrocnemius (GAS), soleus (SOL), and tibialis anterior (TA).

4.2.2 Controller

Muscle activation is regulated by the excitation provided by the motoneurons. The motoneurons are stimulated or inhibited by the different components of the bio-inspired controller: the balance controller of the trunk and the spinal network, composed of the CPGs and spinal reflexes. The balance controller and the CPGs are modeled at an abstract level. Indeed, the former provides balance inputs in specific phases of the gait cycle with Proportional Derivative (PD) controllers, and the latter is composed of two abstract oscillators generating primitive patterns. By contrast, the spinal reflexes are modeled at a lower level of abstraction and are structured in different leaky integrator neurons divided into three types: somatosensory neurons (SNs), interneurons (INs), and motoneurons (MNs). The overall structure of the controller is reported in Figure 4.2. The balance controller of the trunk regulates only the activation of hip muscles in specific phases of the gait cycle, whereas CPGs and spinal reflex controllers provide inputs to all muscles and are not regulated by any state-machine mechanism. We chose to maintain the state machine for the balance controller in order to
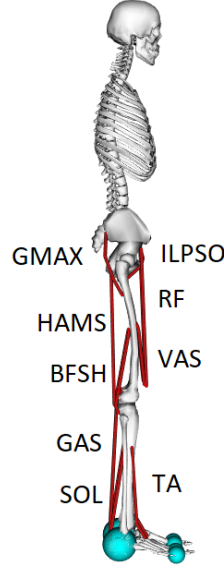
Figure 4.1: Musculoskeletal model used to study human locomotion.
The model is constrained in the sagittal plane and has 9 DoFs: hip and knee flexion/extension, ankle plantar/dorsal flexion for each leg, and a 3-DoFs planar joint between the pelvis and the ground. Movements are generated by the activation of 9 muscles per leg: gluteus maximus (GMAX), biarticular hamstrings (HAMS), biceps femoris short head (BFSH), rectus femoris (RF), iliopsoas (ILPSO), vasti (VAS), gastrocnemius medialis (GAS), soleus (SOL), and tibialis anterior (TA).

simplify the balance control since our main goal is the simulation of locomotor movement. A physiological neuromechanical model of trunk balance control is a complex task that is outside the scope of this study. Muscle excitation is triggered by the motoneuron output with values between 0 and 1 since motoneurons can only provide excitation to muscle fibers and cannot have negative outputs. To keep a reasonable level of abstraction and complexity, we will assume that the neuron's output n_{output} follows the dynamics of a leaky integrator:

$$\tau \frac{dy}{dt} = -y + u_{input},$$
$$u_{output} = f(y) \tag{4.1}$$

where y is the neuronal response, u_{input} is the neural input, τ the time constant (typically 0.01), u_{output} the output of the neuron, and f the activation function. The activation function used for motoneurons is the min-max operator ($f(x) = min(max(0,x),1)$), and the neural input is defined as:

$$u_{input} = \sum_j w_j u_{output\,j} \tag{4.2}$$

where w_j is the weight associated with the jth connection, and $u_{output\,j}$ the output of the jth neuron. The motoneuron receives inputs from the CPGs' network (u_{CPGs}) and the reflex

circuit ($u_{reflexes}$). These inputs are integrated according to equations 4.1 and 4.2:

$$\tau \frac{dy}{dt} = -y + (u_{CPGs} + u_{reflexes}),$$
$$m_{output} = f(y) \tag{4.3}$$

and generate the motoneuron output m_{output}. ILPSO, GMAX, and HAMS also receive inputs from the balance controller ($u_{balance}$). To avoid the activity of the balance controller from being inhibited by the other neural circuits possibly preventing the correct balance of the trunk, $u_{balance}$ is not integrated into the motoneuron dynamics, and the final motoneuron output for hip muscles $\tilde{m}_{output}$ is defined by the following equation:

$$\tilde{m}_{output} = (u_{balance} + m_{output})_+ \tag{4.4}$$

where m_{output} is the motoneuron output resulting from the integration of u_{CPGs} and $u_{reflexes}$ and $u_{balance}$ represents the balance controller effect on the hip muscles. The operator $()_+$ represents only the positive part of the selected signal. The amplitude of all components is regulated by the controller's parameters tuned by the optimization algorithm. The muscle activation a responds to the excitation m_{output} (or $\tilde{m}_{output}$ for hip muscles) as defined by Thelen et al. (2003).
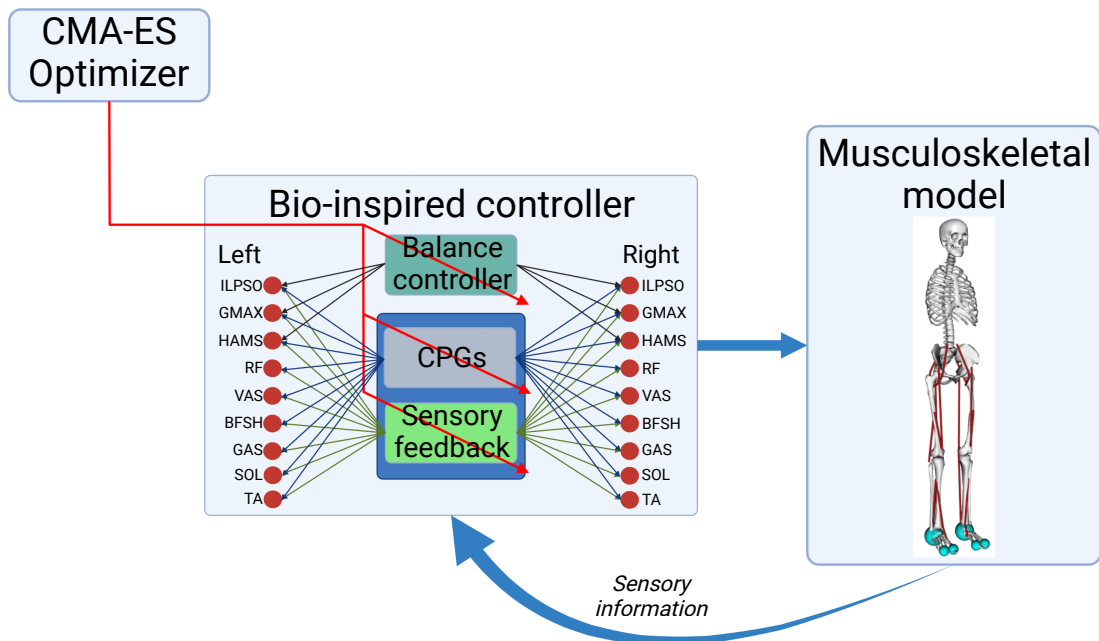
Figure 4.2: Control diagram.
The bio-inspired controller is composed of the balance controller of the trunk and the spinal controller divided into CPGs and spinal reflexes. The balance controller aims at keeping the balance of the trunk by stimulating the hip muscles' motoneurons, whereas CPGs and spinal reflexes generate rhythmic behavior stimulating all muscles' motoneurons. Reflexes and CPGs are integrated by motoneurons, whereas balance inputs are summed separately. (Created with BioRender.com)

The following sections will describe in detail how each neural input is computed ($u_{balance}$, u_{CPGs}, and $u_{reflexes}$).

Balance controller of the trunk

The balance controller is the one proposed by Ong et al. (2019), and it is the only controller part where a state-machine mechanism is present. A proportional derivative control strategy (PD) is used to activate the hip muscles balancing the forward lean angle of the trunk. ILPSO, GMAX, and HAMS receive inputs from the balance controller during the stance phase. The excitation given by the balance controller to the hip motoneurons is described in equation 4.5.

$$u_{balance} = k_p(\theta(t - t_D) - \theta_0) + k_v\dot{\theta}(t - t_D), \tag{4.5}$$

where k_p and k_v are the proportional and derivative controller's gains, and the constant θ_0 is the desired forward lean angle regulating the proportional feedback of the actual forward lean angle θ. t_D represents the time delay, corresponding to $t_D = 5ms$ for the hip muscles. The balance controller has a total of 9 parameters.

Central Pattern Generators (CPGs)

The central pattern generators (CPGs) were implemented as two coupled oscillators (one per side) composed of rhythm generator, and pattern formation layers (McCrea and Rybak, 2008; Rybak et al., 2006) inspired by the work of Aoi et al. (2013, 2010). The rhythm generator dictates a period command synchronized with the environment through afferents triggered by the heel-strike event. Based on Aoi's model, two coupled differential equations govern the CPG dynamics:

$$\dot{\phi}_{left}(t) = \omega - \gamma sin(\phi_{left}(t) - \phi_{right}(t) - \pi)$$
$$\dot{\phi}_{right}(t) = \omega - \gamma sin(\phi_{right}(t) - \phi_{left}(t) - \pi), \tag{4.6}$$

where $\phi_{left/right}$ denotes the phase of each leg, $\omega(t)$ is the basic angular frequency, and γ is the coupling constant.

The differential equation contains events that reset $\phi_{left/right}$ when the leg touches the ground in order to synchronize the CPGs' phases with the environment. This is the only feedback mechanism present in the CPGs model, and it is described in equation 4.7:

$$\phi_{left/right}(t) = \begin{cases} 0, & \text{if the leg touches the ground} \\ \phi_{left/right}(t) & \text{otherwise,} \end{cases} \tag{4.7}$$

In our simulations, the angular frequency ω has a constant value and represents one of the

parameters under optimization.

The pattern formation layer is composed of phase-dependent primitive patterns. Each pattern resembles a bell-shaped waveform with a defined width that can be centered around a specific phase value and is implemented as a raised-cosine function:

$$p(\bar{\phi}; \mu, \sigma) = \begin{cases} \frac{1}{2}\left(1 + cos(\frac{\phi-\mu}{\sigma}\pi)\right), & \mu - \sigma <= \phi <= \mu + \sigma \\ 0 & \text{otherwise,} \end{cases} \qquad (4.8)$$

where $\bar{\phi}$ is the normalized gait phase, μ is the value corresponding to the peak of the bell shape, and σ is the half-width of the curve. The pattern formation layer is composed of five primitives of the same half-width and centered at different times of the gait phase (4.3a):

- P0: $\mu = 0.1$, $\sigma = 0.2$

- P1: $\mu = 0.3$, $\sigma = 0.2$

- P2: $\mu = 0.5$, $\sigma = 0.2$

- P3: $\mu = 0.7$, $\sigma = 0.2$

- P4: $\mu = 0.9$, $\sigma = 0.2$

The choice of modeling the CPG network as the generation of five locomotor primitives has been taken to have smooth an derivable shapes of CPG circuits inputs to motorneuron. More precisely, we took inspiration from the observations done in past experimental studies where five bell-shaped synergies active at different phases of the gait cycle were identified in human studies (Y. P. Ivanenko et al., 2004, 2006). However, it should be noted that those recorded synergies account for the overall motoneuron activity and not just the CPG sub-component. Each motoneuron receives a weighted neural excitation or inhibition u_{CPGs} from all primitive patterns (4.3b) according to the following equation:

$$u_{CPGs} = \sum_{k=0}^{4} w_{m,k} p_k(\phi; \mu_k, \sigma_k), \qquad (4.9)$$

where $w_{m,k}$ is the weight parameter of the pattern k to the motoneuron m to be determined through optimization. The total number of parameters to optimize corresponds to 5 weights per pattern to each specific muscle and the oscillatory frequency. Therefore, the number of parameters for the CPG network is 48. The possible values assigned to $w_{m,k}$ are [-1:1].

Spinal reflexes

To implement a physiologically realistic model of sensory-motor control in human locomotion, we model and investigate five spinal reflexes:

(a) Pattern formation

(b) Synergy motoneuron excitation
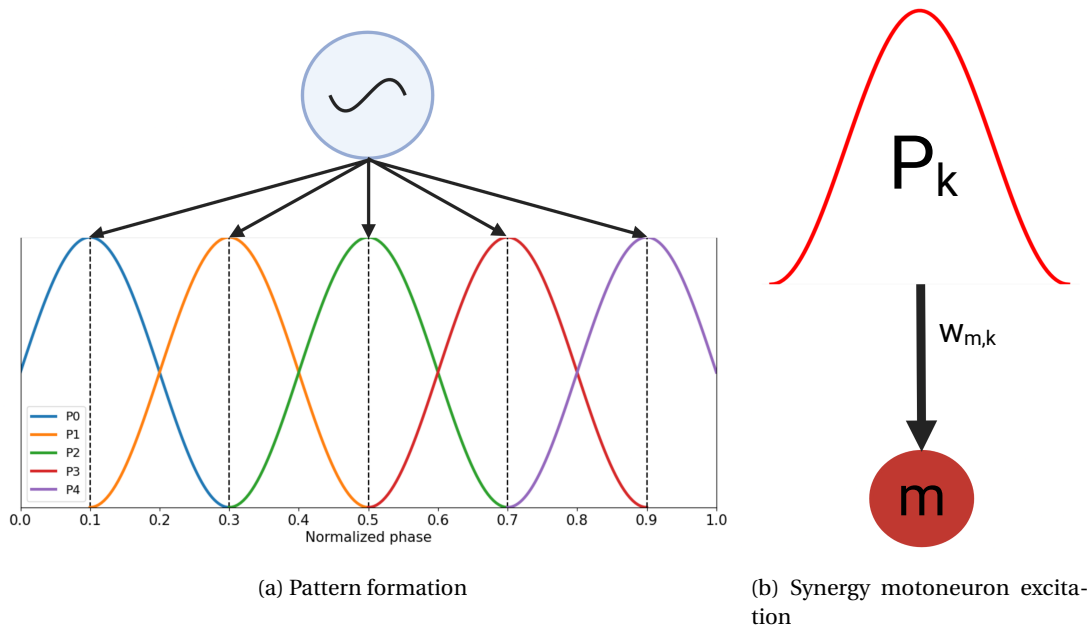
Figure 4.3: CPG structure.

4.3a) The CPG generates five bell-shaped primitives centered at different times of the gait cycle. 4.3b) Each k-pattern stimulates all the m-motoneurons depending on the assigned weight $w_{m,k}$ that can be positive or negative. (Created with BioRender.com)

- Ia afferents provide monosynaptic excitation to motoneurons innervating the same muscle and disynaptic inhibition mediated by Ia inhibitory interneurons to antagonistic motoneurons (4.4a) and model the velocity-dependent response to stretch (Chen et al., 2003).

- II afferents provide disynaptic excitation to motoneurons innervating the same muscle and disynaptic inhibition to antagonistic motoneurons mediated by excitatory and inhibitory interneurons, repectively (4.4b). This reflex models the excitatory role of group II afferents (Lundberg et al., 1987) responding to changes in muscle length during stretch.

- Ib afferents provide disynaptic inhibition to motoneurons innervating the same muscle mediated by inhibitory interneurons.These interneurons reciprocally inhibits with antagonistic Ib-interneurons (4.4c). This reflex is triggered by the Golgi tendon organs and it is introduced to protect muscles when large forces are detected (Capaday, 2001). Additionally, Ib afferents provide dysinaptic excitation to extensor motoneurons innervating the same muscle mediated by excitatory interneurons. These connections model the positive force feedback reversal commonly observed in experimental studies (4.4d) (Geyer et al., 2003; Prochazka et al., 1997; Rybak et al., 2006).

- Renshaw cells are inhibitory interneurons providing inhibitions to motorneurons and Ia-interneurons innervating the same muscle. Additionally, these cells reciprocally inhibits

with antagonistic Renshaw cells (4.4e)(Windhorst, 1990). Renshaw cells are activated by motoneurons innervating the same muscle though synaptic excitation inhibiting these motoneurons when a large activity is detected.

The spinal sensory feedback network is composed of three types of leaky integrator neurons: somatosensory neurons (SNs), interneurons (INs), and motoneurons (MNs). Each of these neurons model the activities of neural populations in the physiological spinal cord. INs have the same properties of MNs responding to the dynamics described in equations 4.1 and 4.2 and with the same activation function $f(x)$. SNs instead presents a rectifier function ($f(x) = max(0, x)$) as activation function, and also the neural input is slightly different:

$$u_{input} = r(t - dt), \tag{4.10}$$

where $r(t - dt)$ is the receptor function and dt the delayed value of the receptor. Transmission delays are known and can be determined according to the proximity of the receptors (Dzeladini et al., 2014). The expressions of the receptors follow the equations:

$$\begin{aligned}
r_{Ia}(t) &= 65/200\sqrt{max(0, \tilde{v}_m(t))} \\
r_{II}(t) &= \tilde{l}_m(t) \\
r_{Ib}(t) &= \tilde{f}_m(t) \\
r_f(t) &= \tilde{f}_f(t),
\end{aligned} \tag{4.11}$$

where $\tilde{v}_m(t)$, $\tilde{l}_m(t)$, $\tilde{f}_m(t)$, $\tilde{f}_f(t)$ are respectively the normalized quantities for contraction velocity, muscle length, muscle force, and cutaneous forces due to ground-foot contact. We choose to consider the normalized quantities to be able to easily scale for different muscles with different values of length and strength. Here, the expression for r_{Ia} was inspired by Prochazka (1999) and modified such that only lengthening $\tilde{v}_m > 0$ triggers a response while ignoring length and activity-dependent terms. We deliberately simplified these expressions because we wanted to capture the general trend and prevent an excessive number of physiological parameters. In Figure 4.4, we present the primitive reflex pathways that govern the connectivity within a single spinal cord segment. These rules are used to build the topological network by assuming that muscles can be categorized as agonists (A), antagonists (N), and extensors (E) or flexors (F).

The relation between agonist and antagonist muscles defines the mutual inhibitions described in 4.4a, 4.4c, 4.4b, and 4.4e. In addition, a muscle can be defined as extensor of flexor. In case it is an extensor muscle, the additional connections of Ib disynaptic extensor facilitation described in 4.4d are included. Some bi-articular muscles can be considered both extensors and flexors since they have different effects on different joints and the Ib disynaptic extensor facilitation is included also in this case. Table 4.1 describes the relations among agonist and antagonist muscles assigned in our models. Accounting for all the weighted connections, the sensory feedback controller has a total of 183 parameters.

(a) Ia mono-/disynaptic excitation and reciprocal inhibition

(b) II disynaptic excitation and reciprocal inhibition

(c) Ib disynaptic autogenic and reciprocal inhibition

(d) Ib disynaptic extensor excitation

(e) RC recurrent inhibition and reciprocal excitation
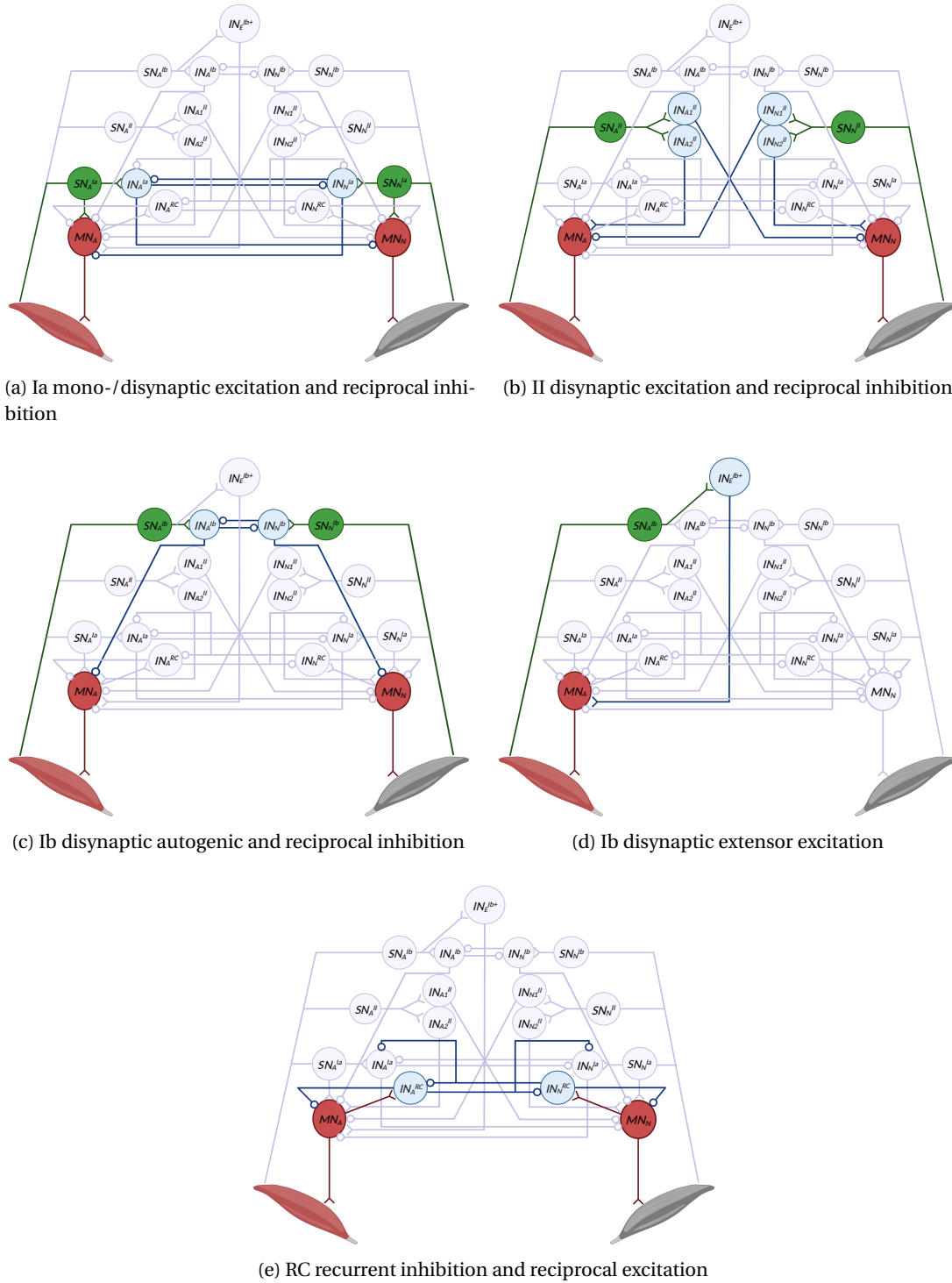
Figure 4.4: Reflex pathways.
Green, blue and red stand for somatosensory ($SN_{A/N}$), inter ($IN_{A/N}$), and motor neurons ($MN_{A/N}$), respectively. The connection tip *o* stands for inhibition while < is for excitation. Subscript letters A, N, and E denote agonist, antagonist, and extensor muscles, respectively. The rules are repeated for all antagonist muscles. (Created with BioRender.com)

Agonist-antagonist muscle relationship

Agonist	Antagonist	Role
ILPSO	GMAX, HAMS	Flexor
GMAX	ILPSO	Extensor
HAMS	VAS, RF	Extensor/Flexor (biarticular)
RF	HAMS, BFSH	Extensor/Flexor (biarticular)
BFSH	VAS, RF	Flexor
VAS	HAMS, BFSH	Extensor
GAS	TA	Extensor/Flexor (biarticular)
SOL	TA	Extensor
TA	GAS, SOL	Flexor

Table 4.1: Agonist-antagonist relationship among muscles modeled.
Each antagonist relationship implies the corresponding reciprocal inhibition of Ia, II, and Ib connections, and the reciprocal excitation connections of RC. The table specifies whether the agonist is considered an extensor, which includes the disynaptic excitation from Ib+, or flexor.

Finally, Figure 4.5 shows the whole spinal network implemented between agonist and antagonist muscles including the reflex pathways and CPGs inputs. On top of this network, ILPSO, GMAX, and HAMS also receive inputs from the balance controller.

4.2.3 Optimization process

In total, the controller's parameters are 256, accounting also for 16 additional parameters regulating initial positions and velocities of the model's DoFs. Because of the large size of the parameters' space and the difficulties in obtaining a stable solution when the network is in an arbitrary state, the optimization process is divided into three steps: imitation objective, optimization for stability, and optimization of metabolic energy. In the first stage, we try determining the network's parameters such that the output of neurons is within a plausible range and motoneurons' activity resembles normal gait solutions. To achieve this, we begin with a previously obtained stable gait simulation generated by a simpler controller (Ong et al., 2019). Given that we know the whole state trajectories of the musculoskeletal system, we can compute the sensory afferent inputs required by the bio-inspired controller. Therefore, we can optimize for network parameters efficiently without numerically integrating the equations of the musculoskeletal system. We call this step imitation learning because we try to imitate a simulated behavior without yet producing dynamically consistent stable gaits. The optimization objective is defined as follows:

$$\underset{\vec{p}}{\text{minimize}} \quad \sum_{t}^{N_t} \sum_{m}^{N_m} \left(e_m^S(t) - e_m^N(t, \vec{x}(t); \vec{p}) \right)^2, \tag{4.12}$$

where $e_m^S(t)$ denotes the target simulated excitation of muscle m at time t, and e_m^N the excitation of the network that depends on time t, the known state variables $\vec{x}(t)$, and parameters $\vec{p}$. The above parameter solution does not produce stable gaits if we evaluate the model by
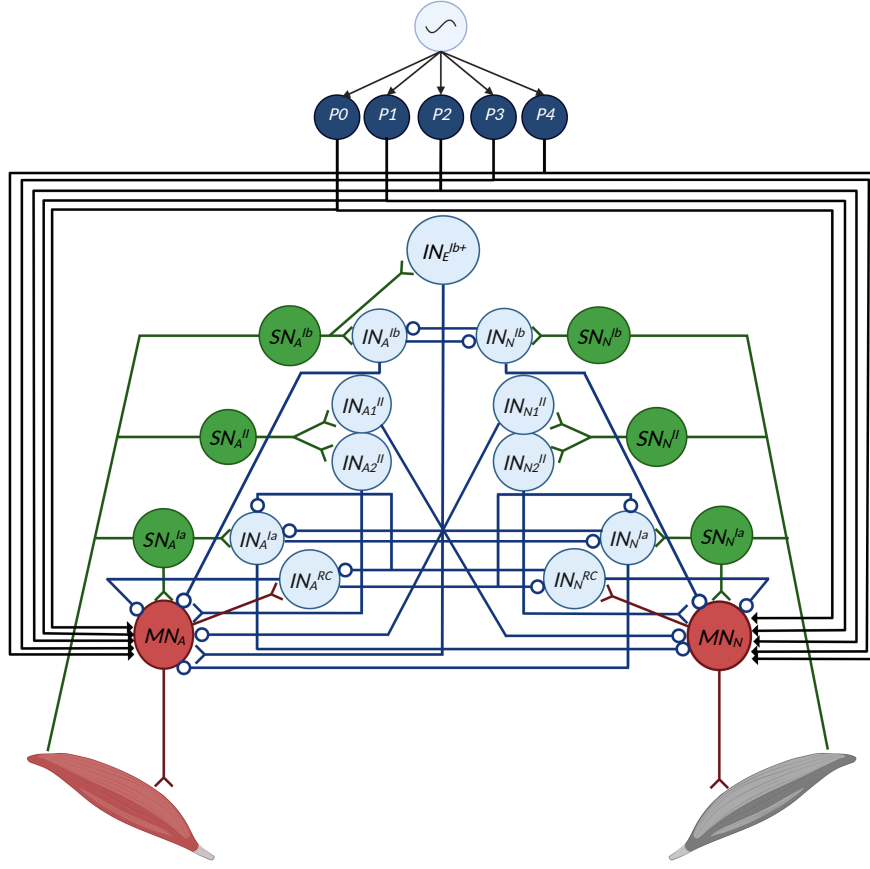
Figure 4.5: Spinal network between a muscle and its antagonist.
The network includes reflexes driven by Ia, II, Ib afferents and Renshaw cells and inputs from CPGs'
patterns. Connections from patterns to motoneurons are represented by back arrows since these
connections be both inhibitory and excitatory. ILPSO, GMAX, and HAMS also receive inputs from the
balance controller. (Created with BioRender.com)

numerically integrating the equations of motion. Our initial goal was to calibrate the network
behavior within a reasonable range of operation in order to avoid neuron activities that are
extreme and always make the model fall and optimization diverge. In fact, the imitation is
only done to obtain a first usable solution for further optimization.

The second optimization aims at obtaining dynamically consistent stable gaits. To do so, we
start integrating numerically the equation of motion producing dynamical gaits by minimizing
the distance between the model's and reference's states as already expressed in equation
4.12, penalizing unstable falling solutions and solutions outside the desired range of speed,
minimizing metabolic effort and joint limit torques. With this process, we aim to obtain stable
solutions generated with our bio-inspired controller with physiological kinematics and muscle
activation. The optimization is done using a CMA-ES algorithm with parameters $\lambda = 40$ and

$\sigma = 5$ (Igel et al., 2007). The cost function for this optimization is defined as follows:

$$\underset{\vec{p}}{\text{minimize}} \quad J_{\text{mimic}} + J_{\text{gait}} + J_{\text{effort}} + J_{\text{limit}} + J_{\text{head}}. \tag{4.13}$$

The term J_{mimic}, represents the model mimicking the reference states as expressed in equation 4.12, J_{gait} penalizes the solution where the center of mass velocity is outside the $[v_{min}, v_{max}]$ range (1.10-1.25 m/s for healthy human gait at normal speed) and the falling solutions. The model is considered to fall when the ratio between its center of mass height (h_{COM}) to the initial state ($h_{COM,i}$) is smaller than a termination height threshold set to 0.8 ($\frac{h_{COM}}{h_{COM,i}} < 0.8$). The term J_{effort} defines the rate of metabolic energy expenditure (Uchida, Hicks, et al., 2016) normalized by the product of body mass and distance traveled. J_{limit} is associated with joint minimization of soft joint limit torques at the knee and ankle joints in order to avoid excessive joint angles (Di Russo et al., 2021). Finally, J_{head} helps to maintain head stability by minimizing horizontal and vertical head accelerations outside the following ranges: $[-4.90 - 4.90]\,m/s^2$ in the vertical direction, and $[-2.45 - 2.45]\,m/s^2$ in the horizontal direction, as previously done by Ong et al. (2019). Concerning the weights, we assigned $w_{\text{mimic}} = 10$, $w_{\text{gait}} = 100$, $w_{\text{effort}} = 1$, $w_{\text{limit}} = 0.1$, and $w_{\text{head}} = 0.25$ in order to promote mainly stability and mimicking. Following this optimization, we use the resulting stable solution as initial condition to find the optimal that minimizes metabolic energy. To do so, we remove the mimicking component of the cost function and optimize for

$$\underset{\vec{p}}{\text{minimize}} \quad J_{\text{gait}} + J_{\text{effort}} + J_{\text{limit}} + J_{\text{head}}. \tag{4.14}$$

J_{gait} allows the stability of future explored solutions and J_{effort} allows convergence toward gait efficiency. In addition, we apply external perturbations to the pelvis and randomized internal perturbations to muscle excitation to obtain more robust and stable gaits. The external perturbation is a force of 100 N applied in the forward and backward direction for a duration of 0.2 s respectively after 3 s and 4 s after the beginning of the simulation. The internal perturbations are applied to sensory receptors. For each controller timestep, a random white Gaussian noise is sampled from a normal distribution with a standard deviation of $s * noise_p$, where $noise_p$ is the proportional standard deviation of the normal distribution, and s is the perturbed sensory signal.

This three steps optimization process was used only to find a proper solution to replicate human gait behavior with a high number of parameters tuning the bio-inspired controller. Stochastic optimization could not converge to a stable solution without these steps and with arbitrary initial conditions. However, using the solution obtained from the three optimization steps as initial condition, different walking patterns can be reached by only optimizing according to equation 4.14 with the different gait behaviors targeted by J_{gait}. Each solution obtained in this way can theoretically be used as initial condition for a new optimization. As long as the initial condition represents a stable solution reproducing human like behavior, similar solutions for a specific gait speed could be achieved from many of these initial conditions.

On the other hand, as previously mentioned, if the initial condition represent an arbitrary state not close to a stable solution, the optimization cannot converge to a stable behavior. The following section will explore the methodology to obtain the different target speeds from the solution obtained from the three optimization steps.

4.2.4 Gait modulation

To study the capability of the proposed bio-inspired controller to reproduce different gait behaviors in human locomotion, we focus mainly on the modulation of locomotor speed. In this way, we aim to evaluate our controller's performance, checking the maximum and minimum speeds it can achieve. Additionally, we evaluate gait analysis and muscle activation for three selected solutions far from the extremes of the achieved speed range since very slow or very fast speeds are more subject to producing artifacts in gait simulations. Therefore the three solutions selected are at 0.6 m/s, 1.2 m/s, and 1.6 m/s representing slow, intermediate, and fast speeds, respectively. To do so, we modulate the optimization parameters $[v_{min}, v_{max}]$ in J_{gait}. Furthermore, we use the data acquired from our model to have possible insights into the contribution of CPGs and spinal reflexes in the neuromotor control of human locomotion and gait modulation. To do so, first, we evaluate the inputs to motoneurons from CPGs and reflexes and how these affect the motoneurons' output at different speeds. We then performed additional optimization where either CPGs parameters or reflexes parameters were fixed to investigate the modulation capabilities of each controller component. The fixed values of parameters are extracted from a reference solution of the model walking at 1.17 m/s with 0.79 m of step length and 0.67 s of step duration. This solution is the one where the optimizer converged without imposing any restriction on the target speed. Finally, we investigate which parameters majorly contribute to gait modulation for the three controller configurations: full control, fixed reflexes, and fixed CPGs. These parameters are identified through a correlation analysis with gait speed, step length, and step duration, were parameters that have a high level of positive or negative correlation with these three gait characteristics (above 0.80 in absolute value) are considered the potential major contributors to gait modulation (Di Russo et al., 2021). The correlation analysis is conducted over 8 samples obtained through different target optimizations for each of the 3 controller configurations.

4.3 Results

Figure 4.6 shows the controller's performance. When minimizing the cost function without imposing restrictions on gait speed, the model converges to a gait at 1.17 m/s of speed, 0.79 m step length, and 0.67 s step duration. 4.6a shows qualitatively the different positions of the model's joints through the gait cycle. The simulated pelvis tilt, hip flexion, knee angle, and ground reaction forces (GRFs) shown in 4.6b faithfully represent the experimental observations from Schwartz et al. (2008) illustrated by the shaded grey areas. Some discrepancies can be observed for the ankle angle that tends to have excessive dorsiflexion and lacks proper

plantarflexion during push-off compared to experimental observations. Indeed, the ankle angle mostly maintains its values above the zero level of plantarflexion/dorsiflexion. However, the simulation replicates the temporal activations observed in experiments from Perry and Burnfield (1992) for TA, GMAX, VAS, GAS, SOL, and HAMS. Concerning ILPSO, the muscle is active also outside its time range, having a consistent activation also in pre-swing. The model converges to different behaviors compared to experimental results for BFSH and RF that are active at the beginning and at the end of the gait cycle, respectively, rather than during swing.

4.3.1 Gait modulation

By optimizing the controller's parameters, the model could reproduce gaits from 0.3 to 1.9 m/s. 4.7a shows the modulation of gait kinematics and GRFs at 0.6, 1.2, and 1.6 m/s representing slow, intermediate, and fast gaits, respectively. As speed increases, the pelvis tilt and the lean angle of the trunk increase in the forward direction by 8 degrees, and the hip flexion oscillates between 35 and -5 degrees at slow speed and 45 and -3 degrees at fast speed. Increasing amplitudes of knee flexion are also observed at high speed, having the peak flexion in swing of 53 degrees at 0.6 m/s and 68 degrees at 1.6 m/s. Fast speed also presents a consistent increase of ankle plantarflexion to -3 degrees of the ankle angle during ankle push-off, whereas this value is maintained at around 10 degrees of ankle dorsiflexion at slow speed. Concerning GRFs, the characteristic double peak shape is very weak at 0.6 m/s. Double peak amplitudes increase with the increase of speed, especially the first peak that shows the reaction with the impact with the ground during heel strike. The duration of the stance phase is reduced from 65% of the gait cycle at 0.6 m/s to 55% at 1.6 m/s. The behaviors of kinematics and GRFs modulation presented resemble the ones observed experimentally by Schwartz et al. (2008). Some differences are observed with the level of ankle dorsiflexion since the model tends to converge to a high-level of dorsiflexion that can differ from experimental data by 7 degrees during heel strike and by 12 degrees during push-off at slow and fast speeds. Additional differences are observed for the level of hip extension at slow speed and knee extension at high speed. In fact, Schwartz et al. observed that the maximum hip extension decreases at low speeds, and knee extension during stance increases at high speeds. In contrast, the model reproduced increased knee flexion during stance at high speeds and a similar level of maximum hip extension at 0.6 m/s compared to 1.2 and 1.6 m/s.

Muscle activity is affected by gait modulation mainly through the increase of activation with the increase in speed. In 4.7b, ILPSO, GMAX, HAMS, TA, and SOL are the muscles that more consistently present an increment in muscle activation. TA and HAMS pass from a maximum activation of 0.2 at slow speed to 0.5 at fast speed, whereas ILPSO has a similar maximum activation at fast speed and a higher activation of 0.3 at slow speed. GMAX has the highest increment of muscle activation, passing from a maximum activity of 0.1 to 0.7. SOL also presents a consistent increase in its activity, passing from a value smaller than 0.1 at slow speed to 0.4 at fast speed. A lower increase is present for VAS at high speed, whereas no consistent variation in muscle activity can be observed for BFSH, RF, and GAS. Therefore,

(a) Gait cycle snapshots

(b) Trunk flex/ext, gait kinematics and GRFs

(c) Muscle activation
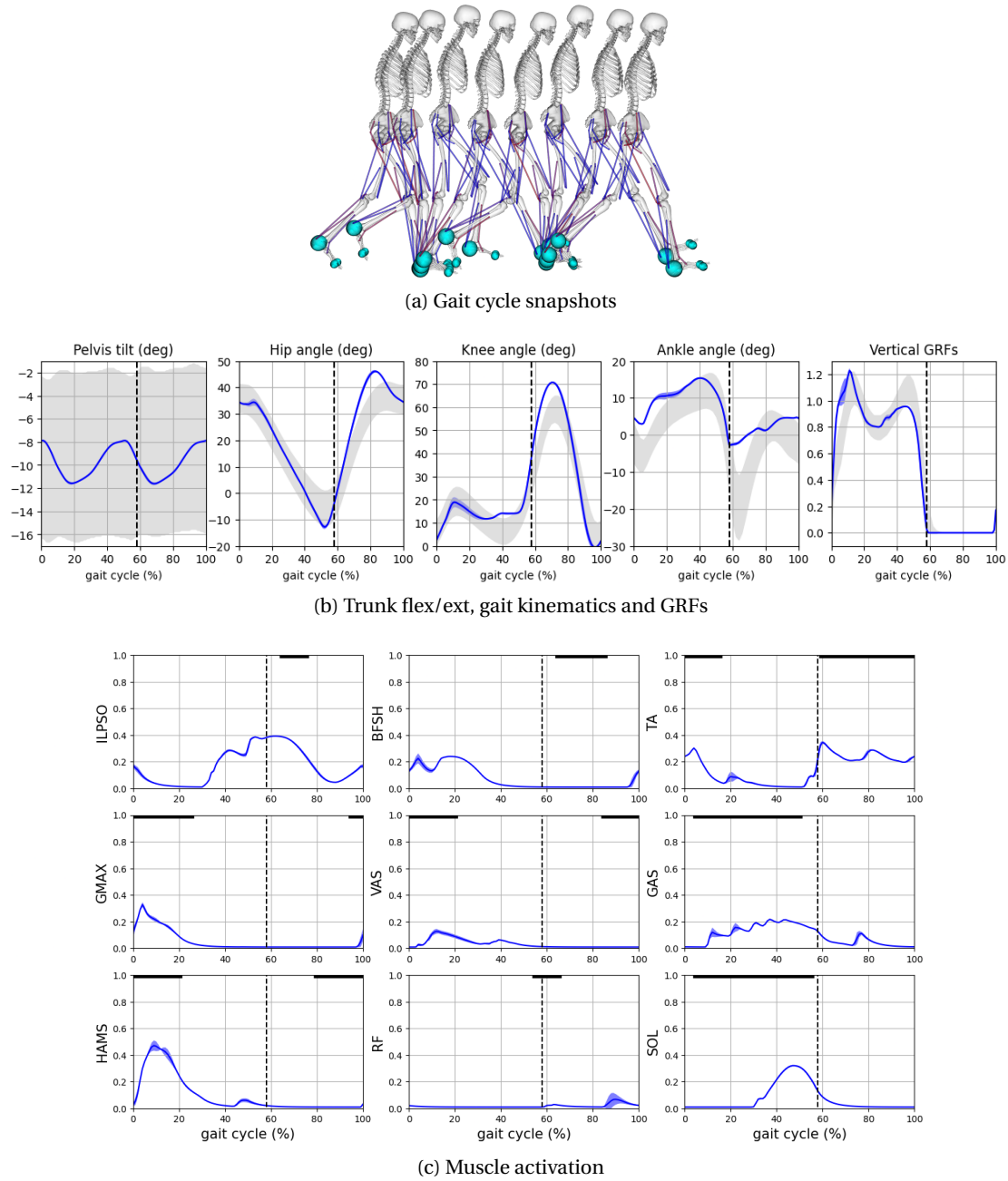
Figure 4.6: Gait analysis of simulated gait at 1.17 m/s.
4.6a) Model position at different times of the gait cycle. 4.6b) Kinematics and GRFs compared to experimental data (Schwartz et al., 2008). Grey areas report the observed experimental ranges for pelvis tilt, hip flexion, knee flexion, ankle dorsiflexion, and vertical GRFs. 4.6c) Muscle activation analysis: muscle activity over a gait cycle for the 9 muscles along the gait cycle. Blue curves represent the means of the gait signals through the gait cycles and the shaded areas the standard deviations. The activation curves are compared with the activation timing observed experimentally (Perry, Davids, et al., 1992) and represented by the solid black lines on the top of the graphs.
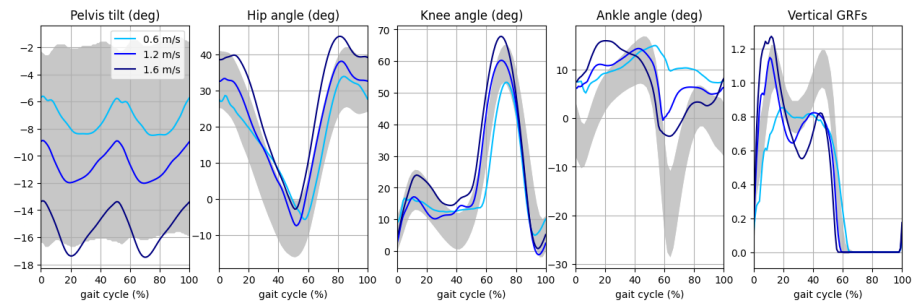
(a) Gait modulation: trunk flex/ext, gait kinematics and GRFs
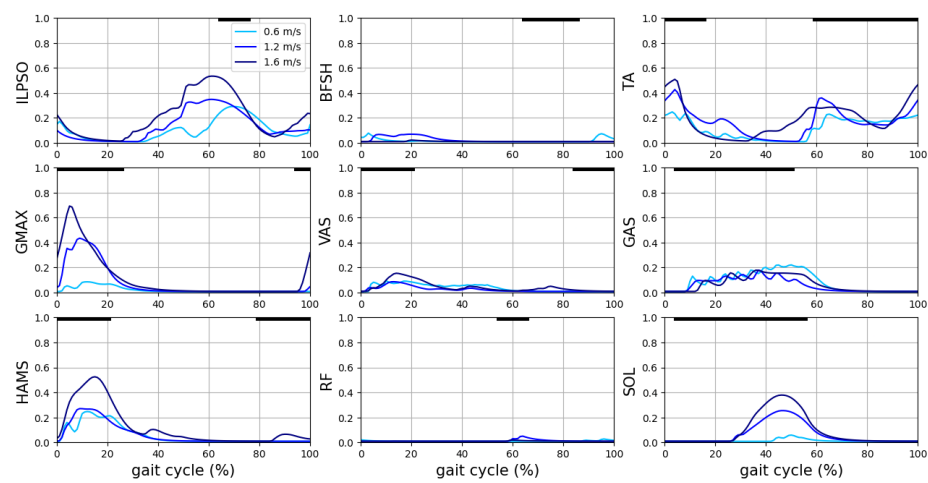
(b) Gait modulation: muscle activation

Figure 4.7: Gait modulation at 0.6, 1.2, and 1.6 m/s.
4.7a) Comparison of kinematics and GRFs among the three speeds. 4.7b) Changing muscle activation at different speeds. The activation curves are compared with the activation timing observed experimentally and represented by the solid black lines on the top of the graphs.

the increased plantarflexion with speed mainly depends on the increased activity of the soleus. In general, the activation amplitude of all muscles increases with speed, as observed experimentally by Cappellini et al. (cappellini2006motor).

4.3.2 Gait modulation: CPGs and reflexes

Past controllers suggested spinal reflexes may be sufficient to generate human locomotion in simulations (Geyer and Herr, 2010; Ong et al., 2019). These reflexes were regulated by state-machine mechanisms. We tested our controller to check whether the spinal connection implemented could generate rhythmic locomotion without the state-machine regulation or the presence of CPGs. With the removal of CPGs, the remaining parameters to optimize are 208. Even if the dimensional reduction could in principle simplify the convergence to a stable solution, no rhythmic gait could be reproduced, suggesting the need for the CPG networks to provide rhythm and timing in the absence of a state machine activating sensory feedback commands at specific times of the gait cycle. The simulation resulting from removing CPG parameters led to the human model in a standing position with the right leg in front of the left leg. The reflexes could generate the muscle activation necessary to maintain this position until the balance controller failed to stabilize the trunk, causing the model to fall. Dzeladini et al. (2014) suggested that the tuning of CPGs applied only to hip muscles could easily modulate human locomotion where other muscles were controlled by sensory feedback. In order to test this hypothesis in our model, we set to 0 the CPG parameters for all muscles except hip muscles and re-optimized the parameters according to the step explained in section 5.2.4. The resulting simulation showed very similar behavior to the one obtained without any CPG parameters, suggesting CPGs inputs may have an important contribution also for knee and ankle muscles. It should be noted that our CPG model provides only a rough waveform (made of the 5 primitives), while Dzeladini's CPG provides a detailed waveform replicating the sensory-driven control signals.

To investigate the contribution of each controller component in gait modulation, we investigated the inputs from CPG circuits, spinal reflexes, and balance controller provided to the motoneurons. Figure 4.8 shows how these signals contribute to generating motoneurons inputs and outputs following equation 4.4. Generally, in the model, the net effect of the reflex circuits tends mainly to inhibit the motoneurons providing a negative stimulation through the whole gait cycle with the exception of ILPSO and TA. Reflexes also facilitate the activation of VAS and GAS during swing for all the speed ranges and the activation of BFSH and HAMS at slow speeds. Instead, for each muscle, CPGs present specific regions of the gait cycle where they excite or inhibit the motoneuron. In this regard, CPGs prevent the activation of specific muscles in specific cycle phases, such as VAS and GAS in swing that were stimulated by the reflex circuits. CPGs' patterns tend to increase the amplitude of inhibition or excitation with increasing speed. This is especially the case for SOL, where the growing muscle activation with speed is primarily due to the increased excitation from CPGs circuits. CPGs activity also helps to have a consistent muscle activation of ILPSO in swing, but it tends to increase the activity at

slow speed, and the lower muscle activity in swing is achieved by reflexes that inhibit ILPSO during swing at 0.6 m/s. The balance controller is applied only to ILPSO, GMAX, and HAMS, and seems to be the leading cause of HAMS activation since the CPGs excitation is entirely inhibited by spinal reflexes.
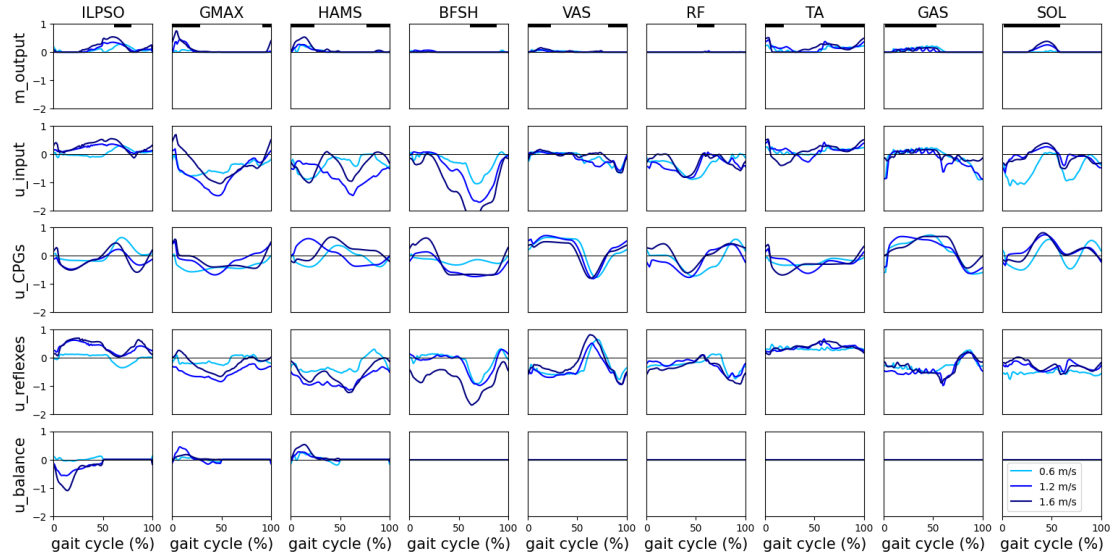
Figure 4.8: CPGs, reflexes, and balance inputs at 0.6, 1.2, and 1.6 m/s.
CPGs, reflexes, and balance generate motoneurons inputs and outputs according to equation 4.4. The contribution of the three controller components is compared through the three speeds selected.

Additionally, we performed optimizations for different target speeds by keeping fixed reflexes parameters or CPGs parameters. Table 4.2 compares the achieved ranges of speed, step length, and step duration for the controller optimizing all parameters (full control), maintaining reflexes parameters fixed (fixed reflexes), and maintaining CPGs parameters fixed (fixed CPGs). The optimization of all parameters allows reaching wide ranges of speed from 0.30 to 1.86 m/s with small and large step lengths (0.23 to 1.08 m) and step durations (0.53 to 0.84 s). Removing reflexes parameters' optimization allows reaching ranges similar to the ones obtained in full control. However, the missing optimization of CPGs parameters significantly limits the controller's capabilities to modulate step duration, passing from a range covering 0.53-0.84 s to 0.64-0.67 s. Consequently, the optimization tends to achieve slow or fast speeds, mainly modulating the step length to reach large values of 1.21 m at high speed. The achieved value of step length is higher than the one in full control because the model converges to a more energetically efficient gait reducing the step duration when all parameters are optimized. By maintaining only the oscillatory frequency fixed and optimizing all the other parameters, the controller covered a similar range compared to the configuration with fixed CPGs, suggesting that the CPG frequency could be the principal modulator of step duration. However, we verified that the modulation of CPG frequency alone is insufficient to converge to different gait behaviors. Indeed, the model loses stability without significant changes in gait speed when only the CPG frequency is tuned. This result implies that the modulation of CPG frequency alone may be necessary but not sufficient to modulate step duration.

	Full control	Fixed reflexes	Fixed CPGs
Speed (m/s)	[0.30-1.91]	[0.30-1.91]	[0.44-1.91]
Step length (m)	[0.23-1.08]	[0.23-1.08]	[0.30-1.21]
Step duration (s)	[0.53-0.84]	[0.56-0.84]	[0.64-0.67]

Table 4.2: Evaluation of speed, step length, and step duration ranges achieved by the bio-inspired controller in 3 configurations
Full control where all parameters are optimized, fixed reflexes where all reflexes parameters are fixed, and fixed CPGs where all CPGs parameters are fixed.

Correlation analysis

The correlation analysis reported in Table 4.3 gives indications on which parameters had a correlation higher than 0.8 with the main gait characteristics and, therefore, those that could be the main responsible for gait modulation in the three controllers configurations. Specific parameters are identified as:

- $Pk \rightarrow M.MN$ for the input pattern Pk weighted connections to motoneuron $M.MN$, where M is the muscle name.

- ω for phase oscillator frequency.

- $M.N_A^s \rightarrow M.N_A^d$ for parameters regulating the weighted synaptic connections between the source neuron of a specific muscle ($M.N_A^s$) and the destination neuron of the target muscle ($M.N_A^d$). N represents the type of neuron and can be either SN, IN, or MN, and A represents the type of afferent and can be either Ia, II, Ib, $Ib+$, or RC

- $M.N_A.w0$ is the activation offset of the neuron N_A regulating the neuronal response.

In full control, both reflexes and patterns' connections seem to contribute to gait modulation. The first (P0) and third (P2) patterns connections to extensor muscles like GMAX and SOL positively correlate with increasing speed and step length and decreasing step duration. The CPGs' frequency (ω) has a highly consistent correlation with gait speed and step duration, suggesting again the direct influence of this parameter on gait frequency. The only reflex parameter representing an excitatory connection is the monosynaptic excitation of Ia afferents from TA ($TA.SN_{Ia} \rightarrow TA.MN$), having a negative correlation with speed and favoring increased dorsiflexion during slow gaits. Another relevant parameter is the length offset of the II somatosensory neuron of GMAX ($GMAX.SN_{II}.w0$) with a positive correlation with speed and step length meaning a higher level of stretch is needed to activate length feedback from II afferents. The other reflex parameters presented are inhibitory connections, which implies that a highly negative correlation with a gait characteristic (either speed, step length, or step duration) means an increased inhibition with the increase of that gait characteristic. The II interneuron of ILPSO tends to decrease its inhibition to GMAX motoneuron ($ILPSO.IN_{II} \rightarrow GMAX.MN$) when speed increases and step duration increases, favoring the activation of GMAX in these

conditions. The same mechanism is involved in facilitating the activation of SOL through the decreasing inhibition from II interneuron of TA ($TA.IN_{II} \rightarrow SOL.MN$). The last two reflex parameters for the controller in full control configuration involve the reciprocal inhibition mechanisms of interneurons and Renshaw cells. GAS's Ia interneuron increases the inhibition to TA's Ia interneuron with increasing speed ($GAS.IN_{Ia} \rightarrow TA.IN_{Ia}$), enhancing the activation of GAS itself because of the decreased inhibition from $TA.IN_{Ia}$. Then, the Renshaw cell of RF decreases its inhibition to the Renshaw cell of HAMS ($RF.IN_{RC} \rightarrow HAMS.IN_{RC}$) with increasing speed, favoring the inhibition of the hamstrings muscle. Indeed, from the previous analysis, the increased activation of HAMS with speed was mainly due to the input from the balance controller.

Concerning the configuration with fixed reflexes, CPGs' frequency (ω) highly correlates with speed and step duration also in this case. Another modulator for step duration is the input from the fifth pattern to TA's motoneuron ($P4 \rightarrow TA.MN$), which indeed increases its activation at the end of the gait cycle with increasing speed. The first pattern ($P0$) tends to increase the inhibition to GAS and GMAX at the very beginning of the gait cycle with increasing speed. Then, speed modulation through modulation of step length is enhanced by tuning the excitation from the second pattern ($P1$) to SOL motoneuron ($SOL.MN$) in order to increase propulsion in stance.

When CPGs parameters are fixed, speed modulation happens mainly through step length changing because of the controller's limited capability to modulate step duration without tuning CPGs' frequency. The controller tends to increase step length by increasing the offset to enhance the length feedback of ILPSO ($ILPSO.SN_{II}.w0$). II afferents are also involved with the decreased length feedback of VAS muscle with speed rising through the excitation of $VAS.IN_{II}$ from $VAS.SN_{II}$. The last two relevant parameters concern the inhibitory connections of Renshaw cells and Ib afferents. The Renshaw cell interneuron of GAS ($GAS.IN_{RC}$) decreases its inhibition to the Ia interneuron of TA ($TA.IN_{Ia}$), decreasing the activation of GAS itself at fastest speeds. Higher speeds should, in principle, increase the activation of GAS, but in the modulation of muscle activation, we previously observed that the optimizer tends to maintain the same activation level for the gastrocnemius muscle during speed modulation. Finally, the Ib inhibitory interneuron of TA ($TA.IN_{Ib}$) decreases its inhibition to the Ib interneuron of SOL, allowing the inhibition of this muscle. Indeed, we previously observed that the increased muscle activation of soleus at higher speeds was not due to the input from spinal reflexes but primarily due to increasing excitatory inputs from CPGs.

4.4   Discussion

In this study, we aim to investigate the possibility of controlling human locomotion by relying only on spinal reflexes not regulated by a state machine mechanism and to investigate the contribution of both CPGs and spinal reflexes in generating locomotor output. To do so, we developed a bio-inspired controller composed of a balance controller, a CPG network, and a

Full control	Speed	Step length	Step duration
$P0 \rightarrow GMAX.MN$	0.92	0.86	-0.9
$P2 \rightarrow SOL.MN$	0.80	0.80	-0.87
$GAS.IN_{Ia} \rightarrow TA.IN_{Ia}$	-0.82	-0.86	0.81
$GMAX.SN_{II}.w0$	0.82	0.81	-0.86
$ILPSO.IN_{II} \rightarrow GMAX.MN$	0.96	0.89	-0.98
$RF.IN_{RC} \rightarrow HAMS.IN_{RC}$	0.83	0.85	-0.8
$TA.IN_{II} \rightarrow SOL.MN$	0.9	0.89	-0.87
$TA.SN_{Ia} \rightarrow TA.MN$	-0.92	-0.83	0.9
ω	0.97	0.88	-0.98

Fixed reflexes	Speed	Step length	Step duration
$P0 \rightarrow GAS.MN$	-0.84	-0.74	0.83
$P0 \rightarrow GMAX.MN$	-0.83	-0.8	0.83
$P1 \rightarrow SOL.MN$	0.85	0.94	-0.54
$P4 \rightarrow TA.MN$	0.79	0.70	-0.85
ω	0.92	0.83	-0.99

Fixed CPGs	Speed	Step length	Step duration
$GAS.IN_{RC} \rightarrow TA.IN_{Ia}$	0.81	0.83	-0.67
$ILPSO.SN_{II}.w0$	0.91	0.91	-0.83
$TA.IN_{Ib} \rightarrow SOL.IN_{Ib}$	0.89	0.87	-0.94
$VAS.SN_{II} \rightarrow VAS.IN_{II}$	-0.85	-0.85	0.82

Table 4.3: Correlations coefficients of controller's parameters contributing to the modulation of speed, step length, and step duration in the 3 controller's configurations: full control, fixed reflexes, and fixed CPGs.

sensory feedback network based on physiological spinal reflexes maintaining a state-machine mechanism only for the balance of the trunk. The proposed controller could replicate human kinematics and ground reaction forces (GRFs) with some limitations in the ankle angle in which the model converges to an excessive dorsiflexion behavior. Regarding muscle activation, the model could reproduce most of muscle activation timings observed experimentally, with the exception of BFSH, which is active outside its range in human recording. The proposed network could probably generate muscle activation closer to physiological activity with additional optimizations. However, finding this global optimal solution results challenging because of the large number of parameters.

Many aspects of speed modulation from human recordings, such as the increased amplitudes of flexion/extension movements and the increased muscle activation with growing speed, are also matched by the model. Concerning the role of CPGs and spinal reflexes in the neural control of human movement, we investigated the possibility of finding stable solutions without relying on CPGs as suggested by previous neuromechanical studies (Geyer and Herr, 2010;

Ong et al., 2019). In our optimizations, we could not find any stable rhythmic behavior in the absence of CPGs' commands even if the number of parameters to optimize significantly decreased, suggesting the need for the CPG network to provide rhythm and timing in the absence of a state machine activating sensory feedback commands at specific times of the gait cycle. Therefore, reflex-based circuits are always active through self-regulation by the afferents, lacking any timing information without CPGs. Similarly, a pure CPG network without reflexes leads to unstable solutions. While we cannot rule out that a different network topology might give rise to high-quality gaits, our model highlights the need for both types to achieve stable and natural movements. Indeed, natural locomotor behavior emerges when both CPGs and spinal reflexes are active. Our study suggests that the state-machines used in previous sensory-driven models (Geyer et al., 2003; Ong et al., 2019) could, in fact, be replaced by CPGs and that one of the main roles of CPGs, in addition to simplifying speed control (Dzeladini et al., 2014), is to serve as gating mechanism that ensures that reflexes do not affect muscles all the time but only at specific moments of the locomotor cycle.

More specifically, the performances on gait modulation while either reflex circuits or CPGs commands were fixed, and the corresponding correlation analysis highlighted the importance of CPGs' frequency in changing the step duration. Therefore, in the model, CPGs have a crucial role in determining gait timing. Additionally, the analysis of neural inputs to motoneurons showed that the net inputs of reflexes are mainly inhibitory through the gait cycle for the proposed model, except for ILPSO and TA, which globally receive excitatory inputs. CPGs' patterns excite or inhibit motoneurons in specific phases of the gait cycle to allow or prevent muscle activation. Therefore, CPGs seem to be important to determine activation timing other than gait frequency. Such a control strategy is similar to the one proposed by Laquaniti et al. (2012) where the timing and magnitude of EMG activity are tuned via proprioceptive feedback and CPGs that control the basic rhythms and patterns of motoneuron activation. However, it should be highlighted that the five locomotor primitives described by Ivanenko et al. (2004) and Laquaniti et al. (2012) were not equally spaced in the gait cycle phase as they are in our controller. This is because, in these studies, the primitives were extracted with factorization of EMG activity. Yet, this activity is the result of the global input received by muscles without being able to distinguish which input was coming from spinal reflexes and which one from CPGs circuits. Therefore, we decided to simplify the distribution of the five primitives and equally space the patterns through the gait cycle since the primitives measured in experiments could hardly be generated by the CPGs commands alone. This choice still leads to largely reproducing the experimental activation timing.

The modulation of gait reflexes alone could still regulate muscle activation to achieve different gait behaviors, mainly through the modulation of step length. The correlation analysis highlighted the possible parameters responsible for this behavior, such as the offset of II fibers regulating the level of stretch necessary to activate length feedback for ILPSO and GMAX. Indeed, increasing these parameters allowed larger amplitude for hip flexion/extension, promoting larger step lengths.

In general, the proposed controller presents a highly redundant system where several different combinations of neural inputs can generate the same muscle activation. The correlation analysis gave possible insights into which parameters could be the most relevant in the control of gait modulation. Yet, given the high redundancy, a separate and more extensive study would be necessary. Possibly, this study should include a large dataset of optimizations and additional elements of the cost function that could guide toward the best combination of neural inputs to generate specific muscle excitation, such as the minimization of the total neuronal activation. Then, the results should ideally be validated by experimental measurements.

Some limitations of the proposed controller should be considered. Because of the large number of parameters, finding a stable solution replicating human walking with the proposed controller may be challenging since it requires the three optimization stages described in section 5.2.4. However, once this solution is found, it can be used as a starting point to explore different gait behaviors by only performing the last optimization stage. In this way, we could reproduce a wide range of speeds comparable to or larger than the ones previously obtained by other neuromechanical controllers (Di Russo et al., 2021; Ong et al., 2019; Song and Geyer, 2012). Yet, the used cost function is very sensitive to the changing of optimization variables. Therefore, the optimization method used might require a good initial guess. For this reason, the initial stage of the optimization requires the imitation objective from a previous solution found with a different neuromechanical controller. This step was necessary because some parameter combinations can quickly saturate the neurons' output and overexcite or excessively inhibit the network resulting in permanent or no muscle activation and leading to model failures during volatile movements. There is a low probability that a random initialization of parameters can make the convergence to a stable solution. If the model falls initially, it is hard to learn a good solution to improve the gait and escape the local minimum. However, the use of the imitation objective implies that any lack of performance from the imitated solution in replicating human movement will probably reflect a lack of performance of the bio-inspired controller. This has probably been the case for the excessive dorsiflexion behavior performed by our model since many solutions of the reflex-based controller proposed by Ong et al. (2019) that we used as imitation objective presented the excessive dorsiflexion behavior. Therefore, the proper choice of the initial imitation objective is crucial for the correct optimization of our model.

Further considerations should also be made for the design of the reflex controller. In paragraph 4.2.2, we explained how we simplified the expressions for the sensory receptors to capture the general trend and prevent an excessive number of physiological parameters. In reality, the dynamics of these receptors are very complex (M. P. Mileusnic et al., 2006; M. Mileusnic and Loeb, 2009), and there is little evidence why the same model identified in specific animal experiments can generalize to humans in the presence of dynamic movements.

Despite these limitations, the bio-inspired controller we propose is a promising tool for investigating spinal circuits in human locomotion. Indeed, we have already shown the insights this model could give into the relationship between CPGs and spinal reflexes. Further suggestions

could be provided in investigating pathological gaits. Past studies tried reproducing neural pathologies with neuromechanical simulation by extending previous controllers, including specific connections to model the pathology in the desired degree of freedom (Bruel et al., 2022). However, the controller proposed could be more suitable for studying neuropathologies like hyperreflexia considering the effects of both excessive inputs from Ia fibers and the lack of reciprocal inhibition. Furthermore, further aspects of gait modulation regulating standing to walking transitions and acceleration and deceleration mechanisms can be investigated. Additionally, this controller could be used as a starting point to further extend the modeling of the neuromotor system by including the implementation of additional spinal neural connections like γ-motoneurons (Ellaway et al., 2015) and descending inputs from the brainstem and other supra spinal brain areas, even though this would increase even more the controller's complexity and the total number of parameters. Additionally, future implementations could include less abstract and more realistic CPG models, for instance, based on more detailed models previously proposed for mammalian circuits that could potentially be taken as a reference for modeling human locomotion (Ausborn et al., 2019; Ausborn et al., 2018; Danner et al., 2017; Danner et al., 2016). Additional connections between CPGs and spinal reflexes may be implemented, allowing somatosensory neurons to interact and modulate CPGs' patterns and CPGs' patterns to interact with spinal interneurons other than motoneurons.

4.5   Conclusions

This study proposes a novel physiologically plausible neuromechanical controller maintaining a good balance between complexity and realism to investigate the spinal components governing human locomotion. The controller is composed of a balance controller from Ong et al. (2019), a CPG network inspired by Aoi et al. (2010), and a sensory feedback network that takes into account the main reflex connections in the spinal cord without being tuned by a state machine. The controller demonstrated the ability to reproduce key behaviors of human locomotion and its modulation in simulations. Results from optimizations suggested that rhythmic locomotion could not be achieved with the only contribution of spinal reflexes without accounting for a state machine mechanism. This suggests the possible need for CPG networks to generate rhythmic movements by guiding muscle activation timing in specific phases of the gait cycle. The modulation of either CPGs or reflexes parameters or both could reproduce wide ranges of gait behaviors, highlighting the high level of redundancy in human locomotor control. The modulation of CPGs' frequency appeared to be crucial for regulating gait cycle duration. The proposed controller demonstrated to be a promising tool to provide many other indications on how the spinal cord may produce locomotor outputs.

Having investigated the capability of this new controller to reproduce healthy human locomotion, the following chapter will focus on the modeling of pathological gaits.

Supplementary materials

All the codes necessary to replicate our experiments and the parameters and files of our simulation can be found in https://github.com/DiRussoAndrea/Spinal_controller. The SCONE version containing the implementation of the proposed controller can be found in https://gitlab.com/simgait/SCONE.

5 Modeling hamstrings spasticity and contracture leading to crouch gait in cerebral palsy patients using neuro-muscular simulations

Overview

In the last chapter, we presented a new neuromuscular controller for human locomotion. In this last study, we will explore the modeling of spasticity and contracture using this new controller. In chapter 3, we have already investigated the gait deviations of toe and heel walking. Here, we will focus on crouch gait, another common gait deviation observed in CP. To achieve this behavior, by applying neural and biomechanical impairments to the hamstring muscle. Furthermore, we will estimate the benefits of hamstring lengthening surgery in these conditions.

> **Reference publication:**
> This work has not been submitted yet.
>
> **My contributions:**
> - I conceptualized the study and optimizations to perform.
>
> - I run the optimization to generate the results shown.
>
> - I wrote the first draft of the chapter and updated it according to suggestions by my supervisor and collaborators.

Abstract

Cerebral palsy is one of the major motor disorders affecting children and generating different gait deviations. These deviations are generated by biomechanical and neural impairments, and it is often difficult to identify the influence of each impairment to then evaluate the correct treatment. In this study, we use neuromuscular simulations to evaluate the effects of isolated contractures, isolated spasticity, and combinations of these two impairments on the hamstring muscle-inducing crouch gait conditions. Contractures are modeled by reducing the muscle's optimal fiber length and increasing the stiffness parameter. On the other hand, neural spasticity is modeled by increasing inputs from Ia afferents and removing reciprocal inhibition connections with antagonist muscles. Furthermore, we simulate the potential benefit of hamstring lengthening surgery in these conditions. The results suggest that crouch gait conditions can be generated by any combination including contractures where the optimal fiber length is reduced by 80% or more or any combination where spasticity levels have the synaptic weights from Ia afferents equal to 3.0 or higher. Hamstring lengthening reduces crouch gait conditions, increases ankle dorsiflexion, decreases muscle coactivation, reduces stretched conditions in the muscle fibers, and drastically decreases passive forces. Surgeries are more beneficial when gait deviations are induced by muscle contractures, whereas significant gait deviations are still present when weights from Ia afferents are equal to 3.0 or higher. Severe surgeries may decrease gait deviations also for high spastic conditions, but this surgery level leads to difficulties in generating meaningful muscle tension in the hamstring muscle-tendon unit. The proposed model of impairments and surgeries could further contribute to our understanding of the effects of isolated biomechanical and neural impairments in several other gait deviations in CP.

5.1   Introduction

Cerebral palsy (CP) is characterized by early injuries to the developing brain, and it is the most frequent cause of motor impairments in children in Europe (Rosenbaum et al., 2014; Sellier et al., 2016). This pathology is often characterized by muscle weakness and contractures (Gracies, 2005a), impaired coordination of muscles, and spasticity characterized by hypertonia, hyperreflexia, clonus, spasms, and co-contraction (Cappellini et al., 2020; Gracies, 2005b). Muscle weakness is a lack of muscle strength due either to lack of the neural descending drive or by muscle atrophy (Thomas et al., 1997), whereas muscle contractures are characterized by an excessive resistance during passive joint mobilization (Gaudreault et al., 2009) due to overstretched conditions of sarcomere lengths and lower sarcomere number because of the reduced ability for muscle growth (Dayanidhi and Lieber, 2018). In addition, contractures present increased collagen in the extracellular matrix leading to higher passive stresses (L. R. Smith et al., 2011). On the other hand, spasticity is traditionally defined as velocity-dependent hyperexcitability to the stretch reflex (Lance, 1980b) due to increased alpha motor neuron excitability (Leech et al., 2018; Marque et al., 2001), reduction of presynaptic inhibition (Calancie et al., 1993; Faist et al., 1994), and reduction of reciprocal inhibition (Knikou and Mummidis-

etty, 2011). However, the difficulty in characterizing precisely the mechanism of spasticity (Malhotra et al., 2009) led to a lack of consensus around this definition. A European consensus proposed to use the term hyper-resistance to describe the phenomenon of impaired neuro-muscular response during the passive stretch (van den Noort et al., 2017), highlighting the necessity to distinguish the biomechanical component of muscle contracture from the neural component of muscle overactivation in the hyper-resistance. For simplicity, we will use the term contracture for the biomechanical component and spasticity for the neural component.

Neuromuscular simulations are powerful tools allowing the modeling and isolation of different kinds of impairments in a virtual environment. Several neuromuscular models to study human locomotion have been developed over the years (Aoi et al., 2010; Aoi et al., 2019; Di Russo et al., 2021; Di Russo et al., 2023; Geyer and Herr, 2010; Ong et al., 2019; Ryu and Kuo, 2021; Song and Geyer, 2015; Taga, 1995). In terms of simulations of pathological behaviors, Van der Krogt et al. (2016) modeled muscle contracture by altering the passive muscle properties and neural spasticity by altering the linear gain of the velocity-dependent stretch reflex replicating EMG global shape during passive stretching but did not reproduce EMG fast variations. Similarly, Jansen et al. (2014) simulated increased length and velocity feedbacks and altered the reflex modulation of lower limb muscles reproducing hemiparetic gait deviations. Then, Falisse et al. (2018) reproduced spasticity in CP by comparing three models based on velocity, acceleration, and force feedback finding the force feedback better correlated with measured activity during gait. Successively, Bruel et al. (2022) modeled spasticity by augmenting the stretch reflex gain and by altering the reciprocal inhibition pathways among soleus, gastrocnemius, and tibialis anterior. On the purely biomechanical level, Ong et al. (2019) modeled SOL and GAS weakness and contracture with respectively reduced maximal isometric force and reduced muscle fiber optimal length reproducing heel and toe walking. Another aspect that has been recently investigated by neuromuscular simulations is the effect of surgeries in improving gait deviations in CP. Mansouri et al. (2016) investigated the role of rectus femoris tendon transfer surgery on balance recovery, finding that tendon transfer of rectus femoris negatively affects balance recovery in children with CP. Successively, Pitto et al. (2019) developed the SimCP framework simulating the effect of different surgeries on gait performance enabling virtual surgery on the models. More recently, Hayford (2022) simulated the effect of Femoral Derotation Osteotomy (FDO), estimating longitudinal changes over time of clinical measures and outcomes after surgical intervention.

In this study, we aim to evaluate the gait deviations associated with the isolated effect of spasticity, contracture, and the combination of these two impairments affecting the hamstring muscle using neuromuscular simulations. These impairments on the hamstring muscle often lead to crouch gait conditions in CP. In literature, there is not an o unambiguous definition of crouch gait (Van der Krogt et al., 2007). Most studies define crouch gait as excessive knee flexion ranging between 10 and 30 degrees during the stance phase (O'Sullivan et al., 2020). This gait deviation is often treated with orthopedic surgeries like hamstring lengthening, characterized by cuts applied to the hamstring's aponeurosis leading to an increased resting length of connective tissue and muscle weakness (Kruse et al., 2018; Lieber and Theologis,

2021; Pierz et al., 2022). After having modeled hamstring spasticity and contracture, our goal is to model the effect of hamstring lengthening in presence of different combinations of these impairments. In order to evaluate the amount of deviations for the different simulations, we use the Gait Variable Score (GVS) for individual joint deviations and the Gait Profile Score (GPS) for the general gait deviations (Baker et al., 2009; Cimolin and Galli, 2016). Finally, we aim to answer the following questions:

- What are the effects of isolated hamstring contracture and spasticity on crouch gait behaviors?

- What kinds of gait deviations produce the combinations of these impairments?

- How can different levels of hamstring lengthening reduce gait deviations produced by hamstring contracture and spasticity?

We found that crouch gait conditions can result from both isolated spasticity or contracture or a combination of both. The severity of crouch gait increased with the increasing severity of impairments. Mild crouch gaits also present excessive ankle dorsiflexion, whereas more severe conditions lead to increased plantarflexion in stance and toe walking. Mild surgeries improve the gait deviations of mild impairments, moderate surgeries appear to be very effective for all contracture levels and low spasticity levels, and severe surgeries generate exaggerated forward pelvis tilt and overactivation of the hamstring because of the difficulty in maintaining a meaningful tension on the muscle-tendon unit.

5.2   Methods

We used the SCONE software simulation framework (2019) to optimize the spinal controller and to generate gait simulations of 10 s. The SCONE simulation is composed of the following four blocks:

- An OpenSim musculoskeletal model.

- A controller.

- Measures that are minimized through the optimization as components of the cost function

- An optimizer that optimizes the initial conditions and controller parameters to minimize the cost function.

5.2.1   Musculoskeletal model

In the musculoskeletal model shown in Figure 5.1, we used the skeletal structure presented by Delp et al. (1990) with height = 1.8 m and weight = 75.16 kg. The model is constrained

in the sagittal plane with a total of nine degrees of freedom (DoFs): a 3-DoFs planar joint between the pelvis and the ground and 3 rotational DoFs per leg: hip flexion/extension, knee flexion/extension, and ankle dorsiflexion/plantarflexion. The contact model with the ground relies on three spheres per leg: one of radius 5 cm at the calcaneus and two of radius 2.5 cm at the toes. Nine Hill-type muscles per leg actuate the musculoskeletal model: gluteus maximus (GMAX), biarticular hamstrings (HAMS), biceps femoris short head (BFSH), rectus femoris (RF), iliopsoas (ILPSO), vasti muscle group (VAS), gastrocnemius (GAS), soleus (SOL), and tibialis anterior (TA).
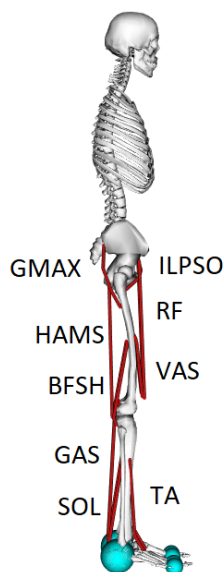
Figure 5.1: Musculoskeletal model.

The model is constrained in the sagittal plane and has 9 DoFs: hip and knee flexion/extension, ankle plantar/dorsal flexion for each leg, and a 3-DoFs planar joint between the pelvis and the ground. Movements are generated by the activation of 9 muscles per leg: gluteus maximus (GMAX), biarticular hamstrings (HAMS), biceps femoris short head (BFSH), rectus femoris (RF), iliopsoas (ILPSO), vasti (VAS), gastrocnemius medialis (GAS), soleus (SOL), and tibialis anterior (TA).

5.2.2   Controller

The spinal controller used to replicate muscle hypertonia is the same we proposed in our previous study (Di Russo et al., 2023) and it is composed of a balance controller from Ong et al. (2019), a CPGs controller based on Aoi et al. (2010), and a reflex controller accounting for sensory feedback from Ia, II, Ib fibers and Renshaw cells. Figure 5.2 shows the spinal connections between a muscle and its antagonist. Table 5.1 describes the agonist-antagonist relationship among the 9 muscles modeled. Accounting for all connections, the controller has a total of 256 parameters. For additional information about the controller structure, we recommend referring to our previous study (Di Russo et al., 2023).
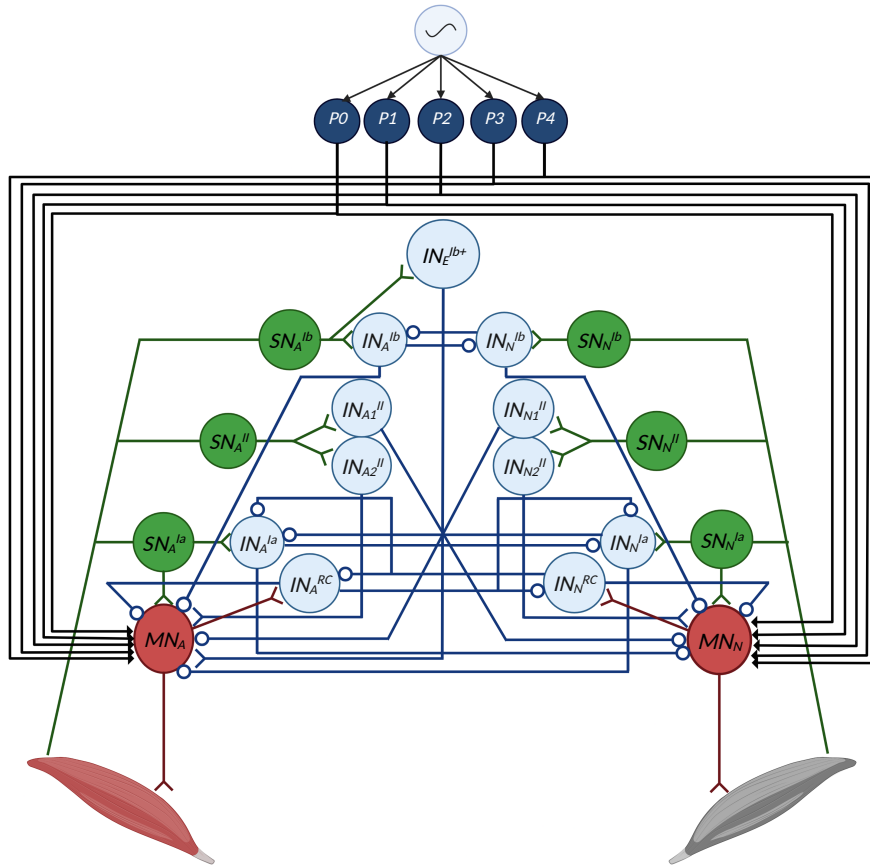
Figure 5.2: Spinal connections between an agonist and antagonist muscles
The controller models GPG networks, Ia, II, and Ib fibers connections together with Renshaw cells inhibitory connections. Green, blue and red neurons represent sensory, inter, and motor neurons, respectively. The connection tip *o* stands for inhibition, < for excitation, and → can be both inhibitory or excitatory. Subscript letters A, N, and E denote agonist, antagonist, and extensor muscles, respectively. The rules are repeated for all antagonist muscles. Ib+ connections are present only if the muscle is identified as an extensor.

5.2.3 Pathological modeling

Modeling muscle contractures

In order to model the biomechanics of muscle contractures, we need to replicate the stretched condition due to fewer sarcomeres in series and the increased passive response to stretch due to the increased collagen fibers in the muscle matrix. The former aspect can be modeled in the Hill-type structure, decreasing the value of the optimal fiber length. This would favor the muscle state in being on the right side of the bell-shaped curve corresponding to the stretched condition. The Hill-type muscle models the number of collagen fibers producing a passive response to stretch as a passive element in parallel with the contractile element. A parameter of this element defined in OpenSim describes the amount of muscle strain necessary to produce a maximum force equal to the muscle's maximum isometric force. A decreased value of this

Agonist-antagonist muscle relationship

Agonist	Antagonist	Role
ILPSO	GMAX, HAMS	Flexor
GMAX	ILPSO	Extensor
HAMS	VAS, RF	Extensor/Flexor (biarticular)
RF	HAMS, BFSH	Extensor/Flexor (biarticular)
BFSH	VAS, RF	Flexor
VAS	HAMS, BFSH	Extensor
GAS	TA	Extensor/Flexor (biarticular)
SOL	TA	Extensor
TA	GAS, SOL	Flexor

Table 5.1: Agonist-antagonist relationship among muscles modeled.
Each antagonist relationship implies the corresponding reciprocal inhibition of Ia, II, and Ib connections, and the reciprocal excitation connections of RC. The table specifies whether the agonist is considered an extensor, which includes the disynaptic excitation from Ib+, or flexor.

parameter would produce a minor amount of muscle strain to reach a passive response equal to the muscle's maximum isometric force and, therefore, higher muscle stiffness. Equation 5.1 defines the equations for the force-length function of the muscle (f_l) and the normalized passive force (F_{PE}) as described in Thelen and Darryl (2003).

$$
\begin{aligned}
f_l &= l_{opt} \cdot e^{-(l_{fiber}-1)^2/\gamma}, \\
F_{PE} &= \frac{e^{k_{PE}(l_{fiber}-1)/\epsilon_0} - 1}{e^{k_{PE}} - 1}
\end{aligned}
\tag{5.1}
$$

where l_{opt} is the optimal fiber length that is equal to 0.069 m for the hamstrings muscle, l_{fiber} the muscle fiber length, γ is a shape factor equal to 0.45, k_{PE} is an exponential shape factor with a value equal to 5, and ϵ_0 is the passive muscle strain due to maximum isometric force equal to 0.6 (Thelen, 2003). Therefore, muscle contracture can be modeled by decreasing the values of l_{opt} and ϵ_0. Figure 5.3 shows the force-length curves for the nominal values of biomechanical parameters that we consider healthy and the same curves for the impaired values. In this study, we apply a scaling factor to l_{opt} and ϵ_0 from 1.0 to 0.6 to study the effect of the decreasing values of these parameters.

Modeling neural spasticity

The modeling of muscle hypertonia can be achieved by altering the spinal connections of the reflex controller. Hypertonia is associated with increased input from Ia afferents, lack of inhibition from Ib afferents, and reciprocal inhibition with the exception of reciprocal inhibition related to Renshaw cells network (Gracies, 2005b). To model this behavior, we disable (synaptic weight equal to 0) the inhibitory connections from Ib fibers and the reciprocal inhibition with antagonist muscles and increase the synaptic weights of connections from the Ia sensory neuron. In this study, we explore the increasing values of Ia weights from 1.0 to 5.0.
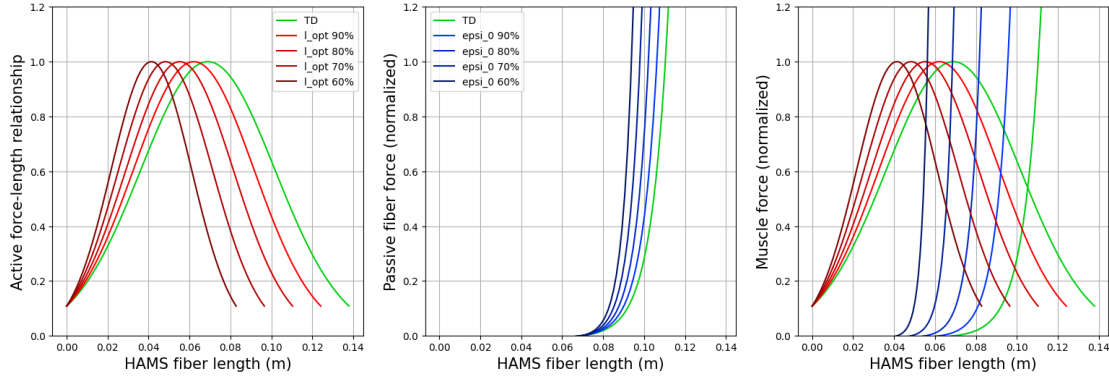
Figure 5.3: Active and passive force-length curves for HAMS in TD and CP.
With the active force-length relationship with decreased values of l_{opt}, the width of the Gaussian curve decreases with the decrease of l_{opt} decreasing the ranges where the muscle can produce a meaningful active force. In the normalized passive force in the muscle fiber, decreasing values of ϵ_0 result in the growing exponential behavior of the passive response when the muscle is stretched.

Modeling muscle surgeries

Similarly to contractures, the modeling of hamstring lengthening can be achieved by altering the parameters of the Hill-type muscle. Specifically for tendon lengthening, the modeling can be done by increasing the slack length l_{slack} of the element in series with the contractile element, and by decreasing the muscle's maximum isometric force F_{max} to model muscle weakness. In this study, we apply a scaling factor to l_{slack} from 1.0 to 1.15 and another scaling factor to F_{max} from 1.0 to 0.85.

Gait deviation measures

To identify the amount of gait deviation compared to the healthy solution, we consider the difference between the healthy and the pathological kinematics for hip flexion, knee flexion, and ankle dorsiflexion. To quantify the amount of gait deviation for each specific solution obtained through optimization, we perform the Movement Analysis Profile (MAP) consisting of assigning a score to the solution's global gait deviations (GPS: Gait Profile Score), and scores to the deviations related to a specific degree of freedom (GVS: Gait Variable Score) (Cimolin and Galli, 2016). The mathematical expressions of GVS and GPS are defined by the following equation:

$$GVS_{joint} = RMS(traj_{joint}^{TD} - traj_{joint}^{CP})$$
$$GPS = RMS([GVS_{pelvis}, GVS_{hip}, GVS_{knee}, GVS_{ankle}]),$$
(5.2)

where GVS_{joint} is the Gait Variable Score related to a specific joint (either pelvis tilt, hip, knee, or ankle), RMS is the root mean square operator, $traj_{joint}^{TD}$ is the trajectory of a specific joint for the healthy condition, $traj_{joint}^{CP}$ is the trajectory of a specific joint for the pathological condition and GPS is the Gait Profile Score.
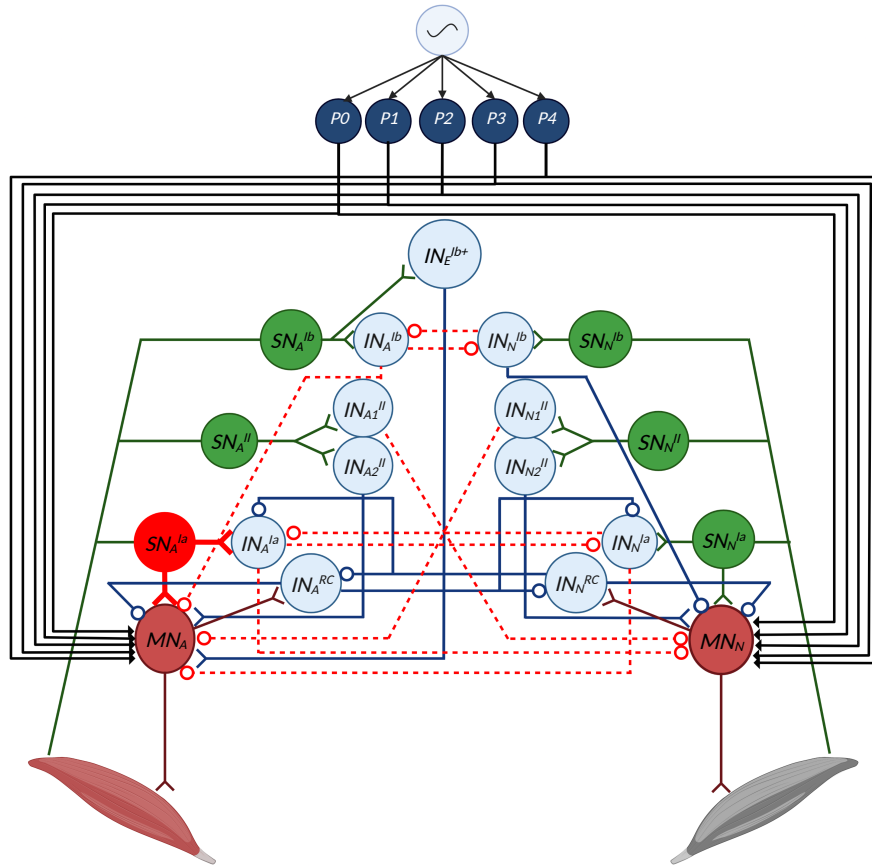
Figure 5.4: Modeling of muscle hypertonia.
Increased inputs from Ia afferents to drive spastic muscle's over-excitability are highlighted by the red color and the sizes of Ia excitatory connections. The lack of inhibition from Ib fibers and the lack of reciprocal inhibition from antagonist muscles are highlighted by the disabled inhibitory connections indicated in red dashed lines.

Through the GVS, the MAP can provide useful insights into which joint variables contribute to the GPS. GPS and GVS are computed as the direct root mean square distance between the evaluated impaired solution and the healthy reference solution computed across the gait cycle for the same joint angles of one side (Baker et al., 2009). In this study, the MAP is represented by colormaps in which the columns represent different levels of biomechanical contracture, the raws different levels of Ia inputs, and the colors the corresponding GPS or GVS. We first present the MAP for the gait deviations without the modeling of surgeries and then for the different surgery levels.

5.2.4 Optimization process

In total, the controller's parameters are 256. When fixing the Ia afferents connections for a spastic muscle and removing the reciprocal inhibitions with antagonist muscles like in the configuration shown in Figure 5.6, the number of parameters decreases depending on the

number of spastic muscles considered and the number of antagonist muscles missing their inhibitory connections. In our case, the only spastic muscle considered is the hamstrings, and the reciprocal inhibitory connections with the antagonist vasti and rectus femoris are fixed to 0. Therefore, the parameters to optimize are 233. The reference healthy solution from which we perform the changing of fixed parameters is taken from the one already presented in our previous study (Di Russo et al., 2023) that represents a simulated gait at 1.17 m/s.

The cost function we use to optimize the parameters penalizes unstable falling solutions and minimizes metabolic effort, joint limit torques, and head accelerations. The optimization uses a CMA-ES algorithm with parameters $\lambda = 40$ and $\sigma = 5$ (2007). The cost function for this optimization is defined as follows:

$$J_{\text{gait}} + J_{\text{effort}} + J_{\text{limit}} + J_{\text{head}} \tag{5.3}$$

The term J_{gait} penalizes the falling solution, meaning when the ratio between the model's center of mass height (h_{COM}) to the initial state ($h_{COM,i}$) is smaller than a termination height threshold set to 0.8 ($\frac{h_{COM}}{h_{COM,i}} < 0.8$). The term J_{effort} defines the rate of metabolic energy expenditure (2016) normalized by the product of body mass and distance traveled. J_{limit} is associated with joint minimization of soft joint limit torques at the knee and ankle joints in order to avoid excessive joint angles (2021). Finally, J_{head} helps to maintain head stability by minimizing horizontal and vertical head accelerations outside the following ranges: $[-4.90 - 4.90] m/s^2$ in the vertical direction, and $[-2.45 - 2.45] m/s^2$ in the horizontal direction, as previously done by Ong et al. (2019). Concerning the weights, we assigned $w_{\text{gait}} = 100$, $w_{\text{effort}} = 1$, $w_{\text{limit}} = 0.1$, and $w_{\text{head}} = 0.25$ to promote mainly stability. Considering the model's structure, where the pelvis and the trunk are merged in a unique segment, high forces applied in the direction of the hamstrings muscle given by the spastic state may result in the trunk being pulled backward, simulating trunk kinematics that could hardly be observed in experiments. Therefore, we assign an additional measure J_{trunk} where we restrict pelvis tilt position to reach values higher than -6 degrees, being the negative the trunk leaned in the forward direction. To this new measure, we assign the weight $w_{\text{trunk}} = 1$. Therefore, the new cost function will be:

$$J_{\text{gait}} + J_{\text{effort}} + J_{\text{limit}} + J_{\text{head}} + J_{\text{trunk}} \tag{5.4}$$

Considering the large number of parameters, finding a stable solution may be challenging. For this reason, the inhibitory connection parameters that should be fixed are changed iteratively. Therefore, we fix no more than three parameters at a time, perform a new optimization where the model can converge easily, and take the new combination of parameters resulting from the new solution as reference for the following optimization, where other parameters are changed until all the connections modeling spasticity are altered. However, once all the necessary inhibitory connections are fixed, the final solution obtained can be used as reference to optimize different levels of Ia inputs.

5.3   Results

We performed different optimizations with combinations of biomechanical and neural impairments to the hamstring muscle.
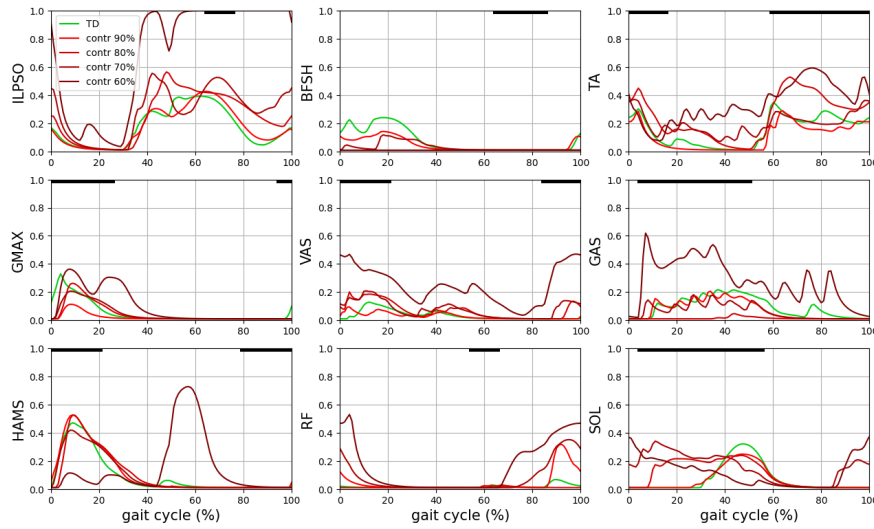
5.3.1   HAMS contracture

The biomechanical contracture is modeled by changing l_{opt} and ϵ_0 parameters of the Hill-type model. Here, we present four different levels of contractures: contr 90% (scaling factor = 0.9 for l_{opt} and ϵ_0), contr 80% (scaling factor = 0.8 for l_{opt} and ϵ_0), contr 70% (scaling factor = 0.7 for l_{opt} and ϵ_0), contr 60% (scaling factor = 0.6 for l_{opt} and ϵ_0). These are compared with the simulated gait for typically developed (TD) that represents our healthy solution, as shown in Figure 5.5. 5.5a compares the gait analysis for the different impairments. A mild contracture of 90% has little effect on the gait behavior. Crouch gait conditions can be observed from contr 80% where the knee angle remains above 20 degrees of flexion throughout the whole gait cycle with high ankle dorsiflexion. As the contracture becomes more severe, the excessive knee flexion increases, remaining above 30 degrees for contr 60%, and the ankle tends to present an excessive plantarflexion during stance leading the model to walk on toes. No meaningful changes can be observed for hip flexion, whereas the pelvis tilt tends to increase the amplitude of its oscillation for severe contractures. From 5.5b, we can observe that the HAMS contracture leads to the increased activation amplitudes of ILPSO, VAS, and RF to counterbalance the high tension from HAMS. In the extreme case of contr 60%, we can also observe an abnormal activation of HAMS during pre-swing and the saturation of ILPSO during pre-swing and swing, and the overactivation of GAS. 5.5c shows the biomechanics of HAMS muscle-tendon unit (MTU). The contracture condition increases the gait cycle duration when HAMS is in a stretched condition generating high passive forces enhanced by the increased stiffness. Indeed, the total forces generated in the HAMS MTU are mainly due to passive forces rather than active forces.

5.3.2   HAMS spasticity

Neural spasticity is modeled by removing the reciprocal inhibitions among HAMS, RF, and VAS, the inhibitions from Ib afferents, and increasing the inputs from Ia afferents. Here we compare the TD solution with three different severities of spasticity: Ia inputs = 1.0, Ia inputs = 3.0, and Ia inputs = 5.0, as shown in Figure 5.6. From 5.6a, consistent gait deviations can be observed from a level of spasticity severity with Ia = 3.0 and above. In these conditions, we can observe mild crouch gait conditions with knee flexion above 20 degrees throughout the whole gait cycle. In addition, knee flexion is maintained below 50 degrees. Concerning the ankle angle, limited dorsiflexion can be observed in stance. Furthermore, increased spasticity leads to higher oscillations of pelvis tilt. In 5.6b, we can observe an overactivation of HAMS, especially during swing. The increased input from Ia afferents generates high peak artifacts with a frequency of approximately 20 Hz. In addition we can observe coactivation of RF and ILPSO. Moreover,
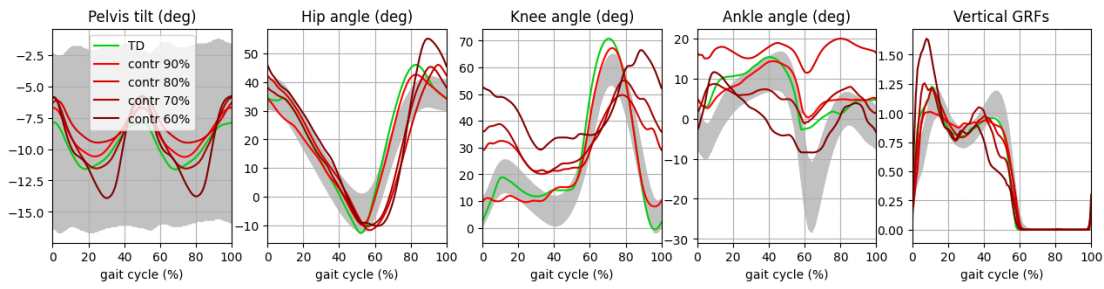
(a) HAMS contracture: Trunk flex/ext, gait kinematics and GRFs

(b) HAMS contracture: Muscle activation
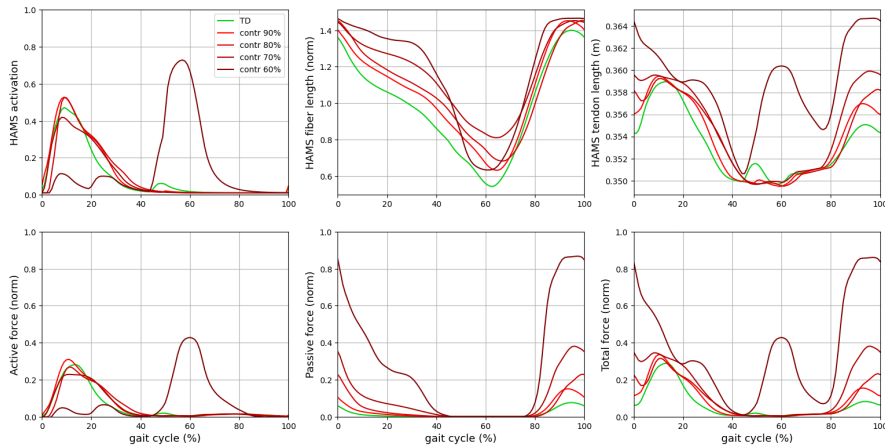
(c) HAMS contracture: HAMS biomechanics

Figure 5.5: HAMS contracture: Comparison among TD (green line), and various levels of contracture: contr 90%, contr 80%, contr 70%, contr 60%.

5.5a) Gait analysis: The increasing contracture leads to a progressive inability to perform knee extension, and compensation mechanisms promote high plantarflexion in stance. The grey areas represent the experimental healthy data from Schwartz et al (2008). 5.5b) Increasing HAMS contracture leads to compensatory mechanisms to increase amplitudes in muscle activation of ILPSO, VAS, and RF. Solid black lines represent the healthy activation timing observed experimentally (Perry, Davids, et al., 1992). 5.5c) Increasing HAMS contracture leads to a stretched condition of the muscle and to high passive forces.

the optimizer converged to solutions where GAS is silent in spastic conditions, leaving the plantarflexor movement to be generated by SOL. The muscle biomechanics shown in 5.6c describes HAMS length to be largely below l_{opt} in spastic conditions, consistently reducing the amount of passive forces generated. Indeed, the total force in HAMS MTU is largely due to active forces generated by muscle activation.

5.3.3   HAMS spasticity and contracture

Here we simulate the combination of neural spasticity and biomechanical contracture: Ia input = 1.0 and contr 90%, Ia input = 3.0 and contr 80%, Ia input = 5.0 and contr 70%, as shown in Figure 5.7. From 5.7a, we can observe limited capability of knee flexion already with the minimum level of spasticity and contracture. Crouch gait conditions can be observed in more severe conditions with knee flexion constantly above 20 degrees and largely above 30 degrees for Ia = 5.0 and contr 70%. The ankle angles show a high dorsiflexion behavior for mild impairments and a progressive excessive plantarflexion in stance, leading the model to walk on toes for the most severe condition. Similarly to what was observed previously, severe conditions of spasticity and contracture lead to high oscillations amplitudes of the pelvis tilt. The muscle activation observed in 5.7b showed HAMS overactivity similar to what has been previously in 5.6b with coactivation and saturation of RF and ILPSO. Similarly to the isolated spasticity condition, GAS muscle is largely silent for impaired solutions leading to increased activity of SOL. In 5.7c, the muscle biomechanics describes increased stretched conditions with the increasing severity of the impairment. This leads to high passive forces generated, and the total force generated in the MTU is due both to passive forces and the active forces generated by the spastic conditions.

5.3.4   HAMS surgery

Here, we model hamstring lengthening for the most severe conditions previously analyzed: contr 60 % for isolated contractures, Ia input = 5.0 for isolated neural spasticity, Ia input = 5.0 and contr 70% for the combination of neural and biomechanical impairments. The surgery is modeled by increasing l_{slack} and F_{max}. We consider four different surgery levels: no surgery (scaling factor = 1.0 for l_{slack} and F_{max}), mild surgery (scaling factor = 1.05 for l_{slack} and 0.95 for F_{max}), moderate surgery (scaling factor = 1.10 for l_{slack} and 0.90 for F_{max}), severe surgery (scaling factor = 1.15 for l_{slack} and 0.85 for F_{max}).

HAMS surgery with contr 60 %

Figure 5.8 describes the simulated effects of the different levels of surgeries with a severe contraction condition (contr 60%) without the presence of neural impairments. From 5.8a, we can observe that a mild surgery can decrease the severity of crouch having the minimum knee flexion passing from 30 degrees to 20 degrees. The ankle angle is also closer to the
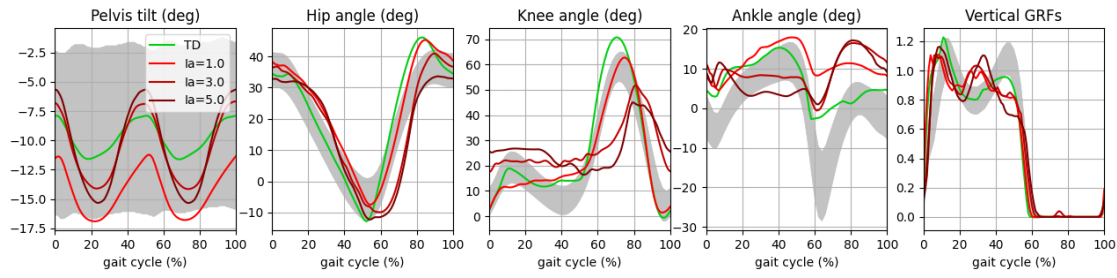
(a) HAMS spasticity: Trunk flex/ext, gait kinematics and GRFs
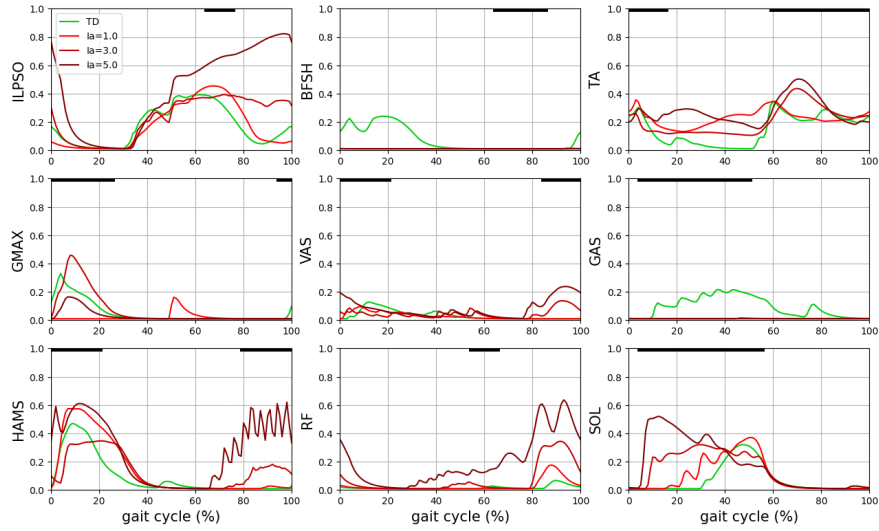
(b) HAMS spasticity: Muscle activation
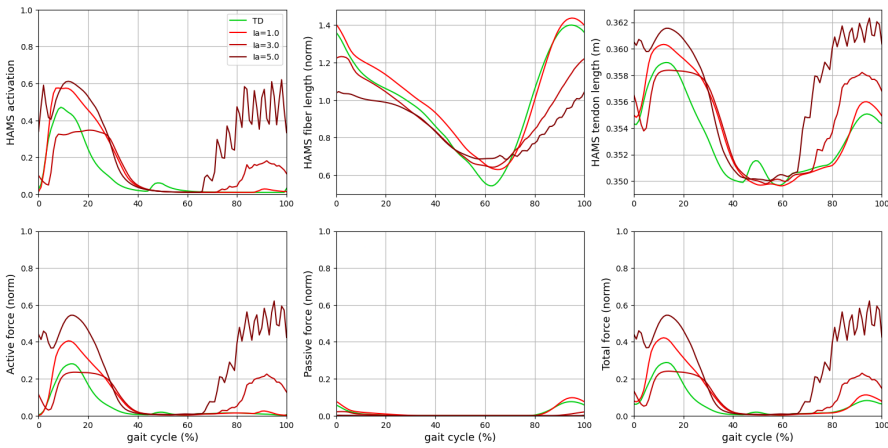
(c) HAMS spasticity: HAMS biomechanics

Figure 5.6: HAMS spasticity: Comparison among TD (green line), and various levels of spasticity: Ia inputs = 1.0, Ia inputs = 3.0, Ia inputs = 5.0.
5.6a) Gait analysis: The increasing Ia input to HAMS leads to increased knee flexion, and compensation mechanisms promote reduced dorsiflexion in stance. The grey areas represent the experimental healthy data from Schwartz et al (2008). 5.6b) Increasing spasticity generates HAMS overactivity in swing and early stance. Compensatory mechanisms lead to increased activation amplitudes in ILPSO and HAMS. Solid black lines represent the healthy activation timing observed experimentally (Perry, Davids, et al., 1992). 5.5c) With the increasing spasticity, HAMS maintains a contraction condition, and the total force produced is mainly due to the active force generated by HAMS activation.
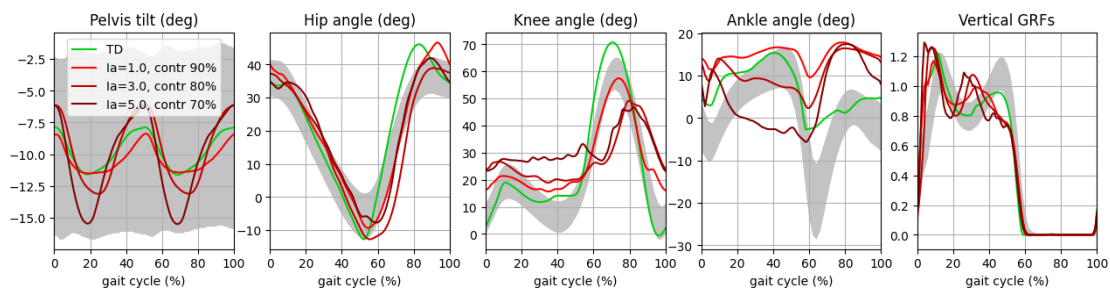
(a) HAMS spasticity and contracture: Trunk flex/ext, gait kinematics and GRFs
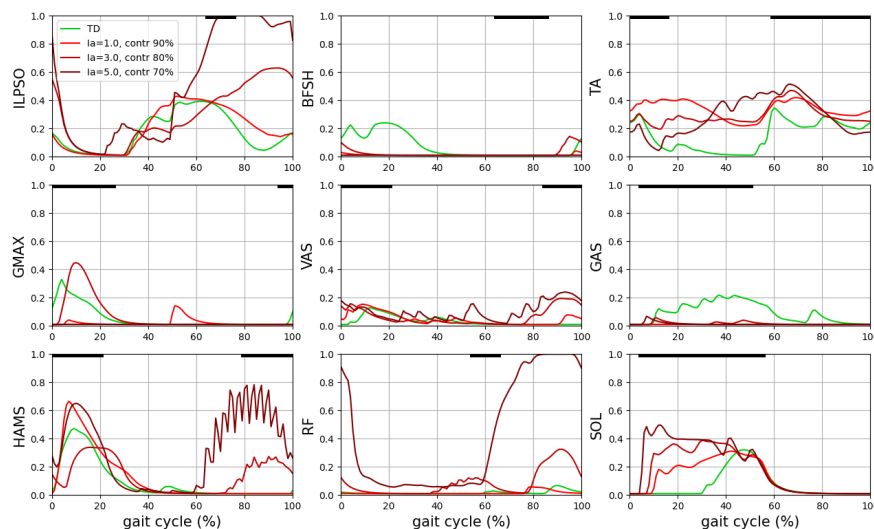
(b) HAMS spasticity and contracture: Muscle activation
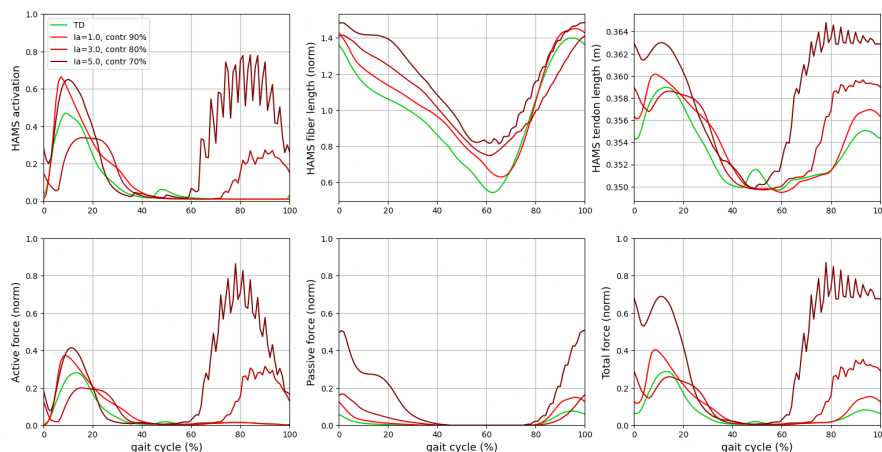
(c) HAMS spasticity and contracture: HAMS biomechanics

Figure 5.7: HAMS spasticity and contracture: Comparison among TD (green line), and various levels of spasticity and contractures: Ia inputs = 1.0 and contr 90%, Ia inputs = 3.0 and contr 80%, Ia inputs = 5.0 and contr 60%

5.7a) Gait analysis: Increasing contracture and spasticity enhance constant knee flexion and decreased dorsiflexion in early stance. The grey areas represent the experimental healthy data from Schwartz et al (2008). 5.7b) Increasing HAMS spasticity and contracture lead to overactivation of HAMS in swing and overactivation of ILPSO, and RF. Solid black lines represent the healthy activation timing observed experimentally (Perry, Davids, et al., 1992). 5.7c) Increasing HAMS spasticity and contracture leads to a stretched condition of the muscle and to high passive and active forces.

115

healthy condition preventing the toe walking condition. For moderate and severe surgeries, the knee angle converges to a kinematic close to TD, and the model does not show a crouch gait behavior anymore. On the other hand, the ankle angle converges to high dorsiflexion behaviors. Concerning the pelvis tilt, decreased oscillations amplitudes can be observed for mild and moderate surgeries, but severe surgery presents high oscillations amplitudes and a forward-leaning of the pelvis. This behavior is probably due to the difficulty in maintaining tension in HAMS for severe surgeries, and a forward-leaning pelvis allows the generation of the necessary muscle tension. The muscle activation described in 5.8b shows HAMS reaching muscle activation close to TD for mild and severe surgeries with decreasing of coactivation with VAS, RF, and ILPSO. GAS, SOL, and TA activation also converge to behaviors similar to TD. However, severe surgery leads to high HAMS activation with values close to saturation. From 5.8c, we can observe how the surgeries prevent the stretched condition of HAMS having the muscle length below l_{opt} for a large duration of the gait cycle. In severe surgery, the muscle reaches its minimum length and maximum contraction. The decreased stretched condition prevents the excessive generation of passive forces, with the resulting total force generated mainly by active forces.

HAMS surgery with Ia input = 5.0

Figure 5.9 describes the simulated effects of the different levels of surgeries with severe hamstring spasticity (Ia input = 5.0) without the presence of neural impairments. In the gait analysis shown in 5.9a, we can observe that the crouch gait condition with knee flexion always above 20 degrees is present for all the surgery levels. For severe surgery, knee flexion between 60% and 80% of the gait cycle is closer to TD with a maximum of 60 degrees. Increasing the severity of surgeries leads to increasing dorsiflexion behaviors and decreasing amplitudes of oscillations of pelvis tilt. From the muscle activation in 5.9b, the increasing severity of surgeries does not present a consistent change in HAMS muscle activation. However, severe surgery leads to decreased coactivation of ILPSO and RF. Severe surgery also presents a weak activation of GAS, whereas this muscle is entirely silent in the other conditions. On the other hand, severe surgery leads to an activation level of TA close to 0.4 throughout the whole gait cycle. In the HAMS biomechanics shown 5.9c, the increasing level of surgery severity, the muscle length progressively decreases, being constantly below l_{opt} and below $l_{opt}/2$ for severe surgery. This leads to the absence of passive force generation. Therefore, the total force is entirely due to active forces generated by the spastic HAMS. The more severe the surgery, the more the active force generated decreases because of the distance of the muscle length from l_{opt} and the weakness induced by the surgery, decreasing the tension given by the spastic activity.

HAMS surgery with Ia input = 5.0 and contr 70%

Figure 5.10 describes the simulated effects of the different levels of surgeries with the combined impairment of neural spasticity (Ia input = 5.0) and biomechanical contracture (contr 70%).
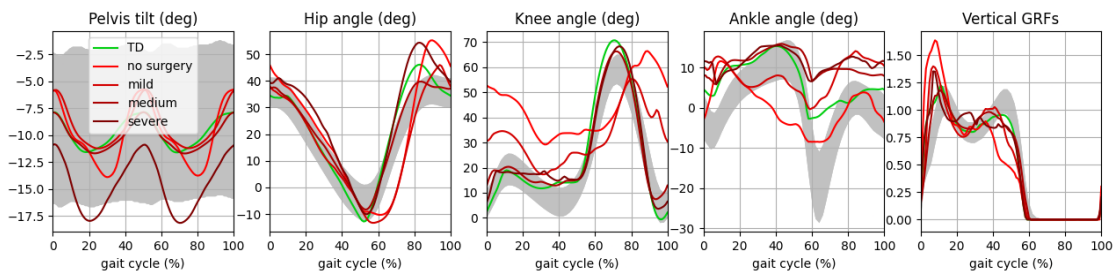
(a) HAMS surgery with contr 60 %: Trunk flex/ext, gait kinematics and GRFs
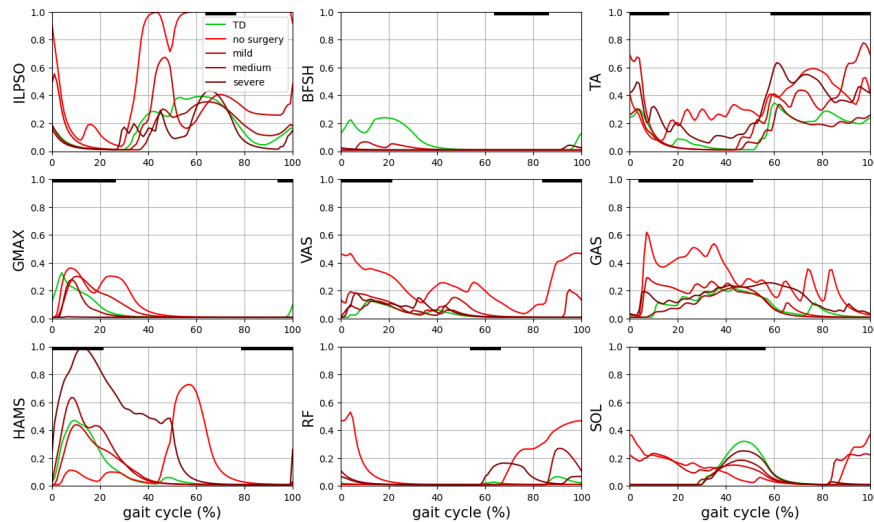
(b) HAMS surgery with contr 60 %: Muscle activation
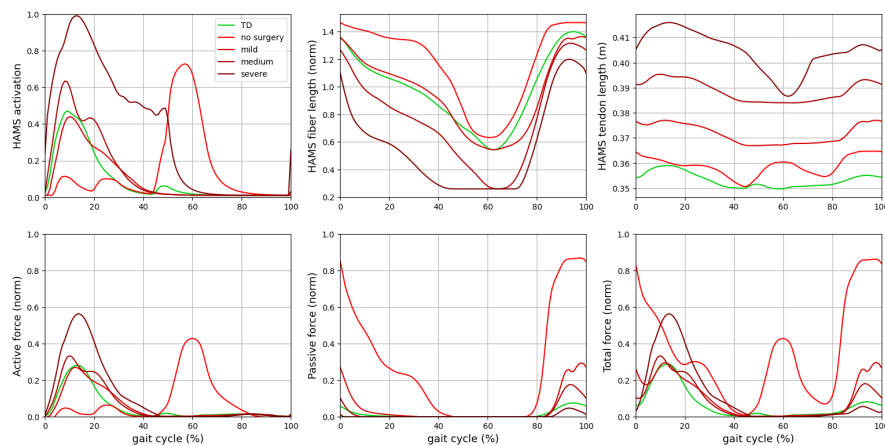
(c) HAMS surgery with contr 60 %: HAMS biomechanics

Figure 5.8: HAMS surgery with contr 60 %: Comparison among TD (green line), and various levels of surgery: no surgery, mild surgery, moderate surgery, severe surgery.
5.8a) Gait analysis: Mild surgery decreases the crouch gait condition. Knee flexion behavior close to TD is reached for moderate and severe surgeries. The grey areas represent the experimental healthy data from Schwartz et al (2008). 5.8b) HAMS activity amplitude is close to TD for mild and moderate surgery, whereas an overactivity is observed for severe surgery. Coactivation of ILPSO, VAS, and RF is drastically reduced for moderate and severe surgery. Solid black lines represent the healthy activation timing observed experimentally (Perry, Davids, et al., 1992). 5.8c) moderate and severe surgeries prevent the stretch condition of HAMS and the generation of high passive forces.

117
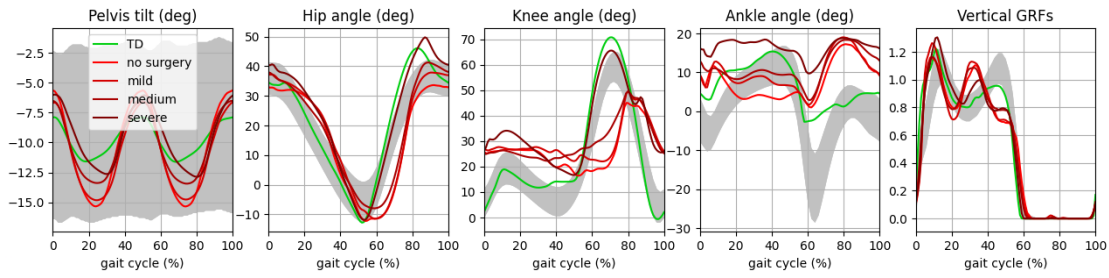
(a) HAMS surgery Ia input = 5.0: Trunk flex/ext, gait kinematics and GRFs
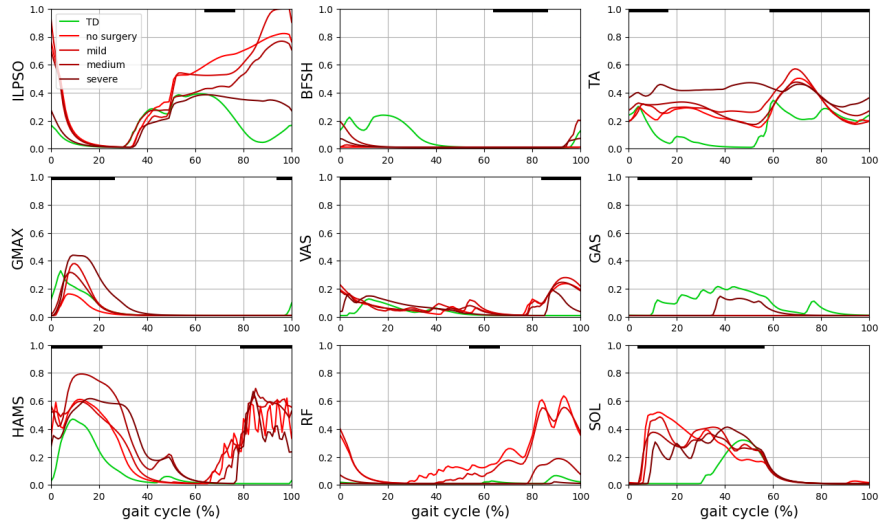
(b) HAMS surgery with Ia input = 5.0: Muscle activation

(c) HAMS surgery with Ia input = 5.0: HAMS biomechanics

Figure 5.9: HAMS surgery with Ia input = 5.0: Comparison among TD (green line) and various levels of surgery: no surgery, mild surgery, moderate surgery, severe surgery.
5.9a) Gait analysis: All surgery levels maintain a crouch gait condition, with the severe one closer to TD concerning knee flexion in swing, and with ankle angle with progressive dorsiflexion. The grey areas represent the experimental healthy data from Schwartz et al (2008). 5.9b) Surgeries generate little changes in HAMS activation. Severe surgery prevents excessive coactivation of ILPSO and RF but generates a high activation of TA. Solid black lines represent the healthy activation timing observed experimentally (Perry, Davids, et al., 1992). 5.9c) Surgeries decrease the active force generated by the spastic HAMS.

From the gait analysis in 5.10a, crouch gait conditions are maintained for mild and moderate surgery, with knee flexion always above 20 degrees and with excessive plantarflexion in stance, leading the model to walk on toes. For severe surgery, knee flexion converges to a solution close to TD with high ankle dorsiflexion. Concerning pelvis tilt, surgeries decrease the amplitudes of oscillations except for mild surgery, which presents oscillations between -5.0 and -15.0. In the muscle activation shown in 5.10b, we can observe that HAMS activation amplitude in swing decreases with the increasing surgery severity. However, HAMS activation increases in stance with severe surgeries until reaching saturation. Coactivation of ILPSO and RF decreases with increasing levels of surgery. GAS is mostly silent throughout the gait cycle for all surgery levels, whereas SOL has an activation shape similar to TD for severe surgeries. The effects of surgeries in the biomechanics of HAMS (5.10c) result in decreasing the stretch level of HAMS fiber until reaching its minimum fiber length for severe surgeries. This condition leads to reducing drastically the amount of passive forces generated since HAMS fiber length is largely below l_{opt}. the total force generated is reduced because of the fiber length range far from the optimal length that can generate the maximum isometric force. In addition, F_{max} decreases with the increase of the surgery severity. In severe surgery conditions, the tension on the HAMS MTU is achieved by activating the muscle until saturation.

5.3.5 Gait deviation measures

Figure 5.11 shows the GPS and GVSs for the three joint angles for different combinations of neural spasticity and biomechanical contractures without any surgery application. We can observe that the GPS increases with the increasing severity of contractures and spasticity. The largest deviations are observed for solutions including contr 60%. The largest deviations contributing to GPS are due to the knee angle, which presents the highest values of GVS up to 30. Lower values of GVS can be found for hip and ankle angles. The hip angle presents the major deviations for high levels of contractures (contr 60 %) and spasticity (Ia input = 3.0 and 5.0). The ankle angle pass from excessive dorsiflexion for mild impairments to excessive plantarflexion in early stance for severe impairments. Indeed, this joint present the highest values of GVS both in mild (contr 80% with no spasticity) and severe (Ia = 5.0 and contr 70%) impairments.

When a mild surgery is applied, we can observe from Figure 5.12 consistent decreased values of GPS for contr 80% and contr 70% in absence of spasticity and with Ia input = 1.0. Increased GPS values compared to the no-surgery condition can be observed for contr 90% without spasticity and with Ia input = 1.0. These solutions were already close to the TD condition and probably the mild surgery augmented the gait deviations. For severe impairments, including solutions with contr 60% and Ia input = 3.0 and 5.0, there are still consistent gait deviations highlighted by high GPS levels, with the highest peak reached at Ia input = 5.0 and contr 60%. Also in this case, the GVS of knee flexion is the main contributor to the GPS. Some improvements in gait deviations at the hip angle can be also observed for contr 80% and contr 70% in absence of spasticity and with Ia input = 1.0. Concerning the ankle angle, no consistent

(a) HAMS surgery with Ia input = 5.0 and contr 70%: Trunk flex/ext, gait kinematics and GRFs
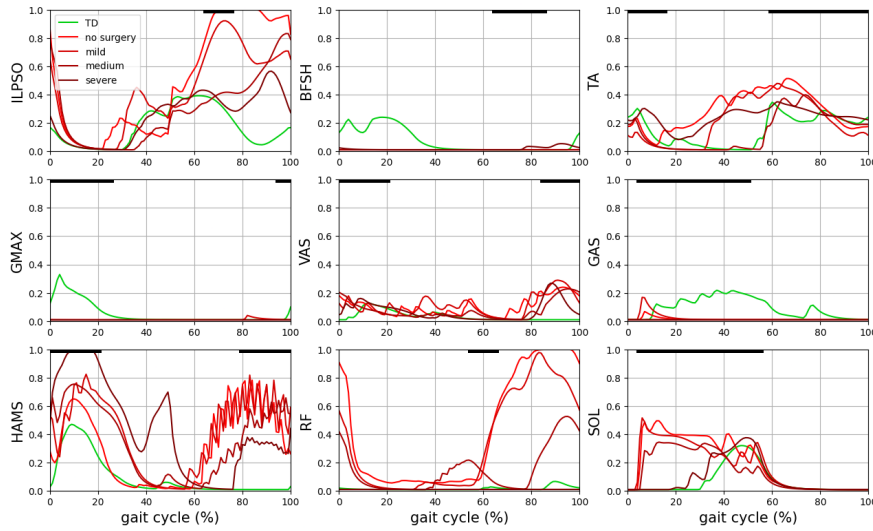
(b) HAMS surgery with Ia input = 5.0 and contr 70%: Muscle activation
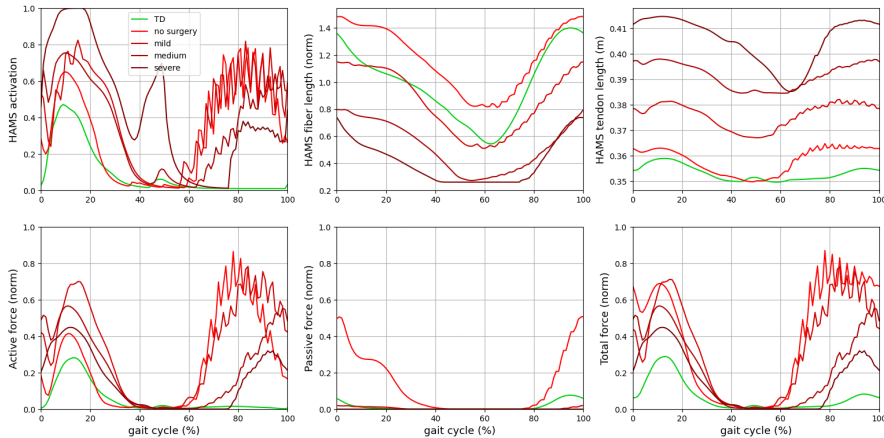
(c) HAMS surgery with Ia input = 5.0 and contr 70%: HAMS biomechanics

Figure 5.10: HAMS surgery with Ia input = 5.0 and contr 70%: Comparison among TD (green line), and various levels of surgery: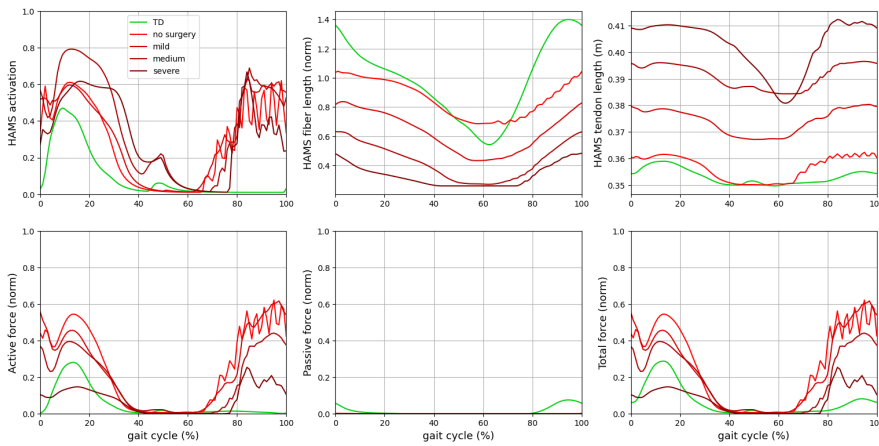 no surgery, mild surgery, moderate surgery, severe surgery. 5.10a) Gait anal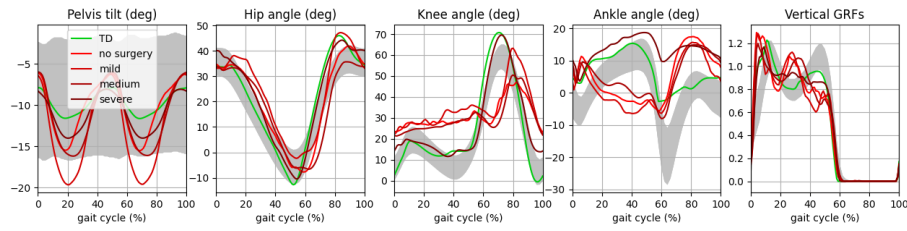ysis: Crouch gait condition is maintained for mild and moderate surgery with no significant changes in the ankle angle. Severe surgery could reproduce knee flexion close to TD with high dorsiflexion. The grey areas represent the experimental healthy data from Schwartz et al (2008).5.10b) Increasing surgery severity leads to decreasing activation of RF and ILPSO. Severe surgery leads to overactivation of HAMS in stance. Solid black lines represent the healthy activation timing observed experimentally (Perry, Davids, et al., 1992). 5.10c) Surgeries decrease the stretch level of muscle fibers, reducing consistently passive forces.

(a) No surgery: GPS

(b) No surgery: GVS Hip angle

(c) No surgery: GVS Knee angle

(d) No surgery: GVS Ankle angle
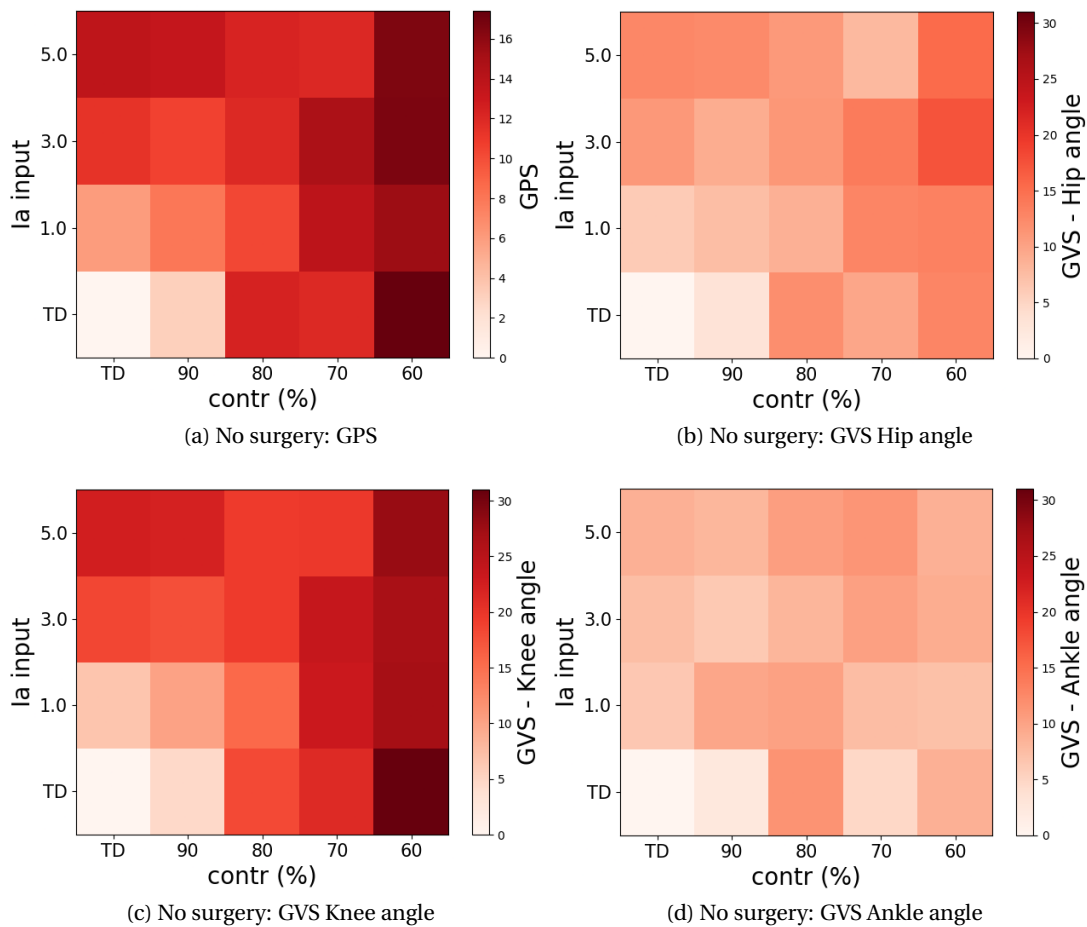
Figure 5.11: MAP - No surgery.

5.11a) GPS: Gait deviations increase with increasing severity of contractures and spasticity with highest values of GPS for contr 60%. 5.11b) GVS for the hip angle: small deviations are observed for increasing severity of biomechanical and neural impairments. The highest values of GVS are observed for the highest contracture and spasticity severity. 5.11c) GVS for knee angle: the major contributor to GPS. Deviations increase with increasing severity of contractures and spasticity. 5.11d) GVS ankle angle: Small deviations can be observed for both mild and severe impairments.

deviations are observed, with the highest level of GVS reached with contr 60% and Ia input = 5.0.

In presence of moderate levels of surgery shown in Figure 5.13, decreasing values of GPS can be observed for severe contracture levels (contr 60 %) without spasticity or with Ia input = 1.0. The GVS knee angle is again the main contributor to the GPS. The moderate surgery is effective on the knee angle in absence or with low levels of spasticity (Ia input = 3.0) for all levels of biomechanical contractures. The slightly higher GPS for Ia input = 1.0 compared to the absence of spasticity is due to the GVS level of the ankle angle. Gait deviations are also improved for the hip angle in presence of extreme contractures (contr 60%).

(a) Mild surgery: GPS

(b) Mild surgery: GVS Hip angle

(c) Mild surgery: GVS Knee angle

(d) Mild surgery: GVS Ankle angle
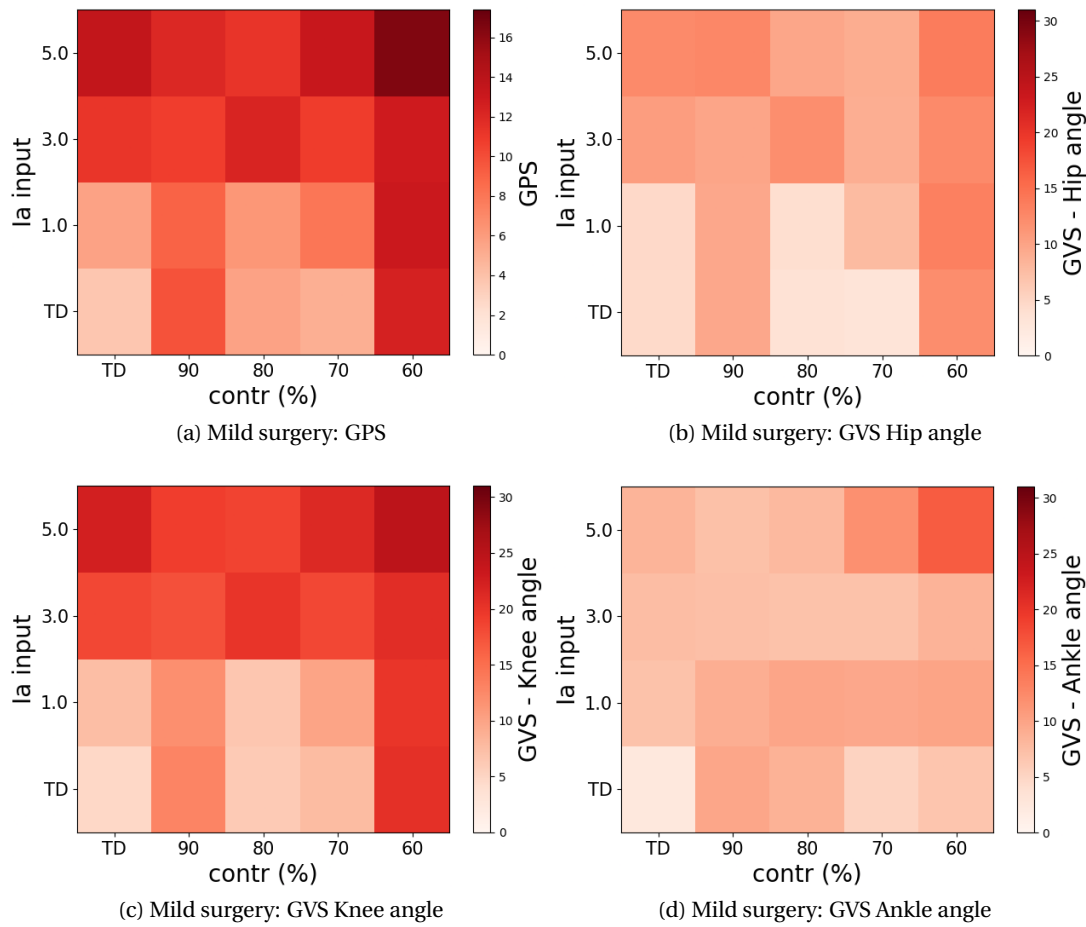
Figure 5.12: MAP - Mild surgery.
5.12a) GPS: Gait deviations improve in the absence or with mild levels of spasticity. Extreme contractures still maintain high levels of gait deviations. 5.12b) GVS for the hip angle: Small reduction of GVS can be observed for the same solutions showing improvements in GPS. 5.12c) GVS for knee angle: the major contributor to GPS. Consistent reduction of GVS can be observed for the same solutions showing improvements in GPS. 5.12d) GVS ankle angle: No consistent improvements are observed.

For severe surgery (Figure 5.14), there are decreasing GPS levels for the combinations including Ia input = 3.0, 5.0 and contr 80%, 70%. GVSs of hip, knee, and ankle angles contribute to the level of GPS. Indeed, consistent knee deviations can be observed only for combinations of spasticity and biomechanical impairments with Ia input = 3.0. 5.0 and contr 0.9, 0.6, or absence of contracture. However, the GVS of the hip angle affects the GPS for all contracture levels in absence of spasticity and the GVS of the ankle angle for all contracture levels, except contr 60%, with Ia input = 1.0.

(a) Moderate surgery: GPS

(b) Moderate surgery: GVS Hip angle

(c) Moderate surgery: GVS Knee angle

(d) Moderate surgery: GVS Ankle angle
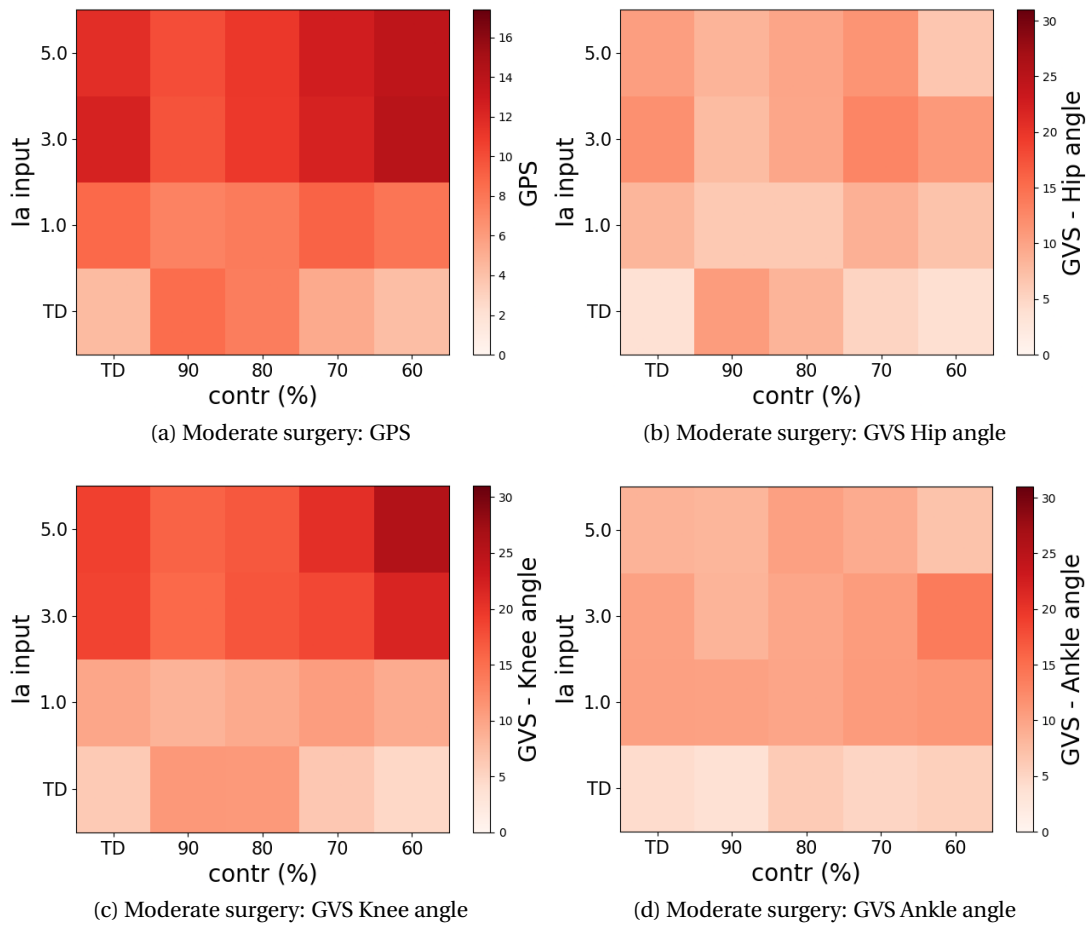
Figure 5.13: MAP - Moderate surgery.

5.13a) GPS: Gait deviations improve in the absence or with mild levels of spasticity for all levels of contractures. 5.13b) GVS for the hip angle: reduction of GVS are observed for severe contractures. 5.13c) GVS for knee angle: the major contributor to GPS. Consistent reduction of GVS can be observed for the same solutions showing improvements in GPS. 5.13d) GVS ankle angle: Small improvements are present in absence of spasticity, whereas Ia input = 1.0 show slightly higher GVS values compared to mild surgery.

5.4 Discussion

In this study, we reproduced the gait deviations generated by isolated hamstring spasticity, contracture, and the combination of these two impairments on a generic musculoskeletal model. Past studies modeled muscle contracture either by altering the passive stiffness parameters (van der Krogt et al., 2016) or by reducing the optimal fiber length (Bruel et al., 2022; Ong et al., 2019). In our study, we modeled both passive stiffness and reduced optimal fiber length since experiments suggest that both stretched sarcomere condition and increased collagen in the extracellular matrix are essential components of muscle contracture (Dayanidhi and Lieber, 2018; L. R. Smith et al., 2011). Furthermore, past models of neural spasticity represented the stretch reflex as a linear response to muscle length or velocity

(a) Severe surgery: GPS

(b) Severe surgery: GVS Hip angle

(c) Severe surgery: GVS Knee angle

(d) Severe surgery: GVS Ankle angle
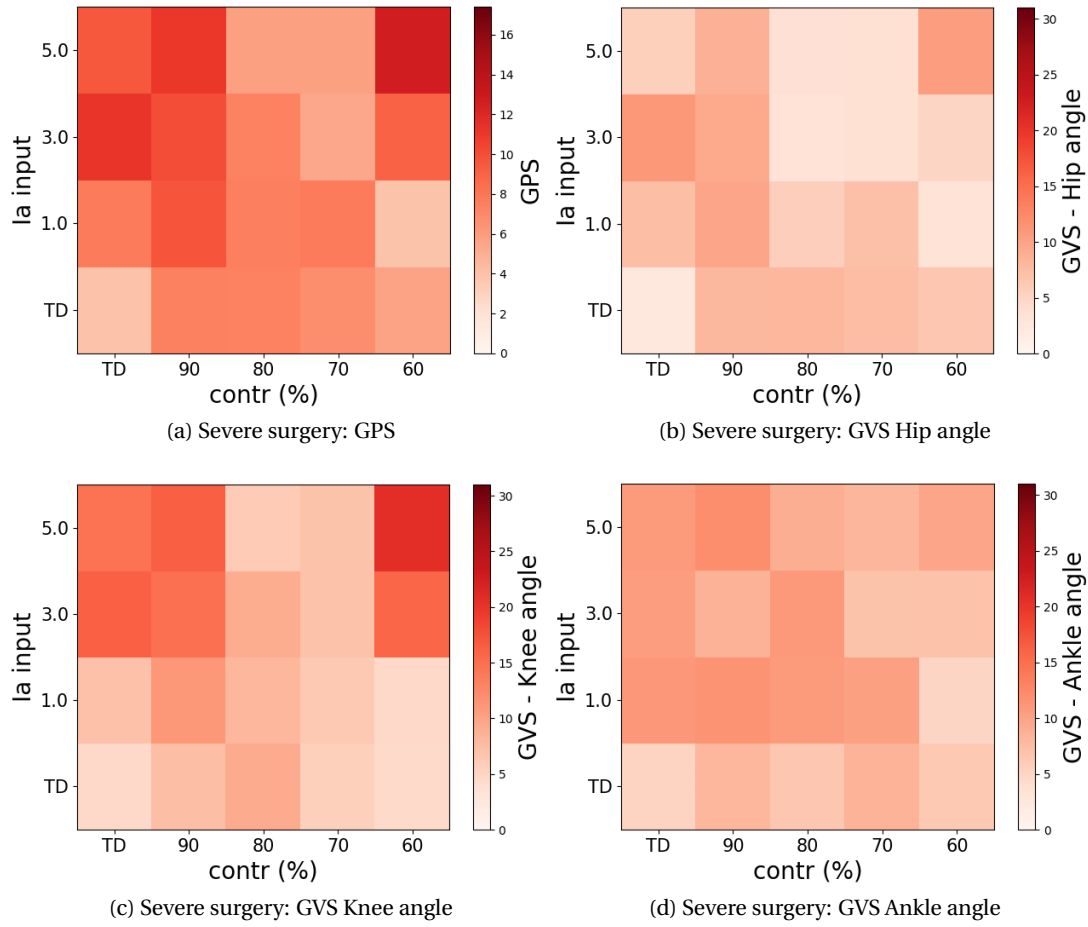
Figure 5.14: MAP - Severe surgery.

5.13a) GPS: Gait deviations improve also for some levels of severe spasticity and contractures. 5.13b) GVS for the hip angle: slightly increased levels of GVS compared to moderate surgery are observed for contractures without spasticity. 5.13c) GVS for knee angle: consistent levels of GVS are present for severe spasticity and mild or extreme contractures. 5.13d) GVS ankle angle: slightly increased levels of GVS compared to moderate surgery are observed for contractures with Ia input = 1.0.

(Jansen et al., 2014; van der Krogt et al., 2016). Bruel et al. (2022) extended this model by integrating the missing reciprocal inhibition between agonist and antagonist muscles. In our study, we decreased the level of abstraction by modeling the reflex connections as a leaky-integrator neural network, including both increased input from Ia afferents, which respond non-linearly to stretch velocity, and lack of inhibition from Ib fibers and reciprocal inhibition with antagonist muscles. In their study, Van der Krogt et al. (2016) could reproduce experimental muscle activation global shape but not the fast variations at approximately 15 Hz. This frequency is close to the variations we observed in hamstring activation in swing with our spasticity model.

We observed that the crouch gait behavior could be generated for any combination in which contr = 0.8 or higher or Ia input = 3.0 or higher. Additionally, the mildest impairments that

could generate crouch gait also show excessive dorsiflexion behavior. As the impairment becomes more severe, the ankle angle gradually progresses to an excessive plantarflexion behavior in stance leading to toe walking. Both excessive dorsiflexion and plantarflexion behaviors have been observed experimentally in crouch gait (O'Sullivan et al., 2020; Perry, Davids, et al., 1992; Rodda et al., 2004; Sutherland and Davids, 1993). Increasing impairment severity also augments the coactivation of rectus femoris and iliopsoas. In general, neural and biomechanical impairments generate similar gait deviations, with slightly more severe deviations observed for extreme contractures. Despite the similar effects of the two impairments on gait deviations, the effect on the hamstring biomechanics is significantly different. Indeed, in the presence of isolated muscle contracture, the hyper-resistance force reacting to stretch is mainly generated by the high stiffness of passive components. By contrast, in presence of isolated spasticity, this hyper-resistance is due to active forces generated by muscle overactivity.

Hamstring lengthening seems particularly effective in reducing gait deviations due to isolated muscle contractures or with a low level of spasticity (Ia input = 1.0), reproducing a gait kinematic very close to TD. Severe surgeries may improve crouch gait conditions for selective combinations of contractures and severe spasticity, also reproducing behaviors similar to TD. In general, hamstring lengthening alleviates crouch gait conditions, promotes ankle dorsiflexion behaviors, as already observed experimentally (Pierz et al., 2022), reduces coactivation of iliopsoas and rectus femoris, decreases fiber stretch, and drastically decreases passive forces. Crouch gaits affected by muscle contractures benefit from the reduced passive forces that are the main causes of gait deviations, whereas crouch gaits affected by spasticity may benefit from the weakness induced by the surgery and the reduced capability of generate maximum isometric force because the fiber length is largely below l_{opt}. However, simulations show that hamstring lengthening seldom significantly benefits conditions with high spastic levels. Indeed, normally other interventions like selective dorsal rhizotomy (SDR), intrathecal baclofen pump (ITB), and anti-spasticity injections and medications are used to treat spastic conditions (Munger et al., 2019). It should be highlighted that the level of severe surgery modeled always leads the muscle fiber to reach the minimum length and the tendon length to fall below the slack length. In these conditions, there is no tension applied to the hamstring muscle-tendon unit. In addition, severe surgery leads the hamstring to show excessive activity until saturation in order to try to generate meaningful tension. Furthermore, severe surgery often leads to increased anterior pelvic tilt, as also observed experimentally (Hoffinger et al., 1993), since this movement helps to generate tension in the hamstring. These conditions are surely not optimal and should be avoided in real interventions.

The present study provides resourceful information on how impairments and surgeries applied to the hamstring muscle may affect gait deviations. Yet, in clinical experiments, crouch gait is seldom induced by impairments to the hamstring alone. Indeed, contractures in hip flexors, high patella, and plantarflexion weakness are other common impairments that can be found in crouch gait conditions (Kedem and Scher, 2016; Perry, Davids, et al., 1992; Steele et al., 2012; Stout et al., 2008). Future studies could use the model we propose to simulate impairments to

different muscles by basing on patients' specific clinical assessments, possibly with precise measures of sarcomere lengths, stiffness, muscle forces, and spasticity levels, and by replicating the specific patient's morphology.

However, having a precise patient-specific model is very challenging. Previous studies reproduced patients' biomechanics and morphologies by measuring specific bone malformations with CT scans and by estimating the muscles' maximum isometric forces from the muscles' cross-sectional areas (Pitto et al., 2019). A methodology to personalize parameters for specific motor impairments like contracture and spasticity has been proposed by van der Krogt et al. (2016). They performed clinical assessments for patients with hyper-resistance of the knee by passively stretching the hamstring with slow and fast movements. Spasticity and contracture were modeled by optimizing the velocity feedback gain and the passive stiffness parameter, respectively. The subject-specific parameters were tuned to match experimental knee angle, muscle activity, and fiber length and velocity. The same experimental protocol could be adopted in our study to optimize the synaptic weight from Ia sensory afferent to the motoneuron. Concerning contracture, our model considers also the stretched sarcomere condition other than increased stiffness. Muscle fiber length could first be experimentally measured with ultrasound imaging (Mathewson et al., 2015) and the optimal fiber length tuned accordingly in the model; then, passive stiffness can be determined as suggested by van der Krogt et al. (2016).

In addition, other treatments can be modeled other than surgical orthopedic ones. For example, selective dorsal rhizotomy can be simulated by modeling the spastic condition and then optimizing the controller setting the Ia inputs to 0. Optimizations can possibly be improved by including elements in the cost function specific for the pathological condition, such as minimizing movements that in CP patients would induce pain in long term.

5.5 Conclusions

In this study, we reproduced crouch gait behaviors with different levels of neural spasticity and biomechanical contracture to the hamstring muscle. Contractures are modeled by increasing passive stiffness and reducing the muscle's optimal fiber length and spasticity by reproducing the high inputs from Ia afferents and the lack of reciprocal inhibitions from a previously proposed neural network modeling spinal reflexes. In addition, we modeled various levels of hamstring lengthening surgery by increasing the tendon slack length and reducing the muscle maximum isometric force. Crouch gait conditions could be reproduced either with isolated contractures, isolated spasticity, or a combination of both. Indeed, the two impairments show similar effects in gait deviations, maintaining significant differences in the type of hyper-resistance to stretch since contractures generate mainly high passive forces and spasticity high active forces from muscle overactivity. Hamstring lengthening results in being more beneficial for biomechanical contractures rather than spasticity. Severe surgeries may also produce undesired effects inducing serious difficulties in maintaining meaningful tension on

the hamstring's muscle-tendon unit.

6 Conclusions

In this doctoral thesis, we explored the capabilities of existing and new predictive neuromuscular controllers in simulating the modulation of healthy human locomotion, pathological gaits observed in CP patients, and the effects of orthopedic surgeries. All these studies have been conducted using OpenSim human musculoskeletal models available in the literature and simulated in the framework SCONE (Geijtenbeek, 2019).

With these simulations, we aim to address the following research questions:

- RQ1: How can the modulation of spinal cord circuits like reflexes and CPGs produce different target behaviors in healthy human locomotion?

- RQ2: Can we identify the effects of specific biomechanical and neural impairments inducing pathological gait deviations and predict the effects of orthopedic treatments using neuromuscular models?

The first research question has been explored in chapter 2 and chapter 4 using a previously assessed finite state-machine reflex-based controller and a newly developed controller including CPG and reflex network, respectively.

The second research question has been explored in chapter 3 and chapter 5 using an extension of a previously assessed finite state-machine reflex-based controller and a newly developed controller including CPG and reflex network, respectively.

6.1   RQ1: Healthy modulation of human locomotion

The modulation of human locomotion results from the interactions of conscious non-automatic neural circuits and other brain areas with the automatic circuits in the spinal cord (Capelli et al., 2017; Clark, 2015; Kiehn, 2016). The studies conducted in this thesis analyze how these spinal networks are modulated by the descending circuits by simulating different gait behav-

iors by optimizing the controller parameters. The variation of spinal parameters represents the effects of descending modulation on the spinal network.

In chapter 2, we investigated the reflex parameters changing in a phase and task dependent manner with the neuromuscular controller proposed by Ong et al. (2019). The tasks investigated are different ranges of speed, step length, and step duration reached through optimization, and the phase dependency is modeled through the finite state-machine regulation of reflex parameters. The results obtained from the optimizations show that the reflex controller could generate large ranges of the three gait characteristics, from slow to fast walking (0.48 and 1.71 m/s), small and large step lengths (0.43 and 0.88 m), and step durations (0.51 and 0.98 s). Depending on the target gait characteristics, the optimizer changes reflex gains and thresholds that facilitate or prevent changes generated by the muscle states. Nine reflex parameters were identified as possible modulators of human gait:

- The threshold parameter activating the hamstring stretch length feedback in stance can regulate speed and step length by allowing larger hamstring stretch due to knee extension and hip flexion at high speeds and step lengths.

- The positive force feedback of soleus and gastrocnemius in stance can regulate speed and step length by giving the main propulsion to gait.

- The iliopsoas stretch length feedback gain in pre-swing and stretch length feedback threshold in swing can regulate the three gait characteristics by lowering leg lifting at slow speed, and allowing large hip extensions during larger step lengths.

- The stretch length feedback gain of gluteus maximus during landing preparation can regulate the three gait characteristics by allowing a faster landing of the foot, increasing the frequency of the gait.

- The threshold parameter activating the tibialis anterior stretch length feedback during landing preparation can regulate the three gait characteristics by increasing ankle dorsiflexion at fast speeds.

- The hamstring stretch length feedback gain and threshold during landing preparation can regulate step length and duration accordingly by allowing a faster landing and preventing a full extension of the knee, reducing the step length.

These reflexes were found to be sufficient and necessary to modulate a wide range of the three gait characteristics under analysis, suggesting that the modulation of a small subset of reflexes could be involved in the strategies used by descending commands to change the gait behavior. It is well-established that the central nervous system modulates sensory transmission by adjusting reflex gains and thresholds to develop adaptive responses to the environment (Mutha, 2017; Prochazka, 1989, 2010). The modulation of sensory feedback relies on controlling reflex responses through reciprocal and presynaptic inhibition in a phase and task-dependent

manner (Mutha, 2017; Prochazka, 1989, 2010). In past studies, few neuromuscular models investigated which reflexes could play an important role in gait modulation since most of them explored supra-spinal or feedforward spinal mechanisms (Dzeladini et al., 2014; Song and Geyer, 2015). Song and Geyer (2012) investigated the possible controller components of a reflex-based controller that were mostly influencing speed modulation. They identified nine control parameters showing a significant trend at increasing speed from 0.8 to 1.8 m/s. Some of these parameters are delegated to the control of balance, whereas the main physiological reflexes identified were the positive force feedback of soleus in stance, also observed in our study, the threshold parameter activating hamstring length feedback in swing, and the reciprocal inhibition gain from the hamstring to the hip flexor. On the other hand, in our study, we could reproduce a wider range of speed and investigated reflexes that could be involved in the modulation of speed, step length, and step duration.

As previously mentioned, purely reflex-based controllers rely on a state machine mechanism for the cyclic activation of reflexes. This phase dependency on spinal reflexes is most probably delegated to mutual inhibition of antagonist muscle or rhythmic circuits located in the spinal cord. In chapter 4, we overcome these limitations with the development of a new neuromuscular controller composed of CPGs synergies generators and spinal reflexes implemented as neural networks not regulated by finite state-machines. We evaluated the controller's performance in reproducing healthy human behavior and speed modulation. In addition, we investigated the role of CPGs and reflexes in gait modulation. The proposed controller could replicate human kinematics and ground reaction forces (GRFs), and muscle activation. Interestingly, in this model, rhythmic locomotion could not be achieved with the only contribution of spinal reflexes without accounting for a state machine mechanism or an interaction with rhythmic CPG circuits, suggesting the need for these networks as a gating mechanism allowing reflexes to affect muscle activation only on specific gait cycle phases. Concerning gait modulation, the controller could reproduce speeds from 0.3 and 1.91 m/s, and the modulation of both CPGs or reflex parameters alone could reproduce wide ranges of gait behaviors. However, the modulation of reflexes alone had great limitations in reproducing different ranges of step duration, suggesting the CPG plays a crucial role in regulating gait cycle duration. Analyzing the neural inputs to motoneurons in the model, the net inputs of reflexes are mainly inhibitory through the gait cycle, and CPGs' patterns excite or inhibit motoneurons in specific phases of the gait cycle, allowing or preventing muscle activation. Most previous studies using neuromuscular controllers did not consider the inhibitory mechanisms to motoneurons since muscle excitation was mainly generated at specific gait cycle phases either by excitatory reflexes (Geyer and Herr, 2010; Ong et al., 2019), excitatory synergies from CPGs (Aoi et al., 2010; Aoi et al., 2019), or a combination of both (Dzeladini et al., 2014). The correlation analysis highlighted the possible spinal parameters affecting gait modulation. Some findings coincide with the previous analysis performed in chapter 2, like the excitation of soleus during stance and tibialis anterior during landing. However, the controller represents a highly redundant system where several different combinations of neural inputs can generate the same muscle activation creating a large variance in the possible strategies performed in

gait modulation.

6.2   RQ2: Pathological gaits in cerebral palsy

The common gait deviations observed in CP patients concern both biomechanical and neural impairments. Biomechanical impairments comprehend muscle weakness and contracture, whereas neural impairments comprehend neural weakness and spasticity. The studies conducted in this thesis analyze the effect of isolated impairments and different combinations of biomechanical and neural impairments.

In chapter 3, we investigated the motor impairments producing toe and heel using an extension of the state-machine neuromuscular controller proposed by Geyer and Herr (2010). Toe walking is commonly due to spasticity and contracture at plantarflexor muscles, whereas heel walking can be attributed to muscle weakness of biomechanical or neural origin. We modeled various bilateral plantarflexor biomechanical and neural impairments by altering the biomechanical properties of the musculoskeletal model and the parameters of a reflex circuit model, including plantarflexor force, spindle, length direct pathways, and additional reciprocal pathways with tibialis anterior. The variation of reflex parameters was constrained to study the short-term effect of impairments on gait, without accounting for long-term adaptations. Concerning neural impairments, toe gaits could be generated by increasing spindle and force reflex gains as models of hyperreflexia during the stance phase. Furthermore, reducing reciprocal inhibition from the tibialis anterior could also reproduce toe walking. Moreover, these simulations of plantarflexor hyperreflexia reveal excessive knee flexion during the stance phase, leading to a crouch gait behavior. On the other hand, increased reflex gains to plantarflexor muscle during the swing phase do not result in toe gait. However, toe gait could also be reproduced with contractures on plantaflexor muscles by reducing their optimal fiber length. For simulation of heel gait, the reduction of maximal isometric force modeling muscle weakness induces partial heel gait. Similarly, the decreased plantarflexor reflex gains during the stance phase mimicking neural weakness induce partial heel gait. The results obtained in this study are coherent with experimental observation (Armand et al., 2016; Chia et al., 2020). Other studies modeled hypereflexia to plantarflexor muscle with increased length and velocity feedback and lack of reflex inhibition during swing (Jansen et al., 2014). On the other hand, Ong et al. (2019) simulated heel and toe walking with biomechanical contractures by modeling soleus and gastrocnemius weaknesses and contractures, respectively. In our study, we modeled both neural and biomechanical impairments. In addition, other studies mostly considered weakness from the biomechanical level (muscle atrophy), whereas we considered also the neural origin (inability of the neural system to recruit the full muscle force). Furthermore, we verified that combinations of impairments could lead more easily to toe and heel gait.

The necessity of extending the state-machine controller from Geyer and Herr (2010) including reciprocal pathways between agonist and antagonist muscles highlighted the need for a new

neuromuscular controller for human locomotion considering also these neural connections. This new controller was presented in chapter 4, and chapter 5 explored the capabilities of this new controller in reproducing crouch gait behaviors by applying neural and biomechanical impairments to the hamstring muscle. Contrary to what is described in chapter 3, where parameters were constrained to study the short-term effects of impairments, in this last study, we explored the adaptation strategies to stabilize the impaired gait by allowing the free optimization of all parameters. Furthermore, we improved the modeling of muscle contractures by simulating both the decreased number of sarcomeres (reducing the muscle's optimal fiber length) and the increased collagen in the extracellular matrix (altering the muscle's stiffness parameter). In addition, we could perturb the newly developed controller without including any extension to model neural spasticity by increasing the weighted connections of Ia afferents and removing reciprocal inhibition connections. Contractures tend to increase the hyper-resistance to stretch through the generation of high passive forces, whereas spasticity through the generation of high passive forces. We evaluated the effect of isolated hamstring spasticity, contracture, and the combination of these two impairments. Crouch gait behavior could be generated for isolated moderate contractures, isolated moderate spastic levels, and any combinations of moderate or severe contracture and spasticity. Mild crouch gaits were characterized by excessive dorsiflexion, whereas the ankle angle shows excessive dorsiflexion and toe walking in more severe conditions. Some previous studies assumed that spastic stiffness is mainly caused by passive muscle properties (Dietz and Sinkjaer, 2007), and others reported instead a significant activity of hyperreflexia (Lorentzen et al., 2010; Mirbagheri et al., 2001). Our study suggested the significant contributions of both aspects to the emergence of gait deviations, which could be especially useful considering that the contributions of neural spasticity and passive muscle properties in hyper-resistance to stretch can barely be distinguished in clinical examination. In this study, we predicted excessive dorsiflexion and plantarflexion behaviors observed experimentally in crouch gait (O'Sullivan et al., 2020; Perry, Davids, et al., 1992; Rodda et al., 2004; Sutherland and Davids, 1993).

After having reproduced different crouch gait conditions, we simulated the effects of different levels of hamstring lengthening surgery, altering the hamstring's tendon slack length and maximum isometric force. The virtual intervention could significantly improve impairments caused by isolated muscle contractures or with low spastic levels, allowing healthy knee extension, decreasing coactivation, and reducing excessive passive forces. Furthermore, we could predict that hamstring lengthening promotes ankle dorsiflexion behaviors, as already observed experimentally (Pierz et al., 2022). Severe surgeries show improvements in knee kinematics also for high levels of spasticity, but the hamstring is overactivated to produce meaningful muscle tension, meaning a high probability of muscle fatigue outside a virtual environment. We also predicted that severe surgery leads to increased anterior pelvic tilt to help generate tension in the hamstring, as also observed experimentally (Hoffinger et al., 1993). This condition could possibly lead to spinal deformations. Therefore, according to our simulations, severe surgery causing the muscle fiber to reach its minimum length should be avoided, mild surgery should be performed with low spastic levels, and spastic conditions

should probably be treated with alternative treatments, like pharmacological injections or neural surgeries (Azar et al., 2020).

The studies presented in this thesis are an example of the great potentiality of predictive neuromuscular simulations in investigating healthy and pathological human locomotion by isolating the effects of model and controller's components and investigating the cause–effect relationship between impaired mechanisms and gait deviations with the potentiality of assisting the choice of appropriate treatments.

6.3   Future directions

The studies presented in this thesis could be a solid starting point to further develop neuromuscular controllers that could give resourceful insights into healthy and pathological control of locomotion.

Concerning the improvement of the musculoskeletal model, the lack of DoFs above the pelvis delegates the balance control of the trunk to the hip muscles that are generally not involved in trunk balance. This improvement could also be used with the integration of circuits modeling the vestibular and cerebellar networks regulating balance with the consequent possibility of exploring impairments to these systems, like the ataxic behavior observed in some populations of CP. In many of our simulations presented in the previous chapters, we observed excessive dorsiflexion of the ankle. This behavior may be due to convergence to a local minimum in the model proposed by Ong et al. (2019) and to the imitation of a non-optimal solution in the new spinal controller proposed in 4. Alternatively, the presence of this limitation in multiple controllers may be due to limitations in the modeling of contact geometries. Indeed, the excessive dorsiflexion behavior is also observed in previous simulation studies (Falisse et al., 2022; Ong et al., 2019), and additional investigations found the modeling of toes generates ankle motions closer to experimental kinematics (Falisse et al., 2022). Furthermore, neuromuscular controllers modeling sensory feedback, including the one we propose in this thesis, implement shorter reflex pathway delays compared to the ones recorded experimentally (Van der Helm and Rozendaal, 2000). A possible extension of our controller could be the reproduction of experimental neural delays to resemble more physiology. Other extensions may include for each neuron the auto-adaptation, meaning the neuron has a property such that the firing rate decreases when given constant stimulus energy (Matsuoka, 1985). Matsuoka et al. (1985) highlighted how adaptation could generate rhythmic neural activity. Therefore, the integration of such property, together with additional reflexes detecting stance interacting with interneurons, could possibly generate rhythmic motion without the CPG component. Additional extensions may include neural pathways not considered in our implementation, like a connection network between CPG circuits and sensory reflexes with patterns gating spinal interneurons other than motoneurons and with reflexes modulating CPG parameters. Other possible circuits to take into account in the modeling could be the descending modulation from the brainstem and higher brain areas, as well as the activity of γ-motoneurons.

The addition of all these circuits would surely make the optimization problem even more challenging. Moreover, the augmented redundancy would increase more the different combinations of parameters producing the same muscle activation and kinematics. This problem could potentially be solved by including in the cost function a component considering the high redundancy of neural networks aiming at minimizing the global neuronal activation. In this way, it would be possible to generate more unique solutions for specific muscle activations and kinematics, improving the results in the exploration of correlation among parameters and specific gait characteristics as performed in chapter 4. Additionally, other aspects of gait modulation could be explored, like the passage from standing to balance and the acceleration and deceleration mechanisms.

Another extension of the neuromuscular controller could be the control of locomotion to the 3D plane. This extension would require the addition of hip abduction/adduction, hip internal/external rotation, and ankle internal/external rotation. The addition of these DoFs requires additional muscles included in the musculoskeletal model and extending the agonist-antagonist relationship with the consequent increased number of parameters in the spinal reflex network and CPG circuit. Also the balance controller should be extended to regulate the lateral balance and lateral foot placement. With this extension, many different aspects of gait modulation could be explored, like the modulation of step width and steering.

Another sensitive aspect to further develop is the modeling of muscle spindle response. In 4, we modeled this response proportionally to the square root of muscle velocity. More complex models of muscle spindle include the dependency on muscle length and activation (Prochazka, 1999). However, recent studies showed that muscle spindles encode force and force rate (Blum et al., 2017), and a model of spindles encoding aspects of muscle force, yank, length, stiffness, velocity, and acceleration has been proposed (Blum et al., 2020). It would indeed be interesting to model the Ia responses in our spinal controller following the suggestion emerging from this recent model and to predict the effects of proprioceptive sensory signals in health and disease.

Finally, further considerations should be made about the possible validation of our model. In this thesis, we invested our effort in proposing a neuromuscular model reproducing human locomotor behaviors close to what is the current understanding of mammalian circuits of locomotion (Capaday, 2001; Chen et al., 2003; Lundberg et al., 1987; Prochazka et al., 1997; Windhorst, 1989) and that could be used by the community to test different hypotheses about healthy and especially pathological locomotion in a simulation environment. However, the matter of how the proposed model could be representative of actual human neuromotor circuits may still be debated given that multiple bio-inspired controllers can reproduce human movement (Aoi et al., 2019; Geyer and Herr, 2010; Ong et al., 2019; Song and Geyer, 2015) and that the possibility to perform direct experiments in the human spinal cord to uncover its structure and validate models is highly limited. The strength of our model relies on the representation of the spinal reflex circuits based on animal experiments and on the possibility of performing various neural impairments to any modeled muscle without the need to integrate complex model extensions. Possible indirect validation experiments could be performed with

experiments perturbing the feedback signals modeled (Y. Ivanenko et al., 2000; Verschueren et al., 2002) and reproducing the effect of such perturbations in simulations.

Concerning pathological gaits, a motor impairment that has not been investigated is the lack of selective motor control, defined as the inability to isolate the activation of muscles in a selected pattern in response to demands of a voluntary movement or posture (Sanger et al., 2006). This impairment could be modeled as a reduced number of synergies generated by CPGs and an increased width of these patterns. In addition, other CP conditions that could be explored are asymmetric hemiplegic gait. A similar behavior could be modeled using different parameters for the left and right sides with the neuromuscular controller extended to the 3D plane. On the other hand, the possible improvements to the cost function for the simulation of pathological gaits might be the minimization of movements that would induce pain in patients affected by the modeled motor impairments.

Additionally, further explorations could be done in the context of patient-specific modeling. We highlighted in 5 the challenge of obtaining such specific models. Indeed, CP patients normally present multiple impairments in several muscles. Muscle impairments can be modeled as we reported in this thesis. Then, an important step would be the development of a musculoskeletal model shaped on the patient's morphology, similar to what has been done by previous frameworks (Pitto et al., 2019). The proper modeling of specific patients strictly depends on precise measures performed in the clinical assessment. Weakness is often assessed using ordinal scales (Florence et al., 1992) but can be objectively quantified using an isokinetic dynamometer or a hand-held dynamometer (Fosang and Baker, 2006) or by evaluating the muscle cross-sectional area with MRI (Abe et al., 2005). On the other hand, soft tissue contractures are generally assessed with a manual goniometer (Pandya et al., 1985). A more precise measure would be the measure of sarcomeres length using ultrasounds (Got et al., 1999; Mathewson et al., 2015) and by performing slow passive stretch to assess the level of passive stiffness. Concerning neural impairments, spasticity is commonly evaluated through the use of ordinal scales (Ben-Shabat et al., 2013; Charalambous, 2014), but several studies have questioned their validity and reliability (Fleuren et al., 2010; Platz et al., 2005). A more precise measurement could be performed by learning the model spasticity parameter (weight form Ia afferents) reproducing muscle activity, kinematics, and fiber length and velocity in clinical assessment performed during fast passive movements.

Finally, further studies should model other treatments apart from muscle lengthenings, like the removal of parts of bones (osteotomies) and complete surgical cutting of the tendon (tenotomy) (Azar et al., 2020). The former should be modeled having specific deformities information from clinical measurements (Pitto et al., 2019), and the latter either by removing the target muscle from the musculoskeletal model or by increasing the tendon slack length at a point that the muscle fiber length is always at its minimum length. Concerning non-orthopedic surgeries, the surgical cut of afferent fibers generating spasticity (selective dorsal rhizotomy) (Azar et al., 2020) can be simulated by modeling the spastic condition and then optimizing the controller setting the Ia inputs to 0. Further studies might also model the effect

of pharmacological treatments and epidural electrical stimulation.

Bibliography

Abe, T., Hinata, S., Koizumi, K., & Sato, Y. (2005). Day-to-day change in muscle strength and mri-measured skeletal muscle size during 7 days kaatsu resistance training: a case study. *International Journal of KAATSU Training Research, 1*(2), 71–76.

Af Klint, R., Mazzaro, N., Nielsen, J. B., Sinkjaer, T., & Grey, M. J. (2010). Load rather than length sensitive feedback contributes to soleus muscle activity during human treadmill walking. *Journal of neurophysiology, 103*(5), 2747–2756.

Akay, T. (2020). Sensory feedback control of locomotor pattern generation in cats and mice. *Neuroscience, 450*, 161–167.

Akoglu, H. (2018). User's guide to correlation coefficients. *Turkish journal of emergency medicine, 18*(3), 91–93.

Allen, J. L., & Ting, L. H. (2016). Why is neuromechanical modeling of balance and locomotion so hard? In *Neuromechanical modeling of posture and locomotion* (pp. 197–223). Springer.

Alvarez, C., De Vera, M., Beauchamp, R., Ward, V., & Black, A. (2007). Classification of idiopathic toe walking based on gait analysis: development and application of the itw severity classification. *Gait & posture, 26*(3), 428–435.

Angulo-Kinzler, R. M., Mynark, R. G., & Koceja, D. M. (1998). Soleus h-reflex gain in elderly and young adults: modulation due to body position. *The Journals of Gerontology Series A: Biological Sciences and Medical Sciences, 53*(2), M120–M125.

Aoi, S., Kondo, T., Hayashi, N., Yanagihara, D., Aoki, S., Yamaura, H., Ogihara, N., Funato, T., Tomita, N., Senda, K., et al. (2013). Contributions of phase resetting and interlimb coordination to the adaptive control of hindlimb obstacle avoidance during locomotion in rats: a simulation study. *Biological cybernetics, 107*(2), 201–216.

Aoi, S., Ogihara, N., Funato, T., Sugimoto, Y., & Tsuchiya, K. (2010). Evaluating functional roles of phase resetting in generation of adaptive human bipedal walking with a physiologically based model of the spinal pattern generator. *Biological cybernetics, 102*(5), 373–387.

Aoi, S., Ohashi, T., Bamba, R., Fujiki, S., Tamura, D., Funato, T., Senda, K., Ivanenko, Y., & Tsuchiya, K. (2019). Neuromusculoskeletal model that walks and runs across a speed range with a few motor control parameter changes based on the muscle synergy hypothesis. *Scientific reports, 9*(1), 1–13.

Armand, S., Decoulon, G., & Bonnefoy-Mazure, A. (2016). Gait analysis in children with cerebral palsy. *EFORT open reviews, 1*(12), 448–460.

Attias, M., Bonnefoy-Mazure, A., De Coulon, G., Cheze, L., & Armand, S. (2017). Influence of different degrees of bilateral emulated contractures at the triceps surae on gait kinematics: the difference between gastrocnemius and soleus. *Gait & posture, 58*, 176–182.

Ausborn, J., Shevtsova, N. A., Caggiano, V., Danner, S. M., & Rybak, I. A. (2019). Computational modeling of brainstem circuits controlling locomotor frequency and gait. *Elife, 8*, e43587.

Ausborn, J., Snyder, A. C., Shevtsova, N. A., Rybak, I. A., & Rubin, J. E. (2018). State-dependent rhythmogenesis and frequency control in a half-center locomotor cpg. *Journal of neurophysiology, 119*(1), 96–117.

Azar, F. M., Canale, S. T., & Beaty, J. H. (2020). *Campbell's operative orthopaedics, e-book*. Elsevier Health Sciences.

Baker, R. (2006). Gait analysis methods in rehabilitation. *Journal of neuroengineering and rehabilitation, 3*(1), 1–10.

Baker, R., & Hart, H. M. (2013). *Measuring walking: a handbook of clinical gait analysis* (Vol. 1). Mac Keith Press London.

Baker, R., McGinley, J. L., Schwartz, M. H., Beynon, S., Rozumalski, A., Graham, H. K., & Tirosh, O. (2009). The gait profile score and movement analysis profile. *Gait & posture, 30*(3), 265–269.

Ben-Shabat, E., Palit, M., Fini, N. A., Brooks, C. T., Winter, A., & Holland, A. E. (2013). Intra- and interrater reliability of the modified tardieu scale for the assessment of lower limb spasticity in adults with neurologic injuries. *Archives of physical medicine and rehabilitation, 94*(12), 2494–2501.

Biering-Sørensen, F., Nielsen, J., & Klinge, K. (2006). Spasticity-assessment: a review. *Spinal cord, 44*(12), 708–722.

Blum, K. P., Campbell, K. S., Horslen, B. C., Nardelli, P., Housley, S. N., Cope, T. C., & Ting, L. H. (2020). Diverse and complex muscle spindle afferent firing properties emerge from multiscale muscle mechanics. *Elife, 9*, e55177.

Blum, K. P., Lamotte D'Incamps, B., Zytnicki, D., & Ting, L. H. (2017). Force encoding in muscle spindles during stretch of passive muscle. *PLoS computational biology, 13*(9), e1005767.

Bohannon, R. W. (2007). Muscle strength and muscle training after stroke. *Journal of rehabilitation Medicine, 39*(1), 14–20.

Boudarham, J., Roche, N., Pradon, D., Delouf, E., Bensmail, D., & Zory, R. (2014). Effects of quadriceps muscle fatigue on stiff-knee gait in patients with hemiparesis. *PloS one, 9*(4), e94138.

Bouvier, J., Caggiano, V., Leiras, R., Caldeira, V., Bellardita, C., Balueva, K., Fuchs, A., & Kiehn, O. (2015). Descending command neurons in the brainstem that halt locomotion. *Cell, 163*(5), 1191–1203.

Brockett, C. L., & Chapman, G. J. (2016). Biomechanics of the ankle. *Orthopaedics and trauma*, *30*(3), 232–238.

Brooke, J., Cheng, J., Collins, D., McIlroy, W., Misiaszek, J., & Staines, W. (1997). Sensori-sensory afferent conditioning with leg movement: gain control in spinal reflex and ascending paths. *Progress in neurobiology*, *51*(4), 393–421.

Brown, T. G. (1911). The intrinsic factors in the act of progression in the mammal. *Proceedings of the Royal Society of London. Series B, containing papers of a biological character*, *84*(572), 308–319.

Bruel, A., Ghorbel, S. B., Di Russo, A., Stanev, D., Armand, S., Courtine, G., & Ijspeert, A. (2022). Investigation of neural and biomechanical impairments leading to pathological toe and heel gaits using neuromusculoskeletal modelling. *The Journal of Physiology*, *600*(11), 2691–2712.

Büschges, A. (2017). Controlling the 'simple'–descending signals from the brainstem command the sign of a stretch reflex in a vertebrate spinal cord. *The Journal of physiology*, *595*(3), 625.

Büschges, A., & El Manira, A. (1998). Sensory pathways and their modulation in the control of locomotion. *Current opinion in neurobiology*, *8*(6), 733–739.

Calancie, B., Broton, J. G., Klose, K. J., Traad, M., Difini, J., & Ayyar, D. R. (1993). Evidence that alterations in presynaptic inhibition contribute to segmental hypo-and hyperexcitability after spinal cord injury in man. *Electroencephalography and Clinical Neurophysiology/Evoked Potentials Section*, *89*(3), 177–186.

Capaday, C., & Stein, R. (1986). Amplitude modulation of the soleus h-reflex in the human during walking and standing. *Journal of Neuroscience*, *6*(5), 1308–1313.

Capaday, C. (2001). Force-feedback during human walking. *TRENDS in Neurosciences*, *24*(1), 10.

Capelli, P., Pivetta, C., Soledad Esposito, M., & Arber, S. (2017). Locomotor speed control circuits in the caudal brainstem. *Nature*, *551*(7680), 373–377.

Cappellini, G., Sylos-Labini, F., Dewolf, A. H., Solopova, I. A., Morelli, D., Lacquaniti, F., & Ivanenko, Y. (2020). Maturation of the locomotor circuitry in children with cerebral palsy. *Frontiers in Bioengineering and Biotechnology*, *8*, 998.

Charalambous, C. P. (2014). Interrater reliability of a modified ashworth scale of muscle spasticity. *Classic papers in orthopaedics*, 415–417.

Chen, H.-H., Hippenmeyer, S., Arber, S., & Frank, E. (2003). Development of the monosynaptic stretch reflex circuit. *Current opinion in neurobiology*, *13*(1), 96–102.

Chia, K., Fischer, I., Thomason, P., Graham, H. K., & Sangeux, M. (2020). A decision support system to facilitate identification of musculoskeletal impairments and propose recommendations using gait analysis in children with cerebral palsy. *Frontiers in Bioengineering and Biotechnology*, *8*, 529415.

Chiou, I.-I. L., & Burnett, C. N. (1985). Values of activities of daily living: a survey of stroke patients and their home therapists. *Physical Therapy*, *65*(6), 901–906.

Cimolin, V., & Galli, M. (2016). Gait scores–interpretations and limitations. In *Handbook of human motion* (pp. 1–15). Springer International Publishing.

Clark, D. J. (2015). Automaticity of walking: functional significance, mechanisms, measurement and rehabilitation strategies. *Frontiers in human neuroscience, 9*, 246.

Crenna, P., & Frigo, C. (1987). Excitability of the soleus h-reflex arc during walking and stepping in man. *Experimental Brain Research, 66*(1), 49–60.

Crenna, P. (1998). Spasticity andspastic'gait in children with cerebral palsy. *Neuroscience & Biobehavioral Reviews, 22*(4), 571–578.

Crone, C., Hultborn, H., Jespersen, B., & Nielsen, J. (1987). Reciprocal ia inhibition between ankle flexors and extensors in man. *The Journal of physiology, 389*(1), 163–185.

Crone, C., Johnsen, L., Biering-Sørensen, F., & Nielsen, J. (2003). Appearance of reciprocal facilitation of ankle extensors from ankle flexors in patients with stroke or spinal cord injury. *Brain, 126*(2), 495–507.

Cuomo, A. V., Gamradt, S. C., Kim, C. O., Pirpiris, M., Gates, P. E., McCarthy, J. J., & Otsuka, N. Y. (2007). Health-related quality of life outcomes improve after multilevel surgery in ambulatory children with cerebral palsy. *Journal of Pediatric Orthopaedics, 27*(6), 653–657.

Daley, M. A., Felix, G., & Biewener, A. A. (2007). Running stability is enhanced by a proximodistal gradient in joint neuromechanical control. *Journal of Experimental Biology, 210*(3), 383–394.

Danner, S. M., Hofstoetter, U. S., Freundl, B., Binder, H., Mayr, W., Rattay, F., & Minassian, K. (2015). Human spinal locomotor control is based on flexibly organized burst generators. *Brain, 138*(3), 577–588.

Danner, S. M., Shevtsova, N. A., Frigon, A., & Rybak, I. A. (2017). Computational modeling of spinal circuits controlling limb coordination and gaits in quadrupeds. *Elife, 6*, e31050.

Danner, S. M., Wilshin, S. D., Shevtsova, N. A., & Rybak, I. A. (2016). Central control of interlimb coordination and speed-dependent gait expression in quadrupeds. *The Journal of physiology, 594*(23), 6947–6967.

Davids, J. R., Õunpuu, S., DeLuca, P. A., & Davis, R. B. (2003). Optimization of walking ability of children with cerebral palsy. *JBJS, 85*(11), 2224–2234.

Dayanidhi, S., & Lieber, R. L. (2018). Muscle biology of contractures in children with cerebral palsy. In *Cerebral palsy* (pp. 143–153). Springer.

De Groote, F., Kinney, A. L., Rao, A. V., & Fregly, B. J. (2016). Evaluation of direct collocation optimal control problem formulations for solving the muscle redundancy problem. *Annals of biomedical engineering, 44*(10), 2922–2936.

Delp, S. L., Loan, J. P., Hoy, M. G., Zajac, F. E., Topp, E. L., & Rosen, J. M. (1990). An interactive graphics-based model of the lower extremity to study orthopaedic surgical procedures. *IEEE Transactions on Biomedical engineering, 37*(8), 757–767.

Di Russo, A., Stanev, D., Armand, S., & Ijspeert, A. (2021). Sensory modulation of gait characteristics in human locomotion: a neuromusculoskeletal modeling study. *PLOS Computational Biology, 17*(5), e1008594.

Di Russo, A., Stanev, D., Sabnis, A., Danner, S. M., Ausborn, J., Armand, S., & Ijspeert, A. (2023). Investigating the roles of reflexes and central pattern generators in the control and

modulation of human locomotion using a physiologically plausible neuromechanical model. *bioRxiv*, 2023–01.

Dietz, V., Quintern, J., & Berger, W. (1984). Corrective reactions to stumbling in man: functional significance of spinal and transcortical reflexes. *Neuroscience letters*, *44*(2), 131–135.

Dietz, V., & Sinkjaer, T. (2007). Spastic movement disorder: impaired reflex function and altered muscle mechanics. *The Lancet Neurology*, *6*(8), 725–733.

Diong, J. H., Herbert, R. D., Harvey, L. A., Kwah, L. K., Clarke, J. L., Hoang, P. D., Martin, J. H., Clarke, E. C., Bilston, L. E., & Gandevia, S. C. (2012). Passive mechanical properties of the gastrocnemius after spinal cord injury. *Muscle & nerve*, *46*(2), 237–245.

Dzeladini, F., Van Den Kieboom, J., & Ijspeert, A. (2014). The contribution of a central pattern generator in a reflex-based neuromuscular model. *Frontiers in human neuroscience*, *8*, 371.

Edwards, D. H., & Prilutsky, B. I. (2017). Sensory feedback in the control of posture and locomotion. *Neurobiology of Motor Control: Fundamental Concepts and New Directions*, 263–304.

Eggink, H., Kremer, D., Brouwer, O. F., Contarino, M. F., van Egmond, M. E., Elema, A., Folmer, K., van Hoorn, J. F., van de Pol, L. A., Roelfsema, V., et al. (2017). Spasticity, dyskinesia and ataxia in cerebral palsy: are we sure we can differentiate them? *European Journal of Paediatric Neurology*, *21*(5), 703–706.

Elder, G. C., Kirk, J., Stewart, G., Cook, K., Weir, D., Marshall, A., & Leahey, L. (2003). Contributing factors to muscle weakness in children with cerebral palsy. *Developmental medicine and child neurology*, *45*(8), 542–550.

Ellaway, P. H., Taylor, A., & Durbaba, R. (2015). Muscle spindle and fusimotor activity in locomotion. *Journal of anatomy*, *227*(2), 157–166.

Faist, M., Hoefer, C., Hodapp, M., Dietz, V., Berger, W., & Duysens, J. (2006). In humans ib facilitation depends on locomotion while suppression of ib inhibition requires loading. *Brain research*, *1076*(1), 87–92.

Faist, M., Mazevet, D., Dietz, V., & Pierrot-Deseilligny, E. (1994). A quantitative assessment of presynaptic inhibition of ia afferents in spastics: differences in hemiplegics and paraplegics. *Brain*, *117*(6), 1449–1455.

Faist, M., Dietz, V., & Pierrot-Deseilligny, E. (1996). Modulation, probably presynaptic in origin, of monosynaptic ia excitation during human gait. *Experimental brain research*, *109*(3), 441–449.

Falisse, A., Afschrift, M., & De Groote, F. (2022). Modeling toes contributes to realistic stance knee mechanics in three-dimensional predictive simulations of walking. *Plos one*, *17*(1), e0256311.

Falisse, A., Bar-On, L., Desloovere, K., Jonkers, I., & De Groote, F. (2018). A spasticity model based on feedback from muscle force explains muscle activity during passive stretches and gait in children with cerebral palsy. *PLoS One*, *13*(12), e0208811.

Falisse, A., Serrancolı, G., Dembia, C. L., Gillis, J., Jonkers, I., & De Groote, F. (2019). Rapid predictive simulations with complex musculoskeletal models suggest that diverse

healthy and pathological human gaits can emerge from similar control strategies. *Journal of The Royal Society Interface*, *16*(157), 20190402.

Farahani, S. D., de Zee, M., Andersen, M. S., Lund, M. E., & Rasmussen, J. (2011). Prediction of the movement patterns for human squat jumping using the inverse-inverse dynamics technique. *XIII International Symposium on Computer Simulation in Biomechanics.*

Fish, D. J., & Nielsen, J.-P. (1993). Clinical assessment of human gait. *JPO: Journal of Prosthetics and Orthotics*, *5*(2), 39.

Fleuren, J. F., Voerman, G. E., Erren-Wolters, C. V., Snoek, G. J., Rietman, J. S., Hermens, H. J., & Nene, A. V. (2010). Stop using the ashworth scale for the assessment of spasticity. *Journal of Neurology, Neurosurgery & Psychiatry*, *81*(1), 46–52.

Florence, J. M., Pandya, S., King, W. M., Robison, J. D., Baty, J., Miller, J. P., Schierbecker, J., & Signore, L. C. (1992). Intrarater reliability of manual muscle test (medical research council scale) grades in duchenne's muscular dystrophy. *Physical therapy*, *72*(2), 115–122.

Fluit, R., Andersen, M. S., Verdonschot, N. J. J., & Koopman, H. F. (2014). Optimal inverse dynamic simulation of human gait. *Gait & posture*, *39*(Supplement 1).

Fosang, A., & Baker, R. (2006). A method for comparing manual muscle strength measurements with joint moments during walking. *Gait & Posture*, *24*(4), 406–411.

Francis, C. A., Lenz, A. L., Lenhart, R. L., & Thelen, D. G. (2013). The modulation of forward propulsion, vertical support, and center of pressure by the plantarflexors during human walking. *Gait & posture*, *38*(4), 993–997.

Frijns, C., Laman, D., Van Duijn, M., & Van Duijn, H. (1997). Normal values of patellar and ankle tendon reflex latencies. *Clinical neurology and neurosurgery*, *99*(1), 31–36.

Gage, J. R., Schwartz, M. H., Koop, S. E., & Novacheck, T. F. (2009). *The identification and treatment of gait problems in cerebral palsy* (Vol. 180). John Wiley & Sons.

Garcia-Rill, E., & Skinner, R. (1987). The mesencephalic locomotor region. i. activation of a medullary projection site. *Brain research*, *411*(1), 1–12.

Gaudreault, N., Gravel, D., & Nadeau, S. (2009). Evaluation of plantar flexion contracture contribution during the gait of children with duchenne muscular dystrophy. *Journal of Electromyography and Kinesiology*, *19*(3), e180–e186.

Geijtenbeek, T. (2019). Scone: open source software for predictive simulation of biological motion. *Journal of Open Source Software*, *4*(38), 1421.

Gerasimenko, Y., Sayenko, D., Gad, P., Liu, C.-T., Tillakaratne, N. J., Roy, R. R., Kozlovskaya, I., & Edgerton, V. R. (2017). Feed-forwardness of spinal networks in posture and locomotion. *The Neuroscientist*, *23*(5), 441–453.

Geyer, H., & Herr, H. (2010). A muscle-reflex model that encodes principles of legged mechanics produces human walking dynamics and muscle activities. *IEEE Transactions on neural systems and rehabilitation engineering*, *18*(3), 263–273.

Geyer, H., Seyfarth, A., & Blickhan, R. (2003). Positive force feedback in bouncing gaits? *Proceedings of the Royal Society of London. Series B: Biological Sciences*, *270*(1529), 2173–2183.

Giuliani, C., & Smith, J. L. (1987). Stepping behaviors in chronic spinal cats with one hindlimb deafferented. *Journal of Neuroscience, 7*(8), 2537–2546.

Goldberger, M. E. (1977). Locomotor recovery after unilateral hindlimb deafferentation in cats. *Brain research, 123*(1), 59–74.

Got, F., Culioli, J., Berge, P., Vignon, X., Astruc, T., Quideau, J., & Lethiecq, M. (1999). Effects of high-intensity high-frequency ultrasound on ageing rate, ultrastructure and some physico-chemical properties of beef. *Meat Science, 51*(1), 35–42.

Gough, M., & Shortland, A. P. (2008). Can clinical gait analysis guide the management of ambulant children with bilateral spastic cerebral palsy? *Journal of Pediatric Orthopaedics, 28*(8), 879–883.

Gracies, J.-M. (2005a). Pathophysiology of spastic paresis. i: paresis and soft tissue changes. *Muscle & Nerve: Official Journal of the American Association of Electrodiagnostic Medicine, 31*(5), 535–551.

Gracies, J.-M. (2005b). Pathophysiology of spastic paresis. ii: emergence of muscle overactivity. *Muscle & Nerve: Official Journal of the American Association of Electrodiagnostic Medicine, 31*(5), 552–571.

Graham, H. K., & Selber, P. (2003). Musculoskeletal aspects of cerebral palsy. *The Journal of bone and joint surgery. British volume, 85*(2), 157–166.

Granata, K. P., Abel, M. F., & Damiano, D. L. (2000). Joint angular velocity in spastic gait and the influence of muscle-tendon lengthening. *The Journal of bone and joint surgery. American volume, 82*(2), 174.

Grillner, S. (1975). Locomotion in vertebrates: central mechanisms and reflex interaction. *Physiological reviews, 55*(2), 247–304.

Guertin, P. A. (2009). The mammalian central pattern generator for locomotion. *Brain research reviews, 62*(1), 45–56.

Hägglund, M., Borgius, L., Dougherty, K. J., & Kiehn, O. (2010). Activation of groups of excitatory neurons in the mammalian spinal cord or hindbrain evokes locomotion. *Nature neuroscience, 13*(2), 246–252.

Haghpanah, S. A., Farahmand, F., & Zohoor, H. (2017). Modular neuromuscular control of human locomotion by central pattern generator. *Journal of biomechanics, 53*, 154–162.

Hayford, C. F. (2022). *Musculoskeletal models to aid in clinical decision-making in children with cerebral palsy* (Doctoral dissertation). University of Sheffield.

Hoffinger, S. A., Rab, G. T., & Abou-Ghaida, H. (1993). Hamstrings in cerebral palsy crouch gait. *Journal of Pediatric Orthopaedics, 13*(6), 722–726.

Hunt, K. H., & Crossley, F. R. E. (1975). Coefficient of restitution interpreted as damping in vibroimpact.

Igel, C., Hansen, N., & Roth, S. (2007). Covariance matrix adaptation for multi-objective optimization. *Evolutionary computation, 15*(1), 1–28.

Ijspeert, A. J. (2008). Central pattern generators for locomotion control in animals and robots: a review. *Neural networks, 21*(4), 642–653.

Ivanenko, Y., Grasso, R., & Lacquaniti, F. (2000). Influence of leg muscle vibration on human walking. *Journal of neurophysiology, 84*(4), 1737–1747.

Ivanenko, Y. P., Poppele, R. E., & Lacquaniti, F. (2004). Five basic muscle activation patterns account for muscle activity during human locomotion. *The Journal of physiology, 556*(1), 267–282.

Ivanenko, Y. P., Poppele, R. E., & Lacquaniti, F. (2006). Spinal cord maps of spatiotemporal alpha-motoneuron activation in humans walking at different speeds. *Journal of neurophysiology, 95*(2), 602–618.

Jansen, K., De Groote, F., Aerts, W., De Schutter, J., Duysens, J., & Jonkers, I. (2014). Altering length and velocity feedback during a neuro-musculoskeletal simulation of normal gait contributes to hemiparetic gait characteristics. *Journal of neuroengineering and rehabilitation, 11*(1), 1–15.

Jiroumaru, T., Kurihara, T., & Isaka, T. (2014). Establishment of a recording method for surface electromyography in the iliopsoas muscle. *Journal of Electromyography and Kinesiology, 24*(4), 445–451.

Kedem, P., & Scher, D. M. (2016). Evaluation and management of crouch gait. *Current Opinion in Pediatrics, 28*(1), 55–59.

Kerkum, Y. L., Buizer, A. I., Van Den Noort, J. C., Becher, J. G., Harlaar, J., & Brehm, M.-A. (2015). The effects of varying ankle foot orthosis stiffness on gait in children with spastic cerebral palsy who walk with excessive knee flexion. *PloS one, 10*(11), e0142878.

Kiehn, O. (2006). Locomotor circuits in the mammalian spinal cord. *Annual review of neuroscience, 29*(1), 279–306.

Kiehn, O. (2016). Decoding the organization of spinal circuits that control locomotion. *Nature Reviews Neuroscience, 17*(4), 224–238.

Klint, R. a., Nielsen, J. B., Cole, J., Sinkjaer, T., & Grey, M. J. (2008). Within-step modulation of leg muscle activity by afferent feedback in human walking. *The Journal of physiology, 586*(19), 4643–4648.

Knikou, M., & Mummidisetty, C. K. (2011). Reduced reciprocal inhibition during assisted stepping in human spinal cord injury. *Experimental neurology, 231*(1), 104–112.

Koceja, D. M., Markus, C. A., & Trimble, M. H. (1995). Postural modulation of the soleus h reflex in young and old subjects. *Electroencephalography and Clinical Neurophysiology/Electromyography and Motor Control, 97*(6), 387–393.

Koceja, D. M., Trimble, M. H., & Earles, D. R. (1993). Inhibition of the soleus h-reflex in standing man. *Brain research, 629*(1), 155–158.

Kruse, A., Schranz, C., Tilp, M., & Svehlik, M. (2018). Muscle and tendon morphology alterations in children and adolescents with mild forms of spastic cerebral palsy. *BMC pediatrics, 18*(1), 1–9.

Lacquaniti, F., Ivanenko, Y. P., & Zago, M. (2012). Patterned control of human locomotion. *The Journal of physiology, 590*(10), 2189–2199.

Lajoie, Y., Teasdale, N., Cole, J., Burnett, M., Bard, C., Fleury, M., Forget, R., Paillard, J., & Lamarre, Y. (1996). Gait of a deafferented subject without large myelinated sensory fibers below the neck. *Neurology, 47*(1), 109–115.

Lamontagne, A., Malouin, F., Richards, C., & Dumas, F. (2002). Mechanisms of disturbed motor control in ankle weakness during gait after stroke. *Gait & posture, 15*(3), 244–255.

Lance, J. W. (1980a). The control of muscle tone, reflexes, and movement: robert wartenbeg lecture. *Neurology, 30*(12), 1303–1303.

Lance, J. W. (1980b). Pathophysiology of spasticity and clinical experience with baclofen. *Spasticity: disordered motor control*, 185–204.

Leech, K. A., Kim, H. E., & Hornby, T. G. (2018). Strategies to augment volitional and reflex function may improve locomotor capacity following incomplete spinal cord injury. *Journal of neurophysiology, 119*(3), 894–903.

Lenhart, R. L., Francis, C. A., Lenz, A. L., & Thelen, D. G. (2014). Empirical evaluation of gastrocnemius and soleus function during walking. *Journal of biomechanics, 47*(12), 2969–2974.

Levin, M. F., & Feldman, A. G. (1994). The role of stretch reflex threshold regulation in normal and impaired motor control. *Brain research, 657*(1-2), 23–30.

Lieber, R. L., Steinman, S., Barash, I. A., & Chambers, H. (2004). Structural and functional changes in spastic skeletal muscle. *Muscle & Nerve: Official Journal of the American Association of Electrodiagnostic Medicine, 29*(5), 615–627.

Lieber, R. L., & Theologis, T. (2021). Muscle-tendon unit in children with cerebral palsy. *Developmental Medicine & Child Neurology, 63*(8), 908–913.

Lim, Y. P., Lin, Y.-C., & Pandy, M. G. (2017). Effects of step length and step frequency on lower-limb muscle function in human gait. *Journal of biomechanics, 57*, 1–7.

Lorentzen, J., Grey, M. J., Crone, C., Mazevet, D., Biering-Sørensen, F., & Nielsen, J. B. (2010). Distinguishing active from passive components of ankle plantar flexor stiffness in stroke, spinal cord injury and multiple sclerosis. *Clinical neurophysiology, 121*(11), 1939–1951.

Lundberg, A., Malmgren, K., & Schomburg, E. (1987). Reflex pathways from group ii muscle afferents. *Experimental Brain Research, 65*(2), 294–306.

Malhotra, S., Pandyan, A., Day, C., Jones, P., & Hermens, H. (2009). Spasticity, an impairment that is poorly defined and poorly measured. *Clinical rehabilitation, 23*(7), 651–658.

Mansouri, M., Clark, A. E., Seth, A., & Reinbolt, J. A. (2016). Rectus femoris transfer surgery affects balance recovery in children with cerebral palsy: a computer simulation study. *Gait & posture, 43*, 24–30.

Mansouri, M., & Reinbolt, J. A. (2012). A platform for dynamic simulation and control of movement based on opensim and matlab. *Journal of biomechanics, 45*(8), 1517–1521.

Marque, P., Simonetta-Moreau, M., Maupas, E., & Roques, C. (2001). Facilitation of transmission in heteronymous group ii pathways in spastic hemiplegic patients. *Journal of Neurology, Neurosurgery & Psychiatry, 70*(1), 36–42.

Mathewson, M. A., Ward, S. R., Chambers, H. G., & Lieber, R. L. (2015). High resolution muscle measurements provide insights into equinus contractures in patients with cerebral palsy. *Journal of Orthopaedic Research, 33*(1), 33–39.

Matjačić, Z., Olenšek, A., & Bajd, T. (2006). Biomechanical characterization and clinical implications of artificially induced toe-walking: differences between pure soleus, pure gastrocnemius and combination of soleus and gastrocnemius contractures. *Journal of Biomechanics, 39*(2), 255–266.

Matsuoka, K. (1985). Sustained oscillations generated by mutually inhibiting neurons with adaptation. *Biological cybernetics*, *52*(6), 367–376.

Matsuyama, K., Mori, F., Nakajima, K., Drew, T., Aoki, M., & Mori, S. (2004). Locomotor role of the corticoreticular–reticulospinal–spinal interneuronal system. *Progress in brain research*, *143*, 239–249.

Matthews, P. (1959). A study of certain factors influencing the stretch reflex of the decerebrate cat. *The Journal of physiology*, *147*(3), 547–564.

McCrea, D. A., & Rybak, I. A. (2008). Organization of mammalian locomotor rhythm and pattern generation. *Brain research reviews*, *57*(1), 134–146.

Meunier, S., & Pierrot-Deseilligny, E. (1998). Cortical control of presynaptic inhibition of ia afferents in humans. *Experimental brain research*, *119*(4), 415–426.

Mileusnic, M. P., Brown, I. E., Lan, N., & Loeb, G. E. (2006). Mathematical models of proprioceptors. i. control and transduction in the muscle spindle. *Journal of neurophysiology*, *96*(4), 1772–1788.

Mileusnic, M., & Loeb, G. (2009). Force estimation from ensembles of golgi tendon organs. *Journal of neural engineering*, *6*(3), 036001.

Millard, M., Uchida, T., Seth, A., & Delp, S. L. (2013). Flexing computational muscle: modeling and simulation of musculotendon dynamics. *Journal of biomechanical engineering*, *135*(2).

Minassian, K., Hofstoetter, U. S., Dzeladini, F., Guertin, P. A., & Ijspeert, A. (2017). The human central pattern generator for locomotion: does it exist and contribute to walking? *The Neuroscientist*, *23*(6), 649–663.

Mirbagheri, M., Barbeau, H., Ladouceur, M., & Kearney, R. (2001). Intrinsic and reflex stiffness in normal and spastic, spinal cord injured subjects. *Experimental brain research*, *141*(4), 446–459.

Moissenet, F., Leboeuf, F., & Armand, S. (2019). Lower limb sagittal gait kinematics can be predicted based on walking speed, gender, age and bmi. *Scientific reports*, *9*(1), 1–12.

Munger, M. E., Chen, B. P.-J., MacWilliams, B. A., McMulkin, M. L., & Schwartz, M. H. (2019). Comparing the effects of two spasticity management strategies on the long-term outcomes of individuals with bilateral spastic cerebral palsy: a multicentre cohort study protocol. *BMJ open*, *9*(6), e027486.

Mutha, P. K. (2017). Reflex circuits and their modulation in motor control: a historical perspective and current view. *Journal of the Indian Institute of Science*, *97*(4), 555–565.

Mynark, R. G., & Koceja, D. M. (1997). Comparison of soleus h-reflex gain from prone to standing in dancers and controls. *Electroencephalography and Clinical Neurophysiology/Electromyography and Motor Control*, *105*(2), 135–140.

Neyroud, D., Armand, S., De Coulon, G., Da Silva, S. R. D., Maffiuletti, N. A., Kayser, B., & Place, N. (2017). Plantar flexor muscle weakness and fatigue in spastic cerebral palsy patients. *Research in developmental disabilities*, *61*, 66–76.

Nielsen, J., & Sinkjaer, T. (2002). Afferent feedback in the control of human gait. *Journal of electromyography and kinesiology*, *12*(3), 213–217.

Nieuwenhuys, A., Õunpuu, S., Van Campenhout, A., Theologis, T., De Cat, J., Stout, J., Mole-naers, G., De Laet, T., & Desloovere, K. (2016). Identification of joint patterns during gait in children with cerebral palsy: a delphi consensus study. *Developmental Medicine & Child Neurology, 58*(3), 306–313.

Ogihara, N., & Yamazaki, N. (2001). Generation of human bipedal locomotion by a bio-mimetic neuro-musculo-skeletal model. *Biological cybernetics, 84*(1), 1–11.

Ong, C. F., Geijtenbeek, T., Hicks, J. L., & Delp, S. L. (2019). Predicting gait adaptations due to ankle plantarflexor muscle weakness and contracture using physics-based muscu-loskeletal simulations. *PLoS computational biology, 15*(10), e1006993.

O'Sullivan, R., Marron, A., & Brady, K. (2020). Crouch gait or flexed-knee gait in cerebral palsy: is there a difference? a systematic review. *Gait & Posture, 82*, 153–160.

Pandya, S., Florence, J. M., King, W. M., Robison, J. D., Oxman, M., & Province, M. A. (1985). Re-liability of goniometric measurements in patients with duchenne muscular dystrophy. *Physical Therapy, 65*(9), 1339–1342.

Papadonikolakis, A., Vekris, M., Korompilias, A., Kostas, J., Ristanis, S., & Soucacos, P. (2003). Botulinum a toxin for treatment of lower limb spasticity in cerebral palsy gait analysis in 49 patients. *Acta Orthopaedica Scandinavica, 74*(6), 749–755.

Perry, J., Davids, J. R., et al. (1992). Gait analysis: normal and pathological function. *Journal of Pediatric Orthopaedics, 12*(6), 815.

Petersen, N., Morita, H., & Nielsen, J. (1999). Modulation of reciprocal inhibition between ankle extensors and flexors during walking in man. *The Journal of Physiology, 520*(2), 605–619.

Pierrot-Deseilligny, E., & Burke, D. (2005). *The circuitry of the human spinal cord: its role in motor control and movement disorders.* Cambridge university press.

Pierz, K., Brimacombe, M., & Õunpuu, S. (2022). Percutaneous hamstring lengthening in cerebral palsy: technique and gait outcomes based on gmfcs level. *Gait & Posture, 91*, 318–325.

Pitto, L., Kainz, H., Falisse, A., Wesseling, M., Van Rossom, S., Hoang, H., Papageorgiou, E., Hallemans, A., Desloovere, K., Molenaers, G., et al. (2019). Simcp: a simulation plat-form to predict gait performance following orthopedic intervention in children with cerebral palsy. *Frontiers in neurorobotics, 13*, 54.

Platz, T., Eickhof, C., Nuyens, G., & Vuadens, P. (2005). Clinical scales for the assessment of spasticity, associated phenomena, and function: a systematic review of the literature. *Disability and rehabilitation, 27*(1-2), 7–18.

Prochazka, A. (1989). Sensorimotor gain control: a basic strategy of motor systems? *Progress in neurobiology, 33*(4), 281–307.

Prochazka, A. (1999). Quantifying proprioception. *Progress in brain research, 123*, 133–142.

Prochazka, A. (2010). Proprioceptive feedback and movement regulation. *Comprehensive Physiology*, 89–127.

Prochazka, A., Gillard, D., & Bennett, D. J. (1997). Positive force feedback control of muscles. *Journal of neurophysiology, 77*(6), 3226–3236.

Prochazka, A., Gosgnach, S., Capaday, C., & Geyer, H. (2017). Neuromuscular models for locomotion. In *Bioinspired legged locomotion* (pp. 401–453). Elsevier.

Rasmussen, J., Damsgaard, M., & Christensen, S. T. (2000). Inverse-inverse dynamics simulation of musculo-skeletal systems. *Inverse-Inverse Dynamics Simulation of Musculo-Skeletal Systems*.

Riemer, R., & Hsiao-Wecksler, E. T. (2008). Improving joint torque calculations: optimization-based inverse dynamics to reduce the effect of motion errors. *Journal of biomechanics*, *41*(7), 1503–1509.

Rodda, J., Graham, H. K., Carson, L., Galea, M. P., & Wolfe, R. (2004). Sagittal gait patterns in spastic diplegia. *The Journal of bone and joint surgery. British volume*, *86*(2), 251–258.

Rosenbaum, P., Eliasson, A.-C., Hidecker, M. J. C., & Palisano, R. J. (2014). Classification in childhood disability: focusing on function in the 21st century. *Journal of child neurology*, *29*(8), 1036–1045.

Rossignol, S., Dubuc, R., & Gossard, J.-P. (2006). Dynamic sensorimotor interactions in locomotion. *Physiological reviews*, *86*(1), 89–154.

Rybak, I. A., Shevtsova, N. A., Lafreniere-Roula, M., & McCrea, D. A. (2006). Modelling spinal circuitry involved in locomotor pattern generation: insights from deletions during fictive locomotion. *The Journal of physiology*, *577*(2), 617–639.

Ryu, H. X., & Kuo, A. D. (2021). An optimality principle for locomotor central pattern generators. *Scientific Reports*, *11*(1), 1–18.

Sanger, T. D., Chen, D., Delgado, M. R., Gaebler-Spira, D., Hallett, M., Mink, J. W., & on Childhood Motor Disorders, T. (2006). Definition and classification of negative motor signs in childhood. *Pediatrics*, *118*(5), 2159–2167.

Sankar, C., & Mundkur, N. (2005). Cerebral palsy-definition, classification, etiology and early diagnosis. *The Indian Journal of Pediatrics*, *72*(10), 865–868.

Schwartz, M. H., Rozumalski, A., & Trost, J. P. (2008). The effect of walking speed on the gait of typically developing children. *Journal of biomechanics*, *41*(8), 1639–1650.

Sellier, E., Platt, M. J., Andersen, G. L., Krägeloh-Mann, I., De La Cruz, J., Cans, C., of Cerebral Palsy Network, S., Van Bakel, M., Arnaud, C., Delobel, M., et al. (2016). Decreasing prevalence in cerebral palsy: a multi-site european population-based study, 1980 to 2003. *Developmental Medicine & Child Neurology*, *58*(1), 85–92.

Sheean, G. (2002). The pathophysiology of spasticity. *European journal of neurology*, *9*, 3–9.

Sherman, M. A., Seth, A., & Delp, S. L. (2011). Simbody: multibody dynamics for biomedical research. *Procedia Iutam*, *2*, 241–261.

Sinkjær, T., Andersen, J. B., Ladouceur, M., Christensen, L. O., & Nielsen, J. (2000). Major role for sensory feedback in soleus emg activity in the stance phase of walking in man. *The Journal of physiology*, *523*(Pt 3), 817.

Smith, A. C., Rymer, W. Z., & Knikou, M. (2015). Locomotor training modifies soleus monosynaptic motoneuron responses in human spinal cord injury. *Experimental brain research*, *233*(1), 89–103.

Smith, L. R., Lee, K. S., Ward, S. R., Chambers, H. G., & Lieber, R. L. (2011). Hamstring contractures in children with spastic cerebral palsy result from a stiffer extracellular matrix and increased in vivo sarcomere length. *The Journal of physiology, 589*(10), 2625–2639.

Song, S., & Geyer, H. (2012). Regulating speed and generating large speed transitions in a neuromuscular human walking model. *2012 IEEE International Conference on Robotics and Automation,* 511–516.

Song, S., & Geyer, H. (2013). Generalization of a muscle-reflex control model to 3d walking. *2013 35th Annual International Conference of the IEEE Engineering in Medicine and Biology Society (EMBC),* 7463–7466.

Song, S., & Geyer, H. (2015). A neural circuitry that emphasizes spinal feedback generates diverse behaviours of human locomotion. *The Journal of physiology, 593*(16), 3493–3511.

Song, S., & Geyer, H. (2018). Predictive neuromechanical simulations indicate why walking performance declines with ageing. *The Journal of physiology, 596*(7), 1199–1210.

Stanev, D., & Moustakas, K. (2019). Modeling musculoskeletal kinematic and dynamic redundancy using null space projection. *PloS one, 14*(1), e0209171.

States, R. A., Krzak, J. J., Salem, Y., Godwin, E. M., Bodkin, A. W., & McMulkin, M. L. (2021). Instrumented gait analysis for management of gait disorders in children with cerebral palsy: a scoping review. *Gait & Posture, 90,* 1–8.

Steele, K. M., van der Krogt, M. M., Schwartz, M. H., & Delp, S. L. (2012). How much muscle strength is required to walk in a crouch gait? *Journal of biomechanics, 45*(15), 2564–2569.

Stein, R. B. (1991). Reflex modulation during locomotion: functional significance. In *Advances in psychology* (pp. 21–36). Elsevier.

Stein, R. B., & Capaday, C. (1988). The modulation of human reflexes during functional motor tasks. *Trends in neurosciences, 11*(7), 328–332.

Stephens, M. J., & Yang, J. F. (1996). Short latency, non-reciprocal group i inhibition is reduced during the stance phase of walking in humans. *Brain research, 743*(1-2), 24–31.

Stout, J. L., Gage, J. R., Schwartz, M. H., & Novacheck, T. F. (2008). Distal femoral extension osteotomy and patellar tendon advancement to treat persistent crouch gait in cerebral palsy. *JBJS, 90*(11), 2470–2484.

Sutherland, D. H., & Davids, J. R. (1993). Common gait abnormalities of the knee in cerebral palsy. *Clinical orthopaedics and related research,* (288), 139–147.

Taga, G. (1995). A model of the neuro-musculo-skeletal system for human locomotion. *Biological cybernetics, 73*(2), 97–111.

Thelen, D. G. (2003). Adjustment of muscle mechanics model parameters to simulate dynamic contractions in older adults. *J. Biomech. Eng., 125*(1), 70–77.

Thomas, C., Bakels, R., Klein, C., & Zijdewind, I. (2014). Human spinal cord injury: motor unit properties and behaviour. *Acta physiologica, 210*(1), 5–19.

Thomas, C., Zaidner, E., Calancie, B., Broton, J., & Bigland-Ritchie, B. (1997). Muscle weakness, paralysis, and atrophy after human cervical spinal cord injury. *Experimental neurology, 148*(2), 414–423.

Uchida, T. K., Hicks, J. L., Dembia, C. L., & Delp, S. L. (2016). Stretching your energetic budget: how tendon compliance affects the metabolic cost of running. *PloS one, 11*(3), e0150378.

Uchida, T. K., Seth, A., Pouya, S., Dembia, C. L., Hicks, J. L., & Delp, S. L. (2016). Simulating ideal assistive devices to reduce the metabolic cost of running. *PloS one, 11*(9), e0163417.

Umberger, B. R. (2010). Stance and swing phase costs in human walking. *Journal of the Royal Society Interface, 7*(50), 1329–1340.

Umberger, B. R., Gerritsen, K. G., & Martin, P. E. (2003). A model of human muscle energy expenditure. *Computer methods in biomechanics and biomedical engineering, 6*(2), 99–111.

van den Noort, J. C., Bar-On, L., Aertbeliën, E., Bonikowski, M., Brændvik, S. M., Broström, E. W., Buizer, A. I., Burridge, J. H., van Campenhout, A., Dan, B., et al. (2017). European consensus on the concepts and measurement of the pathophysiological neuromuscular responses to passive muscle stretch. *European journal of neurology, 24*(7), 981–e38.

Van der Helm, F. C., & Rozendaal, L. A. (2000). Musculoskeletal systems with intrinsic and proprioceptive feedback. *Biomechanics and neural control of posture and movement*, 164–174.

Van der Krogt, M. M., Doorenbosch, C. A., & Harlaar, J. (2007). Muscle length and lengthening velocity in voluntary crouch gait. *Gait & posture, 26*(4), 532–538.

Van der Noot, N., Ijspeert, A. J., & Ronsse, R. (2015). Biped gait controller for large speed variations, combining reflexes and a central pattern generator in a neuromuscular model. *2015 IEEE international conference on robotics and automation (ICRA)*, 6267–6274.

Van der Noot, N., Ijspeert, A. J., & Ronsse, R. (2018). Bio-inspired controller achieving forward speed modulation with a 3d bipedal walker. *The International Journal of Robotics Research, 37*(1), 168–196.

Van Der Salm, A., Nene, A. V., Maxwell, D. J., Veltink, P. H., Hermens, H. J., & IJzerman, M. J. (2005). Gait impairments in a group of patients with incomplete spinal cord injury and their relevance regarding therapeutic approaches using functional electrical stimulation. *Artificial organs, 29*(1), 8–14.

van der Krogt, M. M., Doorenbosch, C. A., Becher, J., & Harlaar, J. (2010). Dynamic spasticity of plantar flexor muscles in cerebral palsy gait. *Journal of rehabilitation medicine, 42*(7), 656–663.

van der Krogt, M. M., Bar-On, L., Kindt, T., Desloovere, K., & Harlaar, J. (2016). Neuro-musculoskeletal simulation of instrumented contracture and spasticity assessment in children with cerebral palsy. *Journal of NeuroEngineering and Rehabilitation, 13*(1), 1–11.

van Schie, C. H. (2008). Neuropathy: mobility and quality of life. *Diabetes/metabolism research and reviews, 24*(S1), S45–S51.

Veerkamp, K., Waterval, N., Geijtenbeek, T., Carty, C., Lloyd, D., Harlaar, J., & van der Krogt, M. (2021). Evaluating cost function criteria in predicting healthy gait. *Journal of Biomechanics, 123*, 110530.

Verschueren, S. M., Swinnen, S. P., Desloovere, K., & Duysens, J. (2002). Effects of tendon vibration on the spatiotemporal characteristics of human locomotion. *Experimental brain research, 143*(2), 231–239.

Wang, J. M., Hamner, S. R., Delp, S. L., & Koltun, V. (2012). Optimizing locomotion controllers using biologically-based actuators and objectives. *ACM Transactions on Graphics (TOG), 31*(4), 1–11.

Waterval, N., Veerkamp, K., Geijtenbeek, T., Harlaar, J., Nollet, F., Brehm, M., & van der Krogt, M. (2021). Validation of forward simulations to predict the effects of bilateral plantarflexor weakness on gait. *Gait & Posture, 87*, 33–42.

Whelan, P. J. (2010). Shining light into the black box of spinal locomotor networks. *Philosophical Transactions of the Royal Society B: Biological Sciences, 365*(1551), 2383–2395.

Windhorst, U. (1989). Do renshaw cells tell spinal neurones how to interpret muscle spindle signals? *Progress in brain research, 80*, 283–294.

Windhorst, U. (1990). Activation of renshaw cells. *Progress in neurobiology, 35*(2), 135–179.

Wren, T. A., Gorton III, G. E., Ounpuu, S., & Tucker, C. A. (2011). Efficacy of clinical gait analysis: a systematic review. *Gait & posture, 34*(2), 149–153.

Wu, A. R., Simpson, C. S., van Asseldonk, E. H., van der Kooij, H., & Ijspeert, A. J. (2019). Mechanics of very slow human walking. *Scientific reports, 9*(1), 1–10.

Xia, R., & Rymer, W. (2005). Reflex reciprocal facilitation of antagonist muscles in spinal cord injury. *Spinal Cord, 43*(1), 14–21.

Yang, J., Stein, R., & James, K. (1991). Contribution of peripheral afferents to the activation of the soleus muscle during walking in humans. *Experimental Brain Research, 87*(3), 679–687.

Yokoyama, H., Ogawa, T., Shinya, M., Kawashima, N., & Nakazawa, K. (2017). Speed dependency in α-motoneuron activity and locomotor modules in human locomotion: indirect evidence for phylogenetically conserved spinal circuits. *Proceedings of the Royal Society B: Biological Sciences, 284*(1851), 20170290.

Zaaya, M., Pulverenti, T. S., Islam, M. A., & Knikou, M. (2020). Transspinal stimulation downregulates activity of flexor locomotor networks during walking in humans. *Journal of Electromyography and Kinesiology, 52*, 102420.

Zajac, F. E. (1989). Muscle and tendon: properties, models, scaling, and application to biomechanics and motor control. *Critical reviews in biomedical engineering, 17*(4), 359–411.

Zehr, E. P., & Stein, R. B. (1999). What functions do reflexes serve during human locomotion? *Progress in neurobiology, 58*(2), 185–205.

Andrea Di Russo

✉ andreadir92@hotmail.it
📞 +41 78 670 52 24
🏠 Avenue de Beaulieu 1, 1004 Lausanne, Switzerland
🅢 andreadir92
my Linked in profile
◯ GitHub

Strengths

- Computational modeling and analysis of healthy and pathological gait
- Experienced in gait recording
- First author of articles in peer-reviewed international journals
- Work in close collaboration with clinicians and medical professionals

Education

Swiss Federal Institute of Technology of Lausanne (EPFL)   *2018 September – 2023 April*
PhD in Robotics and Intelligent Systems

Swiss Federal Institute of Technology of Lausanne (EPFL)   *2015 September - 2018 April*
MSc in Bioengineering,
Minor in Neuroprosthetics, Orientation in Biomechanics

Università degli studi di Roma - La Sapienza   *2011 September - 2015 July*
BSc in Clinical Engineering

Core Experience

Biorobotics Laboratory (EPFL)   *2018 September - Today*
Research Assistant
SimGait project: Neuromuscular simulations of healthy and pathological gait in children with cerebral palsy (CP)
- Programming and modeling neural controllers for healthy and pathological human locomotion.
- Modeling muscle contracture, weakness, and neural spasticity in OpenSim and SCONE.
- Collaborating with Kinesiology and Machine Learning teams in Geneva
- Close interaction with surgeons to assist clinical decision-making in CP patients.

By isolating the effect of biomechanical contractures and neural spasticity in simulations, my results highlighted how muscle-tendon surgeries might benefit patients with severe contractures and low levels of spasticity and counterproductive for patients with high spastic levels. I also identified the possible spinal mechanisms responsible for modulating spatiotemporal parameters in human gait.

Brown University – Neuromotion Laboratory (RI, USA)   *2017 September – 2018 April*
Visiting Research Fellow
Master Thesis: A Musculoskeletal Model of the Rhesus Macaque's Hindlimbs.
- Musculoskeletal modeling of the rhesus macaque's hindlimbs in MuJoCo.
- Implementation of reflex-based controller generating muscle activation for rhythmic locomotion in Python

I efficiently extended the musculoskeletal model and programmed a sensory controller generating locomotion.

Neurorehabilitation Robotics Laboratory - Fondazione Santa Lucia   *2016 July - September*
Rehabilitation Engineer Intern
- Operator of gait experiments on healthy subjects ad stroke patients.
- Gait analysis (kinetic, kinematic and EMG data) of ultra-slow walking from healthysubjects and patients
- Reconstruct marker trajectories with Motive motion capture software.
- Extract gait data from OpenSim through Inverse kinematics and Inverse Dynamics

My work improved the accuracy in estimating gait impairments in patients and minor deviations in healthy subjects.

Language Skills

Mother tongue: Italian

	Reading	Listening	Writing	Speaking
English	C1	C1	C1	C1
French	B2	B2	B2	B2

Publications

First author

- Di Russo, A., Stanev, D., Armand, S., & Ijspeert, A. (2021). Sensory modulation of gait characteristics in human locomotion: A neuromusculoskeletal modeling study. PLoS computational biology, 17(5), e1008594. (https://doi.org/10.1371/journal.pcbi.1008594)
- Di Russo, A., Stanev, D., Sabnis, A., Danner, S. M., Ausborn, J., Armand, S., & Ijspeert, A. (2023). Investigating the roles of reflexes and central pattern generators in the control and modulation of human locomotion using a physiologically plausible neuromechanical model. Submitted to IOP – Journal of Neural Engineering (https://doi.org/10.1371/journal.pcbi.1008594)
- Di Russo, A., Placidet L., Armand, S., & Ijspeert, A. Neuromuscular simulations predict gait deviations and effects of muscle-tendon lengthening surgery in crouch gait cerebral palsy. (Upcoming submission)

Co-author

- Bruel, A., Ghorbel, S. B., Di Russo, A., Stanev, D., Armand, S., Courtine, G., & Ijspeert, A. (2022). Investigation of neural and biomechanical impairments leading to pathological toe and heel gaits using neuromusculoskeletal modelling. The Journal of Physiology, 600(11), 2691-2712. (https://doi.org/10.1113/JP282609)
- Messara, M., Manzoori, A., Di Russo, A., Bouri, M., & Ijspeert, A. (2023). Novel Implementation of a Neuromuscular Controller on a Hip Exoskeleton for Partial Gait Assistance. Submitted to ICORR 2023 - International Consortium for Rehabilitation Robotics.
- Sabnis, A., Di Russo, A., Finley, J., & Ijspeert, A. Muscle sensory feedback predicts effort expenditure in human locomotion : A neuromuscular modelling study. (Upcoming submission)

Technical expertise

Programming

- Phyton: numpy, Pandas, scipy, matplotlib, opensim, mujocopy ◦ MATLAB ◦ SQL ◦ C++ (basic)

Computer Software

- OpenSim ◦ SCONE ◦ MuJoCo ◦ OptiTrack - Motive - Optical motion capture software
- DbVisualizer ◦ Kinovea ◦ Webots ◦ LaTeX ◦ Microsoft Office

Technical skills

- Data analysis: statistical, descriptive, and predictive analysis
- Machine Learning: supervised learning, regression models, factorization analysis, artificial neural networks
- Designing and conducting experimental protocols on human subjects
- Reaching, selecting, and synthesizing information from different database

Interpersonal skills

- Problem-solving ◦ Quick learning abilities in new scientific fields ◦ Effective presentation skills ◦ Scientific writing
- Supervision and teaching to graduate students

Additional Experience

Swiss Federal Institute of Technology of Lausanne (EPFL)   *2018 September - Today*
Teaching Assistant
- Supervision of full-time bachelor and master thesis, summer internships, and part-time semester projects.
- Preparing and giving lectures, building and correcting exercise sessions, assisting students in assignments (BIOENG-404 - Analysis and modeling of locomotion (2020, 2021, 2023), MICRO-507 - Legged robots (2019, 2020), CS-432 - Computational motor control (2019)).
- Supervision of students developing prototype devices assisting people with disabilities for the course project ATC – Assistive Technology Challenge (2022, 2023).

Biorobotics Laboratory (EPFL)   *2016 September - 2017 June*
Lab Intern
- Development and applications of experimental protocols for human subjects walking on treadmill to investigate slow walking.
- Biomechanical analysis of data recorded using MATLAB (btk), Motive, and OpenSim (Inverse Kinematics). My results suggested different control strategies in generating very slow walking compared to walking at normal speeds.

Interests

- Reading and collecting books, graphic novels and comics in three languages ◦ Running and scheduling a 3h/week personal workout ◦ Gardening culinary herbs on the balcony.

Personal details: Nationality: Italian, Date of birth: 20/12/1992, Driving license: B, Civil Status: Single